

DIGITAL ACCESS TO SCHOLARSHIP AT HARVARD

Size-related Isotopic Heterogeneity in Lipids from the Marine Water Column

The Harvard community has made this article openly available. Please share how this access benefits you. Your story matters.

Citation	Close, Hilary Gwyneth. 2012. Size-related Isotopic Heterogeneity in Lipids from the Marine Water Column. Doctoral dissertation, Harvard University.
Accessed	April 17, 2018 3:29:56 PM EDT
Citable Link	http://nrs.harvard.edu/urn-3:HUL.InstRepos:9789420
Terms of Use	This article was downloaded from Harvard University's DASH repository, and is made available under the terms and conditions applicable to Other Posted Material, as set forth at http://nrs.harvard.edu/urn-3:HUL.InstRepos:dash.current.terms-of-use#LAA

(Article begins on next page)

Size-related Isotopic Heterogeneity in Lipids from the Marine Water Column

A dissertation presented

by

Hilary Gwyneth Close

to

The Department of Earth and Planetary Sciences

in partial fulfillment of the requirements
for the degree of

Doctor of Philosophy

in the subject of

Earth and Planetary Sciences

Harvard University
Cambridge, Massachusetts

May, 2012

© 2012 – Hilary Gwyneth Close
All rights reserved.

Dissertation Adviser: Professor Ann Pearson Hilary Gwyneth Close

Size-related Isotopic Heterogeneity in Lipids from the Marine Water Column

Abstract

Microbes, including Bacteria, are globally important mediators of elemental transformations in the marine water column, but not until recently has their biomass been suggested to contribute significantly to carbon export flux. Here I characterize lipid and carbon isotopic signatures in marine particulate organic matter (POM) explicitly at microbial size scales, and I quantitatively explore how these signatures are transferred down the water column. In the North Pacific Subtropical Gyre (NPSG) an isotopically-enriched pool of submicron POM appears to dominate export to mesopelagic depths, supporting recent observations that bacterioplankton communities contribute to export flux in proportion to their biological abundance. In the Eastern Tropical North Pacific (ETNP) complex pathways emerge for the flux of POM to the deep ocean. I use the largest data set to date for natural ^{13}C signatures of individual water column lipids to reveal that submicron and larger-size suspended POM size classes are isotopically distinct. Results point to *de novo* production of lipids above and within the oxygen minimum zone. I develop quantitative models to deconvolve the signatures of sinking and *in situ* sources of these lipids. Results converge on a best-fit model for downward flux in the ETNP that includes both surface-derived and sub-photic zone lipids. Overall results from the modern ocean suggest that approximately half of total suspended POM is submicron in size, much of it is bacterial in origin, and despite the small size of this material, it participates dynamically in water column export flux. These results also suggest some revised interpretations of organic matter signatures in the geologic record. I formulate a quantitative model of marine microbial production and degradation, and reproduce "inverse" isotopic signatures found in lipids and organic matter preserved in Proterozoic sedimentary rocks. Results suggest that the disappearance of this

inverse ^{13}C pattern was a consequence of the shift from Bacteria to Eukarya as dominant producers of marine autotrophic biomass. Together, results of this thesis reveal that heterogeneity in the isotopic signatures of marine suspended POM is associated with particle size, and by extension, must be a function of the composition of the total planktonic community.

Table of Contents

Acknowledgments

Foremost gratitude goes to Ann Pearson for guiding me along this geochemical pathway. She has taught me virtually everything I know about organic geochemistry and microbiological processes, either directly or by giving me the freedom to learn through numerous conferences and (always tropical) field work. She has been an utterly patient and thorough editor of this dissertation. She has helped me in immeasurable ways in getting this work to come together and in moving forward with even more tropical adventures.

I am grateful to each of my committee members through the years for providing vital external perspective and grounding in the wider world of earth sciences, for always being interested in my work, and for supporting me in my plans for the future. I have learned something important from each and every one of you: Andy Knoll, Peter Huybers, Steve Wofsy, Brendan Meade, Dave Johnston, and Sujoy Mukhopadhyay. Special thanks go to Stuart Wakeham for getting me on the cruise that ultimately determined my direction in graduate school, and for indirectly teaching me so much through his decades of foundational work. I am grateful also to the Geology department at Oberlin College, and particularly my undergraduate advisers Karla Parsons-Hubbard and Bruce Simonson, for teaching me to understand and love what the rock record can tell us.

The Department of Earth and Planetary Sciences at Harvard has been a delightful and supportive place to spend almost six hard-working years. Paul Kelley, Chenoweth Moffatt, Sarah Colgan, Maryorie Grande, Jason Miller, Patricia Fuentes-Cross, Robert Henry, and Olga Kolas have all enabled me to thrive both academically and as an active member of the EPS community. I am indebted to EPS for providing a way for me to flex my geologic muscle and to experience new places in the world through the grad-student field trips.

I also am lucky to have shared this time and place with Paul Hoffman, Dan Schrag, my committee members, and a whole host of post-docs and graduate students, who all have provided imposing examples of the geochemical perspective over the whole range of geologic timescales. I have valued my interactions with all of my officemates and geochemical neighbors— no matter whether our conversations in Hoffman have blossomed into profound insights, general confusion, or the occasional heated exchange: Meytal Higgins, John Higgins, Julie Shoemaker, Sarah Hurley, Kate Dennis, Itay Halevy, Tom Laakso, Sierra Petersen, JC Creveling, Wil Leavitt, Alex Bradley, Lindsay Hays, Stephie Kusch, Wiebke Mohr, Lila, Jack, and Lucy. Special thanks to Suni Shah for teaching me most of what I know about doing work in an organic geochemistry lab, and for instilling in me the delicate balance of paranoia necessary for measuring natural-abundance radiocarbon; to Roderick Bovee for his collaboration on the Proterozoic modeling project and for putting up with my "eclectic" coding style; and to Susie Carter, without whom nothing in our lab would run and I would not have eaten many delicious cakes.

The EPS grad student community has fostered a lot of wild times. What a funny bunch. I've had too many and too-fun times to recall with John Crowley, Kate Dennis, Victor Tsai, Justin Parrella, Ben Lee, Patrick Kim, Steve Turner, and everyone else. Thanks to Antonella D'Eramo and Tracy Warmington for giving me the best refuge during these last couple, craziest years. And to Daryl, Donna, and Meredith Close for their absolutely unconditional love and support from afar.

To my parents and grandparents

List of tables and figures

Tables

Figures

Chapter 1

Introduction

Only within the last few decades has the full spectrum of sizes and interactions of living and dead organic matter (OM) in the oceans started to emerge (Pomeroy, 1974; Azam et al., 1983; McCave, 1984; Fogg, 1986; Koike et al., 1990). Specifically, the importance of marine microbes and their biomass in global element cycles is a relatively recent and continuously-developing concept. Even more so than the ecological roles of microbes, the fate of biomass existing at microbial scales in the marine environment remains unclear. In particular, standard methods typically undersample the submicron (< 1 μm) size class of particulate organic matter (POM) by anywhere from ~40% to 70% (Altabet, 1990; Koike et al., 1990), yet this is the scale at which most Bacteria, Archaea, and their remains exist. This dissertation directly examines marine POM from the microbial submicron size class by employing a novel sampling technique not normally used for organic analysis. The work aims to project how chemical and isotopic distinctions among size classes of POM can affect our interpretation of sources and cycling of modern and ancient OM.

Background: Biomass export

The ubiquity of bacterial photosynthesis was not recognized until 1979, and its magnitude is still being realized (e.g., *Synechococcus*: Johnson and Sieburth, 1979; *Prochlorococcus*: Chisholm et al., 1988; Martiny et al., 2009). With the addition of fluorescence-staining and detection techniques that revealed the abundance of bacterial heterotrophs (Hobbie et al., 1977), the concept of a marine microbial food web – operating differently from the classical, macrobiotic grazing food web – has since become widely accepted (Pomeroy, 1974; Ducklow, 1983; Azam et al., 1983).

Somewhat separately, the idea that the fluxes of carbon and nutrients from plankton in the surface ocean are essential contributors to elemental cycles in the deep ocean spurred interest in ocean ecology as a major factor in global element cycles and climate feedbacks (the "biological pump": Dugdale and Goering, 1967; Eppley and Peterson, 1979; Volk and Hoffert, 1985; Longhurst and Harrison, 1989). Importantly, the relative magnitudes of biological production in the surface ocean, and respiration and recycled production in the remainder of the water column, together determine the flux of organic matter and biomarkers to marine sediments. This long-term balance between OM production and sediment burial strongly influences the concentration of CO_2 in the atmosphere and ultimately determines (1) the initial emergence and sustained balance of O_2 available for respiration in the atmosphere and oceans and (2) the record of marine productivity that is buried in sediments on geologic timescales.

The biological pump has been assumed to operate mostly through the export flux of eukaryotic plankton, organic particles, aggregates, and fecal pellets on the order of ≥ 0.1 mm in diameter, in virtue of their sufficiently large size and density to permit sinking (e.g., Fowler and Knauer, 1986; Longhurst and Harrison, 1989). The "microbial loop" (Azam et al., 1983) was conceived as operating somewhat independently of this zooplankton-mediated grazing food web (e.g., Sherr and Sherr, 1988). POM of microbial origin traditionally was thought to be completely recycled within the upper water column, due to its small size and slow (or zero) sinking rates (e.g., Michaels and Silver, 1988; Azam, 1998; Cullen et al., 2002).

Recently, there has been increased recognition of the interaction between microbial processes and the downward flux of materials in the ocean. The suggestion that the role of microbiota in the biological pump is as important as their role in OM cycling in the surface ocean has become increasingly powerful, with evidence that even bacterial biomass is transported to the deep ocean in significant proportions. New observations have come largely in the form of chemical constituents or cells in sinking POM that are attributable to plankton < 2-3 μm in diameter ("picoplankton"; e.g., Waite et al., 2000; Lomas and Moran, 2011; Sohrin

et al., 2011). Export of biomass from picoplankton is also evident from carbon-budget calculations (e.g., Burd et al., 2010), inverse food web/export modeling (Richardson and Jackson, 2007), and direct observation of aggregation processes (Fukuda and Koike, 2004). It is important to note that in this definition, the picoplankton include all Bacteria, Archaea, and the few species of photosynthetic Eukarya that are < 3 μm in diameter (e.g. *Ostreococcus* spp.).

A microbial role in POM transfer to the deep ocean is not just an interesting detail: a full conceptual model of POM transfer between size classes, among biota and detritus, and across the breadth and depth of the ocean underpins calculations of global element budgets, interpretation of the sedimentary record, and projections of the responsiveness of the global system to change. Examples abound, particularly in carbon cycle models and paleoclimate reconstructions. A recent large-scale meeting of biogeochemists resulted in a report that laments—even curses—our inability to model a balanced carbon budget for the modern ocean/atmosphere system (IMBER IMBIZO meeting; Burd et al., 2010). The consensus of this group emphasizes uncertainties in parameterizing carbon flux pathways among microbes and microbe-scale POM.

The central dilemma concerns the inability to reconcile various proxy measurements of organic carbon flux from the surface ocean (carbon "supply") with various proxy measurements of apparent organic carbon consumption in subsurface waters (carbon "demand"). Apparent OM export is quantified most commonly by measuring new production (f-ratio), sediment trap fluxes of POM, or thorium scavenging onto particles. These measurements have resulted in estimates of global organic carbon export that range as broadly as 5-20 GtC/year, or about 7-30% of gross marine primary production (Henson et al., 2011). The carbon demand in the subphotic ocean, on the other hand, often is calculated from oxygen utilization or organic tracer uptake rates (e.g., ^{3}H-leucine incorporation) and often outweighs its supposed carbon supply globally by a factor of two (del Giorgio and Duarte, 2002), and regionally by up to several orders of magnitude (Henson et al., 2011). There are several acknowledged uncertainties in these measurements, both on the side of carbon flux and on the side of heterotrophic demand. Better parameterization of several

often-assumed values—such as growth efficiency and cellular carbon content in Bacteria (e.g., Rivkin and Legendre, 2001; Kawasaki et al., 2011), or Th/POC ratios and sediment trap efficiency (Buesseler et al., 2006; Buesseler et al., 2007)—could help in closing some gaps in current carbon budgets (Burd et al., 2010). However, it is also frequently suggested that a ubiquitous global source of OM flux is fundamentally missed by sampling efforts and thus missing from carbon budgets. The pool of slowly-settling (suspended) POM is frequently suggested as this source (e.g., Karl et al., 1988; Simon et al., 1992; Ducklow, 1993; Arístegui et al., 2009; Burd et al., 2010).

Our inability to adequately represent the fate of POM in the modern world implicates an even more feeble capacity for interpreting ancient processes through the geologic record. Many interpretations of carbon cycling in ancient oceans adopt the microbial loop concept, assuming that there was little or no export flux on early, prokaryote-dominated Earth (Logan et al., 1995; Rothman et al., 2003), or at later times in the Phanerozoic when ocean geochemistry has favored bacterially-dominated ecology (e.g., Butterfield, 2009). Conversely, the widespread use of lipids from Archaea as a proxy of ancient sea surface temperatures (TEX_{86} proxy) implicitly relies on the idea that biomass from the very smallest free-living cells in the ocean sinks to the seafloor (Wuchter et al., 2006).

The composition of modern plankton communities is highly responsive to changes in climate and biogeochemical fluxes on short timescales (e.g., Karl et al., 2001; Corno et al., 2007). Short-term changes in communities may propagate into the nutrient and carbon cycles of deep water reservoirs that cycle on much longer timescales. More accurate models of OM flux on all size scales are particularly important. This is exemplified by studies that project climate-driven changes in the carbon cycle; these studies depend directly on our understanding of the size distribution of OM and the definitions of POM and dissolved organic matter (DOM). Prominently, Wohlers et al. (2009) and Kim et al. (2011) each find an increased ratio of dissolved organic carbon to particulate organic carbon (DOC/POC) with increased temperature

and/or increased CO_2 concentrations in mesocosm experiments. From this, each projects a future in which more OM is respired (as DOM) and less is contributed to export flux (as POM). However, both authors neglect to distinguish processes on the scale of picoplankton, and instead define POM operationally as > 0.7 μm and DOM as < 0.7 μm; their conclusions could change significantly with consideration of export pathways for submicron POM.

This dissertation aims to address some of the conceptual grey areas in marine OM cycling by examining undersampled size classes, particularly POM < 1 μm in diameter. With better understanding of POM transfer between particle size classes and down the water column, we might develop a better mechanistic underpinning with which to project variations in carbon cycling in the future or in the deep past.

Effect of size on OM export and cycling

As addressed by foundational models of marine OM production and export (Michaels and Silver 1988), the size distribution of the plankton community in the surface ocean has both primary (direct sinking) and secondary (grazing and packaging/transport) effects on the export potential of its biological products. In most regions, the phytoplankton community is largely unicellular, existing within the biological size class considered "microbial" – either "picoplankton" (0.2-2 μm) or "nannoplankton" (~2-60 μm; Sieburth et al., 1978). The major exceptions are high-latitude or coastal upwelling regions dominated by larger plankton such as diatoms or photosynthetic dinoflagellates, both of which often are > 60 μm in diameter.

Most phytoplankton are thus included in the class of POM often referred to as "suspended", "non-sinking", or "slowly-settling". Suspended POM generally is considered to include particles and biomass with a lower size cutoff of 0.2-0.7 μm and an upper size cutoff of ~53-100 μm (Bacon et al., 1995; Wakeham and Lee, 1989). POM < 1 μm in diameter ("submicron") contains the smallest components of the suspended pool and includes biological detritus, some picoeukaryotes, and most cells of Bacteria and Archaea (including autotrophs and

heterotrophs). OM smaller than an operationally-defined size cutoff is considered "dissolved" (DOM); this cutoff is inconsistently defined and may be 0.1, 0.2, 0.45, 0.7, 0.8, or 1 μm. DOM comprises small colloids, viruses, and truly "dissolved" molecular components—and includes recently-synthesized, as well as ancient, recalcitrant products (Repeta et al., 2006; Williams and Druffel, 1987). DOM also may contribute substantially to total OM export (DOM; Carlson et al., 1994; Jiao et al., 2010). The DOM pool in the ocean is larger than the POM pool, and it has been estimated to contribute ~20% of OM export globally (Hansell and Carlson, 1998).

POM larger than 53-100 μm is referred to as "sinking" and is frequently modeled as carrying most or all of the sinking flux of OM (e.g., Fowler and Knauer, 1986). In contrast, suspended POM is usually modeled as experiencing higher rates of decomposition and thus effectively contributing less (or nothing) to sinking flux due to its longer residence time in the water column (Bacon et al., 1985; Fowler and Knauer, 1986; Karl et al., 1988). However, numerous factors can transfer POM originating in suspended size classes into more quickly-sinking POM pools. Most prominent among these processes are aggregation and ballasting, indirect transport through ingestion by larger organisms, and direct sinking mediated by self-aggregation/disaggregation processes.

Classical aggregation models parameterize physical factors that influence collision frequency based on a given particle type and water column environment. In these purely physical models, aggregation of submicron particles is most likely to occur through collision via Brownian motion. The models reviewed by Johnson et al. (1990) suggest that Brownian motion and differential settling also are the physical forces most affecting particle collision in subsurface, open water-column settings. Turbulent shear and bubble formation at the air-water or sediment-water interface, on the other hand, lead to increased particle interactions in surface and benthic boundary layers (Kepkay, 1994). Notably, physical collision models of aggregation act upon both organic and inorganic particles, as well as both whole cells and organic detritus.

Organic aggregates effectively scavenge mineral grains, thus increasing their size, density, and sometimes their sinking rates (Armstrong et al., 2002; Passow and De La Rocha, 2001).

Biological mediation often dominates over these purely physical factors in transporting organic particles in the water column (McCave, 1984; Fukuda and Koike, 2004). Prokaryotic cells generally are too small to be grazed directly by migrating mesoplankton. However, small (< 10 μm) grazing protists such as nanoflagelletes are able to feed effectively on submicron OM. These flagellates may then be grazed by larger (> 200 μm) mesoplankton grazers (e.g., Azam et al., 1983; Waite et al., 2000; Fukuda and Koike, 2000; Arístegui et al., 2009). Mesoplankton such as copepods may then migrate to depth, directly carrying their gut contents through the water column; or they may egest their picoplanktonic diet components as fecal pellets, which also sink faster than picoplankton cells (Fowler and Knauer, 1986).

Additional, indirect biological mediation of aggregation occurs through the production of extracellular biopolymers. Transparent exopolymer particles (TEP) released as biological exudates aid in the spontaneous coagulation of DOM, POM, and intact or living pico- and microplankton (Alldredge et al., 1993). Many biological polymers at the particulate or dissolved scale effectively act as gels (Chin et al., 1998), thus adding chemical and ionic interactions to the dynamic exchange between OM size classes (Verdugo et al., 2004). Marine micro- and macrogels now are considered to be a major pathway of aggregation and exchange among all sizes of DOM and POM (Verdugo, 2012).

Most of these processes appear to favor higher aggregation rates in surface waters than in the subphotic water column, owing to factors such as higher overall concentration of organic particles, locus of grazers, and increased shear forces. While models exist for parameterizing physical aggregation processes at the pressures, temperatures, and particle concentrations found in the subphotic water column, they are rarely considered dominant processes (McCave, 1984; Boyd and Trull, 2007). Incorporation of OM produced *in situ* at subphotic depths into sinking flux is thus also rarely considered (Karl et al., 1984; McCave, 1984). However, within the

organic geochemical literature, there is abundant – although non-quantitative – evidence for export of lipid biomarkers reflecting mid-water chemoautrophy and anammox processes (e.g., Jaeschke et al., 2007; Sáenz et al., 2011). Similarly, debate continues as to the export potential of picoplanktonic biomass originating from the euphotic zone (Richardson and Jackson, 2007; Stukel and Landry, 2010; Lomas and Moran, 2011; Fawcett et al., 2011). Thus, the role of aggregation and its effect on export potential of all prokaryotic communities is a major remaining question.

Instead, disaggregation processes are typically assumed to dominate at depth, thereby steadily transforming organic carbon and nutrients from sinking POM into smaller, dissolved forms that are accessible to the *in situ* subphotic communities (e.g., Cho and Azam, 1988; Karl et al., 1988; Goldthwait et al., 2005; Boyd and Trull, 2007). Disaggregation of particles occurs at all depths in the water column, via the physical activity of swimming and feeding plankton, intense ectoenzymatic activity by heterotrophic bacteria (Smith et al., 1992; Arístegui et al., 2009), whole-cell lysis by bacteria or viruses, or by abiotic shear forces like wind or convection (Goldthwait et al., 2005).

While physico-chemical dynamics of POM do vary with size, clearly there are not strict size-cutoffs for the various aggregation and disaggregation processes. Since size classes can be dynamic, a more accurate model of OM size classes emerges as a size continuum (McCave, 1984; Amon and Benner, 1994; Azam, 1993; Verdugo et al., 2004). This model acknowledges that both living cells and "dead" or "detrital" POM and DOM can exist in overlapping size classes, and thus can be subject to similar physico-chemical effects. It also helps to clarify that strict divisions into "dissolved", "suspended", and "sinking" pools are operational definitions based on sampling restrictions, and they are not necessarily mechanistically or biologically distinct. The present challenge is therefore to combine the conceptual size-continuum model with a practical and comprehensive sampling method to in order to gain meaningful insights into OM transfer processes.

Sampling barriers to testing a size-continuum model

Limited sampling methods may have perpetuated many of the uncertainties associated with models of OM cycling. Historically, direct observation of the abundance and size distribution of marine particles has helped guide expectations for sampling yields and has influenced sampling techniques (e.g., discovery of large and abundant transparent exopolymer particles—Alldredge et al., 1993; identification of abundant prokaryotic photoautotrophs by transmission electron spectroscopy—Johnson and Sieburth, 1979; and by flow cytometry—Chisholm et al., 1988). We thus currently have a relatively complete idea of what biases are involved for the many various sampling methods. However, there is no consensus among the oceanographic community as to which sampling methods are optimal for total POM (e.g., Gardner et al., 2003).

Sediment traps historically have been the most widely used devices for measuring POM flux. These usually comprise a floating, conical or cylindrical device that passively collects sinking particles into a cup filled with poisoned brine. Traps are deployed for days to weeks, and therefore capture a time-integrated flux of material. While many improvements in design have reduced sampling biases associated with capture of swimming zooplankton and hydrodynamic effects, traps are still considered to undersample slowly sinking ("suspended") particles (Buesseler et al., 2007; Burd et al., 2010). For example, the imbalance between heterotrophic carbon demand and POM flux measured by sediment traps has been found to increase by an order of magnitude or more over the first thousand meters of the water column (e.g., Baltar et al., 2009). This potentially indicates an increase with depth in the proportion of slowly-settling POM, and a progressively greater bias in the corresponding sediment trap data (e.g., Benner et al., 1997). However, vertical and lateral advection of DOM and suspended POM, active transport by zooplankton, and *in situ* chemoautotrophy also can provide carbon sources that would not be captured by sediment traps (Karl et al., 1984; Jiao et al., 2010; Steinberg et al., 2008; Carlson et al., 1994; Emerson et al., 1997).

The use of *in situ* submersible pumps has allowed the direct collection of "suspended" POM from large volumes of water onto filters of various pore sizes. While this approach is considered to capture a more complete spectrum of particle sizes, deployments of only a few hours mean that the collection represents a snapshot rather than integrated flux. *In situ* pumps can be fitted with Nylon (Nitex) screens of varying mesh sizes to collect larger particles (generally down to 53 µm); these samples usually are resuspended into solution for analysis. However, the most commonly employed small pore-size filters for POM collection are glass fiber filters, which have an effective pore size down to 0.7 µm (GF/F = glass fiber, class F). Glass fiber filters are combustion-proof and organic solvent-inert. Total POM collected onto glass fiber filters can be directly combusted for elemental analysis or solvent-extracted without prior resuspension. Since this 0.7 µm pore size is the smallest commonly used, *in situ* filtration does not capture a large fraction of submicron particles. Up to 87% of bacterial cells or 50% of biomass may be missed (Taguchi and Laws, 1988; Altabet, 1990; Lee et al., 1995; Benner et al, 1997; Morán et al., 1999). GF/F filters also adsorb significant amounts of DOM, thus sometimes rendering size-based conclusions equivocal (Maske and García-Mendoza, 1994; Morán et al., 1999; Roland et al., 2008). Regardless, because of their analytical convenience, nearly all geochemical studies of suspended POM have utilized GF/F filters. It can be argued that such a uniform sampling approach is preferable, because it renders all results internally consistent. However, the same reasoning suggests that efforts to date likely are also consistently undersampling prokaryotic biomass (e.g., Fuhrman et al. 1989; Altabet, 1990; Koike et al., 1990; Gardner et al., 2003; Brinis et al., 2004; Arístegui et al., 2009).

Filters of pore sizes < 0.7 µm are often composed of synthetic polymers that are solvent-soluble, and all are combustible. The carbon contained in the polymer material is thus difficult to separate from sample carbon. POM collected onto these filters (often 0.2 or 0.45 µm pore-size) therefore usually is resuspended into solution in order to collect for analysis. However, the polymer materials making up these filters are more likely to adsorb and retain significant

amounts of POM even after sample resuspension, rendering quantitative organic analyses nearly impossible (e.g., Benner et al., 1997).

Collection of whole seawater by bottle avoids the lower-cutoff size bias of *in situ* filtering. Bottle collection thus is preferable for total POM and DOM analysis (Gardner et al., 2003). However, for many molecular-scale analyses, bottle collection generally cannot collect a sufficient volume of seawater. The smaller sample size from bottles also reflects the limited snapshot of time and space collected; thus bottle collection also undersamples the more-dispersed, large, quickly-sinking particles (McCave, 1975; Bishop and Edmond, 1976). Additionally, many shipboard protocols call for filtering of bottle-collected water, for which the discussion of filter pore-sizes above applies.

Ultrafiltration by tangential flow is a method by which organic and other particulate components of seawater are concentrated by continuously passing large volumes of seawater over a filter or membrane (e.g., Benner et al., 1997). The concentrated retentate will contain all OM with dimensions greater than the filter pore size, often 0.1 μm. Filtrate can then undergo further ultrafiltration to separate high-molecular weight DOM and POM (HMW; particle and colloid diameters 1-100 nm) from low-molecular weight DOM (LMW; < ~1000 Daltons). While this HMW material is considered part of the DOM pool, it contains viruses and colloids, both of which have chemical reactivity more in common with particles than with true solutes. Only LMW DOM is considered to contain truly dissolved molecular components. Ultrafiltration is less commonly employed because it requires large and complex shipboard sampling devices (Roland et al., 2008). Some loss of POM is also likely through adsorption to the filter, since POM is usually collected only from the seawater concentrate, and not extracted directly from the filter (Benner, 1991; Benner et al., 1997).

Methodologically, however, this ultrafiltered POM (UPOM) typically captures the widest range of "suspended" POM sizes, usually 0.1-60 μm. As such, UPOM has been observed to contain more OM and different carbon isotopic signatures than POM collected onto 0.7 μm

GF/Fs, thus highlighting the importance of characterizing the < 0.7 μm particulate size class (Benner et al., 1997; Hernes and Benner, 2002; Sannigrahi et al., 2005; Roland et al., 2008). In this way Benner et al. (1997) concluded that deeper waters contain a higher proportion of submicron particles and colloids than do surface waters, at least in their Pacific gyre study area.

Observational methods also continue to guide our understanding of the water column dynamics of marine POM. Underwater cameras can visualize the size and sinking rates of larger, mm-scale "marine snow" particles. Oceanographic hydrowire instruments often are equipped with a focused visible-spectrum beam (usually 660 nm wavelength) and detector. Because of light-scattering by suspended particles, the attenuation of the light energy over the distance between emission and detection is proportional to the concentration of particulate matter in intervening water (Claustre et al., 1999; Gardner et al., 2003; Grob et al., 2007). The proportional effect of picoplanktonic cells on beam attenuation can be determined by concurrent flow-cytometric measurement of the abundance of different clades (Claustre et al., 1999). However, the relationship between beam attenuation (C_p) and total POM concentration—including detrital components—must be determined via calibration to measured POM concentrations, which sometimes are biased by the filtration methods reviewed above (e.g., Claustre et al., 1999; Gardner et al. 2003). Like other methods, unless data transformations include a specific calibration to account for submicron POM, beam attenuation measurements of POM concentrations are also likely to underdetermine the submicron detrital concentration. Nonetheless, *in situ* optical techniques and remote sensing by satellites (e.g., Kostandinov et al., 2010) are becoming powerful tools in rapidly determining the oceanic distribution of picophytoplankton.

Radioisotopes also help to constrain POM dynamics and export in the ocean. Most common is the measurement of ^{234}Th, a daughter isotope of ^{238}U decay in seawater. Unlike its parent isotope, ^{234}Th is insoluble and is quickly scavenged onto particles. Dynamic exchange and sinking of particles can be traced in detail due to the short half-life of ^{234}Th (24.1 days); deficits

in measured concentrations of ^{234}Th and its daughter isotopes at a given depth indicate the removal rate of particulate matter. Measurements of ^{234}Th concentrations at different depths and across size classes have been combined with experimental determinations of scavenging rates to produce models of particle exchange and to determine sinking, aggregation, and disaggregation rates for OM in the marine water column (e.g., Bacon and Anderson, 1982; Clegg and Whitfield, 1990; Savoye et al., 2006). These models have helped establish the slow settling rates of suspended marine particles. Thorium-derived particle fluxes then can be translated to organic fluxes to determine POM export; this requires a size-dependent parameterization of the organic content of particles considered (e.g., Moran et al., 1993; Burd et al., 2000; Buesseler et al., 2006; Henson et al., 2011). However, many determinations of OM content with size class depend on collection onto 0.7 µm or 1 µm filters (Buesseler et al., 2006), and the size and aggregation properties of plankton populations, along with sampling methods, have been shown to influence the interpretation of ^{234}Th measurements (e.g., Waite and Hill, 2006). In addition, many prevailing models used to parameterize export employ simplified size classes and exchange parameters and therefore may not account for any export contribution from suspended OM. Nonetheless, simultaneous consideration of biological production rates and ^{234}Th-determined aggregation and removal rates at the submicron scale could provide a powerful tool in determining export potential for picoplanktonic biomass.

Summary of thesis

This dissertation aims to overcome sampling barriers described above and specifically characterize a picoplankton-sized class of particles (0.2-0.7 µm). By measuring this particle size class along with the 0.7-53 µm class, I have examined all sizes of POM generally considered to be "suspended". I explore the properties of this POM across ocean depths and geographic locations by examining variations in the lipid and ^{13}C content of these size classes, collected from surface to mesopelagic depths in the modern ocean.

In **Chapter 2** I characterize the compound distributions, ^{13}C, and ^{14}C content of total hydrolyzed fatty acids from an exclusively "picoplanktonic" (0.2-0.5 μm) size class obtained from surface waters of the North Pacific Subtropical Gyre. This very small size class is found to exhibit a distinctive enrichment in ^{13}C in some compounds. By also measuring and quantitatively comparing the isotope signatures of fatty acids from the > 0.5 μm size class, again from the surface ocean, and from a sample of total POM > 0.2 μm from a mesopelagic depth, I demonstrate that the surface picoplanktonic size class appears to be contributing preferentially to the sinking of lipids in this oligotrophic setting.

For **Chapter 3** I report a novel sampling effort to greatly expand the characterization of the submicron size class. Samples were obtained for two water column profiles spanning from the surface down through the intense oxygen minimum zone of the Eastern Tropical North Pacific (ETNP). Here, the picoplankton size class (0.2-0.7 μm) and the larger suspended size class (0.7-53 μm) also exhibit isotopic heterogeneity in both bulk and individual lipid signatures. I develop a detailed picture of POM dynamics by separating each sample into two classes of polar lipids – nominally phospholipids and glycolipids – as well as a third class, the free fatty acids. Specific fatty acid and ^{13}C signatures emerge from bacterial and algal phytoplankton, oxic bacterial heterotrophs, low-light bacterial photoautotrophs, low-oxygen metabolisms, and hydrolytic break-down of large sinking particles in the core OMZ.

In **Chapter 4** I develop a model by which to approach a best-fit deconvolution of sinking and *in situ* sources of fatty acids in the ETNP. I use lipid distributions and ^{13}C signatures to constrain possible end-member sources for lipids collected at each depth. By also considering the pathways of OM loss and the isotopic fractionations inherent in the degradation of lipids, I am able to postulate the dominant processes involved in transforming lipid signatures at different

depths and in the two size classes. The results enable estimation of the quantitative role of picoplanktonic carbon in POM export.

In **Chapter 5** I explore quantitatively how differences in isotopic content and biomass composition in two distinct pools of primary producers, combined with isotopic alteration by heterotrophic organisms during export of OM, can significantly affect our interpretation of ancient environments. I develop a model of marine organic matter production and degradation that is able to recreate the so-called "inverse" isotopic signatures in lipids and kerogen preserved from the Proterozoic Eon. I also quantify the existing model for heterotrophic enrichment of ^{13}C that has long been used to explain these signatures, and I evaluate the plausibility of each model in the context of Proterozoic oceans.

In **Chapter 6** I describe the development of a new method that allows us to extract lipids directly from 0.2 μm polymer (polysulfone) filters. This method was used to obtain the data for Chapters 3 and 4. The ability to extract lipids from 0.2 μm filters has allowed us to remove the size bias associated with GF/F filtration (> 0.7 μm cutoff) and to avoid sample loss associated with approaches that attempt to re-suspend (rather than extract) OM off of 0.2 μm filters. Our method also allows for simultaneous extraction of lipids, nucleic acids, and proteins from the same filter sample, thus expanding our analytical capabilities for low-biomass samples.

Approaches taken by this study

All chapters address the dynamics of water column POM through the lens of lipid biomarkers and their carbon isotopic content. Lipids represent a relatively small fraction of biological products (~10-20%; e.g., Fernandez-Reiriz et al., 1989), but they have long been used as tracers of biomass in the environment due to (1) the relative recalcitrance and potential for preservation of identifiable lipids in sediments and rocks, and (2) the relative source-specificity of individual

lipid compounds. The former point is in contrast to molecules with high specificity of biological source – such as nucleic acids or proteins – but high lability and thus quick turnover time in the environment. The latter point is in contrast to measurements of total organic matter or more general biochemical classes – which encompass all sources but cannot help in distinguishing complex dynamics among living and dead organic constituents.

In this work, I primarily utilize fatty acids as tracers of combined living and detrital OM. Fatty acids (FA) are the major structural components of cellular membranes in all Bacteria and Eukarya. In cellular membranes FA exist as a component of "intact polar lipids" (IPLs), *i.e.*, fatty acid chains that are ester-linked to a polar head group. Fatty acids also can exist in storage molecules such as triacylglycerols (triglycerides) or wax esters (mostly in eukaryotes), or as free fatty acids within cells or in the environment. The lifetime of IPLs as detrital components in the water column and sediments is under debate (Lipp et al., 2008; Schouten et al., 2010); IPLs generally are assumed to degrade "rapidly" once a cell has died, leaving behind detrital free fatty acids (White et al., 1979). The distribution and isotopic content of fatty acids from IPLs and free fatty acids are examined separately in Chapter 3, thus shedding light on this question of the fate of IPLs in the water column.

Organisms biosynthesize fatty acids of varying carbon chain lengths and with varying numbers and positions of double bonds[1]. The specific ratio of fatty acid structures produced by a given organism is partially controlled by phylogeny and biosynthetic capabilities and partially by environmental conditions such as temperature, since these structures help maintain membrane fluidity and cell function (e.g., Russell, 1989; Freese et al., 2008). Most structures are non-specific and can be synthesized by many organisms. Some specific products are recognized among marine biota, but most of these distinct signatures involve less-abundant compounds (e.g.,

[1] Consistent notation for fatty acid chemical structures will be used throughout this dissertation. Compounds represented as $C_{n:x}$ refer to fatty acids with a chain length of *n* carbon atoms and with *x* double bonds. Prefixes *i-*, *a-*, and *br-* refer to carbon chains with additional methyl groups (branching).

branched-$C_{15:0}$ and -$C_{17:0}$ from Bacteria; polyunsaturated, long-chain lengths predominantly from Eukarya). Because of their ubiquitous presence in most marine cells and their detritus (excluding Archaea) we use fatty acids as a way of tracking general POM dynamics (e.g., Reemtsma and Ittekkot, 1992), without specific biological source interpretations. Importantly, this allows us to include the dynamics of both autotrophic and heterotrophic biomass. Other methods of tracking POM dynamics in the marine system often make use of specific photoautotrophic pigment biomarkers, or of clade-specific sterols (e.g., Tolosa et al., 2008; Lomas and Moran, 2011). These other compounds have the advantage of identifying specific source organisms and physiologies, but they cannot be used as a proxy for bulk biomass partitioning because they are not ubiquitous among all of the biological sources that contribute to marine OM.

Along with lipid distributions, the studies in each chapter utilize the natural-abundance ^{13}C content of individual lipids. The distribution of stable carbon isotopes is widely used as an indicator of regional and global carbon cycling. The ^{13}C content of bulk OM in both modern and ancient oceans generally relates directly to the cycling and ^{13}C content of inorganic carbon, although some regional effects are apparent (e.g., Goericke and Fry, 1994). The relationship between the $\delta^{13}C$ values of organic and inorganic carbon stems from the relative constancy of the fractionation of carbon isotopes during photosynthetic uptake of aqueous DIC (as $CO_{2\text{-aq}}$ or HCO_3^-), coupled with export processes that faithfully transfer this signature, with some modification, to sediments (e.g., Hayes et al., 1999).

The quantitative relationship between the ^{13}C content of marine sedimentary OM and carbonate varies over time in the geologic record, and the explanation for large deviations likely lies in more detailed processes involved in organic matter production and cycling (Hayes et al., 1999). The use of compound-specific measurement of ^{13}C content in lipids has helped expose causes of isotopic variation over time and between environments, either from changes in plankton communities or from biogeochemical disturbances to organic carbon cycling and export.

In modern marine environments, wide variations in compound-specific ^{13}C content can arise both from differences in fractionation by clades of photoautotrophs (e.g., Tolosa et al., 2008; Popp et al., 1998) and from heterotrophic processes in the water column and sediments (e.g., Harvey and Macko, 1997; Gong and Hollander, 1997). Additional complexity is contributed in some settings from the mixing of allochthonous source materials in marine waters (e.g., terrestrial sources; Benner et al., 1997). The ^{13}C content of individual biomarker lipids also has revealed more extreme fractionations involved in methane cycling (Hinrichs et al., 1999) and specific pathways of carbon fixation (e.g., the reverse-tricarboxylic acid pathway: van der Meer et al., 1998). Some patterns of isotopic heterogeneity have been observed that are related at least partially to the interplay between CO_2 availability and the geometry of phytoplankton cells (^{13}C: Popp et al., 1998), or to the size of detrital OM (effects on ^{13}C, Roland et al., 2008; effects on ^{15}N, Altabet, 1988; Meador et al., 2007).

Few studies have examined concurrently the organic components of suspended and sinking POM to infer details of exchange across size classes (e.g., Lee and Cronin, 1982; Sheridan et al., 2002; Abramson et al. 2010). Even fewer have compared compound distributions and compound-specific isotopic signatures in different size classes of suspended and/or sinking size classes of OM (e.g., Tolosa et al., 2004). To our knowledge, only one other study has isolated a picoplankton-sized class of particles for compound-specific isotope analysis (Ingalls et al., 2006), specifically with a sufficiently small size cutoff to include most bacterial cells.

In this study, the specificity of a compound-specific characterization of multiple lipid profiles reveals details of POM cycling. The novel data begin to address many of the questions posed above. The following chapters reveal size-related heterogeneity in the ^{13}C content and vertical patterns of marine suspended POM, thus making a strong case for the importance of collecting submicron-sized particles. The results confound the interpretation of modern samples collected by conventional methods and have important implications for conceptual models applied in interpretation of the ancient organic record.

References

Abramson L, Lee C, Liu Z, Wakeham SG, Szlosek J (2010) Exchange between suspended and sinking particles in the northwest Mediterranean as inferred from the organic composition of in situ pump and sediment trap samples. *Limnology and Oceanography,* **55**, 725-739.

Alldredge A, Passow U, Logan BE (1993) The abundance and significance of a class of large, transparent organic particles in the ocean. *Deep Sea Research I,* **40**, 1131-1140.

Altabet MA (1988) Variations in nitrogen isotopic composition between sinking and suspended particles: Implications for nitrogen cycling and particle transformation in the open ocean. *Deep Sea Research Part A. Oceanographic Research,* **35**, 535-554.

Altabet MA (1990) Organic C, N, and stable isotopic composition of particulate matter collected on glass-fiber and aluminum oxide filters. *Limnology and Oceanography,* **35**, 902-909.

Amon RMW, Benner R (1994) Rapid cycling of high-molecular-weight dissolved organic matter in the ocean. *Nature,* **369**, 549-552.

Armstrong R, Lee C, Hedges J, Honjo S (2002) A new, mechanistic model for organic carbon fluxes in the ocean based on the quantitative association of POC with ballast minerals. *Deep Sea Research II,* **49**, 219-236.

Azam F (1998) Microbial control of oceanic carbon flux: the plot thickens. *Science,* **280**, 694-696.

Azam F, Fenchel T, Field JG, Gray JS, Meyer-Reil LA, Thingstad F (1983) The ecological role of water-column microbes in the sea. *Marine Ecology Progress Series,* **10**, 257-263.

Azam F, Smith D, Steward G, Hagström Å (1993) Bacteria-organic matter coupling and its significance for oceanic carbon cycling. *Microbial Ecology*, **28**, 167-179.

Bacon M, Huh C, Fleer A (1985) Seasonality in the flux of natural radionuclides and plutonium in the deep Sargasso Sea. *Deep Sea Research Part A.,* **32**.

Bacon MP, Anderson RF(1982) Distribution of thorium isotopes between dissolved and particulate forms in the deep sea. *Journal of Geophysical Research,* **87**, 2045-2056.

Baltar F, Arístegui J, Sintes E, Van Aken HM, Gasol JM, Herndl GJ (2009) Prokaryotic extracellular enzymatic activity in relation to biomass production and respiration in the meso- and bathypelagic waters of the (sub)tropical Atlantic. *Environmental Microbiology,* **11**, 1998-2014.

Benner R (1991) Ultrafiltration for the concentration of bacteria, viruses, and dissolved organic matter. In: Hurd DC, Spencer, DW (Eds.) *Marine Particles: Analysis and*

Characterization. Geophysical Monographs, **63**. American Geophysical Union: Washington, D.C., 81–185.

Benner R, Biddanda B, Black B, Mccarthy M (1997) Abundance, size distribution, and stable carbon and nitrogen isotopic compositions of marine organic matter isolated by tangential-flow ultrafiltration. *Marine Chemistry*, **57**, 243-263.

Bishop JKB, Edmond JM (1976) A new large volume filtration system for the sampling of oceanic particulate matter. *Journal of Marine Research*, **34**, 181–198.

Boyd PW, Trull TW (2007) Understanding the export of biogenic particles in oceanic waters: Is there consensus? *Progress In Oceanography*, **72**, 276-312.

Brinis A, Méjanelle L, Momzikoff A, Gondry G, Fillaux J, Point V, Saliot A (2004) Phospholipid ester-linked fatty acids composition of size-fractionated particles at the top ocean surface. *Organic Geochemistry*, **35**, 1275-1287.

Buesseler KO, Antia AN, Chen M, Fowler SW, Gardner WD, Gustafsson O, Harada K, Michaels AF, Loeff MR, Sarin M (2007) An assessment of the use of sediment traps for estimating upper ocean particle fluxes. *Journal of Marine Research*, **65**, 345-416.

Buesseler KO, Benitez-Nelson CR, Moran SB, Burd A, Charette M, Cochran JK, Coppola L, Fisher NS, Fowler SW, Gardner WD, Guo LD, Gustafsson Ö, Lamborg C, Masque P, Miquel JC, Passow U, Santschi PH, Savoye N, Stewart G, Trull T (2006) An assessment of particulate organic carbon to thorium-234 ratios in the ocean and their impact on the application of 234Th as a POC flux proxy. *Marine Chemistry*, **100**, 213-233.

Burd AB, Hansell DA, Steinberg DK, Anderson TR, Arístegui J, Baltar F, Beaupré SR, Buesseler KO, Dehairs F, Jackson GA, Kadko DC, Koppelman R, Lampitt RS, Nagata T, Reinthaler T, Robinson C, Robison BH, Tamburini C, Tanaka T (2010) Assessing the apparent imbalance between geochemical and biochemical indicators of meso- and bathypelagic biological activity: What the @$♯! is wrong with present calculations of carbon budgets? *Deep Sea Research Part II: Topical Studies in Oceanography*, **57**, 1557-1571.

Burd AB, Moran SB, Jackson GA (2000) A coupled adsorption-aggregation model of the POC/Th ratio of marine particles. *Deep-Sea Research I*, **47**, 103-120.

Butterfield NJ (2009) Oxygen, animals and oceanic ventilation: an alternative view. *Geobiology*, **7**, 1-7.

Carlson CA, Ducklow HW, Michaels AF (1994) Annual flux of dissolved organic carbon from the euphotic zone in the northwestern Sargasso Sea. *Nature*, **371**, 405-408.

Chin WC, Orellana MV, Verdugo P (1998) Spontaneous assembly of marine dissolved organic matter into polymer gels. *Nature*, **391**, 568-571.

Chisholm SW, Olson RJ, Zettler ER, Goericke R, Waterbury JB, Welschmeyer NA (1988) A novel

free-living prochlorophyte abundant in the oceanic euphotic zone. *Nature,* **334**, 340-343.

Cho B, Azam F (1988) Major role of bacteria in biogeochemical fluxes in the ocean's interior. *Nature,* **332**, 441-443.

Claustre H, Morel A, Babin M, Cailliau C, Marie D, Marty J-C, Tailliez D, Vaulot D (1999) Variability in particle attenuation and chlorophyll fluorescence in the tropical Pacific: Scales, patterns, and biogeochemical implications. *Journal of Geophysical Research,* **104**, 3401-3422.

Clegg Sl, Whitfield M (1990) A generalized model for the scavenging of trace metals in the open ocean-I. Particle cycling. *Deep-Sea Research,* **37**, 809-832.

Corno G, Karl Dm, Church Mj, Letelier Rm, Lukas R, Bidigare Rr, Abbott Mr (2007) Impact of climate forcing on ecosystem processes in the North Pacific Subtropical Gyre. *Journal of Geophysical Research,* **112**, 1-14.

Cullen J, Franks P, Karl D (2002) Physical influences on marine ecosystem dynamics. *The Sea,* **12**, 297-336.

Del Giorgio Pa, Duarte Cm (2002) Respiration in the open ocean. *Nature,* **420**, 379-384.

Ducklow HW (1983) Production and fate of bacteria in the oceans. *BioScience,* **33**, 494-501.

Ducklow H, Kirchman D, Quinby H (1993) Stocks and dynamics of bacterioplankton carbon during the spring bloom in the eastern North Atlantic Ocean. *Deep Sea Research,* **411**, 245-263.

Dugdale R, Goering Jj (1967) Uptake of new and regenerated forms of nitrogen in primary productivity. *Limnology and Oceanography,* **12**, 196-206.

Emerson S, Quay P, Karl D, Winn C, Tupas L, Landry M (1997) Experimental determination of the organic carbon flux from open-ocean surface waters. *Nature,* **389**, 951-954.

Eppley RW, Peterson BJ (1979) Particulate organic matter flux and planktonic new production in the deep ocean. *Nature,* **282**, 677-680.

Fawcett Se, Lomas Mw, Casey Jr, Ward Bb, Sigman Dm (2011) Assimilation of upwelled nitrate by small eukaryotes in the Sargasso Sea. *Nature Geoscience,* **4**, 1-6.

Fernandez-Reiriz M, Perez-Camacho A, Ferreiro M, Blanco J, Planas M, Campos M, Labarta U (1989) Biomass production and variation in the biochemical profile (total protein, carbohydrates, RNA, lipids and fatty acids) of seven species of marine microalgae. *Aquaculture,* **83**, 17-37.

Fogg GE (1986) Picoplankton. *Proceedings of the Royal Society of London. Series B, Biological Sciences,* **228**, 1-30.

Fowler SW, Knauer GA (1986) Role of large particles in the transport of elements and organic compounds through the oceanic water column. *Progress in Oceanography,* **16**, 147-194.

Freese E, Sass H, Rütters H, Schledjewski R, Rulkötter J (2008) Variable temperature-related changes in fatty acid composition of bacterial isolates from German Wadden sea sediments representing different bacterial phyla. *Organic Geochemistry*, **39**, 1427-1438.

Fuhrman JA, Sleeter TD, Carlson CA, Proctor LM (1989) Dominance of bacterial biomass in the Sargasso Sea and its ecological implications. *Marine Ecology Progress Series* **57**, 207–217.

Fukuda H, Koike I (2000) Feeding currents of particle-attached nanoflagellates — a novel mechanism for aggregation of submicron particles. *Marine Ecology Progress Series,* **202**, 101-112.

Fukuda H, Koike I (2004) Microbial stimulation of the aggregation process between submicron-sized particles and suspended particles in coastal waters. *Aquatic Microbial Ecology*, **37**, 63-73.

Gardner W, Richardson M, Carlson C (2003) Determining true particulate organic carbon: bottles, pumps and methodologies. *Deep Sea Research,* **50**, 655-674.

Goericke R, Fry B (1994) Variations of marine plankton d13C with latitude, temperature, and dissolved CO2 in the world ocean. *Global Biogeochemical Cycles*, **8**, 85-90.

Goldthwait S, Carlson C, Henderson G, Alldredge A (2005) Effects of physical fragmentation on remineralization of marine snow. *Marine Ecology Progress Series,* **305**, 59-65.

Gong C, Hollander DJ (1997) Differential contribution of bacteria to sedimentary organic matter in oxic and anoxic environments, Santa Monica Basin, California. *Organic Geochemistry*, **26**, 545-563.

Grob C, Ulloa O, Claustre H, Huot Y, Alarcón G, Marie D (2007) Contribution of picoplankton to the total particulate organic carbon concentration in the eastern South Pacific. *Biogeosciences,* **4**, 837-852.

Hansell DA, Carlson CA (1998) Net community production of dissolved organic carbon. *Global Biogeochemical Cycles,* **12**, 443-453.

Harvey HR, Macko SA (1997) Catalysts or contributors? Tracking bacterial mediation of early diagenesis in the marine water column. *Organic Geochemistry,* **26**, 531-544.

Hayes JM, Strauss H, Kaufman AJ (1999) The abundance of 13C in marine organic matter and isotopic fractionation in the global biogeochemical cycle of carbon during the past 800 Ma. *Chemical Geology,* **161**, 103-125.

Henson SA, Sanders R, Madsen E, Morris PJ, Le Moigne F, Quartly GD (2011) A reduced estimate of the strength of the ocean's biological carbon pump. *Geophysical Research*

Letters, **38**, 10-14.

Hernes PJ, Benner R (2002) Transport and diagenesis of dissolved and particulate terrigenous organic matter in the North Pacific Ocean. *Deep Sea Research I*, **49**, 2119-2132.

Hinrichs KU, Hayes JM, Sylva SP, Brewer PG, Delong EF(1999) Methane-consuming archaebacteria in marine sediments. *Nature*, **398**, 802-805.

Hobbie JE, Daley RJ, Jasper S (1977) Use of nuclepore filters for counting bacteria by fluorescence microscopy. *Applied and Environmental Microbiology* **33**, 1225-1228.

Ingalls AE, Shah SR, Hansman RL, Aluwihare LI, Santos GM, Druffel ERM, Pearson A (2006) Quantifying archaeal community autotrophy in the mesopelagic ocean using natural radiocarbon. *Proceedings of the National Academy of Sciences of the United States of America*, **103**, 6442-6447.

Jaeschke A, Hopmans EC, Wakeham SG, Schouten S, Sinninghe Damsté JS (2007) The presence of ladderane lipids in the oxygen minimum zone of the Arabian Sea indicates nitrogen loss through anammox. *Limnology and Oceanography*, **52**, 780-786.

Jiao N, Herndl GJ, Hansell DA, Benner R, Kattner G, Wilhelm Sw, Kirchman Dl, Weinbauer Mg, Luo T, Chen F, Azam F (2010) Microbial production of recalcitrant dissolved organic matter: long-term carbon storage in the global ocean. *Nature reviews. Microbiology*, **8**, 593-599.

Johnson BD, Kranck K, Muschenhein DK (1990) Physico-chemical factors in particle aggregation. In: RS Wotton (Ed.) *The Biology of Particles in Aquatic Systems*. CRC Press: Boca Raton, FL.

Johnson P, Sieburth JM (1979) Chroococcoid cyanobacteria in the sea: a ubiquitous and diverse phototrophic biomass. *Limnology and Oceanography*, **24**, 928-935.

Karl D, Bidigare R, Letelier R (2001) Long-term changes in plankton community structure and productivity in the North Pacific Subtropical Gyre: the domain shift hypothesis. *Deep Sea Research Part II: Topical Studies in Oceanography*, **48**, 1449-1470.

Karl DM, Knauer GA, Martin JH (1988) Downward flux of particulate organic matter in the ocean: a particle decomposition paradox. *Nature*, **332**, 438-441.

Kawasaki N, Sohrin R, Ogawa H, Nagata T, Benner R (2011) Bacterial carbon content and the living and detrital bacterial contributions to suspended particulate organic carbon in the North Pacific Ocean. *Aquatic Microbial Ecology*, **62**, 165-176.

Kepkay P (1994) Particle aggregation and the biological reactivity of colloids. *Marine Ecology-Progress Series*, **109**, 293-304.

Kim J-M, Lee K, Shin K, Yang EJ, Engel A, Karl DM, Kim H-C (2011) Shifts in biogenic carbon

flow from particulate to dissolved forms under high carbon dioxide and warm ocean conditions. *Geophysical Research Letters,* **38**, 1-5.

Koike I, Shigemitsu H, Kazuki T, Kazuhiro K (1990) Role of sub-micrometre particles in the ocean. *Nature* **345**, 242-244.

Kostadinov TS, Siegel DA, Maritorena S (2010) Global variability of phytoplankton functional types from space: assessment via the particle size distribution. *Biogeosciences,* **7**, 3239-3257.

Lee C, Cronin C (1982) The vertical flux of particulate organic nitrogen in the sea: decomposition of amino acids in the Peru upwelling area and the equatorial Atlantic. J*ournal of Marine Research,* **40**, 227-251.

Lee S, Kang Y-C, Fuhrman JA (1995) Imperfect retention of natural bacterioplankton cells by glass fiber filters. *Marine Ecology Progress Series,* **119**, 285-290.

Lipp JS, Morono Y, Inagaki F, Hinrichs K-U (2008) Significant contribution of Archaea to extant biomass in marine subsurface sediments. *Nature,* **454**, 991-994.

Logan GA, Hayes J, Hieshima GB, Summons RE (1995) Terminal Proterozoic reorganization of biogeochemical cycles. *Nature,* **376**, 53-56.

Lomas MW, Moran SB (2011) Evidence for aggregation and export of cyanobacteria and nano-eukaryotes from the Sargasso Sea euphotic zone. *Biogeosciences,* **8**, 203-216.

Longhurst A, Harrison WG (1989) The biological pump: profiles of plankton production and consumption in the upper ocean. *Progress in Oceanography,* **22**, 47-123.

Martiny AC, Kathuria S, Berube PM (2009) Widespread metabolic potential for nitrite and nitrate assimilation among Prochlorococcus ecotypes. *Proceedings of the National Academy of Sciences of the United States of America,* **106**, 10787-10792.

Maske H, Garcia-Mendoza E (1994) Adsorption of dissolved organic matter to the inorganic filter substrate and its implications for C uptake measurements. *Applied and Environmental Microbiology,* **60**, 3887-3889.

McCave IN (1975) Vertical flux of particles in the ocean. *Deep-Sea Research,* **22**, 491-502.

McCave IN (1984) Size spectra and aggregation of suspended particles in the deep ocean. *Deep Sea Research Part A. Oceanographic Research Papers,* **31**, 329-352.

Meador T, Aluwihare L, Mahaffey C (2007) Isotopic heterogeneity and cycling of organic nitrogen in the oligotrophic ocean. *Limnology and Oceanography,* **52**, 934-947.

Michaels Af, Silver Mw (1988) Primary production, sinking fluxes and the microbial food web. *Deep-Sea Research,* **35**, 473-490.

Morán XAG, Gasol JM, Arin L, Estrada M (1999) A comparison between glass fiber and membrane filters for the estimation of phytoplankton POC and DOC production. *Marine Ecology Progress Series,* **187**, 31-41.

Moran SB, Buesseler KO, Niven SEH, Bacon MP, Cochran JK, Livingston HD, Michaels AF, (1993) Regional variability in size-fractionated C/^{234}Th ratios in the upper ocean: importance of biological recycling. The Oceanography Society, Seattle, WA.

Passow U, De La Rocha CL (2006) Accumulation of mineral ballast on organic aggregates. *Global Biogeochemical Cycles,* **20**, 1-7.

Pomeroy LR(1974) The ocean's food web, a changing paradigm. *BioScience*, **24**, 499-504.

Popp BN, Laws EA, Bidigare RR, Dore JE, Hanson KL, Wakeham SG (1998) Effect of phytoplankton cell geometry on carbon isotopic fractionation. *Geochimica et Cosmochimica Acta,* **62**, 69-77.

Repeta DJ, Aluwihare LI (2006) Radiocarbon analysis of neutral sugars in high-molecular-weight dissolved organic carbon: Implications for organic carbon cycling. *Limnology and Oceanography,* **51**, 1045-1053.

Richardson TL, Jackson GA (2007) Small phytoplankton and carbon export from the surface ocean. *Science,* **315**, 838-840.

Rivkin RB, Legendre L (2001) Biogenic carbon cycling in the upper ocean: effects of microbial respiration. *Science,* **291**, 2398-2400.

Roland LA, Mccarthy MD, Peterson TD, Walker BD (2008) A large-volume microfiltration system for isolating suspended particulate organic matter: fabrication and assessment versus GFF filters in central North Pacific. *Limnology and Oceanography: Methods,* **6**, 64-80.

Rothman DH, Hayes JM, Summons RE (2003) Dynamics of the Neoproterozoic carbon cycle. *Proceedings of the National Academy of Sciences of the United States of America,* **100**, 8124-8129.

Russell NJ (1989) Adaptive modification in membranes of halotolerant and halophilic microorganisms. *Journal of Bioenergetics and Biomembranes*, **21**, 83-113.

Sáenz J, Wakeham SG, Eglinton TI, Summons R (2011) New constraints on the provenance of hopanoids in the marine geologic record: bacteriohopanepolyols in marine suboxic and anoxic environments. *Organic Geochemistry*, **42**, 1322-1351.

Sannigrahi P, Ingall ED, Benner R (2005) Cycling of dissolved and particulate organic matter at station ALOHA: Insights from 13C NMR spectroscopy coupled with elemental, isotopic and molecular analyses. *Deep Sea Research I,* **52**, 1429-1444.

Savoye N, Benitez-Nelson C, Burd Ab, Cochran Jk, Charette M, Buesseler Ko, Jackson Ga, Roy-Barman M, Schmidt S, Elskens M (2006) 234Th sorption and export models in the water column: A review. *Marine Chemistry,* **100**, 234-249.

Schouten S, Middelburg JJ, Hopmans EC, Sinninghe Damsté JS (2010) Fossilization and degradation of intact polar lipids in deep subsurface sediments: A theoretical approach. *Geochimica et Cosmochimica Acta,* **74**, 3806-3814.

Sheridan C, Lee C, Wakeham S (2002) Suspended particle organic composition and cycling in surface and midwaters of the equatorial Pacific Ocean. *Deep Sea Research I,* **49**, 1983-2008.

Sherr E, Sherr B (1988) Role of microbes in pelagic food webs: a revised concept. *Limnology and Oceanography,* **33**, 1225-1227.

Sieburth JM, Smetacek V, Lenz J (1978) Pelagic ecosystem structure: heterotrophic compartments of the plankton and their relationship to plankton size fractions. *Limnology and Oceanography*, **23**, 1256-1263.

Simon M, Welschmeyer N, Kirchman DL (1992) Bacterial production and the sinking flux of particulate organic matter in the subarctic Pacific. *Deep Sea Research,* **39**, 1997-2008.

Smith D, Simon M, Alldredge A, Azam F (1992) Intense hydrolytic enzyme activity on marine aggregates and implications for rapid particle dissolution. *Nature,* **359**, 139-142.

Sohrin R, Isaji M, Obara Y, Agostini S, Suzuki Y, Hiroe Y, Ichikawa T, Hidaka K (2011) Distribution of *Synechococcus* in the dark ocean. *Aquatic Microbial Ecology*, **64**, 1-14.

Steinberg D, Van Mooy B, Buesseler K, Boyd PW, Kobari T, Karl DM (2008) Bacterial vs. zooplankton control of sinking particle flux in the ocean's twilight zone. *Limnology and Oceanography,* **53**, 1327-1338.

Stukel MR, Landry MR (2010) Contribution of picophytoplankton to carbon export in the equatorial Pacific: A reassessment of food web flux inferences from inverse models. *Limnology and Oceanography,* **55**, 2669-2685.

Taguchi S, Laws EA (1988) On the microparticles which pass through glass fiber filter type GF/F in coastal and open waters. *Journal of Plankton Research,* **10**, 999-1008.

Tolosa I, Miquel J-C, Gasser B, Raimbault P, Goyet C, Claustre H (2008) Distribution of lipid biomarkers and carbon isotope fractionation in contrasting trophic environments of the South East Pacific. *Biogeosciences*, **5**, 949-968.

Tolosa I, Vescovali I, Leblond N, Marty J-C, De Mora S, Prieur L (2004) Distribution of pigments and fatty acid biomarkers in particulate matter from the frontal structure of the Alboran Sea (SW Mediterranean Sea). *Marine Chemistry,* **88**, 103-125.

Van Der Meer MTJ, Schouten S, Sinninghe Damsté JS (1998) The effect of the reversed tricarboxylic acid cycle on the 13C contents of bacterial lipids. *Organic Geochemistry*, **28**, 527-533.

Verdugo P (2012) Marine Microgels. *Annual Review of Marine Science*, **4**, 375-400.

Verdugo P, Alldredge A, Azam F, Kirchman D, Passow U, Santschi P (2004) The oceanic gel phase: a bridge in the DOM-POM continuum. *Marine Chemistry*, **92**, 67-85.

Volk T, Hoffert MI (1985) Ocean carbon pumps: Analysis of relative strengths and efficiencies in ocean-driven atmospheric CO_2 changes. In: Sundquist ET and Broecker WS (Eds.) *The Carbon Cycle and Atmospheric CO_2: Natural Variations Archean to Present*. American Geophysical Union: Washington, D.C., 99-110.

Waite AM, Gustafsson Ö, Lindahl O, Tiselius P (2005) Linking ecosystem dynamics and biogeochemistry: Sinking fractionation of organic carbon in a Swedish fjord. *Limnology and Oceanography*, **50**, 658-671.

Waite AM, Hill PS (2006) Flocculation and phytoplankton cell size can alter 234Th-based estimates of the vertical flux of particulate organic carbon in the sea. *Deep-Sea Research*, **100**, 366 - 375.

Waite AM, Safi KA, Hall JA, Nodder SD (2000) Mass sedimentation of picoplankton embedded in organic aggregates. *Limnology and Oceanography*, **45**, 87-97.

Wakeham SG, Lee C (1989) Organic geochemistry of particulate matter in the sea: the role of particles in oceanic sedimentary cycles. *Organic Geochemistry*, **14**, 83-96.

White DC, Davis WM, Nickels JS, King JD, Bobbie RJ (1979) Determination of the sedimentary microbial biomass by extractable lipid phosphate. *Oecologia*, **40**, 51–62.

Williams PM, Druffel ERM (1987) Radiocarbon in dissolved organic matter in the central North Pacific Ocean. *Nature*, **330**, 246-248.

Wohlers J, Engel A, Zöllner E, Breithaupt P, Jürgens K, Hoppe H-G, Sommer U, Riebesell U (2009) Changes in biogenic carbon flow in response to sea surface warming. *Proceedings of the National Academy of Sciences of the United States of America*, **106**, 7067-7072.

Wuchter C, Schouten S, Wakeham SG, Sinninghe Damsté JS (2006). Archaeal tetraether membrane lipid fluxes in the northeastern Pacific and the Arabian Sea: implications for TEX_{86} paleothermometry. *Paleoceanography*, **21**, 1-9.

Chapter 2

Carbon isotopic evidence for contribution of small particles to the biological pump

Abstract

Sixty percent of the world ocean by area is contained in oligotrophic gyres (Longhurst, 1995), the primary biomass of which is dominated by picophytoplankton, including cyanobacteria and picoeukaryotic algae (Karl et al., 2001, Morán et al., 2010). Despite their recognized importance in carbon fixation, the role of small cells and their detrital remains in the net export of particulate organic matter (POM) remains disputed (Richardson and Jackson, 2007; Stukel and Landry, 2010; Lomas and Moran, 2011; Fawcett et al., 2011). Because oligotrophic marine conditions are projected to expand under current climate trends, a better understanding of the role of small particulates in the global carbon cycle is a timely goal. Here we use the lipid profiles, radiocarbon, and stable carbon isotopic signatures of lipids from the water column of the North Pacific Subtropical Gyre (NPSG) to show that picoplankton-sized POM is chemically distinct from larger POM in the surface ocean. Remarkably, this surface picoplankton-size signature dominates the total lipid collected at mesopelagic depth, suggesting that in this location, mesopelagic OM primarily contains the exported remains of small particles. Delivery of significant picoplankton-sized material below the photic zone is consistent with prior claims that carbon export is proportional to total community production, irrespective of cell size (Richardson and Jackson, 2007). Our data imply that future changes in photic zone communities will be transmitted to the deep ocean, affecting the supply of metabolites, impacting whole ocean ecology, and connecting the surface and deep carbon cycles.

Introduction

Picoplankton are aquatic microorganisms larger than viruses but smaller than 2-3 μm in diameter (e.g., Morán et al., 2010). The size class includes numerous clades of Bacteria, Archaea, and

Eukarya and represents the full spectrum of metabolic diversity. Due to their small size, it has been believed that picoplankton cells cannot sink passively and thus may contribute negligible biomass to the pool of POM that is exported from the euphotic zone (e.g., Michaels and Silver, 1988). However, new understanding of aggregation-disaggregation dynamics (e.g., Burd and Jackson, 2009) raises the prospect that organic matter from all size classes potentially can aggregate, exchange between size classes, and sink directly. Such processes would be important additions to the known pathways for small particle export *via* fecal pellets or mesoplankton guts, because self-aggregation minimizes the co-dependence on large cells (Waite et al., 2000, Burd and Jackson, 2009).

Recent attempts to quantify the specific role of picoplankton in export have focused on autotrophs, either by tracing pigments through the water column (e.g., Lomas and Moran, 2011), or by measuring the $\delta^{15}N$ ratios of taxonomically-sorted cells to model the relative contributions of Cyanobacteria and small Eukarya (Fawcett et al., 2011). Such studies are limited in their ability to scale proportionally to total material in the smallest POM size class, because they do not simultaneously quantify the sinking heterotrophic fraction of picoplankton. These approaches also cannot detect freshly detrital components, and/or the sample collection methods exclude the potential contribution of very slowly-settling, small particles (for further discussion, see Burd et al., 2010).

Here we approach this problem by analyzing fatty acids, compounds ubiquitous in Bacteria, Eukaryotes, and their detritus. We recovered lipids from POM of ≥ 0.2 μm particle size, rather than the 0.7 μm (GF/F filter) size traditionally employed for geochemical analyses. Samples were obtained from the North Pacific Subtropical Gyre (NPSG), a location well characterized in association with the Hawaii Ocean Time-series (HOT; Karl and Lukas, 1996). From a depth of 21 m, we isolated the 0.2-0.5 μm and > 0.5 μm size classes of POM by sequential filtration of seawater; at 670 m we captured the total POM > 0.2 μm. Sampling and extraction techniques have been described previously (Ingalls et al., 2006).

Results

The profile of total fatty acids from the > 0.5 µm size class at 21 m is typical of the NPSG mixed phytoplankton community captured by GF/F filtration (Wakeham, 1995): a dominance of $C_{16:0}$, $C_{16:1}$, and C_{18}-chain lengths with 1 to 3 unsaturations (Figure 2.1a,b). The measured values of $\delta^{13}C$ also are consistent with values reported elsewhere for marine planktonic lipids of the same size class (e.g., Tolosa et al., 2004). The profile of 0.2-0.5 µm POM is markedly different: there is a prominent $C_{18:0}$ peak, slightly less $C_{16:0}$, and all other compounds are minor (Figure 2.1c,d). All saturated, even-chain-length compounds in this size class are 3-4‰ enriched in ^{13}C, not only relative to the unsaturated compounds, but also to all compounds in Figure 2.1b. The

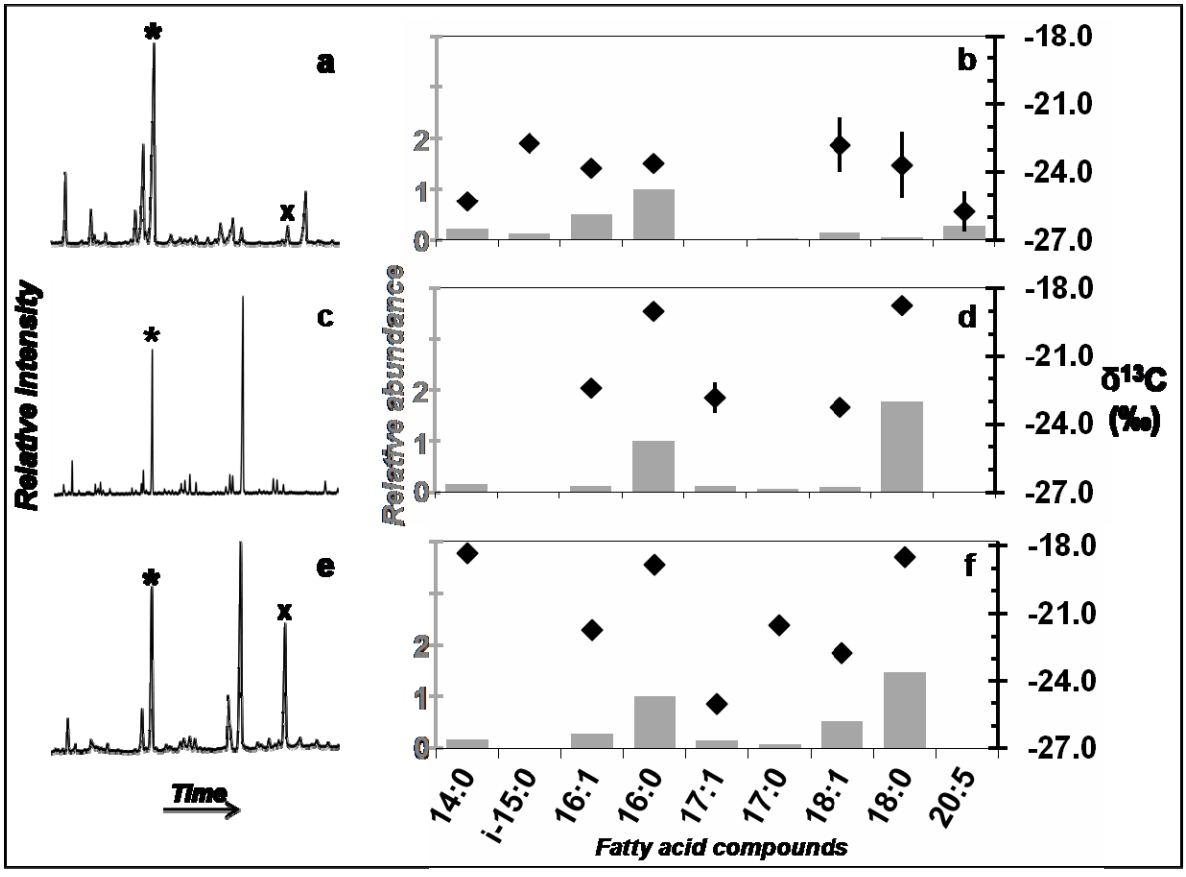

Figure 2.1. **a, c, e**: GC-FID chromatograms of fatty acids; **a**, surface > 0.5 µm; **c**, suface 0.2-0.5 µm; **e**, deep > 0.2 µm. Each peak represents an individual compound. Peaks marked with (*) are $C_{16:0}$ and those marked with (X) are an added $C_{19:0}$ internal standard **b, d, f**: Abundance of compounds in each sample, relative to $C_{16:0}$, from integrated peak areas (grey bars, left-hand axis); and $\delta^{13}C$ values for individual compounds (black points, right-hand axis); **b**, surface > 0.5 µm; **d**, suface 0.2-0.5 µm; **f**, deep > 0.2 µm.

mesopelagic sample (670 m depth; Figure 2.1e,f), which includes total POM > 0.2 μm, has a fatty acid and ^{13}C profile more similar to Figure 2.1d than to Figure 2.1b. All compounds from all samples have natural ^{14}C contents consistent with a carbon source deriving from surface waters ($\Delta^{14}C > 0‰$; Table A2.1; Chapter 2 Appendix).

Given its surface-water ^{14}C signature, the mesopelagic sample could originate solely from sinking of freshly-synthesized POM. If so, an estimate based on mixing the chromatograms of the two surface fractions gives a predicted large:small particle export ratio of 16:84 (Figure A2.1, Chapter 2 Appendix). However, the lipid profile for the deeper sample also must contain some material from the *in situ* mesopelagic community. The mixing model suggests that this *in situ* component must represent at minimum 18% of the total. Conversely, if *in situ* mesopelagic cells synthesize their lipids *de novo* from fresh POM delivered from surface waters and coincidentally generate lipid and $\delta^{13}C$ profiles that are similar to surface picoplankton, these new fatty acids would mimic a surface-derived signature. If so, it could be postulated that up to 100% of the mesopelagic sample represents *in-situ* bacterial consumers living on modern carbon (Cherrier et al., 1999).

Several other data sources are available to help estimate the magnitude of the *in-situ* fraction. Ingalls et al. (2006) used natural ^{14}C signatures to calculate that 14 ± 7% of archaeal lipids recovered at the mesopelagic depth actually derive from sinking of surface-derived material. If we assume that bacterial and archaeal remains sink proportionally, a mixing calculation (Chapter 2 Appendix) based on surface water bacterial (89%) versus archaeal (11%) cell ratios (Karner et al., 2001) can be scaled to suggest that the proportional flux of sinking bacterial lipids would contribute 31-62% of the fatty acids recovered at mesopelagic depths (Figure 2.2). This estimate is a lower bound on the total sinking flux of fatty acids, since it does not account for the additional contribution from sinking eukaryote-derived POM.

In a separate approach, we calculate the expected ^{14}C signature of *in situ* mesopelagic Bacteria and use this value to constrain their maximum contribution to mesopelagic fatty acids.

Radiocarbon measurements from DNA at this location (Hansman et al., 2009) indicate that the integrated mesopelagic community utilizes some "aged", or subsurface, carbon; however, these DNA measurements include contributions from Archaea, which are not a source of fatty acids. Using the entire error-bounded range of mesopelagic $\Delta^{14}C_{DNA}$ values reported in Hansman et al. (2009) and the cell counts mentioned above, we derive a radiocarbon signature between -191 and -37‰ for *in situ* mesopelagic Bacteria by subtracting the contribution from Archaea (Table A2.2; Supplemental Information). The result implies that up to 36% of mesopelagic fatty acids could be contributed by *in-situ* Bacteria.

In sum, we can estimate the sinking component derived from surface bacterial biomass (31-62%) and place boundaries on the *in-situ* mesopelagic bacterial component (18-36%). These calculations are largely independent – the former derives from $\Delta^{14}C$ measurements of lipids of Archaea, and the latter derives from $\Delta^{14}C$ measurements of bulk DNA and from chromatogram mixing models. If we assume that our small surface size class reflects the sinking bacterial end-

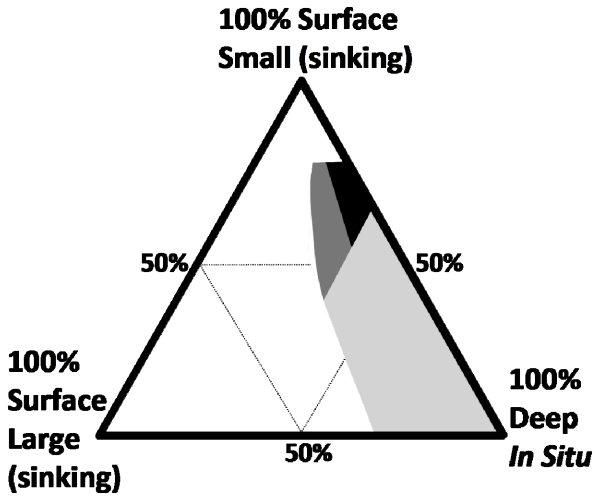

Figure 2.2. Ternary diagram showing possible origin of mesopelagic (670 m) fatty acids as a mixture of three end members. The shaded regions represent the solution spaces determined by models based on lipid profiles and compound-specific natural ^{13}C and ^{14}C content. The light gray defines the boundaries of a mixing model based on fatty acid chromatograms only. The medium gray region is constrained further by the ^{14}C content of mesopelagic DNA (Hansman et al., 2009). The black area includes a final constraint on the upper limit for the contribution from large surface particles, based on the ^{13}C content of fatty acids.

member, then combining these estimates yields the third end-member: the large-size sinking surface component, which could range from 2-51%. However, further isotope-balance calculations using $\delta^{13}C$ values of individual fatty acids show that the allowable boundaries for mixing all three end-members limit the large-size material to < 23% (Figure A2.2— Chapter 2 Appendix). Because of the large uncertainties in these calculations and their partial dependence on equating the size classes directly to cell counts, we resist assigning consensus numbers. Instead, we suggest the data are consistent with contributions to mesopelagic fatty acids from surface small particles > *in-situ* mesopelagic sources ≈ surface large particles (Figure 2.2). Notably, cell count approaches would underestimate the contribution of sinking detrital material in the small POM size class; but chromatogram mixing and isotopic mass balances both are independent of such biases, and all calculations remain consistent with the idea that small POM accounts for at least half of the total export (Figure 2.2).

Our calculations assume that sinking POM can be transmitted through the water column without its originally-associated DNA and RNA, thereby allowing a lipid sinking flux that is not detected by these other signals. This is equivalent to saying that although the sinking POM is "fresh", it is detrital. We verified this assumption using DNA community profiling by PhyloChip (DeSantis et al., 2007). Our surface samples have abundant Cyanobacteria, SAR-11, SAR-86, and other Alpha- and Gammaproteobacteria. The mesopelagic sample is rich in MG-A, Epsilon- and Gammaproteobacteria, and Oceanospiralles (Figure A2.3). Such patterns of community organization in the NPSG are well established (DeLong et al., 2006). These differences suggest that lipids from the living fraction of the mesopelagic and surface bacterial communities should be distinct, and therefore the similarity between Figures 2.1b and 2.1d reflects a common, but largely detrital, sinking source.

Discussion

Several other pieces of data from the NPSG support our conclusions. Roland et al. (2008) observe that bulk POM > 0.1 μm is ~3.5‰ enriched in ^{13}C relative to OM > 0.7 μm. Their results show that the size-based isotopic distinction we observe at the individual-compound level also is reflected in the total POM. Within the POM > 0.1 μm from 500-750 m depth, ≥ 75-80% of bacteria-specific D-amino acids and muramic acid are not associated with living bacterial cells (Kaiser and Benner, 2008; Kawasaki et al., 2011). Inverse modeling in the equatorial Pacific (Richardson and Jackson, 2007; Stukel and Landry, 2010) also indicates that significant prokaryotic biomass must be exported from the upper water column to mesopelagic depths. These findings are consistent with our hypothesis that most of the POM collected at depth is of recent detrital origin, and much of it is from Bacteria.

Power-law models of POM flux attenuation that are based on sediment trap data would predict ~90% loss of POM by 650 m depth (Lamborg et al., 2008). Our results suggest there is a 55-85% reduction in lipid concentration over this same range (Chapter 2 Appendix). Such a result matches observations by Wakeham (1995) for suspended lipids and POM > 0.7 μm. Our data thus may capture an export flux and associated lipid signature that are missing from sediment trap measurements. Estimates of POM export based on respiration (oxygen utilization) rates and nitrogen cycling (f-ratio) also indicate that sediment traps undersample a significant source of exported OM (Steinberg et al., 2008; Burd et al., 2010). Our estimate that picoplankton export contributes at least 31-62% and large particle export contributes a maximum of 23% of the total fatty acid at 670 m equates to a 1:1 to 2:1 estimate for the relative importance of small cells to this missing biochemical fraction.

It has long been recognized that a significant portion of marine POM lies within the 0.2-0.7 μm size range (e.g., Koike et al., 1990), and several studies have identified mechanisms for its unidirectional incorporation into larger particles for export: spontaneous aggregation and sinking, grazing and sinking of fecal pellets, or active transport by mesoplankton (e.g., Waite et

al., 2000; Burd and Jackson, 2009; Verdugo et al., 2004). In contrast, processes that mediate continuous and dynamic aggregation and disaggregation during sinking could transfer submicron POM to depth while subsequently rendering this material invisible to sediment trap measurements, because of the abbreviated time it would spend in association with larger particles (Cho and Azam, 1988; Arístegui et al., 2009).

Our evidence supports such an actively dynamic view, and we re-assert that a size-continuum model of total organic matter is likely the most accurate way to conceptualize export (e.g., Verdugo et al., 2004). However, many broad-reaching carbon cycle studies continue to define dissolved and particulate organic matter (DOM and POM) as *mechanistically* discrete pools. Furthermore, such studies operationally define the DOM/POM distinction with varying filter size cutoffs (0.1, 0.2, 0.45, 0.7, 0.8, or 1 μm) or limit export calculations to sediment trap data, for which no direct small-size cutoff is applicable. Importantly, this operational DOM-POM "grey area" (or "no man's land"; Fuhrman, 1992) universally includes the major portion of planktonic Bacteria and Archaea (Koike et al., 1990). Our measurements specifically suggest that picoplankton-sized OM is exported in the NPSG and thus should not be grouped functionally with true DOM. Care should be taken to include a wider size range of POM in sampling efforts, particularly where quantitative fluxes or mechanistic interpretations will be attributed.

Our results support suggestions that organic matter of picoplanktonic origin should be incorporated into global carbon flux models (Richardson and Jackson, 2007; Stukel and Landry, 2010; Lomas and Moran, 2011). While it remains unknown what fraction of this POM also survives to contribute to sedimentary flux, it is likely an important source of carbon for mesopelagic metabolisms (e.g., Cho and Azam, 1988; Arístegui et al., 2009). With picoplankton-dominated ecosystems projected to expand in a warming climate (Karl et al., 2001; Morán et al., 2010), it will be vital to refine our understanding of the dynamics of small-size POM in the water column.

Acknowledgments

Sampling and analysis for this data set required enormous amounts of effort by my coauthors on this manuscript, including Sunita Shah, Anitra Ingalls, Aaron Diefendorf, Eoin Brodie, Katherine Freeman, Lihini Aluwihare, Roberta Hansman, and Ann Pearson. We thank Tom Daniel, Barbara Lee, Jan War, and the staff of the Natural Energy Laboratory of Hawaii Authority for access to the sampling facility; Susan Carter for laboratory assistance; Sheila Griffin for assistance with AMS preparation and analysis; Li Xu for assistance with PCGC; and John Southon, Tom Guilderson, Ann McNichol, and all of the staff members of the Keck Carbon Cycle AMS facility at the University of California, Irvine, Lawrence Livermore National Laboratories, and National Ocean Sciences Accelerator Mass Spectrometry accelerator facilities. This work was supported by National Science Foundation Grants OCE-0241363 and OCE-0927290 (to A.P.), and by an ExxonMobil Geoscience Grant (to H.G.C.).

References

Arístegui J, Gasol JM, Duarte CM, Herndl G (2009) Microbial oceanography of the dark ocean's pelagic realm. *Limnology and Oceanography,* **54**, 1501-1529.

Burd AB, Hansell DA, Steinberg DK, Anderson TR, Arístegui J, Baltar F, Beaupré SR, Buesseler KO, Dehairs F, Jackson GA, Kadko DC, Koppelman R, Lampitt RS, Nagata T, Reinthaler T, Robinson C, Robison BH, Tamburini C, Tanaka T (2010) Assessing the apparent imbalance between geochemical and biochemical indicators of meso- and bathypelagic biological activity: What the @$#! is wrong with present calculations of carbon budgets? *Deep Sea Research Part II: Topical Studies in Oceanography,* **57**, 1557-1571.

Burd AB, Jackson GA (2009) Particle Aggregation. *Annual Review of Marine Science,* **1**, 65-90.

Cherrier J, Bauer JE, Druffel ERM, Coffin RB, Chanton JP (1999) Radiocarbon in marine bacteria: Evidence for the ages of assimilated carbon. *Limnology and Oceanography,* **44**, 730-736.

Cho B, Azam F (1988) Major role of bacteria in biogeochemical fluxes in the ocean's interior. *Nature,* **332**, 441-443.

DeLong EF, Preston CM, Mincer T, Rich V, Hallam SJ, Frigaard N-U, Martinez A, Sullivan MB, Edwards R, Brito BR, Chisholm SW, Karl DM (2006) Community genomics among stratified microbial assemblages in the ocean's interior. *Science,* **311**, 496-503.

DeSantis TZ, Brodie EL, Moberg JP, Zubieta IX, Piceno YM, Andersen GL (2007) High-density universal 16S rRNA microarray analysis reveals broader diversity than typical clone library when sampling the environment. *Microbial Ecology,* **53**, 371-383.

Fawcett SE, Lomas MW, Casey JR, Ward BB, Sigman DM (2011) Assimilation of upwelled nitrate by small eukaryotes in the Sargasso Sea. *Nature Geoscience,* **4**, 1-6.

Fuhrman J (1992) Bacterioplankton roles in cycling of organic matter: the microbial food web. *Primary Productivity and Biogeochemical Cycles in the Sea*.

Hansman RL, Griffin S, Watson JT, Druffel ERM, Ingalls AE, Pearson A, Aluwihare LI (2009) The radiocarbon signature of microorganisms in the mesopelagic ocean. *Proceedings of the National Academy of Sciences of the United States of America,* **106**, 6513-6518.

Ingalls AE, Shah SR, Hansman RL, Aluwihare LI, Santos GM, Druffel ERM, Pearson A (2006) Quantifying archaeal community autotrophy in the mesopelagic ocean using natural radiocarbon. *Proceedings of the National Academy of Sciences of the United States of America,* **103**, 6442-6447.

Kaiser K, Benner R (2008) Major bacterial contribution to the ocean reservoir of detrital organic carbon and nitrogen. *Science,* **53**, 99-112.

Karl D, Bidigare R, Letelier R (2001) Long-term changes in plankton community structure and productivity in the North Pacific Subtropical Gyre: the domain shift hypothesis. *Deep Sea Research Part II: Topical Studies in Oceanography,* **48**, 1449-1470.

Karl D, Lukas R (1996) The Hawaii Ocean Time-series (HOT) program: Background, rationale and field implementation. *Deep Sea Research Part II: Topical Studies in Oceanography,* **43**, 129-156.

Karner MB, Delong EF, Karl DM (2001) Archaeal dominance in the mesopelagic zone of the Pacific Ocean. *Nature,* **409**, 507-510.

Kawasaki N, Sohrin R, Ogawa H, Nagata T, Benner R (2011) Bacterial carbon content and the living and detrital bacterial contributions to suspended particulate organic carbon in the North Pacific Ocean. *Aquatic Microbial Ecology,* **62**, 165-176.

Koike, I., Shigemitsu, H., Kazuki, T. & Kazuhiro, K. Role of sub-micrometre particles in the ocean. *Nature*, **345**, 242-244 (1990).

Lamborg C, Buesseler K, Valdes J, Bertrand C, Bidigare R, Manganini S, Pike S, Steinberg D, Trull T, Wilson S (2008) The flux of bio- and lithogenic material associated with sinking particles in the mesopelagic "twilight zone" of the northwest and North Central Pacific Ocean. *Deep Sea Research Part II: Topical Studies in Oceanography,* **55**, 1540-1563.

Lomas MW, Moran SB (2011) Evidence for aggregation and export of cyanobacteria and nano-eukaryotes from the Sargasso Sea euphotic zone. *Biogeosciences,* **8**, 203-216.

Longhurst A (1995) Seasonal cycles of pelagic production and consumption. *Progress in Oceanography,* **36**, 77-167.

Michaels AF, Silver MW (1988) Primary production, sinking fluxes and the microbial food web. *Deep-Sea Research,* **35**, 473-490.

Morán XAG, López-Urrutia Á, Calvo-Díaz A, Li WKW (2010) Increasing importance of small phytoplankton in a warmer ocean. *Global Change Biology,* **16**, 1137-1144.

Richardson TL, Jackson GA (2007) Small phytoplankton and carbon export from the surface ocean. Supporting online material. *Science (New York, N.Y.),* **315**, 838-840.

Roland LA, Mccarthy MD, Peterson TD, Walker BD (2008) A large-volume microfiltration system for isolating suspended particulate organic matter: fabrication and assessment versus GFF filters in central North Pacific. *Limnology and Oceanography: Methods,* **6**, 64-80.

Steinberg DK, van Mooy BAS, Buesseler KO, Hole W, Boyd PW, Karl DM (2008) Bacterial vs . zooplankton control of sinking particle flux in the ocean ' s twilight zone. *Methods,* **53**, 1327-

1338.

Stukel MR, Landry MR (2010) Contribution of picophytoplankton to carbon export in the equatorial Pacific : A reassessment of food web flux inferences from inverse models. *Limnology,* **55**, 2669-2685.

Tolosa I, Vescovali I, Leblond N, Marty J-C, De Mora S, Prieur L (2004) Distribution of pigments and fatty acid biomarkers in particulate matter from the frontal structure of the Alboran Sea (SW Mediterranean Sea). *Marine Chemistry,* **88**, 103-125.

Verdugo P, Alldredge A, Azam F, Kirchman D, Passow U, Santschi P (2004) The oceanic gel phase: a bridge in the DOM?POM continuum. *Marine Chemistry,* **92**, 67-85.

Waite AM, Safi KA, Hall JA, Nodder SD (2000) Mass sedimentation of picoplankton embedded in organic aggregates. *Limnology and Oceanography,* **45**, 87-97.

Wakeham S (1995) Lipid biomarkers for heterotrophic alteration of suspended particulate organic matter in oxygenated and anoxic water columns of the ocean. *Deep Sea Research Part I: Oceanographic Research,* **42**, 1749-1771.

Appendix, Chapter 2

Calculations and data tables

Determining the maximum sinking contribution from fatty acid (FA) profiles only:

We derive the best-fit mixing ratio of surface large (G) and small (S) FA profiles to generate a mixture (M) that mimics the mesopelagic, or deep (D) profile. All possible mixing ratios between chromatograms were calculated (0-100% of each endmember, stepping by 0.2%). The relative abundance of each compound in mixture M was calculated as:

$$X_{M,i} = f_S X_{S,i} + (1-f_S) X_{G,i}$$

Where

i = individual fatty acid compound

X = mole fraction of compound "i" in the measured sample (S, small or G, large; Table A2.1) or modeled mixture (M). (Mole fraction is defined as the mass of an individual compound – determined by FID peak area – divided by the summed masses of all compounds in the profile that are considered in this model.)

f_S = proportion of total FA from source S in sinking mixture

The difference between the model mixture and the actual deep profile was calculated for each compound. The best fit model ratio is the one that simultaneously resulted in the smallest mean absolute-value difference across all compounds and the smallest standard deviation in the absolute-value difference across all compounds. This mixture (Figure A2.1a) generally reproduces the observed compound ratios for the deep sample, although with some differences (Figure A2.1b).

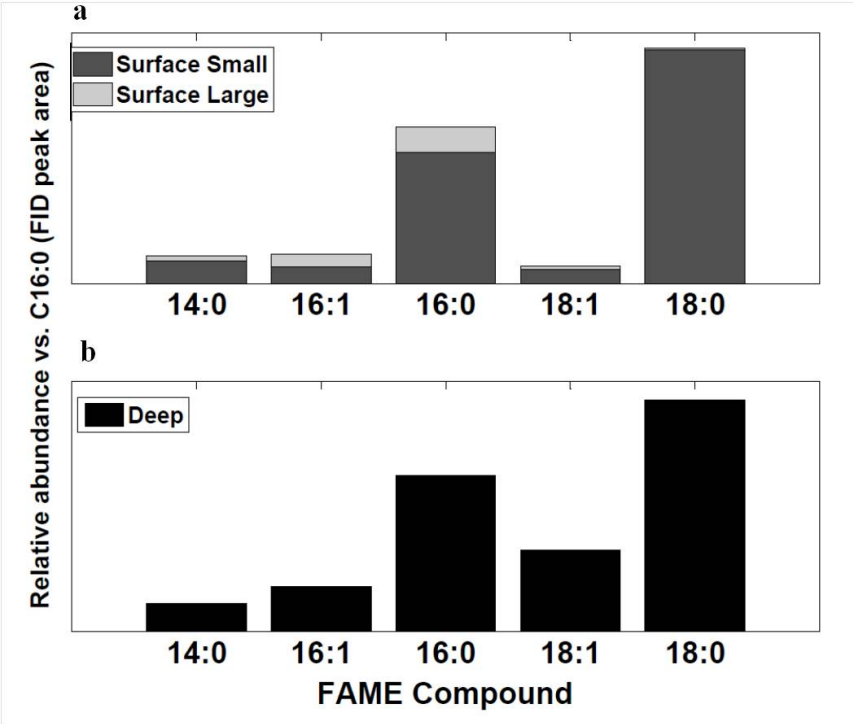

Figure A2.1. **(a)** Derived profile of hypothetical sinking material that is 84% surface small (0.2-0.5 μm) and 16% surface large (> 0.5 μm). **(b)** Fatty acid profile of actual mesopelagic OM.

Using this best-fit model sinking profile (f_S = 0.84, f_G = 1-f_S = 0.16), we then calculated the minimum proportion of the deep profile that must remain unaccounted for by sinking FA, *i.e.*, we computed the residuals. We thus derived the minimum proportion of FA that must be produced *in situ* at depth by calculating the maximum proportion that could derive from the sinking mixture (maximum f_M) while satisfying conservation of mass. To do this, we specify that in total, each deep (D) compound *i* is composed of fractional contributions f_M from the sinking mixture (M) above and 1-f_M from the *in situ* component (I):

$$X_{D,i} = f_M X_{M,i} + (1-f_M) X_{I,i} .$$

To achieve conservation of mass, no solution can be permitted that would allow $(1-f_M)X_{I,i} < 0$. Therefore, f_M is maximized at the highest value for which $(1-f_M)X_{I,i} \geq 0$ for all compounds *i*. (This can be calculated as the minimum among all *i* of $X_{D,i}/X_{M,i}$.)

We find that the deep profile contains, at minimum, 18% of its total peak area that cannot be accounted for by the best-fit sinking model (*i.e.*, minimum f_I=0.18, maximum f_M=0.82). If the contribution from f_I is 18%, then f_G*f_M is 13% (=0.16*0.82) and f_S*f_M is 69% (=0.84*0.82). The correct magnitude of f_I therefore is critical to determine.

Since the distribution of compounds in I is unconstrained, a wide range of values for f_G and f_S can contribute to f_M when we consider larger values for f_I. However, the conservation of mass condition limits the absolute largest contribution of f_M for a given f_S and f_G. Over all allowable values of f_M, the maximum contribution to the total from G (i.e., maximum f_G*f_M) is ~31% and from S, 76%. The present calculations are based only on profile mixing; some further constraints can be imposed using $\delta^{13}C$ data (see below).

The proportionally largest *in-situ* signal (largest individual contributor, *i*, to I) is contributed by $C_{18:1}$. Examining the mass spectrum for $C_{18:1}$ in all samples reveals that the deep sample contains a large peak in a $C_{18:1}$ isomer that is a very minor contributor to both surface

samples. This $C_{18:1}$ isomer is thus the largest unique contributor to – and thus the likeliest representation of – the *in situ* contribution.

Deriving further constraints on S + G = M and M + I = D using compound-specific $\delta^{13}C$ data:

Large variation in measured $\delta^{13}C$ values amongst individual compounds – both within and between samples – provides an additional means to evaluate permissible mixing ratios. Following Lichtfouse and Eglinton (1995), we construct a mass-balance model based on the relative proportion of individual fatty acid compounds within a given sample, along with their $\delta^{13}C$ values. We first model the relative fatty acid profile and $\delta^{13}C$ values of hypothetical sinking OM as a mixture (M) of the measured small (S) and large (G) size class, as above. We calculate the projected $\delta^{13}C$ values ($\delta_{M,i}$) across the entire range of possible mixtures (f_S = 0-100% small size class) using data from Table A2.1, according to:

$$X_{M,i} = f_S X_{S,i} + (1-f_S) X_{G,i}$$

as above, and

$$\delta_{M,i} = [f_S X_{S,i} \delta_{S,i} + (1-f_S) X_{G,i} \delta_{G,i}] / [f_S X_{S,i} + (1-f_S) X_{G,i}] .$$

Where

i = individual fatty acid compound

X = mole fraction of fatty acid "i" in the measured sample (S or G) or modeled mixture (M)

f_S = proportion of total fatty acid from source S in sinking mixture

$\delta = \delta^{13}C$ value of fatty acid "i" in sample or modeled mixture

Table A2.1. Data for NPSG fatty acids: Relative abundance, $\delta^{13}C$, $\Delta^{14}C$ (raw and corrected), and AMS measurement information.

DEEP (>0.2 µm)

FAME	rel abun	$\delta^{13}C$	± σ	$\Delta^{14}C_{raw}$	± σ	$\Delta^{14}C_{corr}$	± σ	notes	size (µgC)	AMS ID #
14:0	0.18	-18.3	0.2	-467	14	114	76	a,b,c	24	OS-49294
***i+a*-15:0**	--	--	--			--	--			
16:1	0.29	-21.7	0.2	-264	12	66	47	a,b,d	36	OS-67905
replicate				*-295*	*4*	*399*	*77*	*a,b,c*	*12*	*(Irvine)*
16:0	1.00	-18.8	0.2	-119	8	49	12	a,b,c	103	OS-49279
split				-106	8	65	13	a,b,c	34	CAMS 114840
17:1	0.15	-25.0	0.2			--	--			
17:0	0.09	-21.5	0.2	-496	13	57	74	a,b,c	23	OS-49295
18:1	0.52	-22.7	0.2	-208	11	72	25	a,b,c	50	OS-49286
replicate				-148	13	43	24	a,b,d	70	OS-66625
18:0	1.48	-18.5	0.2	-35	8	99	10	a,b,c	153	OS-49272
split				-49	7	82	9	a,b,c	58	CAMS 114841
replicate				-45	9	60	11	a,b,d	138	OS-66614
20:5	--	--	--	--	--	--	--			--
22:0	--	--	--	--	--	--	--			--
19:0 std	--	--	--	--	--	--	--			--

		$\delta^{13}C$	± σ	$\Delta^{14}C_{raw}$	± σ	$\Delta^{14}C_{corr}$	± σ	notes	size (µgC)	AMS ID #
19:0 std, pure	--	-31.7	0.1	71	4	71	4	a	242	OS-67848

SURFACE 0.2 (0.2-0.5 µm)

FAME	rel abun	$\delta^{13}C$	± σ	$\Delta^{14}C_{raw}$	± σ	$\Delta^{14}C_{corr}$	± σ	notes	size (µgC)	AMS ID #
14:0	*0.17*	*--*	*--*	*-392*	*17*	*-201*	*261*	*a,b,e*	*7*	*(Irvine)*
***i+a*-15:0**	--	--	--	--	--	--	--		--	--
16:1	0.13	-22.4	0.2	--	--	--	--		--	--
replicate										
16:0	1.00	-19.0	0.2	-76	9	86	28	a,b,e	17	(Irvine)
split										
17:1	0.12	-22.8	0.7	--	--	--	--		--	--
17:0	0.07	--	--	-246	13	86	112	a,b,e	7	(Irvine)
18:1	0.11	-23.3	0.3	-226	13	-2	58	a,b,e	9	(Irvine)
replicate										
18:0	1.78	-18.8	0.2	--	--	--	--		--	--
split										
replicate										
20:5	--	--	--	--	--	--	--		--	--
22:0	--	--	--	--	--	--	--		--	--
19:0 std	--	--	--	--	--	--	--		--	--

SURFACE 0.5 (>0.5 µm)

FAME	rel abun	$\delta^{13}C$	± σ	$\Delta^{14}C_{raw}$	± σ	$\Delta^{14}C_{corr}$	± σ	notes	size (µgC)	AMS ID #
14:0	0.22	-25.3	0.2	--	--	--	--		--	--
***i+a*-15:0**	0.13	-22.7	0.3	-33	8	48	14	a,b,f	105	OS-66618
16:1	0.51	-23.8	0.1	--	--	--	--		--	--
replicate										
16:0	1.00	-23.6	0.2	-14	4	51	5	a,b,f	296	OS-65816
split										
17:1	--	--	--	--	--	--	--		--	--
17:0	0.03	--	--	--	--	--	--		--	--
18:1	0.14	-23.5	0.8	-13	7	52	10	a,b,f	163	OS-66611
replicate		-22.0	1.2							
18:0	0.05	-23.7	1.5	7	12	93	23	a,b,f	60	OS-67899
split										
replicate										
20:5	0.27	-25.7	0.9	--	--	--	--		--	--
22:0	*0.03*	*--*	*--*	*-278*	*14*	*-225*	*24*	*a,b,f*	*46*	*OS-67906*
19:0 std	0.07	-31.7	0.1	-4	11	71	19	a,b,f	78	OS-66626

Notes: Corrections Applied
a- Combustion blank (1.0 µg C)
b- Methyl carbon
c- Residual correction, batch 1 (16.6 µg C)
d- Residual correction, batch 2 (9.8 µg C)
e- Residual correction, batch 3 (1.4 µg C)
f- Internal standard correction, batch 4 (1.7 µg C)

We then consider each iteration of this hypothetical mixed sinking material (M) as a contributor to the measured total deep (D) sample. The other endmember contributing to the total deep sample is the *in situ* mesopelagic community (I).

$$X_{D,i} = f_M X_{M,i} + (1-f_M) X_{I,i} \; ; \; (1-f_M) X_{I,i} \geq 0$$

$$\delta_{D,i} = [f_M X_{M,i} \delta_{M,i} + (1-f_M) X_{I,i} \delta_{Ii}] / X_{D,i}$$

Rearranging, we solve for the proportion and $\delta^{13}C$ value of each fatty acid from the *in situ* community ($X_{I,i}$ and $\delta_{I,i}$, respectively) across the allowable range of M and the full range of S and G (Figure A2.2). The range of allowable solutions for each *in situ* component ($X_{I,i}$ $\delta_{I,i}$) is that which achieves isotopic mass-balance with the deep sample ($X_{D,i}$, $\delta_{D,i}$) within the measurement errors. These ranges are shown outlined in Figure A2.2. The conservation of mass condition limits the absolute largest contribution of f_M for a given f_S and f_G; this limitation is delineated in Figure A2.2 by the boundary between shaded areas and white (non-solution) areas. We have thus calculated $\delta_{I,i}$ for a range of sinking material from 0% to the maximum percentage allowable by profile mixing (satisfying $(1-f_M)X_{I,i} \geq 0$); and within this constraint on f_M, for a range of composition in sinking material from 0% to 100% small (f_S) surface material. In all cases, we further constrain values of $\delta_{I,i}$ to a maximum value of -16‰, or no more than 2.5‰ more positive than the highest measured value of δ, based on the argument of limited trophic-level enrichment of ^{13}C in bacterial heterotrophy (Blair et al., 1985; DeNiro and Epstein, 1978); this further limits the allowable results to only those values that fall below the thick black lines in Figures A2.2a and A2.2b. Since we thus place a constraint on the maximum allowable value for individual *in situ* compounds, we consider the most conservative (minimum) value achieved by calculating over the error ranges for all measured values. The maximum contribution from the large size class to the total is further limited to 23% under this constraint, and down to ~10%

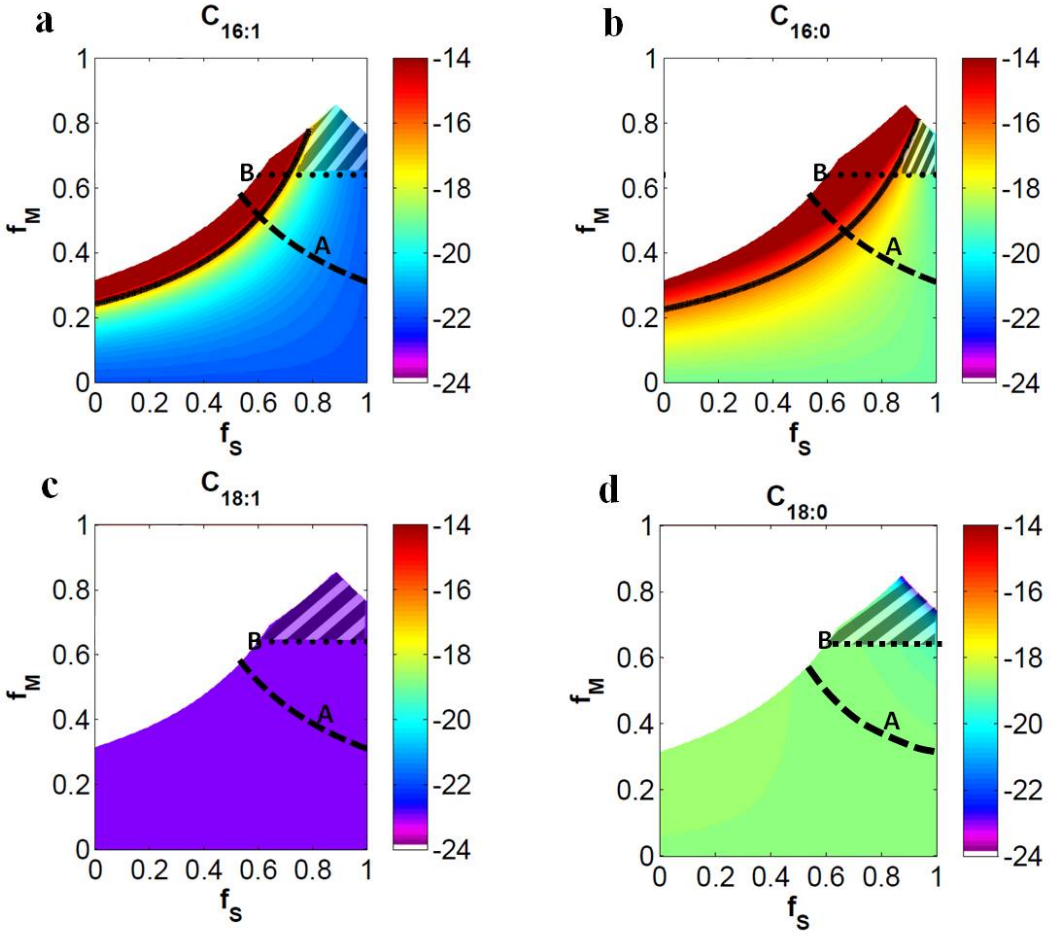

Figure A2.2. Modeled $\delta^{13}C$ values of four individual fatty acids from the *in situ* mesopelagic bacterial community (a, $C_{16:1}$; b, $C_{16:0}$; c, $C_{18:1}$, d, $C_{18:0}$), calculated over all f_S (proportion sinking from S; where S+G=M) compositions contributing to M (total sinking; x-axis) and all allowed f_M (proportion sinking; M+I=D) contributing to D (y-axis; see text for definition of allowed). We stipulate that the upper limit for modeled $\delta^{13}C$ values in the *in situ* population is -16‰, implying that results above the contour outlined in solid black (panels **a**, **b**) are excluded. Additional constraints on S:G ratios and M:I ratios imposed by ancillary data further constrain the estimated results to the striped areas (all panels). Line B is defined in Section 4 of the SI text as the minimum fraction of the total deep sample (D) that must come from the sinking flux (M). Isotopic mass-balance must be reached for all compounds simultaneously; the narrowest solution field (striped area in b) is thus the best constrained.

when this constraint must be met simultaneously with the $^{14}C_{DNA}$-defined lower limit on sinking contribution (calculation 4, below).

Importantly, solving the model in this way does not require that we aim to converge on a single and uniform $\delta^{13}C$ value for the entire *in situ* mesopelagic community, since isotopic heterogeneity among lipids from living communities is observed elsewhere (*e.g.*, the surface sample here). Instead, the model allows each calculated value of $\delta_{D,i}$ to converge on the measured value of $\delta_{D,i}$; and from the four different compounds modeled (Figure A2.2), we derive the boundaries for allowable fractional contributions S, G, and I.

Predicting sinking bacterial lipids by comparison to sinking archaeal lipids:

Ingalls et al. calculate that 14 ± 7% of archaeal lipids measured at 670 m are from sinking surface biomass. Average live archaeal cell counts at 500 m depth (the closest measured depth to our sample) in the NPSG are 2.26×10^4 cells/mL (Karner et al., 2001; Table A2.2). Presuming that all archaeal cells have the same lipid content, and that the sinking cells mainly are dead (*i.e.*, their RNA is sufficiently degraded that they would not be counted by the FISH methods of Karner et al., 2001), the additional sinking component contributes its lipids without being counted as part of the *in-situ* population[1]. Therefore the *in-situ* population by FISH (2.26×10^4 cells/mL) is equivalent to only 86 ± 7%, or 79% to 93%, of the total archaeal lipids. By this reasoning, the number of "cell equivalents" of total archaeal lipids is 2.43×10^4 to 2.86×10^4 cells/mL, meaning the sinking lipid contribution is equivalent to adding lipid from 1700-6000 cells/mL of sinking Archaea to the mesopelagic waters. Using cell counts, this can be translated into an estimate for the addition of surface-derived bacterial lipid. There are 3.78×10^4 archaeal cells/mL in surface waters (Karner et al., 2001), so the sinking proportion that reaches 670 m

[1] This is a reasonable assumption given numerous studies that show strain-level heterogeneity in archaeal and bacterial populations as a function of depth in the water column (e.g., DeLong et al., 2006). If sinking cellular material promiscuously carried DNA and RNA to depth, it would mask these patterns.

Table A2.2. Ancillary data used for NPSG model calculations. H= Hansman et al. (2009); I= Ingalls et al. (2006); C= Close et al. (2012)—this paper; K-supp= Karner et al. (2001), supplementary materials. All $\Delta^{14}C$ values are per mil (‰).

	Mean	± σ	*Reference*
Surface DIC $\Delta^{14}C$	71	3	I
Deep DIC $\Delta^{14}C$	-151	3	I
Surface DNA			
0.2-0.5 µm $\Delta^{14}C$	60	3	H
670 m DNA			
0.2-0.5 µm $\Delta^{14}C$	-140	17	H
>0.5 µm $\Delta^{14}C$	-73	4	H
670 m Archaeal lipid			
Average *in situ* $\Delta^{14}C$, calculated	-112	28	I
Fraction from sinking	0.14	0.07	I
Fatty acids (16:1, 16:0, 18:1, 18:0)			
20 m FA, small			
mass-weighted $\Delta^{14}C$	78	66	C
20 m FA, large			
mass-weighted $\Delta^{14}C$	52	13	C
670 m FA			
mass-weighted $\Delta^{14}C$	68	34	C
25 m cell counts			
Archaea cell/mL	3.78E+04	3.88E+04	K-supp
Bacteria cell/mL	3.07E+05	1.03E+05	K-supp
Arch+Bac cell/mL	3.45E+05		
Fraction Bacterial	0.89	0.11	
500 m cell counts			
Archaea cell/mL	2.26E+04	9.04E+03	K-supp
Bacteria cell/mL	3.01E+04	1.03E+04	K-supp
Arch+bac cell/mL	5.27E+04		
Fraction Bacterial	0.57	0.12	

represents 4.5% to 15.9% of their original concentration in the surface. Assuming that surface ocean bacterial cells and archaeal cells are similar sizes and thus could be predicted to be incorporated into sinking flux in similar proportions, we would expect that the equivalent would be true for Bacteria: 4.5% – 15.9% of the surface ocean concentration of bacteria also would reach mesopelagic depth. Bacteria average 3.07×10^5 cells/mL in surface waters, so lipids from 1.38×10^4 to 4.88×10^4 cells/mL would be expected to reach mesopelagic depths. Bacterial cells at 500 m number 3.01×10^4 cells/mL on average. Addition of lipids from the sinking bacterial component would therefore contribute 31 – 62% of the lipids at depth. This estimate does not account for the additional contribution from sinking eukaryotic biomass. As such, it represents a lower bound on the predicted sinking flux, and the total surface contribution must be higher. The lower bound of this range is defined as line A on Figure A2.2.

Predicting the fraction of mesopelagic fatty acids derived from *in situ* Bacteria using ^{14}C budgets:

Total DNA collected from suspended OM at mesopelagic depths should reflect the combined *in situ* bacterial and archaeal contribution, assuming that eukaryotic cells contribute insignificant DNA at 670 m. Hansman et al. (2009) report $\Delta^{14}C$ values for DNA from two size classes of total OM (0.2-0.5 μm and > 0.5 μm); Table A2.2. Because our sample integrates the total of all OM > 0.2 μm, we constrain the mass balance broadly, to cover the entire range of values reported by Hansman et al. (2009), including error (-157 to -69‰). Ingalls et al. (2006) measured ^{14}C content in archaeal lipids, and by mass-weighted calculation derived an average $\Delta^{14}C$ value of -112‰ for mesopelagic Archaea living *in situ*. If *in situ* mesopelagic Archaea and Bacteria are the only two endmembers contributing to the DNA signature, and mesopelagic bacteria represent 57 ± 12% of the total population at these depths (Karner et al., 2001), then by isotopic mass balance, the *in situ* bacterial $\Delta^{14}C$ value could be between -191 and -37‰.

Similar to Ingalls et al. (2006), we can then calculate a mass-weighted $\Delta^{14}C$ value for fatty acids measured at 670 m. Relative proportions of fatty acids are derived from GC-FID peak areas and indicate that the total mesopelagic FA pool has a mass-weighted $\Delta^{14}C$ value of 68±34‰ (Table A2.1). Assuming that biomass sinking from the surface is the only external contributor to this pool, it would carry the $\Delta^{14}C$ value of surface DIC (71±3‰; Ingalls et al., 2006). Some of our surface $\Delta^{14}C$ values from FA are lower than 71‰; however, the error ranges are large, and choosing a more positive endmember yields the most conservative outcome (i.e., more *in situ* contribution). Creating an isotope mass balance between sinking material and the total sample automatically poses a problem: on average, the mesopelagic lipids are isotopically indistinguishable from the surface. However, since the optimized mixing of FA profiles (above) suggests that at least 18% of FA must derive from the *in situ* mesopelagic component, we can examine if the large error ranges in the ^{14}C data would permit an 18% or greater contribution. The answer is yes: the maximum allowed is 36% based on data in Table A2.2:

$$\Delta^{14}C_{Mesopelagic\_FA\_min} = (0.36)(\Delta^{14}C_{Mesopelagic\_Bacteria\_max}) + (0.64)(\Delta^{14}C_{Surface\_Biomass\_max})$$

Solving: $(68\text{-}34‰) = 34‰ = (0.36)(-37‰) + (0.64)(71+3‰)$

If the *in situ* component contributes 0-36% of total fatty acids collected at the mesopelagic depth, sinking material contributes 64-100%. The lower bound of this range is defined as line B on Figure A2.2. Notably, this sinking component could derive from both bacterial and eukaryotic surface biomass, so it is not inconsistent with the estimate for sinking bacterial contribution calculated above. The boundary regions defined by line B in Figure A2.2 suggest that if the sinking fraction M is defined by line B, it must consist mostly of material from the small particle size class.

The ^{14}C signature for $C_{18:1}$ FA remains problematic. As stated above, $C_{18:1}$ is likeliest to have a large contribution from the *in situ* community, and yet its $\Delta^{14}C$ value is modern. It

therefore seems that the total *in situ* mesopelagic bacterial $\Delta^{14}C$ value calculated above from DNA measurements could be too negative; either the cell count estimates underrepresent Archaea (Karner et al., 2001), or the absolute values reported for $\Delta^{14}C_{DNA}$ are too low (Hansman et al., 2009). Either a greater contribution from modern DNA or greater numbers of Archaea is needed to reconcile all forms of data. Alternately, our mass-weighted total mesopelagic fatty acid $\Delta^{14}C$ value could be too positive. Minor compounds that could not be resolved for ^{14}C measurement, particularly those commonly attributed to bacteria (*e.g.*, branched and odd-chain fatty acids), potentially could represent the more ^{14}C-depleted component of the *in situ* bacterial community but are not counted here.

Regardless of the explanation, however, all estimates point to sinking, modern material being the dominant source of lipids to mesopelagic depths (M ≥ 64% of the total D). If the sinking, small fraction (S) also is 31-62% of D (Section 3), it follows that between half and all of M derives from S. This is consistent with the modeled striped boundary regions shown in Figure A2.2, yielding reasonable values of *in-situ* $\delta_{I,i}$ for all modeled components of the *in-situ* community. Finally, by mass balance, the large surface contribution ($f_G = 1\text{-}f_S$) is limited to ~0-16% of the sinking fatty acids (or 0-10% of the total mesopelagic sample). To invoke contributions greater than 16% from the large size class would require that lipid $\delta^{13}C$ values be > -16‰ for the members of the *in situ* mesopelagic community that produce $C_{16:0}$ and $C_{16:1}$ FA; this is needed to achieve isotope balance (Figure A2.2) and seems unreasonable. The most ^{13}C-enriched FA we measure anywhere in the system has a $\delta^{13}C$ value of -18.5‰.

Authenticity of environmental signature:

The dissimilarity in bacterial phylogenetic profiles between the surface small sample and the mesopelagic sample lead us to conclude that we did not inadvertently incubate an enrichment culture of heterotrophs on the filters during sampling (Figure A2.3). The samples were examined by PhyloChip hybridization of DNA amplicons of 16S ribosomal RNA genes.

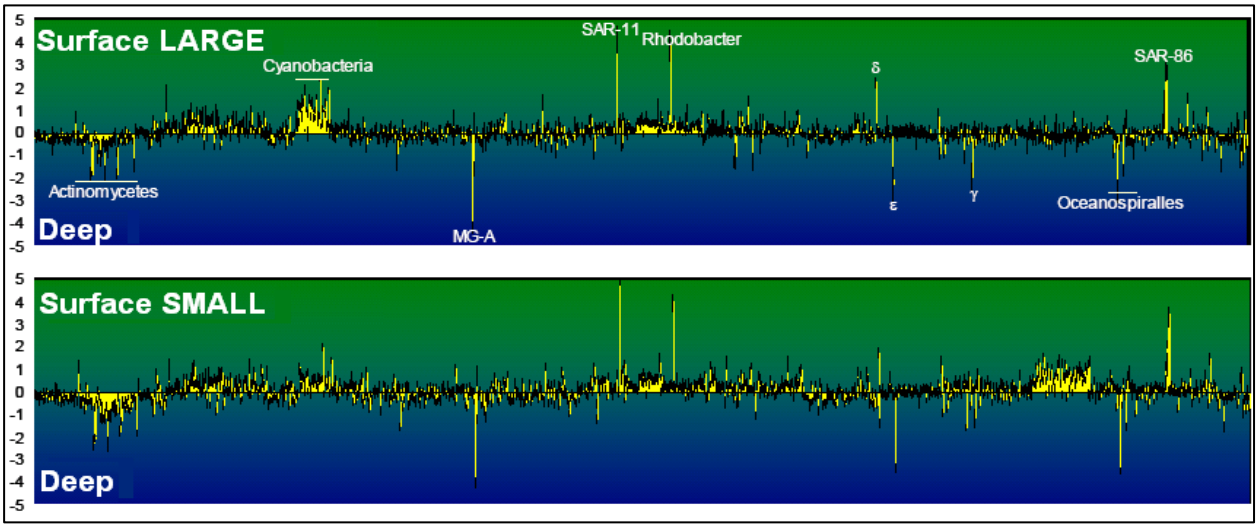

Figure A2.3. Comparison of results for PhyloChip analysis of DNA. Plots are difference spectra, calculated for each OTU (x-axis) on a logarithmic scale of hybridization intensity (y-axis). The data show that similar communities of Bacteria were retained on both the surface (21 m) large size class (> 0.5 µm) and small size class (0.2-0.5 µm) filters; but when each is compared to the deep (670 m) filter, significant differences are detected across OTUs consistent with expected surface and pelagic populations. Yellow peaks represent differences that are significant beyond the error range of the hybridization signal; black peaks are within error ranges and thus insignificantly different for the abundance of the OTU.

PhyloChip is a microarray chip that is capable of detecting >10,000 operational taxonomic units (OTUs); amplification and hybridization protocols, including signal calibrations against known concentration standards were as defined in Brodie et al. (2006) and DeSantis et al. (2007). The similarity between fatty acids in surface and mesopelagic samples is thus an authentic environmental signature.

Sequential filtering technique and relation to size classes

We have simplified our interpretation of collected size classes by equating the "picoplanktonic" fraction to "Bacteria" in calculation (3) above, which results in a minimum S contribution outlined by line A in Figure A2.2. Koike et al. (1990) found that, depending on filter type, 13-34% of bacterial cells in natural seawater passed through a 0.4-0.45 μm filter, so 66-87% would have been captured with the larger particulate size-class material. As noted in the main text, accounting for a significant portion of bacterial cells that we likely captured in the G (> 0.5 μm) size class would reduce the calculated contribution from S. However, this estimate of S is both a conservative minimum (because it derives from considering the full error range in calculations by Ingalls et al., 2006) and it ultimately goes unused; the $^{14}C_{DNA}$ constraint from calculation (4) above imposes a much greater minimum contribution from the S fraction (Line B, Figure A2.2).

Conversely, the use of cell counts in calculation (3) also underestimates the contribution from the S size class: a significant fraction of submicron POM in the surface ocean likely exists in the form of detrital (non-living, non-cellular) particles (e.g., Koike et al., 1990). However, filtering can also break up fragile aggregates, and some of the detrital OM in the S fraction could have existed naturally in a larger size fraction. The estimate of a maximum 62% contribution from Bacteria likely is a low estimate for the maximum contribution from S, due to these additional detrital contributions. The striped solution field in Figure A2.2 includes values for which total contribution from S is as great as 76%.

Finally, we believe that potential size-based biases due to adsorption of organic matter onto filters were avoided here by (1) directly extracting filters rather than resuspending the POM from the solid surfaces; and (2) avoiding use of glass fiber filters, which are known to adsorb dissolved organic matter (Morán et al., 1999). Our 0.5 μm filter was composed of cellulose ester.

Sample Preparation and Analytical Methods

Filters were extracted as described in Ingalls et al (2006). Intact polar components in the total lipid extract (TLE) were cleaved by acid hydrolysis in 5% hydrochloric acid in methanol, heated at 70^{o}C. All free fatty acids and polar lipid fatty acid side chains were methylated in this reaction and converted to fatty acid methyl esters (FAMEs). The same batch of methanol was used for all reactions, and its $\delta^{13}C$ and $\Delta^{14}C$ values were measured separately; these values are used in mass-balance equations that account for the ^{13}C and ^{14}C content of the donor methyl group.

The fraction of TLE containing fatty acid methyl esters was purified by silica gel chromatography (eluted in 90% hexane, 10% ethyl acetate). Separate aliquots of this fraction were then used for three separate gas chromatography (GC) applications: GC-flame ionization detection (FID) to determine relative proportions of individual FAMEs; GC-isotope ratio-monitoring combustion mass spectrometry (GC-C-irMS) to determine $\delta^{13}C$ values of individual FAMEs; and preparative capillary GC (PCGC) to purify and collect individual FAMEs for radiocarbon analysis. GC-mass spectrometry (GC-MS) was also used to identify compounds via their fragmentation patterns. The surface 0.2-0.5 μm filter was not measured via GC-MS due to instrument availability and limited sample size; compounds in this sample were identified via comparison of GC-FID retention time with other samples.

Separation of FAMEs for radiocarbon analysis by PCGC is described in Eglinton et al. (1996). Briefly, individual FAMEs collected by PCGC were dried under N_2 and flame-sealed on a vacuum line in pre-combusted quartz tubes with added cupric oxide. Sealed tubes were heated

for 5 hours at 850°C to convert purified compounds to CO_2. Individual CO_2 samples were released into a vacuum line, quantified manometrically, cryogenically purified and collected, and flame-sealed into glass tubes. CO_2 samples were sent to accelerator-mass spectrometry (AMS) facilities for conversion to graphite and measurement of natural ^{14}C content (Table A2.1).

Relative proportions of fatty acids derive from relative peak area obtained during GC-FID. Absolute sample sizes for radiocarbon analysis (reported in Table A2.1) were determined via vacuum-line quantification of CO_2.

Corrections to Radiocarbon Data

Processing blanks and error corrections for our laboratory radiocarbon-preparation procedure were established and reported previously (Ingalls et al., 2006). Reported AMS-facility values were corrected for biological fractionation as determined by $\delta^{13}C$ values. Following the error-propagation technique described Shah and Pearson (2007), these corrected values of $\Delta^{14}C$ and measurement error were corrected for the blanks, uncertainties, and derivatization carbon as described below (Table A2.1).

Combustion correction. A 1-μg carbon blank can be attributed to the combustion process for purified compounds ($\Delta^{14}C$ value 58.5 ± 208.5‰), and additional error derives from propagation of a ~1.7% uncertainty in vacuum line volume and subsequent calculations of sample size. This blank contribution is accounted for in proportion to the size of the sample.

Residual/contaminant correction. $\Delta^{14}C$ values for three of the four sample sets were found to correlate to sample size, indicating an additional source of contamination that contributes a constant mass of carbon to each sample within a given set. Based on a linear projection of the $\Delta^{14}C$ – sample size correlation, a "true" $\Delta^{14}C$ value for a sample of infinite size was derived for each sample set. From this, the size of the contaminant was calculated and included in correction of $\Delta^{14}C$ and corresponding error values, assuming a $\Delta^{14}C$ value of -1000‰ for the contaminant (i.e., petroleum-derived or otherwise radiocarbon-dead source of carbon).

Contaminant sizes for each sample set are detailed in Table A2.1; size-based correlation is shown in Figure A2.4. A "sample set" refers to compounds separated from the same original filter extract and subsequently processed in the same batches through consecutive procedural stages – PCGC, combustion, and vacuum line quantitation. Values within the sets include replicate measurements from splits of the same CO_2 sample, *i.e.*, the residual must have been introduced downstream of the point of combustion, for example, during graphitization (Shah and Pearson, 2007). Independent confirmation of a contaminant in the deep sample sets was found by comparing $\delta^{13}C$ values reported from NOSAMS against those measured separately by GC-C-irMS. The difference between these two sources of $\delta^{13}C$ measurement for individual compounds correlates well with $\Delta^{14}C$ values, possibly indicating addition of an isotopically-constant (and relatively ^{13}C-depleted) endmember (Figure A2.5).

In the fourth sample set (Surface > 0.5 μm), $C_{19:0}$ FAME was added as an internal standard previous to PCGC separation. The internal standard was collected by PCGC identically to the other compounds in the sample and analyzed for ^{14}C content. An aliquot of $C_{19:0}$ free fatty acid standard from the original manufacturer's bottle (powder) was also analyzed to determine a "true" value. The blank- and methyl-corrected $\Delta^{14}C$ value for the PCGC-separated standard was 48‰, whereas the bottled $C_{19:0}$ had a $\Delta^{14}C$ value of 71‰. We assume that the difference can be attributed to an additional carbon blank with a $\Delta^{14}C$ value of -1000‰; by mass-balance, we calculate an addition of 1.67 μg of carbon. As above, we corrected the $\Delta^{14}C$ values for other compounds from this batch according to mass.

***Methyl correction*.** Methanol used in acid hydrolysis/transesterification reactions was previously measured and had a $\delta^{13}C$ value of -39‰ and a $\Delta^{14}C$ value of -1000‰. Blank-corrected $\Delta^{14}C$ values for samples were corrected for the addition of one carbon atom (as a methyl group) from this methanol, calculated in proportion to the number of carbon atoms in the fatty acid chain of each individual compound. Compound-specific $\delta^{13}C$ values were similarly corrected for the addition of this methyl group from methanol.

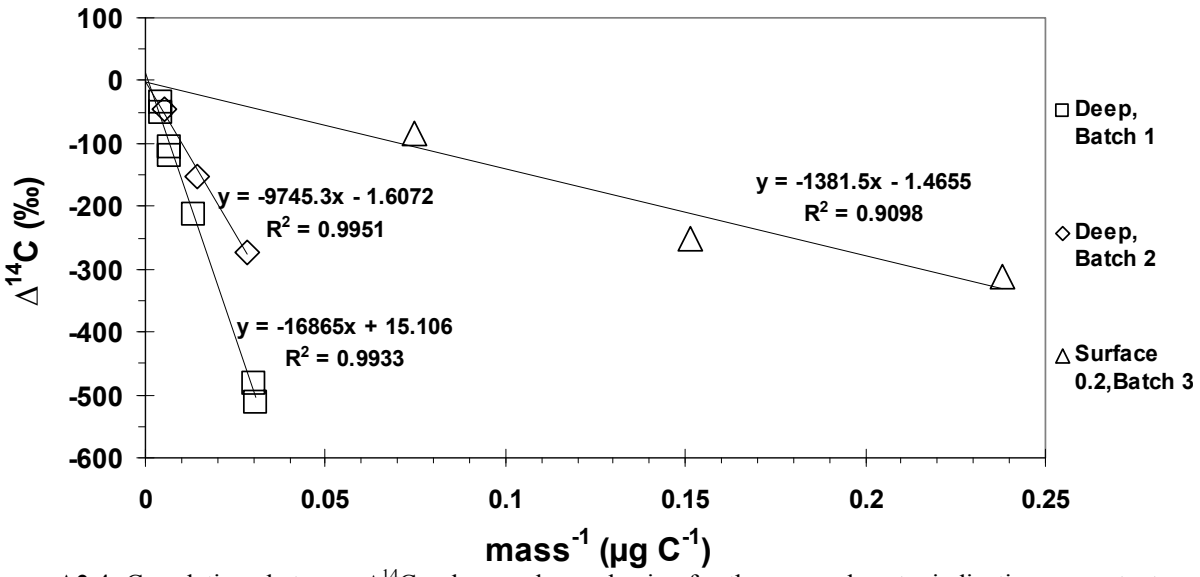

Figure A2.4. Correlations between $\Delta^{14}C$ values and sample size for three sample sets, indicating a constant-mass addition of carbon from a contaminant to each sample in a given set. Projections of linear correlations were used to estimate the mass of the contaminant and, assuming a contaminant $\Delta^{14}C$ of -1000‰, correct the sample $\Delta^{14}C$ values accordingly.

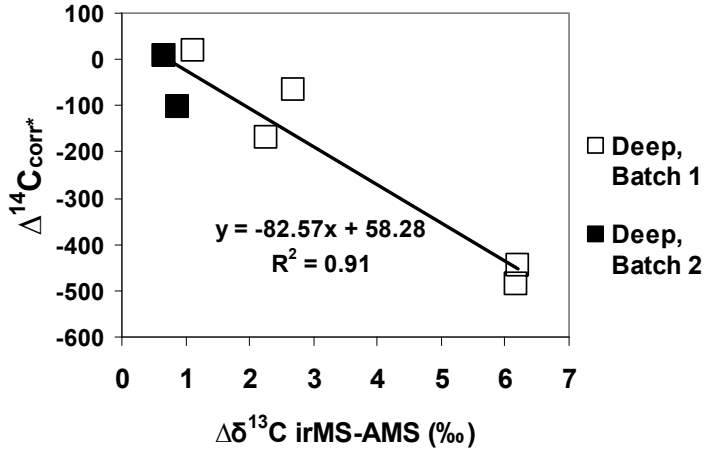

Figure A2.5. Correlation between $\Delta^{14}C$ values (no residual correction) and the offset in $\delta^{13}C$ values derived from measurement by GC-C-irMS and AMS; samples shown only for which AMS and irMS-derived $\delta^{13}C$ values were available. All values have been corrected for addition of one carbon of known ^{13}C and ^{14}C content from methylation, and $\Delta^{14}C_{corr*}$ values also have been corrected for combustion blanks as described.

Estimate of Lipid Attenuation with Depth

We were unable to obtain absolute concentrations of lipid from our samples. However, we can estimate a "cell-equivalent" concentration of lipids at each depth. From our calculations above, we estimate that sinking material derives 84-100% from the small size class. If we equate this size class with the bacterial cells in the surface ocean ($3.07x10^5$ cells/mL; Karner et al., 2001), then the addition of the maximum large size class contribution would raise the equivalent total of cells to $3.65x10^5$ cells/mL. The biomass from $3.07x10^5$ to $3.65x10^5$ cells would then sink and degrade in the water column. At mesopelagic depths, we calculate that 18-36% of FA derive from *in situ* bacteria; therefore 64-82% of FA derive from sinking OM. There are ~$3.01x10^4$ bacterial cells/mL at mesopelagic depths, so the sinking OM would be the equivalent of biomass from $5.35x10^4$ to $1.37x10^5$ cells/mL. Combining high and low estimates for surface and deep, these numbers imply a 55% to 85% reduction in fatty acid concentration over ~650 m of water depth. While we are considering concentrations of lipids rather than fluxes of OM, power-law models of organic carbon flux would predict 84% to 92% loss over similar depth ranges. POM flux as measured by sediment traps commonly is found to relate to depth as a power-law function: $F_Z = F_{100}*(Z/100)^{-b}$, where F_Z is the POM flux at subphotic depth Z (in meters), F_{100} is the flux at 100 m, and b is derived from best-fit to the data. The exponent b has been estimated in the NPSG to be within the range of 0.973 to 1.36 (Martin et al., 1987; Lamborg et al, 2008). Conservatively, if the flux at 100 m is the same as the flux at our sampling depth of 20 m, the sediment-trap POM flux at 670 m would be 7.5% to 15.7% of the flux at 100 m: $F_Z = F_{100}*(0.075,0.157)$. However, as previously mentioned, equating the S fraction with bacterial cells will tend to underestimate its contribution: the concentration of total FA in the surface ocean could be higher, and thus attenuation would be greater than our current estimates.

References

Blair N, Leu A, Muñoz E, Olsen J, Kwong E, Des Marais D (1985) Carbon isotopic fractionation in heterotrophic microbial metabolism. *Applied and Environmental Microbiology,* **50**, 996-1001.

Brodie EL, Desantis TZ, Joyner DC, Baek SM, Larsen JT, Andersen GL, Hazen TC, Richardson PM, Herman DJ, Tokunaga TK, Wan JM, Firestone MK (2006) Application of a high-density oligonucleotide microarray approach to study bacterial population dynamics during uranium reduction and reoxidation. *Applied and Environmental Microbiology,* **72**, 6288-6298.

DeLong EF, Preston CM, Mincer T, Rich V, Hallam SJ, Frigaard N-U, Martinez A, Sullivan MB, Edwards R, Brito BR, Chisholm SW, Karl DM (2006) Community genomics among stratified microbial assemblages in the ocean's interior. *Science,* **311**, 496-503.

DeNiro M, Epstein S (1978) Influence of diet on the distribution of carbon isotopes in animals. *Geochimica et Cosmochimica Acta,* **42**, 495-506.

DeSantis TZ, Brodie EL, Moberg JP, Zubieta IX, Piceno YM, Andersen GL (2007) High-density universal 16S rRNA microarray analysis reveals broader diversity than typical clone library when sampling the environment. *Microbial Ecology,* **53**, 371-383.

Hansman RL, Griffin S, Watson JT, Druffel ERM, Ingalls AE, Pearson A, Aluwihare LI (2009) The radiocarbon signature of microorganisms in the mesopelagic ocean. *Proceedings of the National Academy of Sciences of the United States of America,* **106**, 6513-6518.

Ingalls AE, Shah SR, Hansman RL, Aluwihare LI, Santos GM, Druffel ERM, Pearson A (2006) Quantifying archaeal community autotrophy in the mesopelagic ocean using natural radiocarbon. *Proceedings of the National Academy of Sciences of the United States of America,* **103**, 6442-6447.

Karner MB, Delong EF, Karl DM (2001) Archaeal dominance in the mesopelagic zone of the Pacific Ocean. *Nature,* **409**, 507-510.

Koike, I., Shigemitsu, H., Kazuki, T. & Kazuhiro, K. Role of sub-micrometre particles in the ocean. *Nature*, **345**, 242-244 (1990).

Lamborg C, Buesseler K, Valdes J, Bertrand C, Bidigare R, Manganini S, Pike S, Steinberg D, Trull T, Wilson S (2008) The flux of bio- and lithogenic material associated with sinking particles in the mesopelagic "twilight zone" of the northwest and North Central Pacific Ocean. *Deep Sea Research Part II: Topical Studies in Oceanography,* **55**, 1540-1563.

Lichtfouse E, Eglinton T (1995) 13C and 14C evidence of pollution of a soil by fossil fuel and reconstruction of the composition of the pollutant. *Organic Geochemistry,* **23**, 969-973.

Martin JH, Knauer GA, Karl DM, Broenkow WW (1987) VERTEX: carbon cycling in the northeast Pacific. *Deep Sea Research Part I: Oceanographic Research,* **34**, 267-285.

Moran XAG, Gasol JM, Arin L, Estrada M (1999) A comparison between glass fiber and membrane filters for the estimation of phytoplankton POC and DOC production. *Marine Ecology Progress Series,* **187**, 31-41.

Shah SR, Pearson A (2007) Ultra-microscale (5-25 μg C) analysis of individual lipids by 14C AMS: Assessment and correction for sample processing blanks. *Radiocarbon,* **49**, 69-82.

Chapter 3

Lipid and ^{13}C signatures of suspended organic matter in the Eastern Tropical North Pacific: Implications for the role of Bacteria in the export of marine organic matter

Abstract

The contribution of bacterial biomass to total particulate organic matter (POM) export flux in the ocean is poorly constrained. To examine the export of bacterioplankton and their detrital remains, here we provide the first compound-specific ^{13}C characterization of lipids obtained from a water column profile of exclusively submicron POM. Samples were collected in the Eastern Tropical North Pacific, which contains one of the largest oxygen minimum zones in the world. This environment hosts active subsurface bacterial metabolisms relating to the loss of fixed nitrogen. Significant distinctions appear between submicron POM (0.2-0.7 μm) and the size class typically collected as "suspended" POM (0.7-53 μm). The distribution of phospholipid and glycolipid head groups, fatty acid side chain distributions, and natural ^{13}C contents all vary, both between size classes and with depth in the water column. Results indicate that lipid signatures from the surface ocean are partially conserved in the suspended pool during transit down the water column. However, bacterial heterotrophic degradation and dark autotrophy partially overprint these surface signatures. In addition, active bacterial metabolisms in the oxygen minimum zone appear to mediate the disaggregation of large, detrital aggregates sinking from the surface, thus adding complexity to the pathways of mid-water carbon flux and providing additional organic substrates to the OMZ. This "substrate injection" may provide important fuel for the denitrification and anammox reactions.

Introduction

Export of organic matter (OM) from the surface ocean represents a major flux of carbon into deep reservoirs, thereby removing it from exchange with atmospheric CO_2 on short time-scales. This export also is the largest source of fuel for respiration in the dark ocean. In order to predict

carbon cycle responses to global change, it is vital to accurately parameterize biotic and environmental controls that affect the balance of export versus respiration. Small plankton and other slowly-settling particles – otherwise known as "suspended" POM – recently have been implicated as being overlooked sources of a large fraction of this carbon flux (e.g., Richardson and Jackson, 2007; Lomas and Moran, 2011; Arístegui et al., 2009; Burd et al., 2010). The majority of cellular biomass in the surface ocean is classified within the suspended size class: most phytoplankton and all free-living bacteria are smaller in size than the typical 53 μm cut-off usually defined as the criterion for "sinking" POM (Bacon et al., 1995; Wakeham and Lee, 1989). Because hydrodynamic models dependent on Stokes's Law suggest that this small material should not sink, the downward flux of suspended POM in the water column must involve other dynamic processes.

To provide insight into the conundrum, recent studies have investigated the potential for exchange between "suspended" and "sinking" POM (Sheridan et al., 2002; Goutx et al., 2007; Abramson et al., 2010). Radioisotope tracers indicate that there is significant exchange between these two pools (Bacon et al., 1982), but organic characterization commonly reveals little qualitative similarity in their compositions (Wakeham and Canuel, 1988; Abramson et al., 2010). Perhaps more significantly, none of these previous studies has included POM $< \sim 1$ μm in diameter ("submicron" POM), and this size class remains uncharacterized at most depths in the ocean (Brinis et al., 2004). However, the submicron fraction likely contains the majority of living Bacteria and Archaea in the subsurface ocean. Prokaryotes are critical mediators of particle transformations, and they comprise a significant fraction of POM. These cells are diverse in metabolism and lifestyle, and they participate in exchanging material between size classes, thus potentially contributing to the dynamics of POM sinking (Li et al., 1983; Turley et al., 1986; Fuhrman et al., 1989; Karl et al., 1988; Cho and Azam, 1988; Koike et al., 1990). By neglecting submicron POM, key stages in the production, aggregation, disaggregation, and consumption of organic matter may be missing from our conceptual model of POM export.

Here we begin to address this deficit in knowledge by examining POM from the water column of the Eastern Tropical North Pacific (ETNP). Subsurface waters in the ETNP contain one of the three most expansive oxygen minimum zones in the world ocean (e.g., Ward et al., 2008). The export of organic matter in this location has important implications for global productivity: oxygen minimum zones, including the ETNP, are the sites of the largest discrete losses of fixed nitrogen from the world ocean (Codispoti et al., 2001). Furthermore, the supply of organic matter to denitrifying Bacteria in the OMZ may be the limiting factor in determining the magnitude of nitrogen loss (Ward et al., 2008). The global strength and extent of oxygen minimum zones is increasing with recent climate trends (Stramma et al., 2008), so it is vital to characterize the transformations in POM that reveal the mechanisms and magnitude of its transfer to mesopelagic depths.

We focus on the upper 800 m of the water column in the ETNP, including the entire span of the OMZ. This vertical extent also encompasses the depths over which the attenuation (remineralization) of export flux generally is the greatest but is also highly variable (Martin et al., 1987; Buesseler et al., 2007). We utilize a compound-specific approach to characterize the concentration and $\delta^{13}C$ values of fatty acids from POM in two size classes: 0.2-0.7 μm and 0.7-53 μm. The former most resembles the size class commonly referred to as "submicron" and the latter represents the size class typically collected as the "suspended" pool. This approach allows us to capture the signatures of *in situ* processes as well as evidence for a sinking flux. Fatty acid data are reported for two classes of intact polar lipids (IPLs), nominally distinguished as glycolipids and phospholipids, and for free fatty acids. Such an approach is novel, as compound-specific $\delta^{13}C$ values rarely are reported for lipids from suspended POM, and to date have been reported for submicron POM only for one other study (this work, Chapter 2).

By examining POM at this level of detail, we are able to consider how signatures of autotrophy, heterotrophy, and aggregation/disaggregation are manifested in water column lipids and their ^{13}C content. We evaluate changes in each size class with depth to examine the fate of POM from both surface and subsurface production. In so doing, we also evaluate opposing

models for the fate of intact polar lipids (IPLs): either IPLs are robust indicators of living planktonic communities, or they can persist as detrital components of particles and participate in the dynamic processes of the water column. Results indicate that the submicron size class actively participates in the production, transformation, and translocation of POM as a function of depth in this region of the ocean. A complex combination of sources and pathways of POM dynamics throughout the water column emerges as contributing to the lipid signature that reaches mesopelagic depths.

Methods

Oceanographic stations in the Eastern Tropical North Pacific were defined during the 2007 field season (Figure 3.1). Samples were collected from aboard the R/V *Knorr* in December 2008-January 2009 from Station 1 (13°N 105°W) and Station 8 (9°N 90°W).

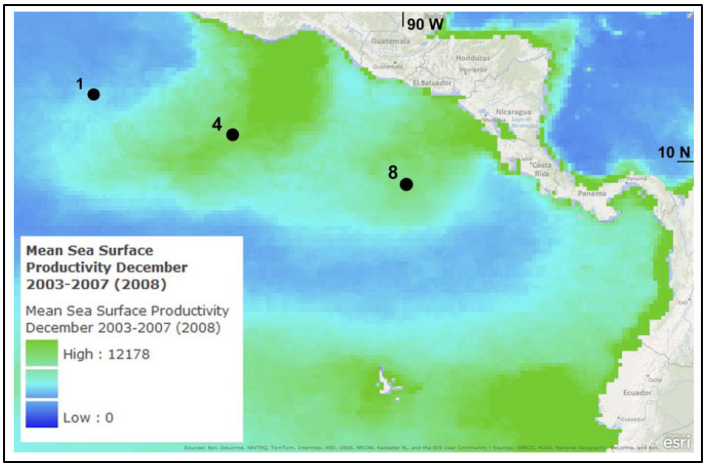

Figure 3.1. Study sites and productivity in the Eastern Tropical North Pacific: Station 1, 13ºN 105ºW; Station 8, 9ºN 90ºW.

In situ filtration. 300-1850 L of seawater were sequentially filtered *in situ* via submersible pumps (McLane Laboratories WTS-LV) deployed on the CTD wire at six or seven depths at each station. Pumps were equipped with three filter tiers, each 142-mm in diameter. The first tier of each pump was fitted with an acid-cleaned 53 µm-mesh Nitex screen. The second tier was fitted with one or two (stacked) 0.7 µm pore-size, pre-combusted glass fiber filters (GF/F). A 0.2 µm pore-size, sterile-packed polyethersulfone (Pall Supor) filter was placed on the bottom tier. Results from two size classes are discussed here: 0.2-0.7 µm ("S"; small) and 0.7-53 µm ("G"; large). Results from Station 8 include both size classes at all depths; at Station 1, the S size class was only collected at two depths in the OMZ.

Each filter was wetted with sterile-filtered deionized water before tiers were assembled for deployment. Pumps were equipped with programmable trigger mechanisms that were employed to ensure passive equilibration with water at the filtering depths for at least 20-30 minutes before pumping commenced. Upon removal from the water, pumps were activated briefly to remove excess seawater from filters. Filters were then removed immediately using cleaned forceps, folded and placed in Whirlpak bags, and frozen in the shipboard -70°C freezer. Samples were packed on dry ice for overnight shipment and were placed in a -80°C freezer upon arrival in lab.

Extraction and separation of polar lipid fractions. Weighed aliquots of each filter were extracted via the detergent method described in Chapter 6. Briefly, organic matter was extracted from filters by adding detergent (1:1 Y-PER and B-PER, Pierce Protein Research Products) and then performing physical disruption *via* bead-beating and freeze-thaw cycling. Nucleic acids were separated into an aqueous phase by standard protocol (Chomczynski and Sacchi, 1987) with Trizol LS extraction reagent (Invitrogen). Proteins were precipitated with isopropanol; the chloroform/phenol supernatant contained the lipids. This lipid phase was washed repeatedly against chilled 5 mM NaOH in water to remove phenol and then washed against plain water. The remaining total lipid extract was dried under N_2 and separated into polarity fractions by column chromatography on 100 mL of 100-200 mesh, 60 Å, pre-combusted SiO_2 gel (~4 cm × 8 cm). TLE was mixed thoroughly with the first 100-mL eluent of solvent to reduce polarity effects from any residual phenol. Free fatty acids were eluted in 85% hexane/15% ethyl acetate (v/v); sterols in 75% hexane/25% ethyl acetate (v/v); glycolipids in 75% ethyl acetate/25% methanol (v/v); and phospholipids in 100% methanol. The polarity of the glycolipid fraction was determined for this method by optimizing separation of intact glycolipid and phospholipid standards (Chapter 6). This fraction is more polar than that used by Pitcher et al. (2009) to elute glycolipids.

The separation of glycolipid and phospholipid fractions was further confirmed by headgroup analysis via HPLC-QToF on an individual sample (Sturt et al., 2004; Schubotz et al.,

2011). Glycosidic head groups were overwhelmingly abundant in the "glycolipid" fraction, with a smaller number of phosphatidylglycerol peaks also detected. Similarly, diverse and abundant phosphatic head groups were present in the "phospholipid" fraction, with few glycolipid peaks also detectable at abundances only a fraction of those seen "glycolipid" fraction. Betaine head groups partitioned into the phospholipid fraction, while sulfolipids were found in the glycolipid fraction. Several fatty acid side chains eventually were detected exclusively in only one or the other fraction, also confirming the specificity of the SiO_2 column separation method. Aliquots of polar lipid fractions from selected samples were derivatized to trimethylsilyl (TMS) ethers before saponification and were found to contain no free fatty acids.

Preparation and isotope analysis of FAMEs. Polar lipid fractions were cleaved via saponification to release fatty acid side chains. Samples were dried under N_2 and heated at 100^{o}C for two hours with 0.5 N KOH in methanol (pH > 11). Neutral lipids were extracted, and the remaining reaction mixture was acidified to pH ~2 with hydrochloric acid. Fatty acids were extracted with multiple aliquots of 90% hexane/10% dichloromethane (v/v) and washed against 5% NaCl in nanopure water and plain nanopure water.

Fatty acids were converted to fatty acid methyl esters (FAMEs) by heating in boron trifluoride/methanol (10% BF_3 in MeOH; Fluka Analytical, Lot BCBC0847) at 70^{o}C for 20-30 minutes. Water was added to stop the reaction, and FAMEs were extracted with hexane and dried over Na_2SO_4 and under N_2. Fatty acid standards of known ^{13}C content were routinely methylated with sample batches in order to determine the ^{13}C content of the carbon added from the BF_3/MeOH solution.

The free fatty acid fraction was found to elute partially with sterols. The two fractions were combined, and the mixture was methylated in BF_3/MeOH. The methylated mixture was washed against 5 mM NaOH, dried, and purified again on a SiO_2 column. FAMEs were eluted in 90% hexane/10% ethyl acetate (v/v), and sterols were eluted in 75% hexane/25% ethyl acetate (v/v). Some residual reagent byproducts coeluted with FAMEs, and chain lengths < 16 could not be analyzed in the free fatty acid fraction.

FAMEs were identified by gas chromatography-mass spectrometry (GC-MS; Agilent 6890N GC – 5973 mass selective detector) equipped with a 30 m HP5-MS column. Samples were injected in hexane via a programmable temperature vaporization (PTV) inlet with a temperature ramp from 65ºC to 450ºC. The GC oven was held at 65ºC for 2 minutes, heated at 20ºC/minute to 130ºC, 6ºC/minute to 280ºC, and 3ºC/minute to 320ºC, where is was held for 25 minutes. Absolute abundance of the natural $C_{16:0}$ FAME in each sample was determined by comparison of the peak area with a nonadecanoate standard added at known concentration.

Natural ^{13}C content of individual FAMEs was determined by gas chromatography – isotope ratio monitoring mass spectrometry via a combustion interface (GC-IRMS: Thermo Scientific Trace GC Ultra-GC Isolink-Conflo IV-Delta V Advantage). Samples were dissolved in hexane and injected through a septum using an autosampler (TriPlus). The inlet was operated in splitless mode at 240ºC. Fatty acids were separated on a DB5-MS column by heating the GC oven from 60ºC to 145ºC at 10ºC/minute, to 230ºC at 2.7ºC/minute, to 275ºC at 5ºC/minute, and to 310ºC at 7ºC/minute, where it was held for 5 minutes. The combustion reactor (nickel and copper oxidants) was held constant at 1030°C. Each sample was measured 3 to 6 times at varying concentrations in order to resolve FAME peaks of varying sizes. Average relative IRMS peak areas were used to determine the concentration of each compound relative to $C_{16:0}$ FAME for each sample. Mean $\delta^{13}C$ values were determined from replicate runs, but including only those replicates for which detected peak amplitudes were > 0.4 V on the mass 44 ion. Values of the original fatty acids were determined by accounting for addition of the methyl carbon from BF_3/MeOH. Error in $\delta^{13}C$ values is reported as 1σ replicate error propagated with 1σ error in the value for the added methyl carbon (Table A1,A2, Appendix). The $\delta^{13}C$ value of the methyl carbon was determined separately via > 40 replicate runs of FAME standards. Absolute instrument performance was checked regularly using the external B3 alkanes reference material; while internal run performance was checked via co-injected C_{32} *n*-alkane (http://mypage.iu.edu/~aschimme/n-Alkanes.html). Errors are reported uniformly as ±1‰ for any compound that was measured only once above the 0.4 V threshold.

Results

Oceanographic setting. Water column properties in the ETNP were similar in 2008 to those reported for 2007 (Rush et al., *in press*; Podlaska et al., *in press*). Station 1 is located in the Tehuantepec Bowl off of southeastern Mexico. Oxygen concentration drops quickly from ~200 µmol/kg in the mixed layer to < 3 µmol/kg at 80 m (Figure 3.2a). The primary chlorophyll maximum is centered around 50-55 m, at the base of the mixed layer. A strong secondary chlorophyll maximum (SCM) occurs at around 90-120 m depth, below the sharp thermocline and within the OMZ. The strength of the fluorescence signal at the SCM was similar to that at the primary chlorophyll maximum, and sometimes larger (~1.4-1.6 mg/m^3). Oxygen concentrations

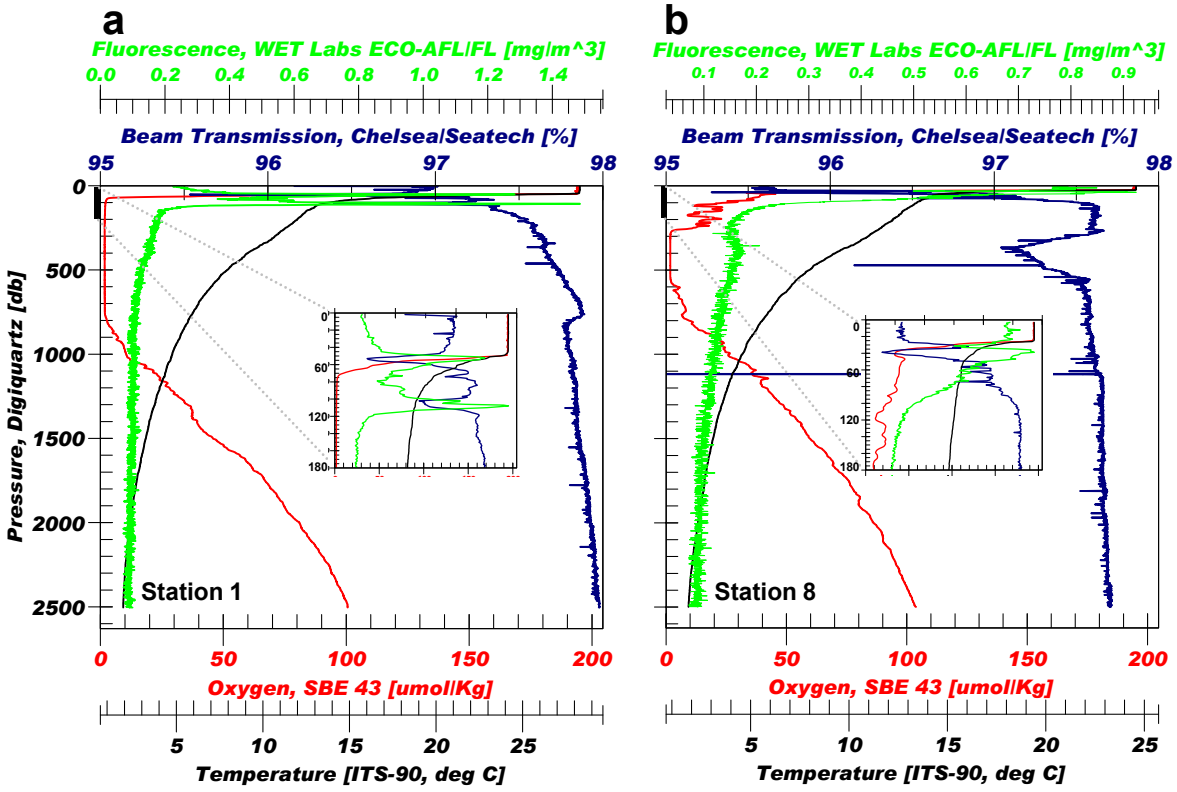

Figure 3.2. Water column properties in the ETNP, Station 1 (13°N, 105°W) and Station 8 (9°N, 90°W). Fluorescence, beam transmission, temperature, and dissolved oxygen concentrations are shown for the first 2500 m. Inlays highlight the relationship between chlorophyll peaks and oxygen concentrations in the surface ocean.

remain < 2 μmol/kg between about 110 m and 760 m before rising again in mesopelagic waters (CTD-mounted SBE 43 sensor, Seabird Electronics, Inc.; Figure 3.2a).

Station 8 is centered over the Costa Rica dome, a year-round upwelling feature. Here oxygen concentration drops sharply below a shallow mixed layer to about 40 μmol/kg at 40 m. The primary chlorophyll maximum at Station 8 was centered around 30-35 m. A poorly-defined SCM at Station 8 was only sometimes evident in fluorescence profiles, just below the primary maximum and within the chemocline/suboxic conditions (O_2, 40-50 μmol/kg).Variably suboxic conditions (10-30 μmol/kg) caused by advection of oxygenated waters (Lewitus and Broenkow, 1985) prevail until an oxygen concentration of < 2 μmol/kg is reached at around 275 m; oxygen concentrations of < 1.5 μmol/kg persist from 350 m to 550 m (Figure 3.2b). In the mid-OMZ a distinct increase in particle concentration is apparent from a broad peak in beam attenuation (i.e., dip in beam transmission; Figure 3.2b).

Absolute abundance of fatty acids. At Station 8 the total yields of intact polar lipids in photic zone G and S size classes were almost identical (~100 ng/L) (Figure 3.3). Lipids from the small size class (0.2-0.7 μm; S) were evenly divided between glycolipids and phospholipids. In the G size class (0.7-53 μm), the highest concentration of FA was in the free fatty acid fraction, and glycolipids exceeded phospholipids. We do not know if free fatty acids in the S size class are similarly abundant in the photic zone, as their absolute concentration could not be estimated due to a large loss in this sample during processing.

Fatty acid concentrations drop quickly to ~4-17% of the maximum between the photic zone and underlying suboxic waters in each size and polarity fraction (Figure 3.3). Attenuation is lowest in the S size class phospholipids; at 170 m the S size class contributes > 60% of total IPL.

At Station 8 the OMZ is marked by a return to higher FA concentrations. In the G size class, the increase in FA concentration begins at the top of the OMZ (~274 m). The most pronounced increases in FA abundance appear in the core OMZ (~400 m), particularly in the glycolipid S size class and the free fatty acid fraction of both S and G size classes. The contribution from the S size class to total IPL again rises from 50% in the upper OMZ to ~60%

in the mid-OMZ. Notably, in the upper OMZ the G size class contributes the greater proportion of glycolipids and in underlying mesopelagic depths the S size class contains the greater proportion of glycolipids. The general increase in FA abundance in the mid-OMZ also correlates with peaks in pigment concentrations (Lewitus and Broenkow, 1985), beam attenuation (Figure 3.2b), total POM concentrations, prokaryotic cell counts, and nitrite concentration (Podlaska et al., *in press*).

Station 1 exhibits higher concentrations of fatty acids in the upper water column than are seen at Station 8. The highest summed concentration of fatty acids coincides with the primary fluorescence maximum in fully oxic waters, but fatty acid concentrations from phospholipids are higher in underlying waters, where the secondary chlorophyll maximum coincides with the upper OMZ. The glycolipid fraction is dominant over the phospholipid fraction at all other depths, by a factor as large as 9:1 in the primary fluorescence maximum. Surface waters above the primary fluorescence maximum (3 m depth) also contain lower overall concentrations of fatty acids.

At Station 1 concentrations of FA below the SCM drop quickly to ~10% of their maximum concentration. FA in the S size class comprise > 50% of the total in the two OMZ depths in which this size class was collected, and the S:G proportion is greatest in the phospholipid fraction. No mid-OMZ increase in FA concentration is observed at Station 1: FA concentrations, total POM, and beam attenuation are all nearly constant from mid- to lower-OMZ. However, insufficient sampling resolution may explain the inability to detect an OMZ particle and lipid-maximum, as such a layer was evident in POM profiles from the same station sampled at higher depth resolution the previous year (Stuart Wakeham, unpublished data). The deepest sample available, from the G glycolipid fraction just below the OMZ, reveals an increase in fatty acid concentrations that may relate to increased aerobic activity of metazoans and related microbes (Wishner et al., 1995; Podlaska et al., *in press*).

Distributions of individual fatty acids

Patterns with depth. Fatty acids from all polarity fractions and size classes are dominated by straight-chain saturated compounds, *n*-$C_{12:0}$-$C_{18:0}$ at all depths (Station 8: 56-87%, Station 1: 34-91%). The primary chlorophyll maximum at both stations contains the fraction with the largest proportion of unsaturated compounds (61% of glycolipid at Station 1; 40% of phospholipid at Station 8), with multiple isomers of $C_{22:6}$, $C_{20:5}$, $C_{18:4}$, $C_{18:3}$, $C_{18:2}$, $C_{18:1}$, $C_{16:2}$, and $C_{16:1}$, and single identifiable isomers of $C_{16:4}$, $C_{17:1}$, and $C_{14:1}$ (Figures 3.3,3.4,3.5). This distribution is characteristic of mixed marine phytoplankton assemblages (Harwood and Russell, 1984; Wakeham, 1995).

At Station 8, the proportion of straight-chain, saturated compounds generally increases with depth below the photic zone. The exception to this pattern is the mid-OMZ: here the relative proportion of unsaturated FA increases compared to immediately overlying depths.

S size class, Station 8. *Glycolipids.* The glycolipid fraction is dominated by large relative proportions of $C_{14:0}$, $C_{16:0}$, and $C_{18:0}$ at all depths (Figure 3.3a, right). Polyunsaturated FA (PUFA) such as $C_{22:6}$ and $C_{18:2}$ are only present in the upper water column and as very minor components. OMZ glycolipids are marked by relative increase in the $C_{18:1\omega9}$ isomer, which peaks in the mid- to lower- OMZ (Figure 3.5a). $C_{12:0}$ also is a significant component, peaking in the lower OMZ, and $C_{16:1}$ is detectable as a minor component at all depths. Notably, $C_{22:1}$ was detected exclusively in the glycolipid fraction, and is a significant minor component at most subphotic depths. The 730-m S glycolipid sample also contains the only detected hydroxy-FA, all with chain length > 20.

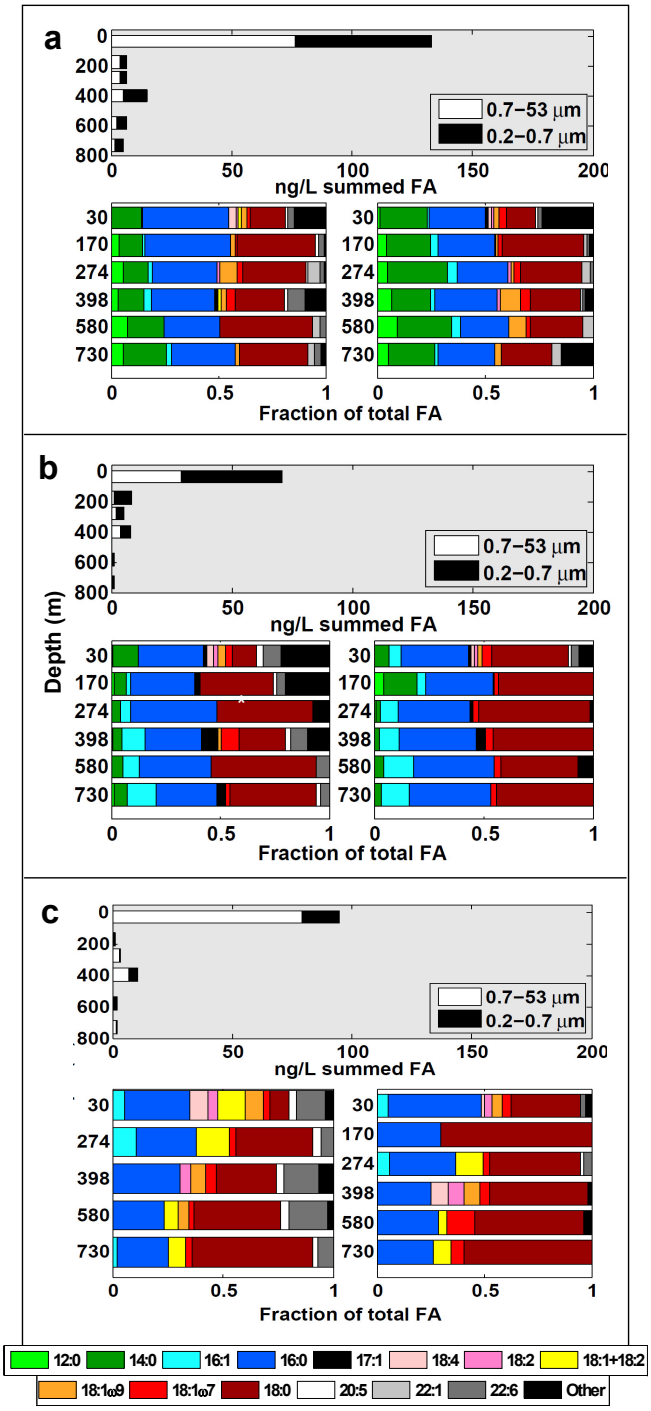

Figure 3.3. Absolute abundances of fatty acids by depth and size class (top), and fractional contribution of 14 major compounds to each size class, by depth (bottom left: 0.7-53 µm; right: 0.2-0.7µm), for three polarity fractions analyzed from Station 8: a- glycolipids; b- phospholipids; c- free fatty acids. Compounds included as "other" are described in the text.

Phospholipids. The phospholipid fraction exhibits comparatively little diversity of FA compounds at subphotic depths (Figure 3.3b, right). $C_{18:0}$ and $C_{16:0}$ are the dominant components at most depths, with $C_{18:0} > C_{16:0}$. However, $C_{16:1}$ comprises a significant component at all depths, particularly in the OMZ. $C_{18:1\omega7}$ and $C_{17:1}$ – both attributed most commonly to bacterial sources – are also present in small proportions at all or most depths, respectively. An increased concentration of $C_{17:1}$ is observed in the mid-OMZ, and the upper- and lower-OMZ also contain a compound identified by its mass spectrum as a branched $C_{18:1}$ FA, which is not observed elsewhere. PUFAs and $C_{18:1\omega9}$ are trace components only detectable in the photic zone. Similarly, $C_{14:0}$ and $C_{12:0}$ are minor or undetectable, with both peaking at the subphotic, suboxic depth (170 m).

Free fatty acids. Saturated $C_{18:0}$ and $C_{16:0}$ dominate the free fatty acid fraction, with $C_{18:0} > C_{16:0}$ at all subphotic depths (Figure 3.3c, right). Unsaturated C_{18} compounds are a sizeable component in all but the 170 m sample, with $C_{18:4}$ and $C_{18:2}$

becoming large components in the mid-OMZ, and $C_{18:1\omega7}$ in the lower OMZ. The 170 m (suboxic) depth contains the lowest diversity of compounds overall, which is true of all size classes and all polarity fractions. C_{12}-C_{15} compounds could not be resolved in any of the free fatty acid fractions due to carryover from extraction reagents, and thus neither their absolute nor relative abundances can be compared directly to polar lipid fractions.

G size class, Station 8. *Glycolipids.* Glycolipids from the G size class show a similar profile of fatty acids as the S size class, but with relatively more $C_{16:0}$ and less $C_{14:0}$ at most depths, and PUFAs present throughout (Figure 3.3a, left). $C_{18:2}$, $C_{18:4}$, and $C_{22:6}$ are present in small proportions in the photic zone. The OMZ again is marked by relative increase in unsaturated compounds, with $C_{18:1\omega9}$ and $C_{22:1}$ peaking in the upper OMZ, and $C_{22:6}$, $C_{18:1\omega7}$, and $C_{17:1}$ peaking in the mid-OMZ (Figure 3.4a). Most unsaturated compounds become very minor in the lower depths, but $C_{22:1}$ and $C_{22:6}$ remain significant components. Here, as in the S size class, $C_{12:0}$ peaks in the lower OMZ, where it is also observed that $C_{18:0} > C_{16:0}$.

Phospholipids. Phospholipids from the G size class also contain FA profiles similar to the S size class, but with significant proportions of $C_{20:5}$ and $C_{22:6}$ at most depths (Figure 3.3b, left). In the mid-OMZ, $C_{17:1}$ and $C_{18:1\omega7}$ constitute a larger portion and $C_{18:0}$ is much smaller than in the S size class. At other subphotic depths, the $C_{18:0}/C_{16:0}$ ratio in the G size class is > 1 and generally increases with depth.

Free fatty acids. Photic zone waters contain a large proportion of $C_{22:6}$ and C_{18} chain lengths with 1 to 4 unsaturations (Figure 3.3c, left). PUFAs are present almost exclusively in this G size class. With increasing depth, $C_{18:0}$ becomes a larger component, as in the free fatty acids obtained from the S size class. An increase in mono- and polyunsaturated C_{18} occurs in the mid-OMZ, with both isomers of $C_{18:1}$ ($C_{18:1\omega7}$ and $C_{18:1\omega9}$) present. $C_{20:5}$ also is present in minor proportions at all depths.

Comparison to Station 1. *Glycolipids.* At Station 1, distributions of fatty acids from subphotic glycolipids are similar to Station 8, but fatty acids from the photic zone show some contrast (Figure 3.4a). In the photic zone, $C_{18:0}$ is present only in low concentrations and instead $C_{18:4}$ and other polyunsaturated C_{18} FA isomers are very abundant. At the SCM, $C_{16:1}$ is the dominant glycolipid component, and $C_{18:4}$ is a trace component. An increase in $C_{18:0}$ with depth in both size fractions is pronounced here, while $C_{14:0}$ decreases in concentration over the same range. The prevalence of $C_{22:1}$, $C_{18:1\omega9}$, and $C_{18:1\omega7}$ at subphotic depths is similar to that seen in glycolipids at Station 8.

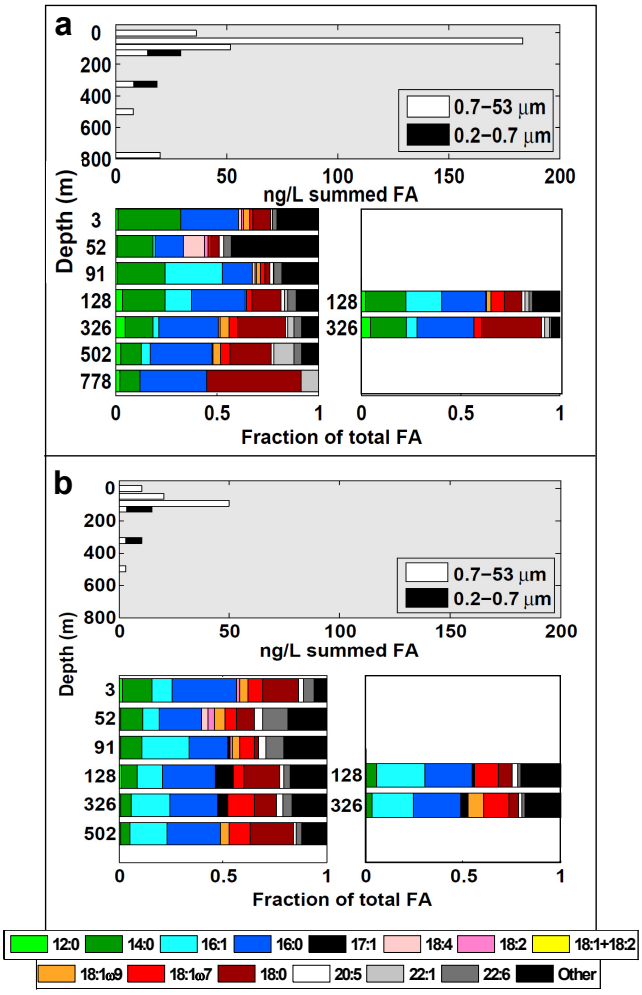

Figure 3.4. Absolute abundances of fatty acids by depth and size class (top), and fractional contribution of 14 major compounds to each size class, by depth (bottom left: 0.7-53 µm; right: 0.2-0.7µm), for each of two polarity fractions analyzed from Station 1: a- glycolipids; b- phospholipids. Compounds included as "other" are described in the text.

Phospholipids. The phospholipid fraction at Station 1 presents the greatest contrast to Station 8 (Figure 3.4b). Most notably, $C_{18:0}$ comprises a much smaller portion of the total in all depths, with $C_{18:0}/C_{16:0}$ always < 1, especially in the S size class. $C_{16:1}$ instead is a prominent component at all depths and both size classes. As with Station 8, $C_{17:1}$ becomes a larger component in the OMZ, and in general, branched and odd-chain compounds become more abundant (14% to 20% of total FA in the upper- and mid-OMZ, both size classes). Notably, the relative content of branched and odd-chain FA at Station 1 is both more diverse and up to > 5

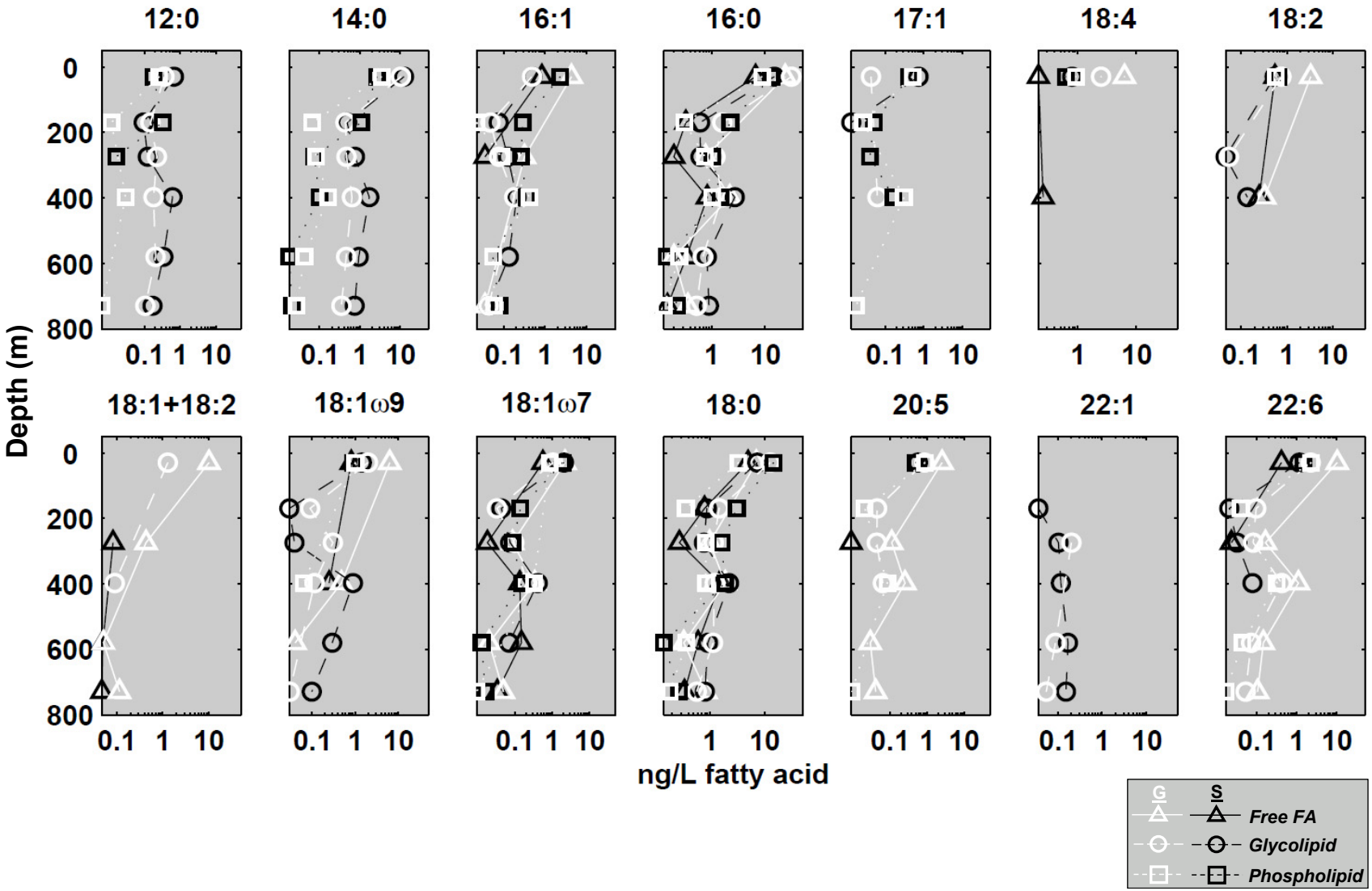

Figure 3.5a. Absolute abundances of 14 major individual fatty acids, by depth, size class (color: G- 0.7-53 µm; S- 0.2-0.7 µm), and polarity fraction (symbol), Station 8. Note that concentrations are displayed on a log scale.

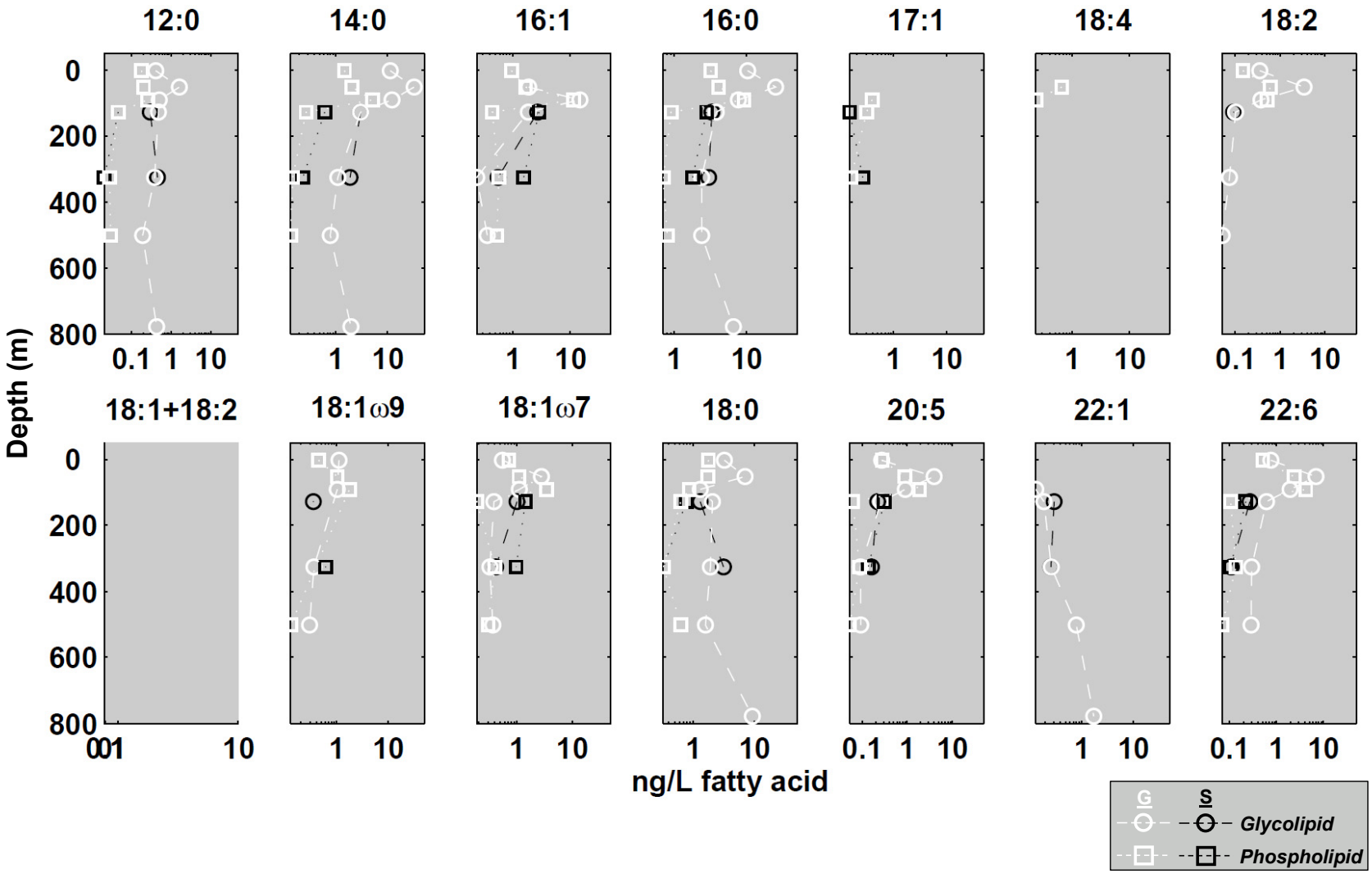

Figure 3.5b. Absolute abundances of 14 major individual fatty acids, by depth, size class (color: G- 0.7-53 µm; S- 0.2-0.7 µm), and polarity fraction (symbol), Station 1. Note that concentrations are displayed on a log scale.

times higher in the phospholipid fraction than in the glycolipid fraction (Table A1, Appendix). Two branched $C_{15:0}$ compounds, distinct from *iso*- or *anteiso*- forms, were identified in the S size class only and were also found to have distinctly depleted $\delta^{13}C$ values (-43‰ to -39‰).

^{13}C content: Total fatty acids. The two stations, 6 or 7 depths, 2 or 3 polarity fractions, and 1 or 2 size classes constitute a total of 35 samples from Station 8 and 17 from Station 1. Within each of these samples, values of $\delta^{13}C$ could be determined for between 2 and 20 individual compounds (Table A1,A2, Appendix). To compare large-scale isotopic patterns across all of the data, first the mass-weighted average $\delta^{13}C$ value for each of the 52 samples was calculated ($\delta^{13}C_{FA\text{-}ave}$; squares, Figures 3.6,3.7). The overall values of $\delta^{13}C_{FA\text{-}ave}$ span from -30‰ to -26.8‰ at Station 8 and -31.5‰ to -24.2‰ at Station 1. Values of $\delta^{13}C_{FA\text{-}ave}$ range from nearly invariant with depth (Station 8, S size class, phospholipids; Figure 3.6b) to ~4‰ deviation over < 100 m in the upper water column (Station 1, G size class, both IPL fractions; Figure 3.7a,b).

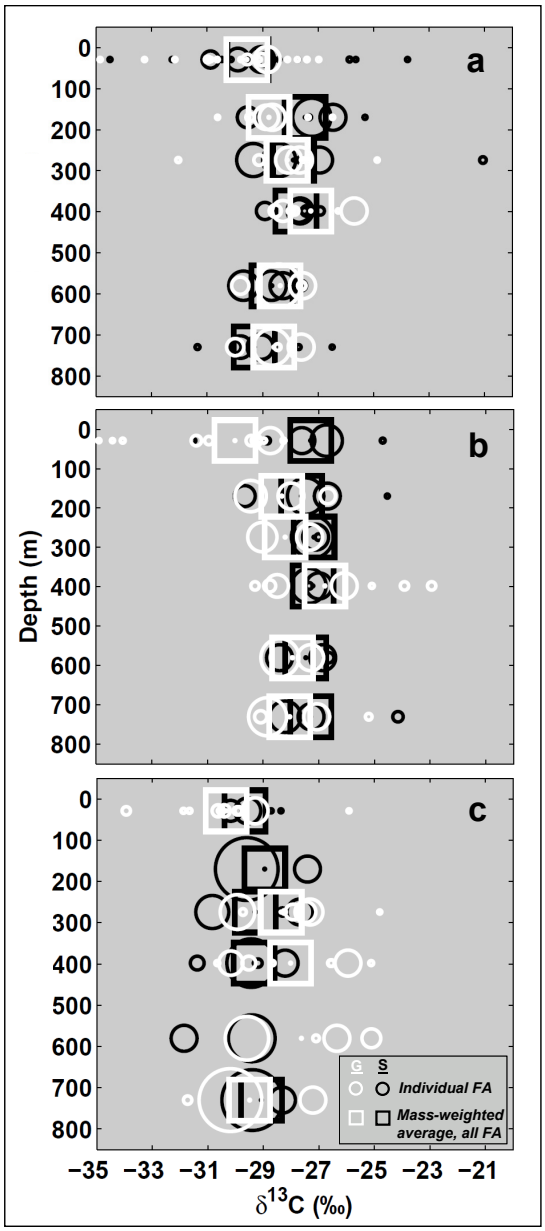

Figure 3.6. Compound-specific and mass-weighted average $\delta^{13}C$ values for all measured fatty acids, Station 8. Data for individual compounds is plotted as circles the sizes of which are proportional to their relative concentration in the sample. Mass-weighted average $\delta^{13}C$ values are plotted as squares. Size classes are indicated by color. a- glycolipids; b-phospholipids; c- free fatty acid fraction. Individual error bars are shown in Figure 3.8a.

The G size class exhibits the most variation with depth in all fractions and at both stations, with the lightest values at the primary chlorophyll maximum and values 2.3‰ to 3.2‰ heavier in the mid-OMZ (Figure 3.6, 3.7). In the lower

OMZ and depths below the OMZ, $\delta^{13}C_{FA\text{-}ave}$ return to lighter values. Fatty acids from the S size class are generally slightly enriched in ^{13}C relative to compounds from the G size class in the same depth and location. This trend is pronounced at Station 1, where the S size class is consistently ~2‰ heavier than the G size class (Figure 3.7a,b). In polar lipid fractions at Station 8, the $\delta^{13}C_{FA\text{-}ave}$ value for the S size class either overlaps with that of the G size class, or is slightly heavier (Figure 3.6a,b). In the phospholipids, the $\delta^{13}C_{FA\text{-}ave}$ value of the S size class is nearly invariant down the water column, but on average is 1‰ more enriched than the G size class (Figure 3.6b). Notably, the photic zone ^{13}C signature for the two size classes is nearly identical in the glycolipids (-29.5‰) but in the phospholipids, the S size class is 2.7‰ more enriched (G: -30.0‰; S: -27.3‰). This pattern mirrors the differences in FA distributions: in the photic zone, the two size classes contain very similar glycolipids but more distinct phospholipids. Isotopic distinction accompanies these compositional differences, with G phospholipids containing abundant, relatively ^{13}C-depleted PUFAs, while S phospholipids contain a large concentration of relatively ^{13}C-enriched $C_{18:0}$ FA.

At Station 1, phospholipids in both size classes are consistently enriched by 1‰ to > 2‰ over glycolipids from the same depth (Figure 3.7). This distinction is most pronounced in the OMZ.

Free fatty acids reflect the general structure of depleted $\delta^{13}C$ values in the photic zone and more enriched values in the OMZ, but with the heaviest values in the lower OMZ (Station 8; Figure 3.6c). The $^{13}C_{FA\text{-}ave}$ content of the S size class of free fatty acids is again roughly invariant down the water column. However, because earlier-eluting FA in the Station 8 free fatty acid fraction could not be analyzed, the mass-weighted average $\delta^{13}C$ values from this fraction may not be directly comparable to the IPL fractions. Free fatty acids from Station 1 were not measured.

^{13}C content: Individual fatty acids. The range in $\delta^{13}C$ values for individual compounds was much larger than the overall mass-weighted averages, spanning from ~ -35‰ to -21‰ at Station 8 and -43.8‰ to -20.3‰ at Station 1. Depth profiles in a few major individual

compounds clearly control the trends in $\delta^{13}C_{FA\text{-}ave}$ values, *e.g.*, $C_{14:0}$ and $C_{16:0}$; but many of the minor compounds with outlying values, *e.g.*, $C_{18:1\omega7}$, also deviate significantly from the average patterns (Figure 3.8a,b).

Across all samples, the C_{16} and C_{18} polyunsaturated fatty acids from the photic zone are relatively depleted in ^{13}C. In the G size class from Station 8, the relative enrichment in ^{13}C in OMZ waters is reflected most greatly in $C_{16:0}$ (all fractions); $C_{22:6}$ (glycolipids and phospholipids); $C_{18:1\omega9}$ (glycolipids and free fatty acids); $C_{18:1}$+$C_{18:2}$, $C_{16:1}$, and $C_{20:5}$ (free fatty acids); and $C_{14:0}$ (phospholipids). Isotopic enrichment is sometimes > 5‰ in $\delta^{13}C$ values of these compounds between the photic zone and mid-OMZ waters (Figure 3.8a).

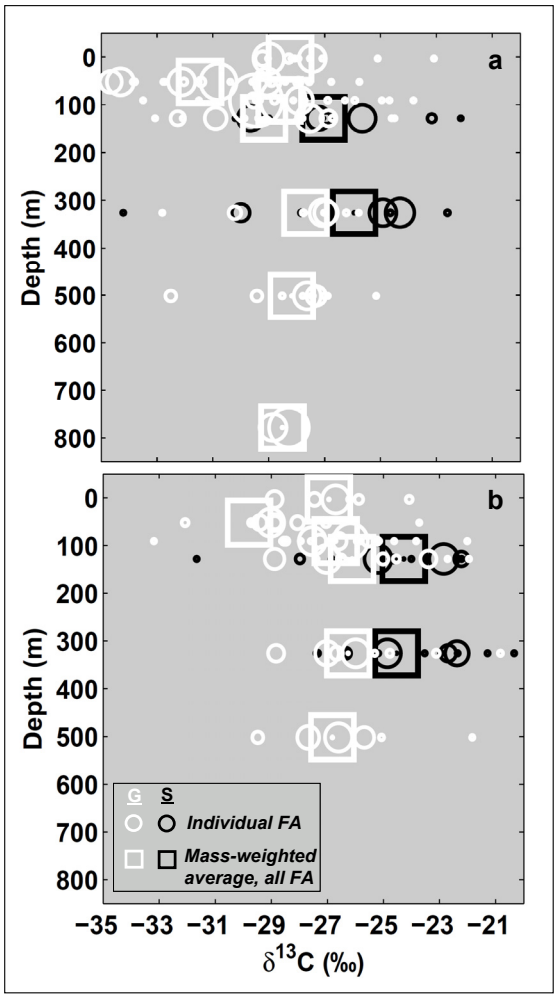

Figure 3.7. Compound-specific and mass-weighted average $\delta^{13}C$ values for all measured fatty acids, Station 1. Data for individual compounds is plotted as circles the sizes of which are proportional to their relative concentration in the sample. Mass-weighted average $\delta^{13}C$ values are plotted as squares. Size classes are indicated by color. a- glycolipids; b- phospholipids. Individual error bars are shown in Figure 3.8b. A few compounds have $\delta^{13}C$ values < -35‰: these are discussed in the text.

In the S size class from Station 8, the glycolipid fraction exhibits the greatest isotopic shifts with depth. $C_{16:1}$, $C_{18:1\omega9}$, and $C_{18:0}$ all are enriched by 2‰ to > 5‰ in the upper- and/or mid-OMZ as compared to the photic zone (Figure 3.8a). In both the free fatty acid and glycolipid fractions, $C_{18:0}$ becomes relatively ^{13}C-enriched in the upper suboxic layers, depleted in the upper OMZ, and enriched again in the mid-OMZ. In the phospholipid fraction of the S size class from Station 8, the large proportion of consistently ^{13}C-enriched $C_{18:0}$ is the primary reason why S-class phospholipids are ^{13}C enriched on average relative to G-class phospholipids.

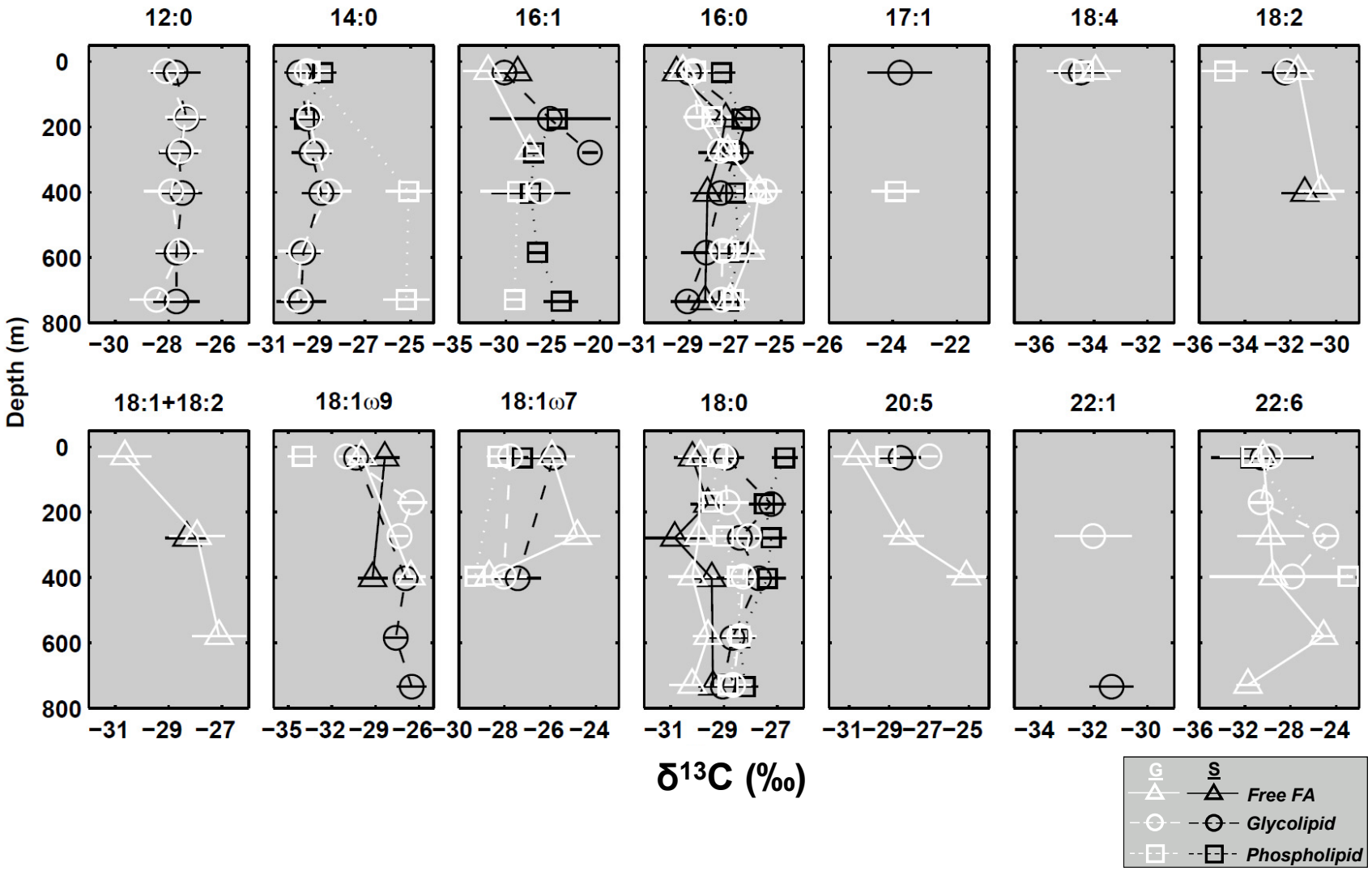

Figure 3.8a. $\delta^{13}C$ values of 14 major individual fatty acids, by depth, size class (color: G- 0.7-53 µm; S- 0.2-0.7 µm), and polarity fraction (symbol) from Station 8. Error bars are 1σ, with error propagated from the 1σ uncertainty in the $\delta^{13}C$ value of the methyl carbon added during derivatization.

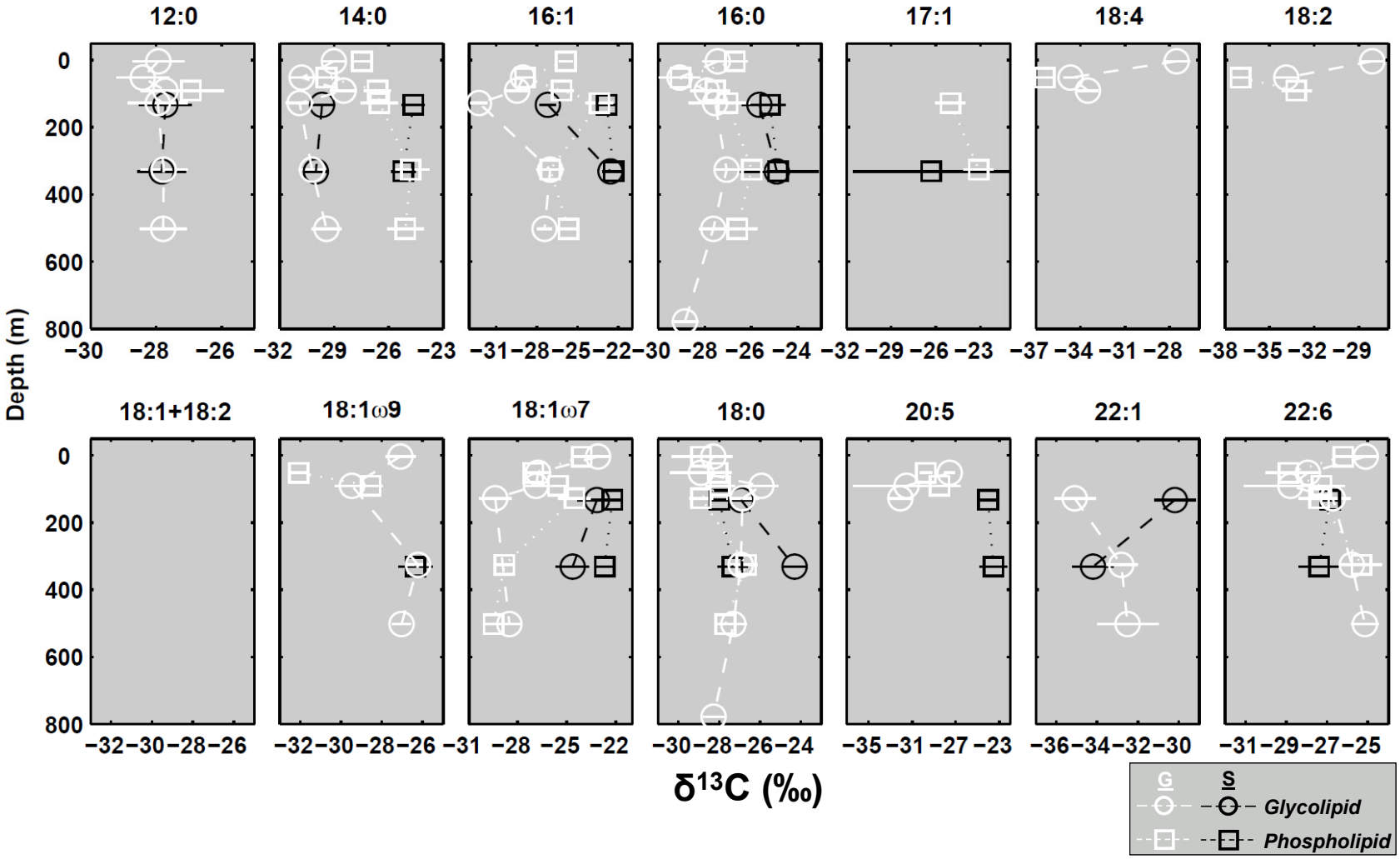

Figure 3.8b. $\delta^{13}C$ values of 14 major individual fatty acids, by depth, size class (color: G- 0.7-53 µm; S- 0.2-0.7 µm), and polarity fraction (symbol) from Station 1. Error bars are 1σ, with error propagated from the 1σ uncertainty in the $\delta^{13}C$ value of the methyl carbon added during derivatization.

At Station 1, $C_{16:0}$ and $C_{18:1\omega7}$ FA in both polar lipid fractions display relative ^{13}C enrichment in the S-class lipids relative to these same compounds in G-class lipids (Figure 3.8b). In the glycolipids this pattern is also apparent for $C_{16:1}$, with the S size class more enriched in ^{13}C than the G size class. In the G size class from the upper OMZ of Station 1, $C_{14:0}$, $C_{16:1}$, and $C_{18:1\omega7}$ from phospholipids are all 4‰ to 6‰ enriched in ^{13}C relative to glycolipids, driving much of the overall pattern of relative ^{13}C enrichment in phospholipids at this station. The distinction is most robust for $C_{14:0}$. In addition, the S size class mirrors many of the patterns seen for the G size class, and the isotopic distinction between phospholipids (heavier) and glycolipids (lighter) is conserved throughout the OMZ. In a partial exception to these patterns, however, for the S size class, the $\delta^{13}C$ values for $C_{16:1}$ and $C_{18:1\omega7}$ become almost identical in the glycolipid and phospholipid fractions in the mid- to lower-OMZ (Figure 3.8b).

At Station 1, $\delta^{13}C$ values were resolvable for *i*- and *a*-$C_{15:0}$ compounds at multiple depths: values were consistently enriched by ~2‰ to 6‰ over the $\delta^{13}C_{FA\text{-}ave}$ values for each sample. Values were usually ~ -25‰ to -24‰, and as high as -22‰ to -20‰ for *i*- and *a*-$C_{15:0}$ components of OMZ phospholipids (Table A1, Appendix). At Station 8, branched $C_{15:0}$ compounds were resolvable for isotopic measurement only in photic zone glycolipids (S and G): *i*-$C_{15:0}$ also is 2‰ to 4‰ enriched in ^{13}C over the $\delta^{13}C_{FA\text{-}ave}$ values at this depth.

Discussion

Properties of the 0.2-0.7 µm (S) size class. The 0.2-0.7 µm size class has been collected previously for lipid compositional analysis only on limited occasions (Brinis et al., 2004), and to our knowledge never has been collected in large samples for compound-specific isotopic analysis before this study. Small particles are expected to contain both detrital components and living, exclusively prokaryotic cells (e.g., Koike et al., 1990; Fuhrman et al., 1989; Brinis et al., 2004). Within this material, polar lipids should best represent the living component (e.g., Van Mooy and Fredricks, 2010; Popendorf et al., 2011). Therefore, IPLs from the S size class are the most likely direct indicators of prokaryotic lipid and ^{13}C signatures in the water column (e.g., Brinis et al.,

2004; Ingalls et al., 2006). However, the contribution from *in situ* living biomass is superimposed upon – and may be overwhelmed by the flux from – detrital POM. Previous studies of submicron POM have concluded that it contains a high proportion of nonliving material (e.g., Koike et al., 1990). This observation justifies the common practice of including submicron POM mechanistically into the dissolved pool (DOM). However, including this material with DOM ignores its living components and particulate nature, masks the potential interaction and exchange of these particles with larger aggregates, and hides the quantitative importance of this pool in the POM cycle.

Our data illustrate the potential impact: concentrations of lipids from the S size class of POM in the ETNP water column are remarkably similar to concentrations of lipids from the G size class (POM > 0.7 μm), *i.e.*, there is quantitatively as much submicron POM as there is classical "suspended" POM. Furthermore, there is no apparent distinction between the size classes in the relative proportions of supposedly "fresh" (intact polar lipid) and "degraded" (free fatty acid) material. This contradicts suggestions that submicron POM is primarily a repository of degraded, detrital organic matter (e.g., Bacon et al., 1985; Koike et al., 1990), and instead supports an extrapolation to submicron POM of the conclusion of Wakeham and Canuel (1988), who argued that "suspended" POM did not show preferential degradation relative to "sinking" POM in the ETNP. Our data argue that submicron and suspended POM contain equally-fresh material.

The S and G size classes do differ in their proportional yields of the two IPL fractions. The S size class is especially rich in phospholipids in the upper water column, while the G size class is dominated by glycolipids. Planktonic bacterial heterotrophs likely synthesize more phospholipids than glycolipids (Van Mooy and Fredricks, 2010; Popendorf et al. 2011), and they should be well-represented in the S size class. In contrast, photosynthetic bacterial and eukaryotic plankton both have been shown to biosynthesize predominantly glycolipids (Harwood, 1998; Wada and Murata, 1998; Van Mooy and Fredricks, 2010; Popendorf et al., 2011). Furthermore, most photosynthetic bacteria are ≥ 0.7 μm in diameter (e.g., Chisholm et al.,

1998), including species of *Synechococcus*, which are especially prominent in the upper photic zone of the Costa Rica dome (Li et al., 1983; Saito et al., 2005). The G size class thus shows strong evidence of more heavily representing phytoplankton in the upper water column, while the S class may be composed mostly of heterotrophs.

Additional support for this distinction comes from the concentration of S-class phospholipids as a function of depth. All size classes and polar lipid fractions experience great attenuation of FA concentrations between the chlorophyll maximum and underlying depths, but the attenuation in S phospholipids is relatively much less than for other lipid classes. Active synthesis of biomass by heterotrophic Bacteria is expected in association with the formation of the intense OMZ, due to the intensive remineralization of OM that must be occurring in the water column. FA from S-class phospholipids in the upper water are dominated by $C_{16:0}$ and $C_{18:0}$, and are enriched in ^{13}C relative to the G size class by > 2‰; this general signature may represent aerobic heterotrophic Bacteria.

However, we resist assigning strict biological sources to specific FA structures. Most of the common FA chain lengths can be synthesized by both Bacteria and Eukarya, and most are present here in both size classes and across both polarity fractions. However, some patterns seen within the size and polarity fractions do correspond to the interpretations above. Most notably, the phospholipid fraction consistently contains FA that are made primarily by Bacteria (branched and odd-chain forms), or that are commonly attributed to Bacteria ($C_{18:1\omega7}$). These bacteria-specific FA occur in the phospholipid fractions in higher absolute concentrations than are measured in the glycolipid fractions. This distinction is especially apparent at Station 1, but it is present in both size classes at both stations.

However, the presence of significant concentrations of "bacterial" FA in the G size class, in addition to the S size class, raises two important points with respect to the filtering method. First, we do expect that a significant fraction of living Bacteria were captured in the G size class; many bacterial cells are > 0.7 μm in diameter, and in addition the effective pore size of the two, stacked GF/F filters we used was probably < 0.7 μm. Second, we are sampling not just cells but

also detrital POM, which often exists as aggregates that are larger or smaller in size than the cells from which the POM originated. Accordingly, the "bacterial" FA accumulate both in the S and G size classes. In contrast, FA that are most often attributed to Eukarya are found predominantly in the G size class: $C_{20:5}$ and $C_{22:6}$ display this pattern most strongly, where they are detected in G by a ratio of anywhere from 1:1 to 10:1 over their presence in S. The general absence of these compounds in the S particle class may indicate that the break-up of larger cellular material is accompanied by the degradation of IPLs.

The ubiquitous saturated FA could be considered to be of little potential use for distinguishing biological signatures. However, both the relative proportion and the ^{13}C content of $C_{14:0}$, $C_{16:0}$ and $C_{18:0}$ FA show patterns in their ^{13}C signatures with depth. These patterns are distinct between the size classes and polarity fractions. For instance, the $\delta^{13}C$ value of $C_{18:0}$ in the G size class shows little variation with depth and thus might reflect a conservative signature of sinking POM. In contrast, in the S size class, $C_{18:0}$ shows more variability in ^{13}C content with depth, perhaps pointing to a greater importance of *in situ* bacterial sources. At both stations, $C_{14:0}$ deriving from phospholipids of both size classes in the OMZ is significantly enriched in ^{13}C. If phospholipids, regardless of size class, are synthesized disproportionately by Bacteria, this could point to a ^{13}C-rich bacterial signature in the OMZ.

Signatures of degradation and sinking. Several patterns in FA concentration and/or ^{13}C content emerge across most samples. Most prominent is the trend in $\delta^{13}C$ values with depth. At both stations, photic zone communities contain FA distinctly depleted in ^{13}C, while just below, in the shallowest subphotic sample, summed IPLs from both size classes, as well as total POM (only collected for the G size class), show a shift toward more enriched $\delta^{13}C$ values (Figure 3.9). Such a distinction (*i*) could reflect the replacement of primary OM with the biomass of heterotrophs (De Niro and Epstein,, 1997; Logan et al., 1995); (*ii*) could reflect sinking primary biomass in which the total residual pool has become isotopically enriched during degradation (e.g., Sun et al., 2004); or (*iii*) could reflect the preferential loss or degradation of a pool of ^{13}C-depleted (eukaryotic) primary biomass from the shallow photic zone, relative to slower

degradation of ^{13}C-enriched (prokaryotic phytoplankton) biomass from the deeper photic zone. Many – but not all – individual compounds follow this trend.

Notably, here we do not consider that trends in $\delta^{13}C$ values with depth could be derived from input of exogenous terrestrial material, as has been suggested for other observations of heterogeneity of $\delta^{13}C$ values among different size fractions of total organic matter (Benner et al., 1997; Sannigrahi et al., 2005). Both study sites in the ETNP were > 600 km from the Central American coastline. We consider there to be little likelihood of transport of intact polar lipid components over this distance, and thus the isotopic signatures of IPLs must be native to the marine environment.

However, we do find evidence that IPLs can survive as intact molecules during sinking over several hundred meters (*cf.*, Schouten et al., 2010). PUFAs such as $C_{20:5}$ and $C_{22:6}$ require oxygen for their biosynthesis (e.g., Russell and Nichols 1999). However, PUFAs are present in IPLs throughout the OMZ, suggesting that these IPLs have survived intact within sinking detrital particles. PUFAs are frequently attributed to eukaryotic production, but are detected here in low abundance in IPLs from the S size class. Association with small particles would be consistent with recent suggestions of significant PUFA biosynthetic capacity within marine bacteria (Russell and Nichols, 1999; Shulse and Allen, 2011a, b). Aerobic bacteria could have produced PUFAs above the OMZ. If the PUFAs are primarily eukaryotic, however, an alternate explanation might be that a portion of the S size class contains a transient pool of freshly-disaggregated POM that has not yet fully degraded into chemical subunits.

In addition, the $\delta^{13}C$ values of some compounds (glycolipid $C_{12:0}$, $C_{14:0}$) are nearly invariant with depth and size class, and could represent an end-member of sinking, relatively unchanged POM. This interpretation fits with the observation that glycolipids persist longer than phospholipids as intact molecules in a degradative setting (Harvey et al., 1986). The detrital component of IPLs thus appears to be significant in the ETNP, but may be more significant for glycolipids than for phospholipids. Sinking POM should be considered as a source of IPLs in other locations; many other IPL studies consider only living sources (e.g., Brinis et al., 2004;

Espinosa et al., 2009; Van Mooy and Fredricks, 2010; Wakeham et al., 2012). The similarity between $\delta^{13}C$ values of certain FA in both the S and G size classes also supports the view that picoplankton-sized POM is participating actively in the overall transfer of POM signatures down the water column. This also could indicate that aggregation/disaggregation processes actively transfer material between the S and G size classes.

Relative ^{13}C enrichment in the S size class relative to the G size class is another consistent pattern across samples, although it mostly is reflected in the major FA: $C_{18:0}$, $C_{18:1\omega7}$, and $C_{16:0}$. Some depths reflect this distinction more strongly; and although the pattern of $\delta^{13}C$ values in S > $\delta^{13}C$ values in G is apparent for the IPL fractions, the free fatty acids do not exhibit isotopic distinction between the size classes. The same pattern of ^{13}C enrichment in S relative to G was also recognized in the North Pacific Subtropical Gyre, where total fatty acids were measured instead of individual polarity classes (Chapter 2). The combined observations suggest that submicron particles – and therefore submicron living cells – are systematically enriched in ^{13}C relative to larger plankton throughout the ocean. Given the three hypotheses for producing signatures of ^{13}C enrichment in the S class, this interpretation is most consistent with option (*iii*), namely, that there is a systematic and pre-existing isotopic difference between Bacteria and Eukarya.

Further support for this interpretation could derive from the relative ^{13}C enrichment in lipids from the secondary chlorophyll maximum (SCM) as compared to the primary chlorophyll maximum at Station 1. POM from the SCM likely reflects a large input from bacterial photoautotrophs that can tolerate the low light conditions and near-absent oxygen at this depth (*e.g.*, Goericke et al., 2000). Bacterial photoautotrophs also are active in the photic zone at Station 8 (Li et al., 1983; Saito et al., 2005), but absence of an SCM indicates they are not as preferentially enhanced at depth. Therefore, the only evidence of their biomass might be in the relative ^{13}C enrichment of the S size class over the G size class in $C_{18:0}$, $C_{18:1\omega7}$, and $C_{16:0}$. Notably, the cells of bacterial photoautotrophs such as *Prochlorococcus* are of similar diameter to the S-G size cutoff. Therefore in all samples, these cells should have been captured in both

size classes; however, at Station 8 their signature in G samples would be overwhelmed by the relatively more abundant algal biomass, while at Station 1, they should make a large contribution to both S and G. This is consistent with the much greater expression of ^{13}C enrichment in the phospholipid fraction at Station 1 relative to Station 8. In and below the SCM at Station 1, $C_{14:0}$, $C_{16:1}$, and $C_{16:0}$ in phospholipids are 2‰ to 4‰ enriched over glycolipids; this signature could derive directly from the synthesis of these compounds by bacterial autotrophs in the SCM. Regardless, the enriched ^{13}C signature is likely to be primary (rather than heterotrophic), because it is quantitatively abundant enough to affect the aggregate average value of $\delta^{13}C$ for the total pool of IPLs in the SCM, which is 4.6‰ heavier than the value at the primary chlorophyll maximum (Figure 3.9).

At subphotic depths the S size class continues to contain more ^{13}C than the G size class, and at Station 8 this is mostly reflected in $C_{18:0}$. At the same depths, $C_{18:0}$ increases in relative abundance in all polarity fractions and in both size classes, leading to many depths at which the abundance of $C_{18:0} > C_{16:0}$. This pattern is not observed in the surface ocean, but it is observed in our other study in the NPSG (Chapter 2). Additionally, high $C_{18:0}$:$C_{16:0}$ ratios are most common among phospholipids and free fatty acids; the former in particular suggests this ratio could be a bacterial chain-length signature. Additional support for this interpretation comes from the increase in $C_{18:0}$ FA seen over the course of degradation experiments in which Bacteria were the only consumers of algal OM (Harvey and Macko, 1997a). $C_{18:0}$ also comprised a larger proportion of fatty acids at mesopelagic depths than in the upper water column in the Atlantic and Pacific gyres when collected on 1μm filters via *in situ* pumps (Loh et al., 2008).

In some previous cases, high relative abundances of $C_{18:0}$ fatty acid have been attributed to zooplankton contributions and were considered to be a signature of generally more "reworked" POM (e.g., Wakeham and Canuel, 1988). Dominance of $C_{18:0}$ in deeper samples and in the free fatty acid fraction would both support this interpretation as a general marker of degradation. However, an origin from zooplankton is not supported by its distribution across the size and IPL polarity classes. If the $C_{18:0}$ FA originated in the biomass or fecal material of

mesoplankton, these materials might be expected to disaggregate and partition indiscriminately into multiple smaller size classes, and with uniform ^{13}C content. Instead, the changes with depth in the proportion of $C_{18:0}$ are distinct between the S and G size classes. In addition, other FA generally considered eukaryotic in origin (*e.g.*, $C_{20:5}$, $C_{22:6}$) partition mostly into the G size class, and their concentrations do not co-vary with the concentration of $C_{18:0}$. Instead, the relative

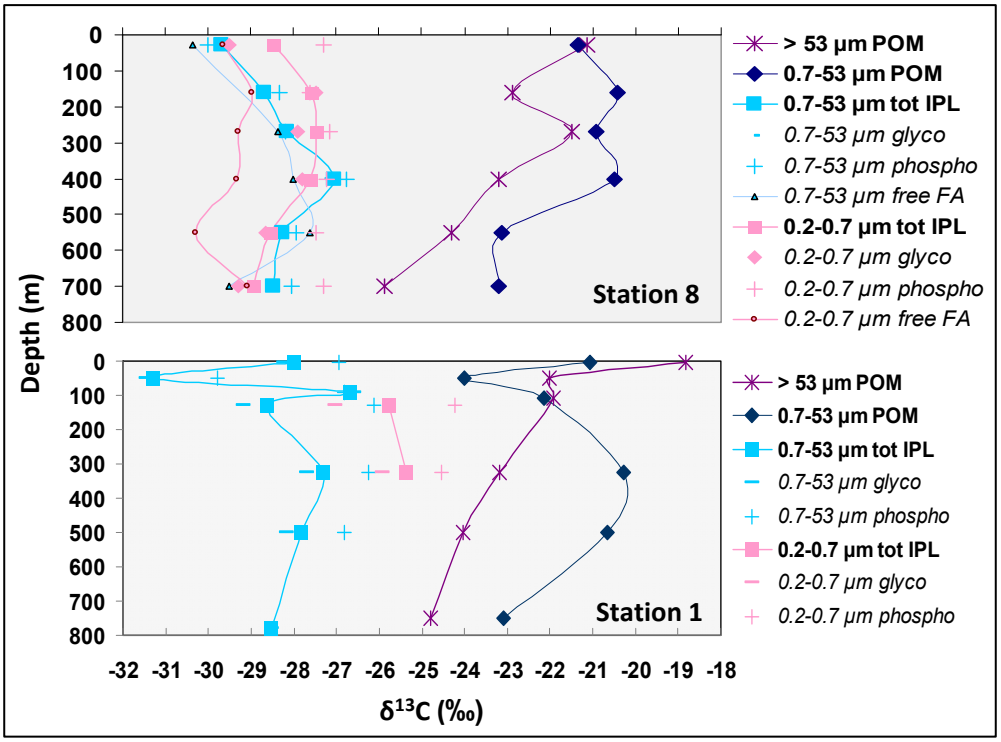

Figure 3.9. Mass-weighted $\delta^{13}C$ values of lipids and POM from three size classes of organic matter in the ETNP. Top- Station 8; bottom- Station 1. POM values represent measurements from total (acidified) organic matter recovered from 53 µm Nitex screens and from 0.7 µm glass fiber filters. Intact polar lipid and free fatty acid values represent the mass-weighted average of $\delta^{13}C$ values measured on individual fatty acids in each sample. "Tot IPL" is the mass-weighted average of the two polar lipid fractions, which are also shown separately ("glyco" – glycolipids; "phospho" – phospholipids).

proportion of $C_{18:0}$ generally displays a gradual increase with depth, and particularly in the S size class. Finally, the general dominance of ^{13}C-enriched – but also ^{13}C-variable – $C_{18:0}$ in the phospholipid S class argues for an active bacterial role in the signature of $C_{18:0}$.

Both $C_{16:0}$ and $C_{18:0}$ are present and/or dominant at all depths, in both size classes. If the large concentrations of $C_{16:0}$ and $C_{18:0}$ in phospholipids from upper, suboxic depths are interpreted as bacterial signatures, by analogy, some fraction of these compounds might be

attributed to living Bacteria at other depths. The $C_{18:0} > C_{16:0}$ signature is more conspicuous in the phospholipid than the glycolipid fraction. This asymmetric distribution across polar lipid fractions may support a dominant origin of the $C_{18:0} > C_{16:0}$ signature from Bacteria, especially because elevated ratios are more pronounced in the phospholipid fraction (Van Mooy and Fredricks, 2010; Popendorf et al., 2011). This effect appears to be important throughout the entire water column below the photic zone. The $\delta^{13}C$ values of $C_{18:0}$ from the S size class also change in parallel down the water column in the glycolipid and free fatty acid classes. This includes cases where values of $\delta^{13}C$ for $C_{18:0}$ alternate between relative depletion and enrichment over the span of the OMZ. Such an observation of consistent changes in $C_{18:0}$ isotope signatures would be consistent with at least a partial origin of $C_{18:0}$ from within the *in situ*, submicron S community. In contrast, if $C_{18:0}$ were mostly detrital, we might expect a more constant or uniformly-trending signature.

Lipid signatures in the OMZ (Station 8). Many individual compounds exhibit different isotopic shifts with depth, both among the size classes and the polarity fractions. The most distinctive down-column features among FA are an OMZ-related increase in absolute concentrations of individual and total FA, and depth-related shifts in $\delta^{13}C$ values in the upper and mid-OMZ. We postulate four sources of OM contributing to FA in the OMZ: (*a*) OM sinking from the same size classes in immediately overlying waters, (*b*) OM newly synthesized through *in situ* chemoautotrophy, (*c*) an "exogenous" source of detrital OM, and (*d*) biomass from *in situ* bacterial heterotrophs utilizing *a, b,* or *c* as carbon sources. "Exogenous" sources in (*c*) could include aggregates or organisms that are not captured in the G or S size class and are sinking quickly from the surface ocean. Exogenous OM also could be advected from adjacent waters.

Due to the reduced efficiency of heterotrophic respiration under low-oxygen conditions (e.g., Harvey and Macko, 1997b), we consider that lipids sinking from above – even if slowly – could be well-preserved (e.g., Devol and Harnett, 2001; Van Mooy et al., 2002). However, the total concentration of many individual FA increases in the OMZ in comparison to the upper, suboxic zone, so the possible contribution from (*a*) can account for only that portion of the total

that is equal in magnitude to the previous depth. On a compound-by-compound basis, a few FA concentrations continue to decrease through the OMZ, and some have relatively uniform $\delta^{13}C$ values at each depth (e.g., $C_{12:0}$, $C_{14:0}$, $C_{18:0}$ in G glycolipids, a probable signature of eukaryotic plankton). This would be consistent with a dominant conserved, sinking source, without additional injection of exogenous POM.

Reports from both the ETNP and other OMZs in the world ocean support a significant contribution from (*b*) – POM production by anaerobic communities of Bacteria and Archaea (e.g., Taylor et al., 2001; Ward et al., 2009; Podlaska et al., *in press*; Rush et al., *in press*). For the same stations in the ETNP, Podlaska et al. and Rush et al. report taxonomic and geochemical evidence for addition of biomass at low-oxygen depths *via* chemoautotrophy (nitrification, anammox), along with elevated rates of heterotrophy (denitrification and sulfate reduction). Wakeham et al. (2012) and Taylor et al. (2001) report similar relationships between prokaryotic cell abundance and redox gradients in the Cariaco Basin. There also is a sharp increase in total POM in the upper anoxic zone of the Cariaco Basin, accompanied by a marked depletion in the ^{13}C content of this POM, which has been attributed to *in situ* chemoautotrophy. In contrast, the upper OMZ in the Baltic Sea exhibits a sharp enrichment in the ^{13}C content of major FA, which has been attributed to carbon fixation via the reverse tricarboxylic acid (rTCA) pathway for carbon fixation by *in situ* bacteria (Glaubitz et al., 2009).

Here in the ETNP the prevailing signature in lipids is an increase in ^{13}C content in the OMZ compared to overlying waters. However, on a compound-by-compound basis, some values are enriched, some are depleted, and some are conservative in comparison to overlying depths. From results by Podlaska et al. (*in press*) and Rush et al. (*in press*), we expect that contributions from anammox, sulfate reduction, and nitrate reduction are present but minor above the OMZ, while nitrification, anammox, nitrate reduction, and denitrification all occur in the uppermost and/or core OMZ. Carbon fixation by anammox bacteria and bacterial nitrifiers would be expected to introduce relatively ^{13}C-depleted biomass and lipids (Schouten et al., 2004; Sakata et

al., 2008), while biomass production by anaerobic heterotrophs would be expected to introduce ^{13}C-enriched biomass and lipids (Blair et al., 1985; DeNiro and Epstein, 1978).

Consistent with our observations that lipid δ^{13}C signatures are zoned by depth, water column profiles of nitrate, nitrite, and ammonium concentrations all imply that metabolisms in the OMZ are somewhat stratified. Maximum nitrate drawdown and nitrite production occur in the uppermost OMZ; this nitrite peak is drawn down to near-zero concentrations just below, in the mid-OMZ (Podlaska et al., *in press*). Accordingly, signatures in lipids from the OMZ may reflect localization of nitrogen-based metabolisms. In the uppermost OMZ, increases in FA abundance and δ^{13}C values mainly are observed in the G size class; this may relate to disaggregation of eukaryote-sourced POM by nitrate reducers in excess of their respiratory metabolic needs. Simultaneous negative shifts in the δ^{13}C values of glycolipid $C_{16:0}$ and $C_{18:0}$ and phospholipid $C_{16:1}$ values also are seen in the S size class and could reflect partial contribution from chemoautotrophy. These compounds also do not decrease as much in their absolute abundances with depth (reduced attenuation) in comparison to other FA, supporting a source of new production for these lipids.

In the mid-OMZ, a pronounced increase in absolute concentrations of FA is evident in both size classes. Here, increased chemoautotrophy by anammox could partially explain nitrite drawdown and increased POM concentrations, along with the slight observed drawdown in ammonium and depleted δ^{13}C values in some IPLs (S glycolipid $C_{16:0}$ and all classes of $C_{18:1\omega7}$, most notably). Nitrification may also add newly-fixed POM in the core OMZ; nitrifiers can function at very low oxygen concentrations (Ward et al., 1989). In general, isotopic shifts to more negative values in the OMZ at Station 8 are reflected mostly in the S size class. If depleted δ^{13}C values are mostly attributable to chemoautotrophic carbon fixation, then this implies that bacterial chemoautotrophs in the OMZ are small cells that may not have been captured in other studies using traditional sampling methods.

Presumably, a supply of newly-fixed carbon would stimulate heterotrophic activity in the OMZ. Bacterial heterotrophs in OMZs are generally very active (e.g., Lipschultz et al., 1990)

and can utilize nitrite, nitrate, or sulfate to oxidize organic matter (e.g., Cline and Richards, 1972; Canfield et al., 2010). Denitrification could account for the remaining apparent drawdown of the nitrite produced by adjacent nitrate reducers (Podlaska et al, *in press*). We postulate that the fresh organic substrate provided by chemoautotrophy in the OMZ also could have a priming effect on the activity of heterotrophs, and they may opportunistically attack sinking aggregates or fecal pellets (e.g., Ward et al., 2009). The hydrolytic activity of mid-water column bacteria can support disaggregation of large particles in excess of *in situ* metabolic needs (e.g., Karl et al., 1988; Smith et al., 1992; Taylor et al., 2009). The disaggregation of large particles thus would introduce "exogenous" detrital OM into the suspended pools and could account for the unexpected presence of PUFAs in the core of the OMZ.

The high abundance of PUFAs in the OMZ is the strongest evidence for such a contribution from exogenous sources (*c*). Similar observation of phytoplankton-derived lipids in the mesopelagic waters of the ETNP previously has been linked to rapid transport and disaggregation of large phytoplankton aggregates (Wakeham and Canuel, 1988). These compounds are likely exported from the photic zone. In the core OMZ, we observe highly elevated concentrations of PUFAs such as $C_{18:2}$, $C_{20:5}$, and $C_{22:6}$, especially in the G size class and in the free fatty acid fraction. This detrital source may be residually enriched in ^{13}C due to degradation of more ^{13}C-depleted constituents during transit (e.g., Sun et al., 2004; Harvey and Macko, 1997a).

Relevant to this point are a few studies showing that fatty acids in a residual pool of autotrophic biomass will be relatively enriched in ^{13}C (by ~2‰ to 7‰) after extensive degradation (Harvey and Macko, 1997a; Sun et al., 2004). However, these studies measured the total pool of FA in the experimental conditions. It is unclear how residual intact polar lipids could exhibit an enrichment effect in their FA side chains during degradation. This would require that enzymatic cleavage of the FA ester bonds to glycerol and/or the bond connecting the glycerol moiety to the polar head group would proceed at a rate that is determined by the ^{13}C content of the FA side chains. Such dependence seems unlikely. Instead, the ^{13}C content of IPLs

must reflect the carbon source and biosynthetic fractionation of their specific biological sources. Such sources might include grazers, which experience isotopic enrichment by feeding on a discrete trophic chain, or autotrophs that are ^{13}C-enriched due to their carbon uptake mechanism (*e.g.*, rTCA cycle). It remains unknown if the microaerophilic conditions in the OMZ could be sufficient for PUFA synthesis; if so, the PUFAs could reflect both disaggregation and *de novo* input from an *in situ*, ^{13}C-enriched community.

At Station 8 the relative ^{13}C enrichment in OMZ PUFAs is most evident in the free fatty acid fraction. Among free fatty acids it is plausible that ^{13}C-depleted components of the detrital pool could be preferentially removed during degradation, leaving the residual pool relatively enriched: enzymes involved in FA degradation would catalyze a quicker reaction on the ^{12}C—^{12}C than on ^{13}C—^{12}C bonds in the fatty acids. However, free fatty acids may derive from degradation of any IPL size class, polarity fraction, or depth – as well as eukaryotic storage lipids such as triacylglycerols or wax esters – and as such their sources are difficult to interpret.

Disaggregation of sinking particles also could explain the relative proportion of phospholipids and glycolipids in the S and G size classes. Above the mid-OMZ, the S size class contains proportionally more phospholipids than the G size class. In the mid-OMZ, the single largest increase in IPL concentrations is in S size class glycolipids. Since we have postulated that glycolipids in the upper water column might be attributed disproportionately to phytoplankton and primarily are abundant in the G class, the addition of abundant glycolipids to the S size class could reflect the physical breakdown of large, sinking aggregates. This agrees with evidence from the Cariaco Basin that indicates that glycolipids make up only a small portion of *de novo* IPL synthesis among mid-water column anaerobic communities (Wakeham et al., 2012).

Finally, identification of a signature from source (*d*) is the most difficult. Fatty acids from heterotrophic bacteria could have $\delta^{13}C$ values that reflect a mixture of substrates, isotopic fractionation during biosynthesis, and/or effects associated with direct assimilation. In general, the expectation is that the biomass of heterotrophs is slightly enriched in ^{13}C compared to its carbon source (e.g., De Niro and Epstein, 1978; Blair et al., 1985; Harvey and Macko, 1997a).

However, heterotrophic bacteria would be expected to consume carbon indiscriminately from multiple sources, including ^{13}C-depleted autotrophs. In addition, the isotopic content of bioavailable organic substrates will vary by depth and will depend on the relative abundance of chemoautotrophic biomass, sinking POM, and re-processed POM. Thus, even if bacterial heterotrophs at two different OMZ depths are both denitrifiers and both synthesize the same distribution of FA, their isotopic content could be different.

The ubiquity of FA synthesis and the complexity of processes leading to their respective $\delta^{13}C$ values in size classes and polarity fractions render a mass-balance approach to deconvolving mixed isotope signatures quite difficult. Furthermore, the relative input of heterotrophic biomass depends on the specific production and degradation rates within the community (e.g., Close et al., 2011), as well as the efficiency of conversion of substrate to heterotrophic biomass, which can vary widely (Rivkin and Legendre, 2001). Rates of heterotrophy and chemoautotrophy have been measured at these stations (Podlaska et al., *in press*), but they do not translate directly to the standing stock of biomass and give no insight into the relative abundance of detrital vs. newly-synthesized POM in depths below the photic zone. Future work with water column models (Chapter 4) will help to decouple some of the potential complexities affecting the distribution of POM in the water column.

Summary and conclusions

Lipids in the ETNP carry complex signatures that reflect production, degradation, and disaggregation processes throughout the water column. Distributions and ^{13}C signatures of fatty acids from IPLs represent at least three distinct processes and/or communities in the water column. (1) A high productivity photic zone contains relatively ^{13}C-depleted biomass and supports aggregation and sinking of relatively-undegraded POM, potentially from all size classes. (2) Intense respiratory activity in the upper water column greatly attenuates the downward flux of OM and results in relative ^{13}C enrichment in several compounds, probably reflecting added biomass of small bacterial heterotrophs. (3) Low-oxygen microbial communities

in the OMZ exploit redox gradients for both heterotrophic and autotrophic metabolisms based on nitrogen and/or sulfur. The activity of the *in situ* community also stimulates disaggregation of large, sinking particles. The overall ^{13}C signature of lipids in the OMZ therefore appears to represent a mixture of photosynthetic POM from both eukaryotic and prokaryotic (*Prochlorococcus*, *Synechococcus*) sources, the biomass of *in situ* chemoautotrophic Bacteria (relatively ^{13}C depleted or enriched), and the biomass of *in situ* heterotrophic Bacteria (slightly ^{13}C enriched). All of this material appears to participate actively in the process of aggregating, disaggregating, and sinking.

Major conclusions:

- Bulk properties of POM reflect major features in the water column: mostly notably, there is evidence for addition of ^{13}C-enriched biomass in the OMZ. In contrast, lipids reflect finer details of POM dynamics in the upper 800 m of the water column, with addition of both ^{13}C-enriched and ^{13}C-depleted biomass, partitioned asymmetrically between size classes and intact polar lipid fractions.

- Total water column concentrations of lipids from the 0.2-0.7 μm size class of lipids are of the same order of magnitude as measured in lipids > 0.7 μm. However, the proportional yields are different between IPL fractions, with the S size class especially rich in phospholipids in the upper water column, perhaps reflecting bacterial heterotrophs. Fatty acid signatures suggest that both S and G size classes of POM can be exported from the surface ocean.

- The 0.2-0.7 μm size class contains many of the same major fatty acid compounds as POM > 0.7 μm, and some $\delta^{13}C$ signatures also seem to be conserved between the two size classes. However, major compounds such as $C_{18:0}$ and $C_{16:0}$ exhibit different patterns in their relative concentrations and $\delta^{13}C$ values between the two size classes, indicating distinct mid-water sources and/or removal processes for some fraction of the two size classes.

- Within individual compounds, significant isotopic heterogeneity exists between depths in the water column. Isotopic heterogeneity also is apparent between polar lipid classes for some compounds (e.g., $C_{14:0}$ in glycolipids vs. phospholipids), and between the two size classes of suspended POM (e.g., $C_{18:0}$ in S vs. G). Because these isotopic distinctions are observed within IPLs, they are expected to represent original biosynthetic signatures and are not a consequence of diagenetic isotope enrichment.

- IPLs appear to have a significant detrital component in the ETNP, *i.e.*, they survive intact while sinking through the water column. Explicit examples are the polyunsaturated fatty acids that require oxygen for biosynthesis (e.g., $C_{20:5}$ and $C_{22:6}$) but are present as IPLs throughout the OMZ. The presence of PUFAs in the OMZ suggests a substantial contribution of POM from a sinking source, overwhelming the lipid signatures of the *in situ* community in the OMZ.

- The 0.2-0.7 μm size class tends to be slightly enriched in ^{13}C in comparison to the 0.7-53 μm size class, particularly in the upper water column and particularly among intact polar lipids. Isotopic enrichment in the 0.2-0.7 μm size class could derive from the inherent biosynthetic fractionation by bacterial autotrophs, or from enrichment during heterotrophic growth on POM. The former possibility is supported at Station 1, where a depth likely dominated by *Prochlorococcus* exhibits relative ^{13}C enrichment. A contribution from bacterial heterotrophs also may be supported by the ubiquitous and intense sub-photic zone respiration (attenuation) of the POM sinking flux in this location.

- The upper- to mid-OMZ hosts a net increase in the concentration of lipids and a change in their ^{13}C content. The increase in biomass likely is due to a combination of chemoautotrophy and enhanced disaggregation of large, sinking particles. A mixture of surface-derived POM from both photoautotrophs and grazers, as well as *in situ* production of new POM by

chemoautotrophs and heterotrophs leads to a wide range of $\delta^{13}C$ values among individual lipids in the OMZ. This influx of POM in the upper- to mid-OMZ again is attenuated efficiently in the mid- to lower-OMZ, presumably by denitrifiers.

Acknowledgments

We thank the crew and science party of R/V Knorr, Voyage 195, Leg 2 for outstanding technical and scientific support, particularly chief scientist Kendra Daly (USF); Monica Heintz (UCSB) for sampling and shipping advice; Steve Manganini (WHOI) and Tim Shanahan (McLane Labs) for *in situ* pump training; Susan Carter for cruise preparation and Meytal Higgins for receiving samples; Florence Schubotz (MIT) for IPL analysis; and Stuart Wakeham for the opportunity to participate in the cruise, as well as filtering preparation and POC analysis. This work was supported by National Science Foundation Grant OCE-0927290 (to A.P.), and by an ExxonMobil Geoscience Grant (to H.G.C.).

References

Abramson L, Lee C, Liu Z, Wakeham SG, Szlosek J (2010) Exchange between suspended and sinking particles in the northwest Mediterranean as inferred from the organic composition of in situ pump and sediment trap samples. *Limnology and Oceanography,* **55**, 725-739.

Arístegui J, Gasol JM, Duarte CM, Herndl G (2009) Microbial oceanography of the dark ocean's pelagic realm. *Limnology and Oceanography,* **54**, 1501-1529.

Bacon M, Huh C, Fleer A (1985) Seasonality in the flux of natural radionuclides and plutonium in the deep Sargasso Sea. *Deep Sea Research Part A.,* **32**, 273-286.

Bacon MP, Anderson RF(1982) Distribution of thorium isotopes between dissolved and particulate forms in the deep sea. *Journal of Geophysical Research,* **87**, 2045-2056.

Blair N, Leu A, Muñoz E, Olsen J, Kwong E, Des Marais D (1985) Carbon isotopic fractionation in heterotrophic microbial metabolism. *Applied and Environmental Microbiology,* **50**, 996-1001.

Brinis A, Méjanelle L, Momzikoff A, Gondry G, Fillaux J, Point V, Saliot A (2004) Phospholipid ester-linked fatty acids composition of size-fractionated particles at the top ocean surface. *Organic Geochemistry,* **35**, 1275-1287.

Buesseler KO, Lamborg CH, Boyd PW, Lam PJ, Trull TW, Bidigare RR, Bishop JKB, Casciotti KL, Dehairs F, Elskens M, Honda M, Karl DM, Siegel DA, Silver MW, Steinberg DK, Valdes J, Van Mooy B, Wilson S (2007) Revisiting carbon flux through the ocean's twilight zone. *Science,* **316**, 567-570.

Burd AB, Hansell DA, Steinberg DK, Anderson TR, Arístegui J, Baltar F, Beaupré SR, Buesseler KO, Dehairs F, Jackson GA, Kadko DC, Koppelman R, Lampitt RS, Nagata T, Reinthaler T, Robinson C, Robison BH, Tamburini C, Tanaka T (2010) Assessing the apparent imbalance between geochemical and biochemical indicators of meso- and bathypelagic biological activity: What the @$#! is wrong with present calculations of carbon budgets? *Deep Sea Research Part II: Topical Studies in Oceanography,* **57**, 1557-1571.

Canfield DE, Stewart FJ, Thamdrup B, De Brabandere L, Dalsgaard T, Delong EF, Revsbech NP, Ulloa O (2010) A cryptic sulfur cycle in oxygen-minimum-zone waters off the Chilean coast. *Science,* **330**, 1375-1378.

Chisholm SW, Olson RJ, Zettler ER, Goericke R, Waterbury JB, Welschmeyer NA (1988) A novel free-living prochlorophyte abundant in the oceanic euphotic zone. *Nature,* **334**, 340-343.

Cho B, Azam F (1988) Major role of bacteria in biogeochemical fluxes in the ocean's interior. *Nature,* **332**, 441-443.

Chomczynski P, Sacchi N (1987) Single-step method of RNA isolation by acid guanidinium thiocyanate-phenol-chloroform extraction. *Analytical Biochemistry*, **162**, 156–159.

Cline JD, Richards FA (1972) Oxygen deficient conditions and nitrate reduction in the eastern tropical North Pacific Ocean. *Limnology and Oceanography,* **17**, 885-900.

Close HG, Bovee R, Pearson A (2011) Inverse carbon isotope patterns of lipids and kerogen record heterogeneous primary biomass. *Geobiology,* **9**, 250-265.

Codispoti LA, Brandes JA, Christensen JP, Devol AH, Naqvi SWA, Paerl HW, Yoshinari T (2001) The oceanic fixed nitrogen and nitrous oxide budgets: Moving targets as we enter the anthropocene? Scientia Marina, **65**, 85-105

Deniro M, Epstein S (1978) Influence of diet on the distribution of carbon isotopes in animals. *Geochimica et Cosmochimica Acta,* **42**, 495-506.

Devol AH, Hartnett HE (2001) Role of the oxygen-deficient zone in transfer of organic carbon to the deep ocean. *Limnology and Oceanography,* **46**, 1684-1690.

Espinosa LF, Pantoja S, Pinto LA, Rullkötter J (2009) Water column distribution of phospholipid-derived fatty acids of marine microorganisms in the Humboldt Current system off northern Chile. *Deep Sea Research Part II: Topical Studies in Oceanography,* **56**, 1063-1072.

Fuhrman JA, Sleeter TD, Carlson CA, Proctor LM (1989) Dominance of bacterial biomass in the Sargasso Sea and its ecological implications. *Marine Ecology Progress Series*, **57**, 207–217.

Glaubitz S, Lueders T, Abraham W-R, Jost G, Jürgens K, Labrenz M (2009) 13C-isotope analyses reveal that chemolithoautotrophic Gamma- and Epsilonproteobacteria feed a microbial food web in a pelagic redoxcline of the central Baltic Sea. *Environmental Microbiology,* **11**, 326-337.

Goutx M, Wakeham SG, Lee C, Duflos M, Guigue C, Liu Z, Moriceau B, Sempéré R, Tedetti M, Xue J (2007) Composition and degradation of marine particles with different settling velocities in the northwestern Mediterranean Sea. *Limnology and Oceanography,* **52**, 1645-1664.

Harvey HR, Fallon RD, Patton JS (1986) The effect of organic matter and oxygen on the degradation of bacterial membrane lipids in marine sediments. *Geochimica et Cosmochimica Acta*, **50**, 795–804.

Harvey H, Macko S (1997) Kinetics of phytoplankton decay during simulated sedimentation: changes in lipids under oxic and anoxic conditions. *Organic Geochemistry,* **27**, 129-140.

Harvey HR, Macko SA (1997) Catalysts or contributors? Tracking bacterial mediation of early diagenesis in the marine water column. *Organic Geochemistry,* **26**, 531-544.

Harwood JL (1998) Membrane lipids in algae. In: Siegenthaler, P., Murata, N. (Eds.), *Lipids in Photosynthesis: Structure, Function and Genetics*. Kluwer Academic Publishers, 53–64.

Ingalls AE, Shah SR, Hansman RL, Aluwihare LI, Santos Gm, Druffel Erm, Pearson A (2006) Quantifying archaeal community autotrophy in the mesopelagic ocean using natural radiocarbon. *Proceedings of the National Academy of Sciences of the United States of America,* **103**, 6442-6447.

Karl DM, Knauer GA, Martin JH (1988) Downward flux of particulate organic matter in the ocean: a particle decomposition paradox. *Nature,* **332**, 438-441.

Koike I, Shigemitsu H, Kazuki T, Kazuhiro K (1990) Role of sub-micrometre particles in the ocean. *Nature*.

Lewitus AJ, Broenkow WW (1985) Intermediate depth pigment maxima in oxygen minimum zones. *Deep-Sea Research*, **32**, 1101-1115.

Li WKW, Subba Rao DV, Harrison WG, Smith JC, Cullen JJ, Irwin B, Platt T (1983) Autotrophic picoplankton in the tropical ocean. *Science*, **219**, 292-295.

Lipschultz F, Wofsy SC, Ward BB, Codispoti LA, Friedrich G, Elkins JW (1990) Bacterial transformations of inorganic nitrogen in the oxygen-deficient waters of the eastern tropical South Pacific Ocean. *Deep Sea Research,* **37**, 1513-1541.

Loh AN, Canuel EA, Bauer JE (2008) Potential source and diagenetic signatures of oceanic dissolved and particulate organic matter as distinguished by lipid biomarker distributions. *Marine Chemistry,* **112**, 189-202.

Lomas MW, Moran SB (2011) Evidence for aggregation and export of cyanobacteria and nano-eukaryotes from the Sargasso Sea euphotic zone. *Biogeosciences,* **8**, 203-216.

Martin JH, Knauer GA, Karl DM, Broenkow WW (1987) VERTEX: carbon cycling in the northeast Pacific. *Deep Sea Research Part I,* **34**, 267-285.

Pitcher A, Hopmans E, Schouten S (2009) Separation of core and intact polar archaeal tetraether lipids using silica columns: insights into living and fossil biomass contributions. *Organic Geochemistry,* **40**, 12-19.

Podlaska A, Wakeham SG, Fanning KA, Taylor GT. Microbial community structure and productivity in the oxygen minimum zone of the Eastern Tropical North Pacific. *Deep-Sea Research I*, in press.

Popendorf KJ, Lomas MW, Van Mooy BAS (2011) Microbial sources of intact polar diacylglycerolipids in the Western North Atlantic Ocean. *Organic Geochemistry,* **42**, 803-811.

Richardson Tl, Jackson GA (2007) Small phytoplankton and carbon export from the surface ocean. *Science,* **315**, 838-840.

Rivkin RB, Legendre L (2001) Biogenic carbon cycling in the upper ocean: effects of microbial respiration. *Science,* **291**, 2398-2400.

Rush D, Wakeham SG, Hopmans EC, Schouten S, Sinninghe Damsté JS (2012) Biomarker evidence for anammox in the oxygen minimum zone of the Eastern Tropical North Pacific. *Organic Geochemistry*.

Russell NJ, Nichols DS (1999) Polyunsaturated fatty acids in marine bacteria- a dogma rewritten. *Microbiology,* **145**, 767-779.

Saito MA, Rocap G, Moffett JW (2005) Production of cobalt binding ligands in a Synechococcus feature at the Costa Rica upwelling dome. *Limnology and Oceanography,* **50**, 279-290.

Shulse CN, Allen EE (2011a) Diversity and distribution of microbial long-chain fatty acid biosynthetic genes in the marine environment. *Environmental Microbiology*, **13**, 684-695.

Shulse CN, Allen EE (2011b) Widespread Occurrence of Secondary Lipid Biosynthesis Potential in Microbial Lineages. *PloS ONE*, **6**, e20146.

Schubotz F, Lipp JS, Elvert M, Hinrichs K-U (2011) Stable carbon isotopic compositions of intact polar lipids reveal complex carbon flow patterns among hydrocarbon degrading microbial communities at the Chapopote asphalt volcano. *Geochimica et Cosmochimica Acta,* **75**, 4399-4415.

Sheridan C, Lee C, Wakeham S (2002) Suspended particle organic composition and cycling in surface and midwaters of the equatorial Pacific Ocean. *Deep Sea Research I,* **49**, 1983-2008.

Smith D, Simon M, Alldredge A, Azam F (1992) Intense hydrolytic enzyme activity on marine aggregates and implications for rapid particle dissolution. *Nature,* **359**, 139-142.

Stramma L, Johnson GC, Sprintall J, Mohrholz V (2008) Expanding oxygen-minimum zones in the tropical oceans. *Science,* **320**, 655-658.

Sturt HF, Summons RE, Smith K, Elvert M, Hinrichs K-U (2004) Intact polar membrane lipids in prokaryotes and sediments deciphered by high-performance liquid chromatography/electrospray ionization multistage mass spectrometry--new biomarkers for biogeochemistry and microbial ecology. *Rapid communications in mass spectrometry,* **18**, 617-628.

Sun M-Y, Zou L, Dai J, Ding H, Culp RA, Scranton MI (2004) Molecular carbon isotopic fractionation of algal lipids during decomposition in natural oxic and anoxic seawaters. *Organic Geochemistry,* **35**, 895-908.

Taylor G, Iabichella M, Ho T-Y, Scranton M, Thunell RC, Muller-Karger F, Varela R (2001) Chemoautotrophy in the redox transition zone of the Cariaco Basin: a significant midwater source of organic carbon production. *Limnology and Oceanography,* **46**, 148-163.

Taylor GT, Thunell R, Varela R, Benitez-Nelson C, Scranton MI (2009) Hydrolytic ectoenzyme activity associated with suspended and sinking organic particles within the anoxic Cariaco Basin. *Deep Sea Research I,* **56**, 1266-1283.

Turley CM, Newell RC, Robbins DB (1986) Survival strategies for two small marine ciliates and their role in regulating bacterial community structure under experimental conditions. *Marine Ecology Progress Series*, **33**, 59–70.

Van Mooy B, Keil RG, Devol AH (2002) Impact of suboxia on sinking particulate organic carbon: Enhanced carbon flux and preferential degradation of amino acids via denitrification. *Geochimica et Cosmochimica Acta,* **66**, 457-465.

Van Mooy BAS, Fredricks HF (2010) Bacterial and eukaryotic intact polar lipids in the eastern subtropical South Pacific: Water-column distribution, planktonic sources, and fatty acid composition. *Geochimica et Cosmochimica Acta,* **74**, 6499-6516.

Wada H, Murata N (1998) Membrane lipids in cyanobacteria. In: Siegenthaler, P.- A., Murata, N. (Eds.), *Lipids in Photosynthesis: Structure, Function and Genetics*. Kluwer Academic Press, 65–81.

Wakeham SG, Canuel EA (1988) Organic geochemistry of particulate matter in the eastern tropical North Pacific Ocean: Implications for particle dynamics. *Journal of Marine Research,* **46**, 183-213.

Wakeham SG, Lee C (1989) Organic geochemistry of particulate matter in the sea: the role of particles in oceanic sedimentary cycles. *Organic Geochemistry*, **14**, 83-96.

Wakeham SG, Turich C, Schubotz F, Podlaska A, Li XN, Varela R, Astor Y, Sáenz JP, Rush D, Sinninghe Damsté JS, Summons RE, Scranton MI, Taylor GT, Hinrichs K-U (2012) Biomarkers, chemistry and microbiology show chemoautotrophy in a multilayer chemocline in the Cariaco Basin. *Deep Sea Research I,* **63**, 133-156.

Ward B, Glover H, Lipschultz F (1989) Chemoautotrophic activity and nitrification in the oxygen minimum zone off Peru. *Deep Sea Research,* **36**, 1031-1051.

Ward BB, Devol AH, Rich JJ, Chang BX, Bulow SE, Naik H, Pratihary A, Jayakumar A (2009) Denitrification as the dominant nitrogen loss process in the Arabian Sea. *Nature,* **461**, 78-81.

Ward BB, Tuit CB, Jayakumar A, Rich JJ, Moffett J, Naqvi SWA (2008) Organic carbon, and not copper, controls denitrification in oxygen minimum zones of the ocean. *Deep Sea Research I,* **55**, 1672-1683.

Wishner KF, Ashjian CJ, Gelfman C, Gowing MM, Kann L, Levin LA, Mullineaux LS, Saltzman J (1995) Pelagic and benthic ecology of the lower interface of the Eastern Tropical Pacific oxygen minimum zone. *Deep Sea Research I,* **42**, 93-115.

Chapter 4

Modeling the sources and degradation of particulate organic matter in the marine water column

Abstract

Particles < 50 μm in diameter comprise the majority of actively-cycling living and detrital particulate organic matter (POM) in the ocean. However, it is unknown to what extent these small, "suspended" phases contribute to downward flux and therefore to long-timescale sequestration of carbon in the deep ocean and sediments. Here we address the fate of suspended POM in the water column of the Eastern Tropical North Pacific by testing three potential models of POM export against the measured distributions and ^{13}C signatures of biologically-ubiquitous fatty acids obtained from intact polar lipids (IPLs). Each model predicts the relative sinking versus *in situ* contributions to suspended POM as a function of depth in the upper to mid-water column. By comparing results from the three models, we propose a likely scenario for lipid production and preservation in this low-oxygen water column: significant proportions of IPLs in the mid-water column are contributed by the surface-derived POM flux, but bacterial communities in the mid-water column also contribute to downward flux, even in POM of submicron size. We also track the specific fate of the IPLs produced in the photic zone to calculate their predicted degradation rates. The models suggest that degradation rates for IPLs in the oxygenated upper water column are comparable to other semi-labile phases of OM. Decreased degradation rates for IPLs are identified in the oxygen minimum zone (OMZ). These results indicate significant potential for the downward flux of chemical signatures within suspended particles produced in the subphotic water column, including within IPLs. Transfer of both biomass and chemical signatures from dark ocean bacterial metabolisms to deep ocean biota and to the sedimentary record could follow the pathways identified here.

Introduction

The cycling of organic matter (OM) in marine water columns includes complex interactions between living biota and detrital OM. Both biota and detritus partition into a range of particulate, colloidal, and dissolved size classes that are subject to different rates of sinking and remineralization. The balance between production and degradation ultimately controls the flux of OM to bathypelagic depths and the seafloor – and thus to long-timescale reservoirs for atmospheric CO_2. It is critical to understand the processes that affect OM export, including how these processes may respond to environmental change.

Organic compounds can be used to track the fate of OM in the water column, and individual compound classes can reveal relative rates of reactivity and different degradative processes (e.g., Wakeham et al., 1997). Fatty acids (FA) are such a class of organic compounds, and due to their ubiquity in bacterial and eukaryotic cells, they can be useful tracers of total OM. For example, Reemtsma and Ittekot (1992) applied a quantitative multivariate treatment to identify factors controlling the distribution of FA in marine particulate matter from the Bay of Bengal. Using principal-component analysis (PCA), they identified sources for key fatty acids that were heavily-loaded on single factors and applied a multiple regression procedure to quantify the contribution of each factor (interpreted as mechanisms of production or degradation) to a given sample. Subsequent work has adopted the PCA method to determine relationships between fatty acid distributions and source attribution in other water column environments (Sheridan et al., 2002; Niggemann and Schubert, 2006; Espinosa et al., 2009). PCA methods can illuminate major, source-specific signatures. However, specific organic compounds, including FA, frequently derive from non-specific biological or detrital sources. Therefore a PCA approach to analyzing FA distributions cannot identify molecular patterns or signatures that may change dynamically, and it likely would not elucidate the overprinting of dynamic OM processing.

Alternatively, mass-balance approaches frequently are used to quantify sources of environmental lipids. These methods typically rely on compound distributions and natural carbon isotope content. By defining the isotopic composition of all but one end-member, the magnitude

of each input and the isotopic content of the remaining, unconstrained contributor can be determined quantitatively through mass-balance calculations (usually by iterative calculations converging on replication of the observed mixture; Lichtfouse and Eglinton, 1995; Pearson and Eglinton, 2000; Ingalls et al., 2006). Such a mass-balance approach again requires that end-members are well-defined; it thus, like PCA, may overlook unidentified sources of organic matter and/or dynamic effects on the fate of OM in a particular setting.

Regardless of limitations, these previous examples have demonstrated how the use of isotopic measurements – particularly on specific organic components – can help deconvolve source signatures and processing among organic pools. Compound-specific analyses can expose the diversity of metabolic and biosynthetic isotopic effects in environmental settings. Lipid biomarkers that are specific to single clades and distinct metabolic pathways can be interpreted definitively (e.g., ladderane lipids from anammox bacteria; Sinninghe Damsté et al., 2002). In contrast, the larger and more complex the set of available data, the more challenging are the interpretations. This is especially true for general biomarkers such as FA and sterols. A need remains for approaches that can discern signatures of wholesale OM processing in marine settings.

Here we consider the water-column properties of fatty acids derived from intact polar membrane lipids (IPLs). IPLs are frequently considered to degrade rapidly after cell death, and are thus considered to represent the living community in various environments (e.g., Lipp et al., 2008; Van Mooy and Fredricks, 2010). Each compound has only limited capacity for specific biological interpretation, but as a whole, IPLs are representative of the majority of biological sources (excluding Archaea). In contrast to the purely "living cell" interpretation, however, it has been suggested that there is significant detrital flux of IPLs in marine water columns (Schouten et al., 2010; Chapter 3). These lipids thus can trace broad-scale OM cycling in the water column. Here we aim to use a particle size-specific and IPL class-specific data set from the Eastern Tropical North Pacific (ETNP) to characterize the degradation – and conversely, the production and preservation potential – of IPLs in the water column. The ETNP is characterized by a strong

oxygen minimum zone (OMZ) spanning several hundred meters. Recent work has revealed significant rates of mid-water microbial metabolic activity that corresponds to redox gradients in the OMZ of the ETNP (Podlaska et al., *in press*). This area thus has the potential to mediate a diversity of *in situ* metabolic processes that affect both the rate of IPL degradation and the potential for synthesis of new IPLs in the sub-photic water column.

This work specifically examines three conceptual models for the cycling of IPLs. Each model separately treats two size classes of suspended OM and controls whether exchange is allowed between these size classes. The small size class (S: 0.2-0.7 μm) should contain small prokaryotes, along with detrital (non-living) OM. The larger size class (G: 0.7-53 μm) is presumed to contain larger prokaryotes, small eukaryotes, and aggregates of detrital OM. Among the detrital components, it has been suggested that extensive exchange between the size classes occurs *via* aggregation and disaggregation processes (e.g., Bacon and Anderson, 1982; Armstrong et al., 2009; Lomas and Moran, 2011). Disaggregation of detrital OM by mid-water column microbial communities has been considered to be a dominant process supplying organic substrates to communities in subphotic waters (e.g., Karl et al., 1988; Cho and Azam, 1990). Our models test the effects of these processes by varying the permitted modes of exchange between particle size classes.

The model results suggest that IPLs survive within both small and large detrital particles as they sink through the water column. The results also suggest that subphotic production adds significant content to the downward flux of POM. Finally, the models also point to disaggregation of rapidly-sinking particles as an additional source of lipids within the OMZ. Because each model deconvolves sinking from *in situ* lipid sources, the fraction of lipids at each depth that derives originally from the surface can be determined. By multiplying this fraction by the total lipid concentration measured at each depth, we can reconstruct the concentration of surface-derived lipids and calculate a degradation profile. The models converge on degradation rates for IPLs in the oxygenated water column that are similar to degradation rates previously determined for pigments within sedimenting particles (Lamborg et al., 2008). In contrast, our

models suggest that degradation rates in the OMZ may be as much as an order of magnitude slower.

Models

Three models of particle mixing were developed to analyze the compound-specific $\delta^{13}C$ data and compound distributions measured for the water column of the ETNP. Sampling methods, fatty acid distributions, and $\delta^{13}C$ values are described in Chapter 3. All models use intact polar lipid (IPL) data from one station (Station 8, 9°N, 90°W), six depths spanning 700 m of the upper water column, two size classes (S: 0.2-0.7 μm, and G: 0.7-53 μm), and two IPL fractions in each size class (glycolipids and phospholipids). To model a dynamic view of particles in the ocean, sinking of all size classes and exchange between size classes both are permitted in various combinations. No exchange is permitted between the lipid fractions, as head-group conversion between glycolipids and phospholipids is assumed not to occur without breakdown (and therefore loss) of the IPL.

The models provide three different conceptual, mechanistic frameworks for how particles sink and mix. Each model considers simple two end-member mixing to account for the lipid distributions and $\delta^{13}C$ values in each sample. The notation S_z or G_z represents a sample from the small or large size class, respectively, at depth z. We generalize the two end-members contributing to a given sample S_z or G_z as I, the unknown *in situ* source of lipids, and K, the sinking source of lipids. The sample(s) used to define the contributions to K are defined separately for each model.

The model results are based on the goodness-of-fit between the assumed sources K and the observational data for each fatty acid compound i in each sample S_z or G_z. The portion of S_z or G_z that cannot be accounted for by contribution from K represents, by difference, I. That is, the measured relative concentrations and $\delta^{13}C$ values of individual fatty acids, i, (Chapter 3) are used to determine f_K (fraction contributed by the sinking source) and the *in situ* fraction $f_I \equiv (1\text{-}f_K)$

for all models. Because all models are mathematically the same and differ only in the specific components used to define the sinking end-members, *K*, all models can be generalized as:

$$\textit{Lipids}\ (S_{i,z}) = f_{K,z,S} * \textit{Lipids}\ (K_{i,z,S}) + (1\text{-}f_{K,z,S}) * \textit{Lipids}\ (I_{i,z,S}),$$

$$\textit{Lipids}\ (G_{i,z}) = f_{K,z,G} * \textit{Lipids}\ (K_{i,z,G}) + (1\text{-}f_{K,z,G}) * \textit{Lipids}\ (I_{i,z,G}),$$

where

Lipids ($S_{i,z}$) = lipid data for compound *i* in sample S at depth *z*,

Lipids ($G_{i,z}$) = lipid data for compound *i* in sample G at depth *z*,

Lipids ($K_{i,z,S}$) = lipid data for compound *i* in source K contributing to S_z (and equivalent for G_z),

Lipids ($I_{i,z,S}$) = calculated *in situ* lipid data for compound *i* at depth *z*, within S_z (and equivalent for G_z), and

$f_{K,z,S} = f_K$, calculated specifically for a given source K, defined by the individual model, and a given sample S_z at depth *z* (and equivalent for G_z).

Once f_K has been determined, the resulting *in situ* fatty acid profile (Equation 1, below) and individual-compound $\delta^{13}C$ values (Equation 2, below) can be calculated via specific individual-compound mass-balance equations (after Lichtfouse and Eglinton, 1995; Pearson and Eglinton, 2000; Ingalls et al., 2006; Chapter 2). As written for a sample from the S size class, these mass-balance equations, respectively, are calculated as:

$$X_{i,z,S} = f_{K,z,S}X_{K,i} + (1\text{-}f_{K,z,S})X_{I,i} \qquad \text{(Equation 1)}$$

and

$$\delta_{i,z,S} = [f_{K,z,S}X_{K,i}\delta_{K,i} + (1\text{-}f_{K,z,S})X_{I,i}\delta_{I,i}] / X_{i,z,S} \qquad \text{(Equation 2)}$$

where

i = individual fatty acid compound;

X = mole fraction of compound *i* in the measured sample S at depth *z*, source *K*, which varies depending on the model, or modeled *in situ* component *I*; and

$\delta_i = \delta^{13}C$ value of fatty acid *i* in sample S at depth *z*, source *K*, or modeled *in situ* component *I*.

Mole fraction is defined as the relative abundance of an individual compound – determined by GC-irMS peak area – divided by the summed relative abundance of all compounds in the profile that are considered in this model. Equations 1 and 2 above are written identically for the G component, but substituting the subscript G for S in all cases. In model formulations below, both classes of individual-compound data, X_i and δ_i, are referred to together within the $S_{i,z}$, $G_{i,z}$, $K_{i,z}$, and $I_{i,z}$ notations.

Conceptual basis and formulation of three models.

Model 1: Canonical export. "Suspended" organic matter generally is defined as all particles of diameter < 53 μm. This implies that both of the size classes (S and G) addressed here would be considered canonically to be "suspended". Suspended OM generally is not believed to contribute to sinking flux, as it is thought to degrade relatively completely due to its long residence time (slow sinking rate) in the water column (Bacon et al., 1985; Fowler and Knauer, 1986; Karl et al., 1988). Virtually all sinking OM is considered to derive from the photic zone, where high rates of production and aggregation produce large particles (> 53 μm) with high sinking rates (e.g., Fowler and Knauer, 1986). It has been claimed that at subphotic depths, the low concentrations of OM and near-absence of turbulent and shear forces permit minimal aggregation, resulting in little or no incorporation of suspended POM into these larger particles (e.g., Johnson et al. 1990). We formulate what we consider to represent this "canonical" model of particle dynamics by allowing only large particles to sink. Therefore, each sample S_z or G_z, must comprise a mixture of only *in situ* (*I*) production, plus lipids derived from packaging, sinking, and disaggregation of surface-derived material (sinking source, *K*). The composition of *K* must be defined: we assert that its closest measured analogue is the surface-most G (0.7-53 μm) sample, which includes biomass that likely would be included in sinking aggregates. This photic-zone sample likely contains the highest proportion of eukaryotic algae and grazing protists, as well as some Bacteria. Model 1 therefore involves strict two-end-member mixing, and each sample S_z or G_z consists of only *in situ* material plus surface-derived detritus (*I* and *K*, Figure 4.1a).

In Model 1, for each compound *i*, source *K* contributing to S_z or G_z at depth *z* can be expressed as:

$$K_{i,z,S} = G_{i,30m}$$

$$K_{i,z,G} = G_{i,30m}$$

Therefore, for each compound *i* at a given depth *z*, and within size fractions S or G, the measured total is:

$$S_{i,z} = f_{K,z,S}G_{i,30m} + (1-f_{K,z,S})I_{i,z,S}$$

$$G_{i,z} = f_{K,z,G}G_{i,30m} + (1-f_{K,z,G})I_{i,z,G}$$

Model 1 does not allow any transmission of detrital lipids from depth-to-depth within the subphotic water column, as all S and G particles at these depths are assumed to be truly "suspended", with zero entrainment into sinking material. We consider this to be an extreme formulation of the canonical view in order to provide the greatest contrast with the other models.

Model 2: Conservative sinking size classes. The second model addresses the possibility that the two pools of OM, S and G, are distinct from one another, but that each – despite being part of the classically "suspended" size classes – is able to sink and contribute to the same size class lower in the water column. This implies that although S sinks, it remains S and cannot exchange with material in G, and vice-versa. Since sinking and mixing occurs sequentially through the water column – i.e., depth *z* receives material sinking from depth *z*-1 – a portion of detrital components from the upper, subphotic water column can persist even at mesopelagic depths (Figure 4.1b).

In Model 2, for each compound *i*, source *K* contributing to S_z or G_z at depth *z* can be expressed as:

$$K_{i,z,S} = S_{i,z-1}$$

$$K_{i,z,G} = G_{i,z-1}$$

Therefore, for each compound *i* at a given depth *z*, and within size fractions *S* or *G*, the measured total is modeled as the sum of two end-members in Model 2 is

$$S_{i,z} = f_{K,z,S}S_{i,z-1} + (1-f_{K,z,S})I_{i,z,S}$$

$$G_{i,z} = f_{K,z,G}G_{i,z-1} + (1-f_{K,z,G})I_{i,z,G}$$

This model encapsulates the idea of "slowly settling" particles that do not aggregate or disaggregate sufficiently to exchange across size classes, and thus may retain the characteristics of their respective biological sources. This model could be plausible in a low-oxygen water column such as the ETNP, where even very slowly-settling particles could be preserved over hundreds of meters of sinking (e.g., Van Mooy et al., 2002).

Model 3: Indiscriminate packaging and disaggregation. The third model incorporates the most dynamic view of particle size exchange and sinking. At each depth, particles from both size classes are mixed together before sinking (i.e., they aggregate). The lipid pool at each depth thus is quantitatively and indiscriminately homogenized during sinking. This mixture is then allowed

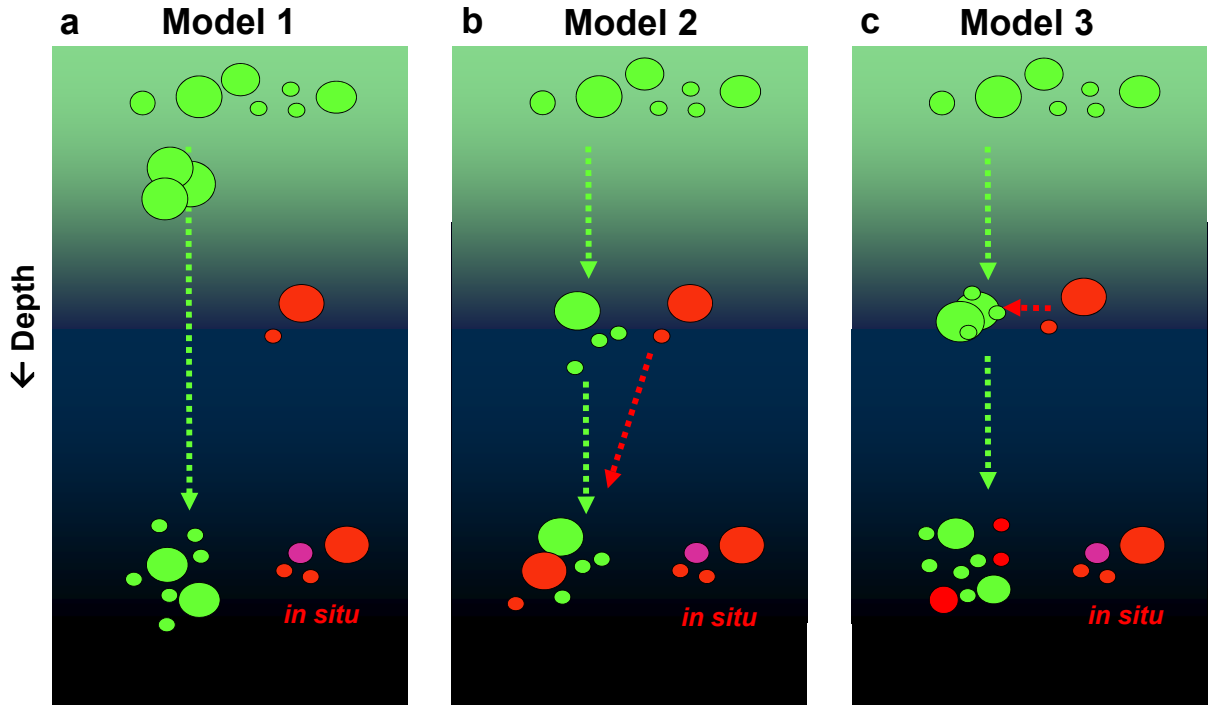

Figure 4.1. Particle mixing allowed by each of three model formulations (a,b,c). Green represents surface contributions, while red and magenta indicate subsurface biomass. Both large and small particles are shown (relative circle sizes). a- In Model 1, only large particles from the surface can sink and contribute to the total measured at depth *z*. The other source of lipids at depth *z* is *in situ* production. b- In Model 2, both size classes can sink, but size classes are constant and their properties remain separate. c- In Model 3, both small and large particles aggregate together and sink, and *in situ* subphotic biomass is similarly added. At depth *z*, these mixed particles disaggregate and add to both size classes at that depth.

to contribute to both size classes at the subsequent depth (i.e., it disaggregates randomly into both the S and G size classes). Therefore the total material, S_z or G_z, at each depth contains the components of *K* from both particle size classes of the preceding depth (Figure 4.1c). Again, because sinking and disaggregation occur sequentially over depth, a proportion of detrital lipids from the upper water column continuously accumulates and can survive within the sinking pool, *K*.

We model the mixture *K* by combining S and G pools at depth *z*-1 in proportions determined by their respective total measured water column concentrations, i.e.,

$$f_{S,z-1} = C_{z-1,S}/(C_{z-1,S} + C_{z-1,G})$$

where *C* = concentration in ng/L, and

$$C_{z-1,S} = \sum C_{i,z-1,S}$$

for all model compounds *i* in S, and analogously for G.

Then the mole fraction and $\delta^{13}C$ value, respectively, of each compound *i* in the total sinking source *K* are calculated as

$$X_{K,z-1,i} = f_{S,z-1}X_{S,z-1,i} + (1-f_{S,z-1})X_{G,z-1,i} \text{ and}$$

$$\delta_{K,z-1,i} = [f_{S,z-1}X_{S,z-1,i}\delta_{S,z-1,i} + (1-f_{S,z-1})X_{G,z-1,i}\delta_{G,z-1,i}] / [f_{S,z-1}X_{S,z-1,i} + (1-f_{S,z-1})X_{G,z-1,i}] .$$

Significantly, measured water column concentrations are used here only to derive the proportions in which S and G are mixed before normalizing to mole fractions. In all other model parameterizations, only mole fractions are used.

In Model 3, for each compound *i*, source *K* contributing to *S* at depth *z* therefore can be expressed as:

$$K_{i,S,z} = f_{S,z-1}S_{i,z-1} + (1-f_{S,z-1})G_{i,z-1} ,$$

and the equivalent can be written for G.

Therefore, for each compound *i* at a given depth *z*, and within size fractions S or G, the measured total is modeled as the sum of two end-members in Model 3 such that:

$$S_{i,z} = f_{K,z,S}[f_{S,z-1}S_{i,z-1} + (1-f_{S,z-1})G_{i,z-1}] + (1-f_{K,z,S})I_{i,z,S}$$

$$G_{i,z} = f_{K,z,G}[f_{S,z-1}S_{i,z-1} + (1-f_{S,z-1})G_{i,z-1}] + (1-f_{K,z,G})I_{i,z,G} .$$

Model parameterization: inputs and outputs. To determine f_K we compare the relative distribution of individual fatty acid compounds *i* in the source *K* and in the total measured sample (S_z or G_z). We calculate the minimum proportion of the S_z or G_z profile that must remain unaccounted for by the source *K*, *i.e.*, we subtract profile *K* from profile S_z or G_z. We thus derive the minimum proportion of FA in S_z or G_z that must be produced *in situ* at depth (Equation 1) – whether *de novo* or by transformations (saturation, structural alteration).

To achieve conservation of mass in the fatty acid profiles, no solution can be permitted that would allow $(1-f_K)X_{I,i} < 0$ (the *in situ* source must either be zero or positive). Therefore, f_K is maximized at the highest value for which $(1-f_K)X_{I,i} \geq 0$ for all compounds *i*. This is calculated as the minimum among all *i* of $X_{Z,i}/X_{K,i}$. Compounds *i* used in this calculation were limited to only those compounds *i* for which X_i comprised > 4% of the total lipid profile for a given sample S_z or G_z; i.e., we parameterize the model with only the major compounds. Minor compounds (those with abundance < 4% of the total) may be vulnerable to detection-limit biases, and including them in the parameterization would have the effect of amplifying measurement errors into large errors in f_K.

Next, we impose an additional limitation to derive an "allowable maximum" f_K. This limitation is based on individual-compound $\delta^{13}C$ values. It is necessary to impose this boundary to reduce potential artifacts: small differences in source and sample fatty acid concentration profiles that are accompanied by proportionally larger differences in $\delta^{13}C$ values will tend to result in arbitrarily high or low values of $\delta^{13}C$ calculated by isotope mass balance for the *in situ* component. We thus prescribe -15‰ and -45‰ as the maximum and minimum allowed values of $\delta^{13}C$ for compounds in *I*. These limits span an approximate ±5‰ range around the range of natural values measured across all FA compounds and samples from the ETNP in this study (Chapter 3). The range is generous to allow for potential contribution by novel mid-water chemoautotrophs whose carbon-fixation pathways fractionate carbon isotopes particularly weakly or strongly. The "allowable maximum" f_K for each sample is calculated by testing all

values from 0 to $f_{K\text{-}max}$, stepping by 0.01, and is the largest value for which, for all individual FA compounds *i*, -45‰ < $\delta_{I,i}$ < -15‰, calculated according to Equation 2.

This value of f_K is is determined uniquely for each sample S_z or G_z, as it is defined by the relative fatty acid profiles and $\delta^{13}C$ values of the specific sample and source. As described, it is then used to calculate the mole fractions, $X_{I,i}$, and $\delta^{13}C$ values, $\delta_{I,i}$, for each fatty acid compound *i* in the *in situ* (I) component, using Equations 1 and 2. This yields the relative distribution of fatty acids in *I*. Isotopic content was not measurable for every compound in every sample and its source. For compounds for which the *in situ* relative abundance could be calculated and the $\delta^{13}C$ value was measured for the sample S_z or G_z, but for which the $\delta^{13}C$ value was not measured in the sinking source, K_i, the *in situ* component *I* was assigned a $\delta^{13}C$ value equal to that of the sample $S_{i,z}$ or $G_{i,z}$.

The outputs of each model are the predicted lipid signatures of Bacteria living at sub-photic depths. We clarify here that while the models are designed to calculated the "predicted" *in situ* lipid signatures, the sinking fraction f_K represents the *maximum* possible proportion of lipids that the sinking source could contribute. Subtracting the sinking fraction yields the *minimum* unique, *in situ* contribution *I*, both for fatty acid distributions ($X_{I,i}$ for all *i* in *I*) and $\delta^{13}C$ values ($\delta_{I,i}$ for all *i* in *I*). The calculated lipid and isotopic signature of I_z thus represents the characteristics of each sample S_z or G_z that cannot be accounted for by other lipid sources within that model framework. In other words, the fractional contribution from *in situ* sources that is coincidentally identical to sinking photosynthetic biomass cannot be distinguished; however, any component that has any unique lipid or isotopic fingerprint can be detected.

Surface-derived sinking component. Separately, the fraction of each sample S or G deriving specifically from the surface-most sample (here, 30 m ≡ z_{30}) can be back-calculated through the depth-to-depth mixing within each model framework. We refer to the fraction of sinking material *K* that is from total surface-derived material S_{30}+G_{30}, within the sample S_z as $f_{S30+G30,z,S}$, and analogously for G_z.

In Model 1, the fraction of residual surface small component S_{30} at depth *z*>30, in both S_z and G_z, is zero: the small size class in Model 1 does not sink. The fraction of S_z (depth *z* > 30)

deriving from the residual surface large component, G_{30}, in Model 1 is simply

$$f_{S30+G30,z,S} = f_{K,z,S}$$

since $K_{z,S}=G_{30m}$ and analogously for G_z.

In Model 2, sinking occurs sequentially within the separate size classes, so the back-calculation of the surface-derived fraction is recursive with respect to $f_{K,z,S}$ and $f_{K,z,G}$:

$$f_{S30+G30,z,S} = f_{K,z,S} * f_{K,z-1,S} * f_{K,z-2,S} * \ldots * f_{K,z30,S}$$

$$f_{S30+G30,z,G} = f_{K,z,G} * f_{K,z-1,G} * f_{K,z-2,G} * \ldots * f_{K,z30,G}$$

where $f_{K,z30,S} = f_{K,z30,G} = 1$.

In Model 3, sinking also is sequential, but mixing occurs between size classes at each depth. The fraction of surface-derived material at depth $z > 30$ is thus the mass-weighted sum of the fraction in S_z and G_z. Therefore, the relative concentrations of S and G – represented as $f_{z,S}$ and $1\text{-}f_{z,S}$, respectively – again must be considered, and the back-calculation of the surface-derived fraction at depth z in Model 3 is also recursive:

$$f_{S30+G30,z,S} = f_{S30,z,S} + f_{G30,z,S} \text{ and}$$

$$f_{S30+G30,z,G} = f_{S30,z,G} + f_{G30,z,G} :$$

$$f_{S30,z,S} = f_{K,z,S} * [f_{z-1,S} * f_{S30,z-1,S} + (1\text{-}f_{z-1,S}) * f_{S30,z-1,G}];$$

$$f_{S30,z,G} = f_{K,z,G} * [f_{z-1,S} * f_{S30,z-1,S} + (1\text{-}f_{z-1,S}) * f_{S30,z-1,G}];$$

$$f_{G30,z,S} = f_{K,z,S} * [f_{z-1,S} * f_{G30,z-1,S} + (1\text{-}f_{z-1,S}) * f_{G30,z-1,G}]; \text{ and}$$

$$f_{G30,z,G} = f_{K,z,G} * [f_{z-1,S} * f_{G30,z-1,S} + (1\text{-}f_{z-1,S}) * f_{G30,z-1,G}].$$

For z=30, $f_{G30,z,S}=0$; $f_{S30,z,G}=0$; $f_{G30,z,G}=1$; and $f_{S30,z,S}=1$.

Accumulated subsurface sinking component. We have defined the fraction of lipids at depth z deriving from the surface and from *in situ* production. Thus, the fraction of sinking lipids accumulated from the subsurface water column can be calculated by difference:

$$f_{SUB,z,S} = 1 - f_{S30+G30,z,S} - f_{I,z,S} \text{, and analogously for } G_z.$$

Or equivalently, since the surface-derived component and the subsurface accumulated component comprise the entirety of f_K,

$$f_{SUB,z,S} = f_{K,z,S} - f_{S30+G30,z,S} \text{, and the equivalent for } G_z.$$

Lipid concentrations at z. Since we have defined the fraction of a given sample S_z or G_z deriving from each of three sources (surface sinking lipids, subsurface sinking lipids, lipids produced *in situ*), we can calculate the total concentration of lipids at depth *z* contributed by each of the three sources. For S_z fractional contributions $f_{S30+G30,z,S}$, $f_{SUB,z,S}$, and $f_{I,z,S}$ are multiplied by the concentrations of lipids at depth *z* ($C_{z,S}$, in ng/L; Chapter 3, Figure 3.3) to derive the modeled absolute concentration of each constituent pool (and the equivalent for G_z).

Alternatively, we calculate the total remaining concentration of the original S_{30} and G_{30} separately at depth *z*, which must be summed from the concentrations of S_{30} and G_{30} present in both the S_z and G_z samples at depth $z>30$:

$$C_{S30,z} = f_{S30,z,S}C_{z,S} + f_{S30,z,G}C_{z,G} \text{ and}$$

$$C_{G30,z} = f_{G30,z,S}C_{z,S} + f_{G30,z,G}C_{z,G}.$$

For Model 1, $f_{G30,z} = f_{S30+G30,z}$ and $f_{S30,z}=0$. For Model 2, $f_{G30,z} = f_{S30+G30,z,G}$ and $f_{S30,z} = f_{S30+G30,z,S}$. For Model 3, $f_{G30,z}$ and $f_{S30,z}$ were defined previously.

The resulting concentrations reflect the total residual surface material from each size class remaining after degradation over z-z_{30} meters. We thus use these concentrations to calculate degradation constants for surface material (below).

Results and Discussion

The total fractional contributions of FA deriving from *in situ*, surface, and subsurface accumulated sources are presented in Figure 4.2 for each depth and for each of the three model calculations. The analogous calculated absolute abundances of FA from each of these three sources are presented in Figure 4.3, for each depth and for each of the three models. The mass-weighted ^{13}C signature of FA for the calculated *in situ* source *I* is presented in Figure 4.6. Figures 4.4 and 4.5 present the raw model output of FA distributions, individual-compound $\delta^{13}C$ values, and fractional contribution of calculated *in situ* components. Figure 4 shows the results for the G size class (a, glycolipids; b, phospholipids), while Figure 5 shows the results for the S size class (a, glycolipids; b, phospholipids)

Fatty acid distributions. All models suggest new fatty acids are produced throughout the water column. The most specific production pattern with depth appears to be the net increase in total new lipid in the mid-OMZ, although some production is detected across all samples and at all depths (Figure 4.2, 4.3). Interestingly, the magnitude of *in situ* production in glycolipids is similar at all low-oxygen depths outside of the core OMZ (all but 398 m; Figure 4.3a,b,c,g,h,i), with modeled concentrations for FA produced *in situ* of ~1 to 2 ng/L. In contrast, phospholipids from the S size class are the only sample class to show a consistent decrease in *in situ* production with depth, which is roughly conserved across all models (Figure 4.3j,k,l). In general, phospholipids from both size classes display higher proportions of overall modeled subphotic productivity but lower overall concentrations than the glycolipids in all models. Production of phospholipids appears to be highest in the uppermost OMZ in both size classes and all models (except mid-OMZ in Model 1 G phospholipids; Figure 4.2d,e,f,j,k,l). This large production pulse is propagated to lower depths in Models 2 and 3, thus leading to a proportionally large flux of accumulated subsurface phospholipids in these two models.

In the large size class (G), $C_{16:0}$ and $C_{18:0}$ dominate the *in situ* signature at many depths (Figure 4.4a,b). This signature is especially apparent among the phospholipids, where modeled *in situ* profiles at and below 170 m – but with the exception of the mid-OMZ sample – are dominated by $C_{16:0}$ and $C_{18:0}$ and have a $C_{18:0}$:$C_{16:0}$ ratio > 1. The modeled profiles also identify additional spatial heterogeneity in FA signatures that is attributable to *in situ* sources. The 274 m (upper OMZ) modeled FA distribution shows a distinct signature in the glycolipids (Figure 3a), with a high relative proportion of monounsaturated compounds ($C_{18:1\omega9}$, $C_{18:1\omega7}$, $C_{22:1}$) compared to other depths. In the phospholipids, the 398 m (mid-OMZ) and 730 m (lower oxycline) modeled FA distributions stand out as unique (Figure 4.3b), with large relative increases in $C_{16:1}$, $C_{17:1}$, $C_{18:1\omega7}$, and $C_{22:6}$; and $C_{14:0}$, $C_{16:1}$, and $C_{17:1}$, respectively. These depths could be hypothesized as locations where chemoautotrophic processes add new signatures to G. Supporting this interpretation is the relative increase in typical bacterially-produced FA:

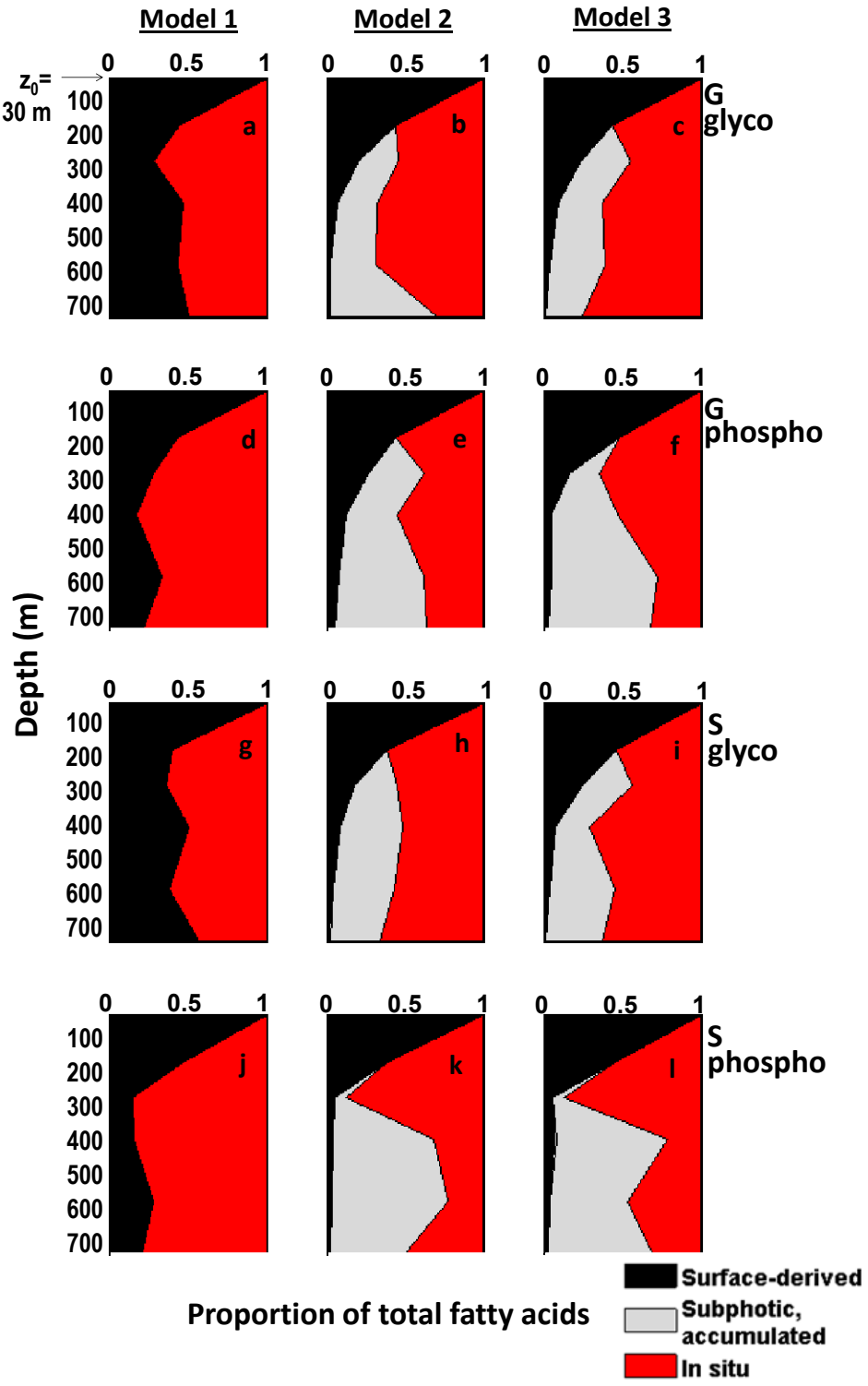

Figure 4.2. Predicted fractional composition of lipid samples from each of three models (Model 1, a,d,g,j; Model 2, b,e,h,k; Model 3, c,f,I,l), shown as the proportion of surface-derived, accumulated subphotic, and *in situ*-produced lipids that sum to the total content of fatty acids at each depth. Results are shown separately for the G size class (a-f) and the S size class (g-l), and within these, from the glycolipid (a-c, g-i) and phospholipid (d-f,j-l) fractions.

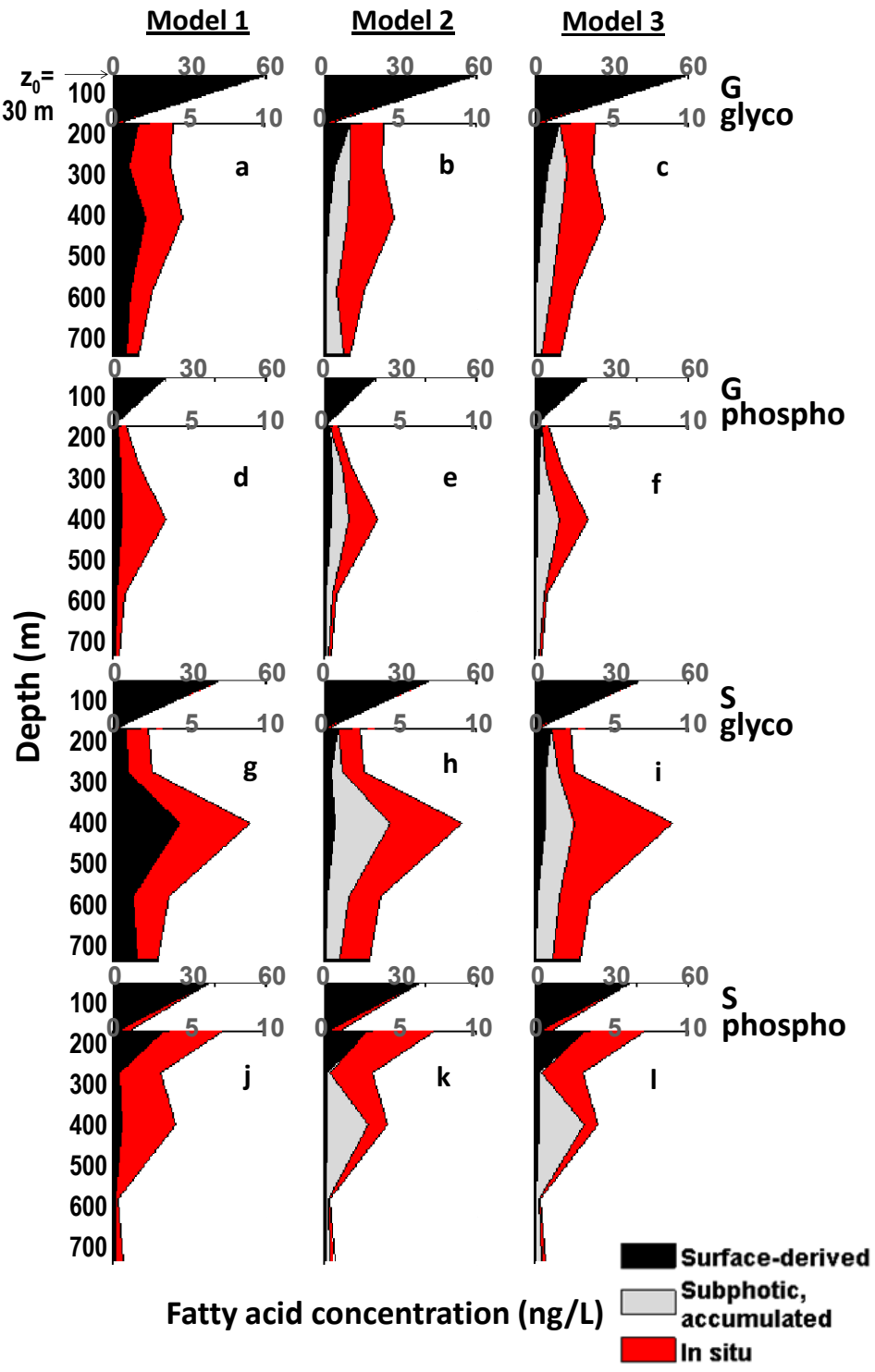

Figure 4.3. Predicted absolute composition of lipid samples from each of three models (Model 1, a,d,g,j; Model 2, b,e,h,k; Model 3, c,f,I,l), shown as the proportion of surface-derived, accumulated subphotic, and *in situ*-produced lipids that sum to the total measured concentration of fatty acids at each depth. Results are shown separately for the G size class (a-f) and the S size class (g-l), and within these, from the glycolipid (a-c, g-i) and phospholipid (d-f,j-l) fractions.

monounsaturated compounds, and specifically, $C_{17:1}$ and $C_{18:1\omega7}$. Particle-associated chemoautotrophy may account for the presence of these bacterial signatures in the G size class.

In all of the models, the differences between measured samples and the hypothesized sinking end-member sources are equated to *in situ* production (Figure 4.2, 4.3). The major assumption in this calculation is that we have characterized all possible end-members through the use of the different models. However, at least one observation suggests that all models must be missing an additional component of sinking, surface-derived material – possibly from very rapidly-sinking, larger (> 53 μm) particles. Evidence comes from the relatively large proportion of $C_{22:6}$ detected in both polarity fractions from the G size class in the mid-OMZ. Since polyunsaturated fatty acids require oxygen for biosynthesis (Russell and Nichols, 1999), $C_{22:6}$ would not be expected to be attributable to *in situ* production in the OMZ. But because this signature is "new", i.e., it is relatively more abundant in the OMZ than it is in overlying depths, the models must assign a significant proportion of $C_{22:6}$ to *in situ* production. The presence of excess $C_{22:6}$ points to an additional external source of FA that we did not capture at these sampling scales; or, it could reflect temporal variability in the FA distribution produced in the surface ocean and transported downward. In either case, Model 1 is the only formulation that could account for the "injection" of surface-derived material at a given depth *z* but not at depth *z*-1. Since large proportions of $C_{22:6}$ are not detected at depths between the surface and the core OMZ, the mechanistic processes represented by Model 1 thus must be at least partially correct. A mechanism for the processes in Model 1 would be consistent with the "particle injection" idea introduced in Chapter 3. We have postulated that fresh organic substrate produced by chemoautotrophs in the OMZ also could have a priming effect on the activity of heterotrophs, and they may opportunistically attack sinking aggregates or fecal pellets (e.g., Ward et al., 2009). The hydrolytic activity of mid-water column bacteria can support disaggregation of large particles in excess of *in situ* metabolic needs (e.g., Karl et al., 1988; Smith et al., 1992; Taylor et al., 2009). The disaggregation of large particles sinking from the surface ocean thus would

introduce fresh detrital OM into the suspended pools and could account for the unexpected presence of PUFAs in the core of the OMZ.

Considerable distinctions between models exist within the S size class, and derive largely from the strong zonation in the concentrations of glycolipids versus phospholipids in the upper water column. Glycolipids are abundant in the photic zone, but phospholipids become dominant just below, especially in the S size class (Chapter 3). However, the concentration of both glycolipids and phospholipids increases in the OMZ when compared to immediately overlying depths. Models 2 and 3, which allow for only sequential sinking and mixing processes, must attribute much of the large increase in glycolipids at the OMZ to *in situ* production, since the pool of potential detrital glycolipids decreases greatly between the surface ocean and underlying depths. Model 1 instead accounts for the increase in OMZ glycolipids with a large flux of directly-sinking surface-derived material, which presumably would escape remineralization through rapid packaging and sinking. Conversely, because Model 1 does not allow for sinking of subsurface lipids (e.g., the large pool of phospholipids in upper subsurface depths), it accounts for the increase in phospholipids the OMZ mostly through *in situ* production.

This last point is notable in terms of overall mass transfer down the water column. The upper subphotic sample (170 m) contains a high abundance of saturated FA in both size classes and polarity fractions (mostly $C_{16:0}$ and $C_{18:0}$). These saturated FA continue to dominate the overall signatures further down the water column. Because subphotic lipids are not "allowed" to sink by Model 1, it assigns these an *in situ* source. As a result, the Model 1 calculated *in situ* fatty acid distribution is almost entirely uniform over depth, because the model must newly produce this same signature at every depth (it cannot inherit it from above). This is particularly evident in phospholipids (Figure 4.5b). Models 2 and 3 instead can account for the persistence of prominent saturated components as detrital remnants from the upper water column. The preservation of signatures in sinking IPLs might be plausible even for slowly-settling particles due to the low oxygen concentrations.

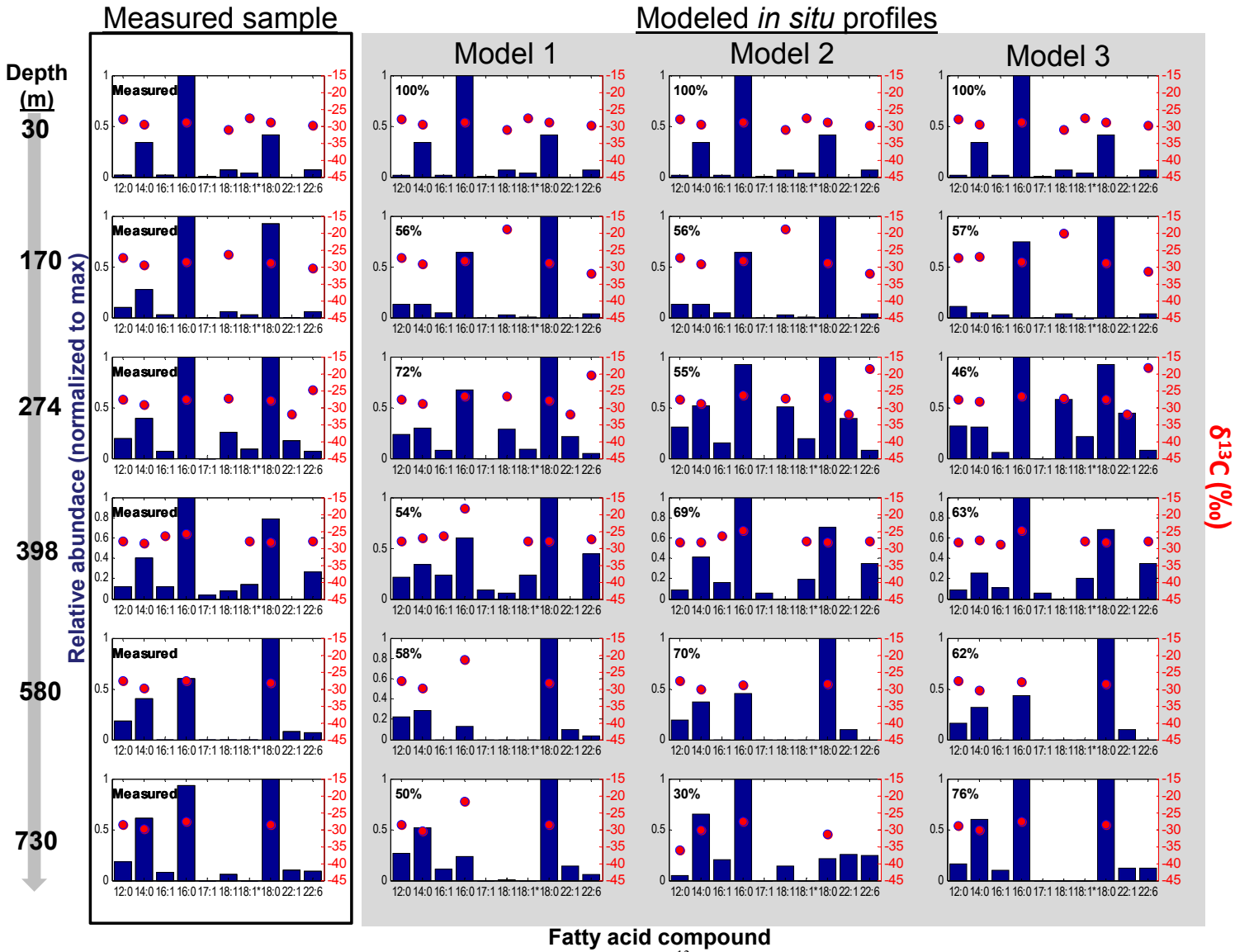

Figure 4.4a. Full model results for fatty acid distributions and individual-compound $\delta^{13}C$ values of *in situ* G size-class glycolipids (right three columns), compared to the measured samples (left column). Numbers in upper-left corners are the percentage of total lipids calculated as deriving from the *in situ* population for a given model. Fatty acid notation is (number of carbon atoms):(number of double bonds). "18:1" indicates 18:1ω9; "18:1*" indicates 18:1ω7.

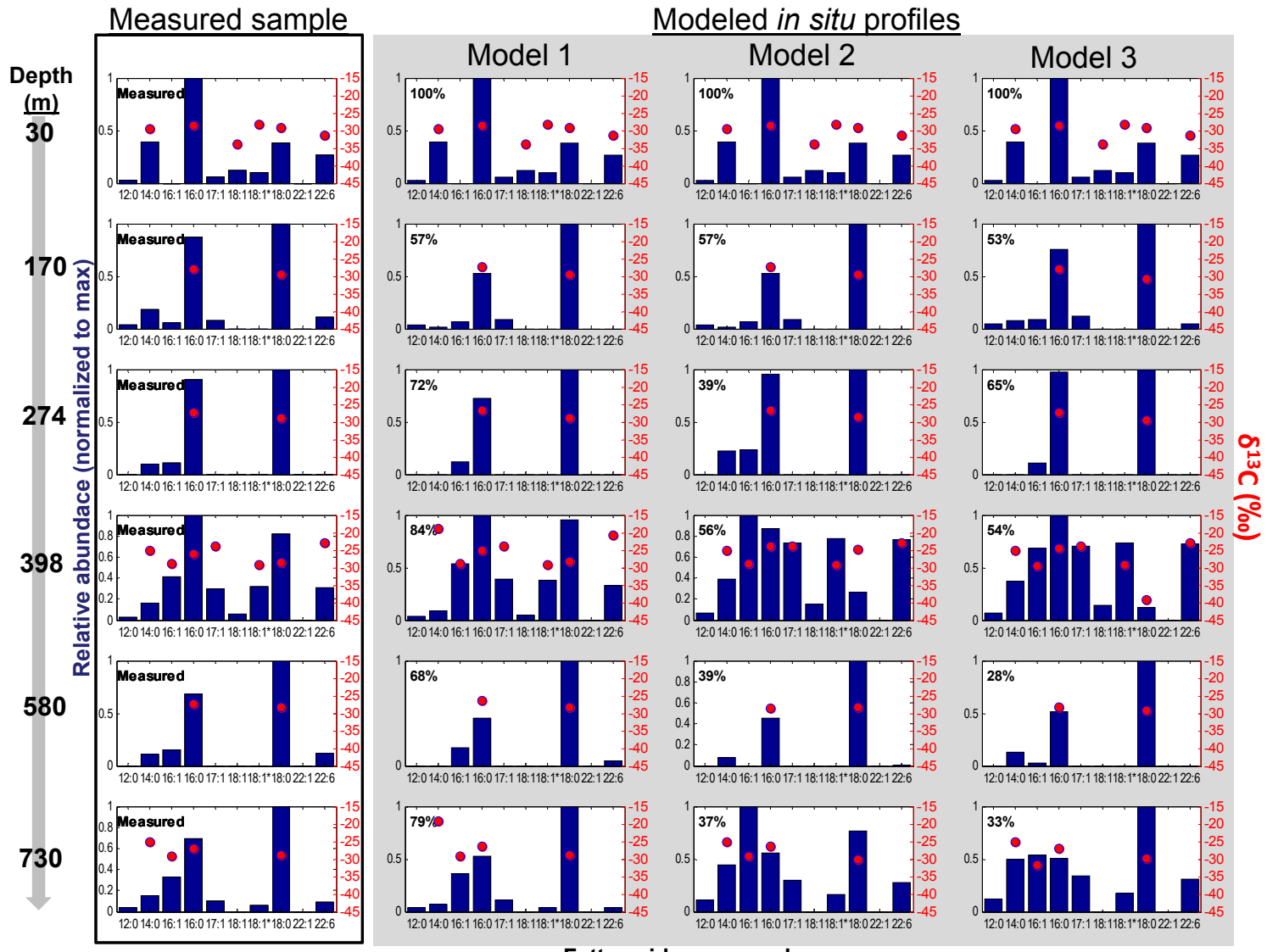

Figure 4.4b. Full model results for fatty acid distributions and individual-compound $\delta^{13}C$ values of *in situ* G size-class phospholipids (right three columns), compared to the measured samples (left column). Numbers in upper-left corners are the percentage of total lipids calculated as deriving from the *in situ* population for a given model. Fatty acid notation is (number of carbon atoms):(number of double bonds). "18:1" indicates 18:1ω9; "18:1*" indicates 18:1ω7.

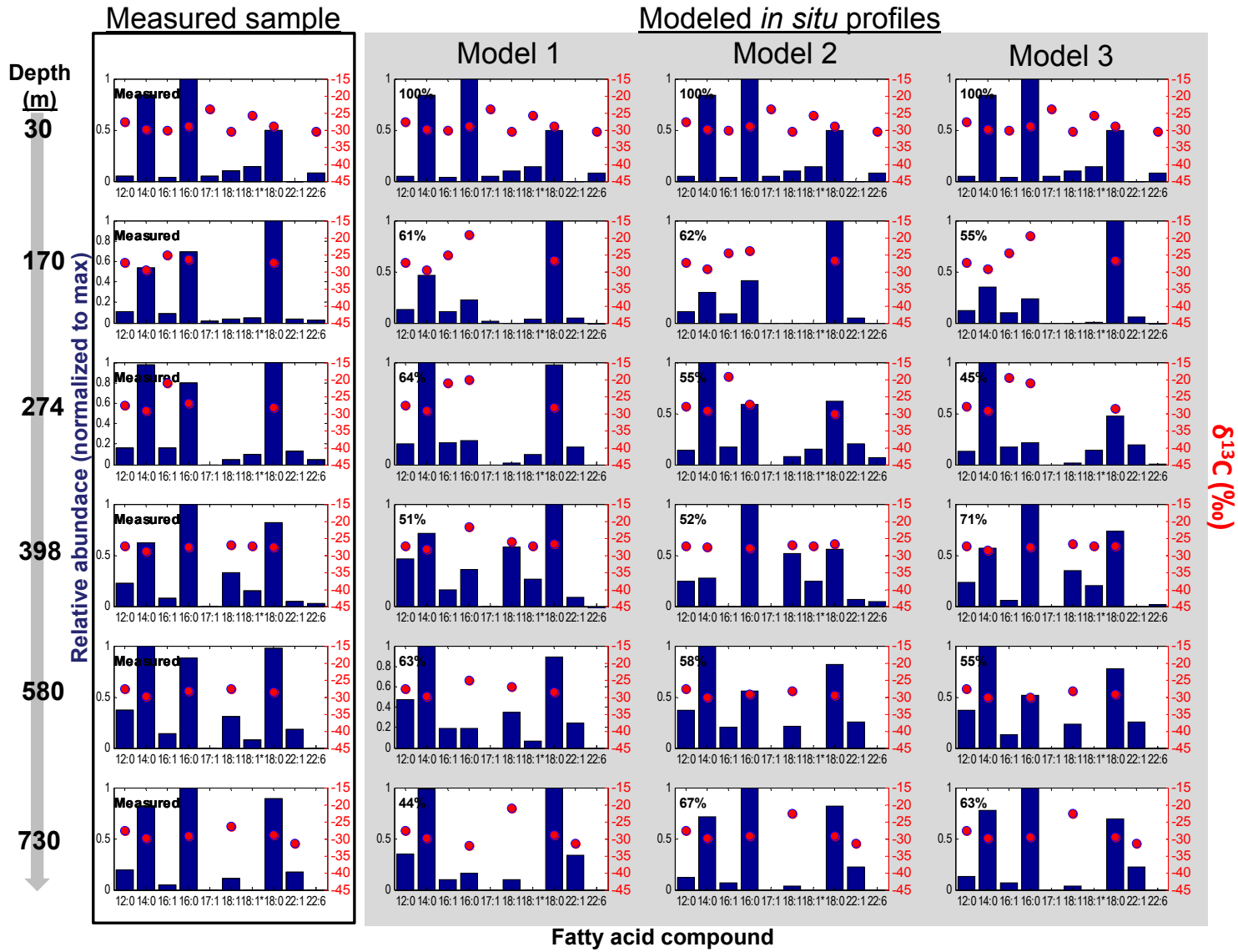

Figure 4.5a. Full model results for fatty acid distributions and individual-compound $\delta^{13}C$ values of *in situ* S size-class glycolipids (right three columns), compared to the measured samples (left column). Numbers in upper-left corners are the percentage of total lipids calculated as deriving from the *in situ* population for a given model. Fatty acid notation is (number of carbon atoms):(number of double bonds). "18:1" indicates 18:1ω9; "18:1*" indicates 18:1ω7.

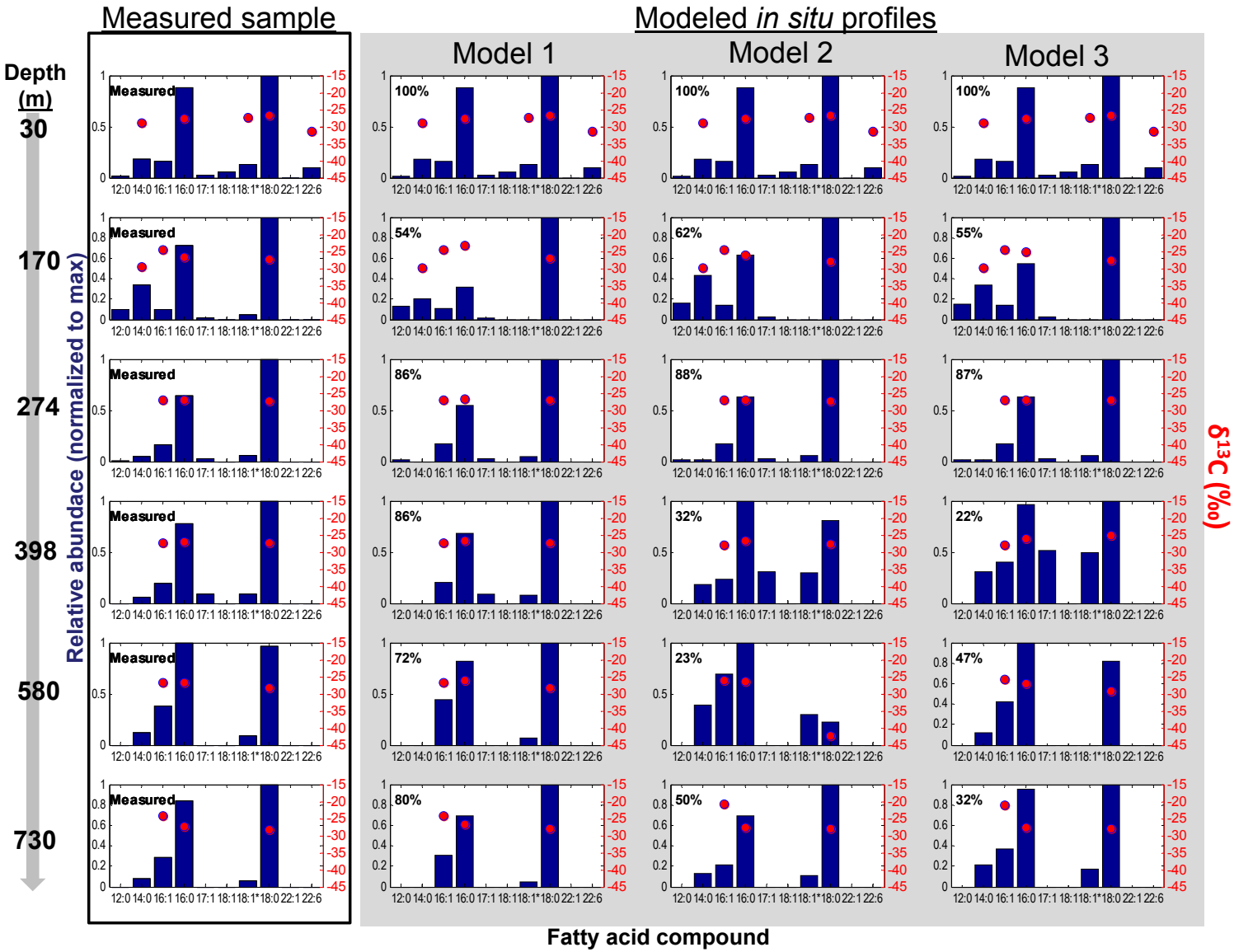

Figure 4.5b. Full model results for fatty acid distributions and individual-compound $\delta^{13}C$ values of *in situ* S size-class phospholipids (right three columns), compared to the measured samples (left column). Numbers in upper-left corners are the percentage of total lipids calculated as deriving from the *in situ* population for a given model. Fatty acid notation is (number of carbon atoms):(number of double bonds). "18:1" indicates 18:1ω9; "18:1*" indicates 18:1ω7.

In Models 2 and 3, distinct zonations arising within the *in situ* signature. In particular, among phospholipids from the S size class, a marked increase in $C_{16:1}$, $C_{17:1}$, and $C_{18:1\omega7}$ appears in the mid-OMZ (398 m). As with the G size class, these components represent plausible *in situ* bacterial contributions from the native low-oxygen community. These distinction arise in Models 2 and 3 because they attribute the otherwise overwhelming concentrations of $C_{16:0}$ and $C_{18:0}$ to inheritance from overlying depths.

Isotopic trends. The predicted ^{13}C content for total (mass-weighted) *in situ* lipids from the G size class at each depth is remarkably similar among the three models. Specifically, all models predict a particular enrichment in the ^{13}C content of *in situ* lipids with increasing depth, coming to a maximum in the mid-OMZ (Figure 4.6a,b). Values of $\delta^{13}C$ are ~3 to 4‰ more positive than those in the photic zone sample (~ -26 to -27‰, versus ~ -30‰ at 30 m). As models converge on this value for *in situ* production, it could be postulated to derive from some proportion of bacterial metabolisms unique to the OMZ; the agreement between models is closest in the G size-class phospholipids. However, if there is an unaccounted-for source of lipids

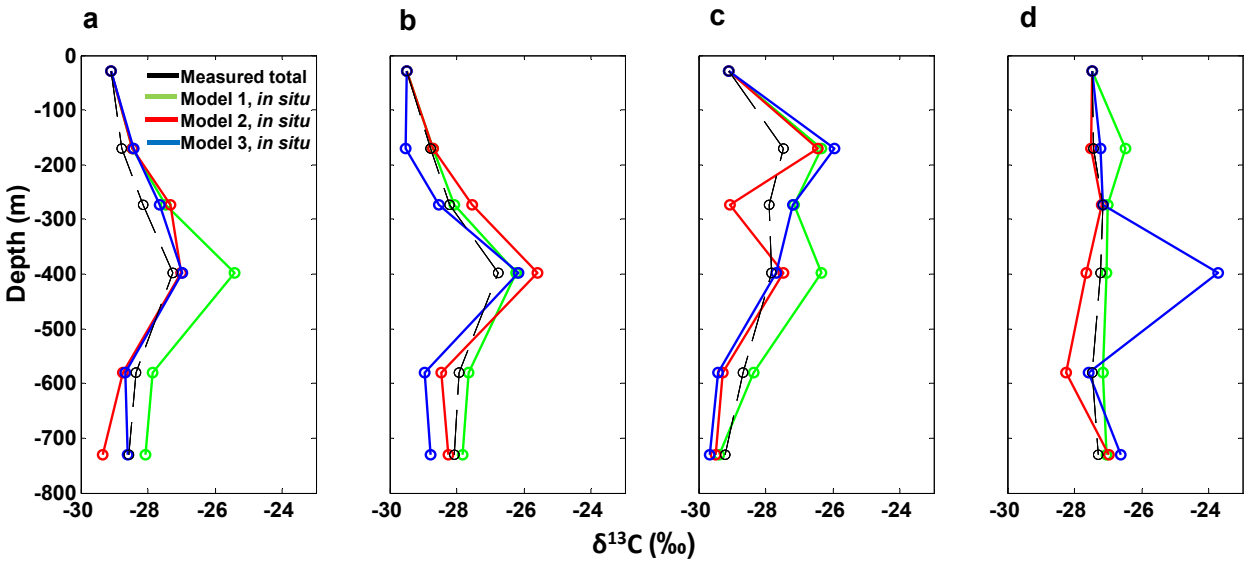

Figure 4.6. Mass-weighted $\delta^{13}C$ value of fatty acids from modeled *in situ* production in the ETNP water column (three models: green, red, blue), compared to mass-weighted $\delta^{13}C$ value of fatty acids in the total measured sample (black). a- G size-class glycolipids; b- G size-class phospholipids; c- S size-class glycolipids; d- S size-class phospholipids.

in the OMZ, the coupling of ^{13}C enrichment and elevated concentrations of PUFA could point instead to this exogenous source being enriched in ^{13}C.

The mass-weighted ^{13}C signature of the small size class shows more distinctions among the models. Model 3 generally predicts *in situ* $\delta^{13}C$ values distinct from Models 1 and 2. For instance, Model 3 predicts an isotopic enrichment in the mid-OMZ phospholipids that could relate to the ^{13}C enrichment seen in the G size class phospholipids at the same depth (Figure 4.6d). Models 1 and 2 instead predict a remarkably constant $\delta^{13}C$ value for the S phospholipids at all depths, varying only slightly from a value around -27‰, and virtually identical to the total measured sample. However, the mean $\delta^{13}C$ values for these S phospholipids were calculated from only three compounds. The individual-compound distributions and $\delta^{13}C$ values are distinct among the models, so the correspondence in mean values seems to be a coincidental result.

In the S glycolipids, all models predict a pronounced enrichment in the *in situ* ^{13}C content at 170 m in comparison to the signature at 30 m. Model 3 is again distinct in underlying waters, calculating a monotonic decrease in overall *in situ* lipid ^{13}C content over increasing depth. Models 1 and 2, in contrast, predict more varied *in situ* signatures, with comparative ^{13}C-depletion at 274 m and enrichment at 398 m. Model 2 displays the greatest variation (~ 2 to 3‰) over successive depths in the S glycolipids. Since Model 2 also treats the size classes individually over successive depths, it could be considered to represent the best approximation of absolute unique characteristics for each size class at each depth, especially if we consider the case in which our "sinking" sources instead could be representing similarities in communities at adjacent depths.

Model synthesis. A possible best-fit combination of models emerges from these results. Consistent with Model 1, POM produced in the photic zone may be either packaged and exported, or respired rapidly. This requires an active population of respiring heterotrophic organisms in the upper water column, which then dominate the signature of suspended lipids between the base of the photic zone and the upper OMZ. Because oxygen concentrations are low here, this upper subphotic signature (the 170 m sample) appears to be well-preserved as it settles

slowly through the OMZ. The physical processes represented by Model 2 and/or Model 3 are required to permit this material to sink. At redox boundaries in the OMZ, *in situ* chemoautotrophs and denitrifying heterotrophic Bacteria are the likely contributors of unique biomass and isotopic signatures to both the suspended and sinking pools. The contribution of this subphotic biomass to sinking flux again requires Model 2 and/or 3. A exogenous source of $C_{22:6}$ also appears to enter the OMZ, possibly deriving from large, sinking particles that are attacked and disaggregated by the *in situ* community. This source can be supported only by the proposed mechanism operating in Model 1, and only by assuming that our sinking source as estimated in Model 1 actually has failed to account for the largest, most rapidly-settling particles that may be richer in PUFAs.

Because of these complex processes, no single model can capture all of the mechanistic features necessary to fully characterize the biological sources of measured FA signatures. However, because the three models produce similar isotopic predictions (Figure 4.6), all models come to some of the same general conclusions: the OMZ is a major zone of new lipid production, and on average, these new lipids are ^{13}C-enriched. It would therefore be useful to use an external metric of *in situ* production to quantitatively test the details of the different model hypotheses. Concurrent measurements of water column bacterial activity are not available for this particular data set. In the future both biotic activity and nutrient availability would be useful to compare to the model predictions. However, we can postulate gross-scale effects due to redox zonation of the water column. Given the sharp contrast in oxygen concentration, and accompanying redox gradients in nitrogen speciation (Podlaska et al., *in press*), we expect that the composition of *in situ* communities will have distinct zones across depths in the water column. Presuming that these different bacterial communities produce different membrane lipids, strong redox-zonation also should be evident in the FA profiles of these *in situ* populations. Models 2 and 3 demonstrate such zonation of unique signatures by identifying the profiles within the upper- to mid-OMZ (274 m and 398 m) as being different from the detrital carryover of IPLs predicted from the slowly-settling particle classes (Figure 4.4a, 274 m, Models 2 and 3; Figure

4.4b, 398 m and 730 m, Models 2 and 3; Figure 4.5b, 398 m, Models 2 and 3). This is the best piece of evidence that aggregation and sinking of POM throughout the water column (Model 2 and/or 3) is a required mechanistic view of how carbon export occurs. By extension, similar mechanisms could explain how prokaryotic lipids from major redox boundaries throughout the water column can reach the sediments, even when these lipids are produced far from the photic zone depths where initial processes of large particle aggregation and export likely are concentrated. Well known examples of prokaryotic export include isorenieratene from anoxygenic photosynthesis (e.g., Repeta, 1993), tetraether lipids of ammonia-oxidizing archaea (e.g., Wuchter et al., 2006), and possibly ladderane lipids of anammox bacteria (e.g., Jaeschke et al., 2009). Our models suggest some mechanisms for how prokaryotic export might occur, and are consistent with the observational FA and $\delta^{13}C$ data.

A final question stimulated by the differences between these models is the capacity for mid-water column Bacteria to produce glycolipids. Few studies have addressed the IPL biosynthesis of subphotic Bacteria, and they indicate that they produce mostly phospholipids (e.g., Wakeham et al., 2012; Van Mooy and Fredricks, 2010). However, Model 1 predicts the most phospholipid production (versus detrital carryover) at subphotic depths, but it also predicts that the FA distribution and isotopic signature of subphotic production is almost uniform through the water column, even across strong redox gradients. The other models predict a more unique FA signature for phospholipids produced in the OMZ, but also require a large flux of sinking, detrital phospholipids and significant *de novo* production of glycolipids in the OMZ. If Models 2 and 3 are capturing an actual signature of glycolipid production by Bacteria in the mid-OMZ, this production could relate to the availability of phosphorus at these depths (e.g., Van Mooy et al., 2006; Popendorf et al., 2011).

Implications for degradation. An additional important outcome of our models is the ability to track the fate of surface-derived lipids separately from the accumulation of *in situ* lipids in deeper layers. Because the models separate the pools of *in situ* production, surface lipids, and other subphotic detritus (Figure 4.2, 4.3), they effectively isolate a degradation curve for surface-

derived lipids. We use this result to probe the degradation rate, and conversely, preservation potential of both classes of intact polar lipids in the water column. Importantly, our model formulations are independent of the measured absolute concentrations of compounds. Instead, we calculate the fraction of remaining surface-derived lipids according to fatty acid distributions and ^{13}C content, as described previously. From this, we back-calculate the concentration of remaining lipids; i.e., by multiplying the proportion f_K by the total concentration of IPL-FA measured at each depth, we can construct a modeled concentration curve for surface-derived lipids (Figure 4.7, black). Using a nonlinear least squares fitting routine to determine constants for power-law and exponential-decay curves that best fit these concentration profiles, we extract degradation constants for each polarity fraction within each water column size class (Table 4.1). Notably, for the ETNP raw (measured) data, the same curve-fitting routines cannot determine a decay profile, because large increases in FA concentrations cannot be fit with a decay function.

The degradation constants in Table 4.1 can be compared to other published attenuation profiles. The "*b*" (power-law) values for IPLs in Models 2 and 3 are higher (~1.7-2) than those typically observed for total POM sinking through the water column (~0.85-1.3; e.g., Martin et al., 1987; Lamborg et al. 2008; Table 4.1a). However, these values are quite similar to pigment degradation rates within particles sinking from the photic zone (e.g., up to 2.05, Lamborg et al., 2008; Figure 4.7). This lability is expected due to the presumed rapid remineralization of IPLs. Similarly, the calculated exponential decay constants "*k*" (units of depth^{-1}) can be compared to published inherent degradation rate constants (units of time^{-1}) for the molecules, by using a sinking rate to interconvert between time and depth. Derived values of *k* for the photic zone degradation model are also high (Table 4.1b), and could correspond either to slow sinking rates, high lability, or particularly intense aerobic reworking. Both *b* and *k* are lower for Model 1 than Models 2 or 3. This is expected, since Model 1 simulates a scenario in which surface material may sink and disaggregate without participating in intermediate – possibly more dynamic – processes of aggregation, disaggregation, and degradation. Interestingly, no significant differences in degradation rates are calculated for G versus S lipids, indicating that the

Power-law fit "b", where $C_Z = C_0 (Z / Z_0)^{-b}$

a. Photic zone lipids

	Model 1	Model 2	Model 3
G glyco	1.40	2.05	2.03
G phospho	1.13	2.08	1.71
S glyco	inf	2.12	2.03
S phospho	inf	1.67	1.71

c. Subphotic lipids

	Model 1	Model 2	Model 3
G glyco	inf	2.02	1.46
G phospho	inf	0.57*	3.83
S glyco	inf	1.0*	1.46
S phospho	inf	5.98	3.83

Exponential decay fit "k", where $C_Z = C_0 e^{-k (Z-Zo)}$

b. Photic zone lipids

	Model 1	Model 2	Model 3
G glyco	0.021	0.025	0.025
G phospho	0.012	0.028	0.020
S glyco	inf	0.027	0.025
S phospho	inf	0.019	0.020

d. Subphotic lipids

	Model 1	Model 2	Model 3
G glyco	inf	0.0079	0.0052
G phospho	inf	0.0019*	0.018
S glyco	inf	0.0032*	0.0052
S phospho	inf	0.028	0.018

Table 4.1. Calculated degradation constants (degradation as loss m^{-1}) for lipids deriving from surface (a,b: photic zone, 30 m) and upper subsurface (c,d: subphotic, 170 m) size classes/polarity fractions (G and S size classes, glyco- and phospholipid fractions). Power-law and exponential decay curves were fit to lipid concentrations derived from model results; constants for the best-fit curves (*b* and *k*, respectively in a,c; b,d) are shown. The models separate sinking surface material from *in situ* production in order to derive a degradation curve. *Indicates constants for which curve-fitting routine yielded low r^2 values (~0.5-0.7).

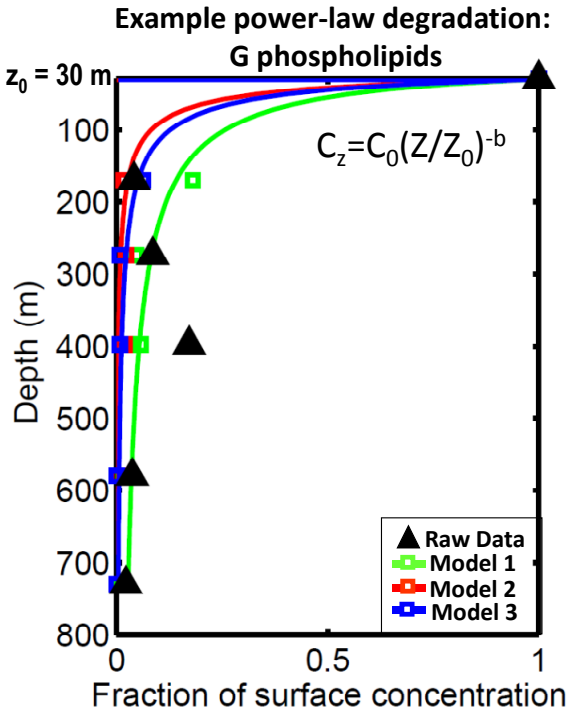

Figure 4.7. Modeled concentrations of sinking phospholipids deriving from the surface G size-class in the upper water column of the ETNP (colored squares), and best-fit power-law degradation profiles for each of three sinking models (colored lines). Here, z_0 refers to 30 m. Black triangles show measured total FA concentrations from each depth (raw data), whereas modeled concentrations have separated the likely surface-derived component from the total. The values for the exponent "b" in modeled degradation curves are 1.13, 2.08, and 1.71 for Models 1,2, and 3, respectively.

preservation potential might be uniform across size classes within the suspended pool. Alternatively, it may indicate that the exchange of material between G and S size-class particles is an important homogenizing process (Model 3).

Our results also may suggest secondary lessons about heterogeneity in the spatial distribution of glycolipids and phospholipids in the water column. There is no significant difference between our calculated degradation rates for glycolipids and phospholipids. This is unexpected, as there is debate as to whether inherent degradation rate constants for phospholipids are higher than for glycolipids. This question is difficult to evaluate, as the degradation experiments typically test ester-linked phospholipids versus ether-linked glycolipids – hence, differences in degradation cannot be attributed uniquely to the head groups (e.g., Harvey et al., 1986; Schouten et al., 2010; Logemann et al., 2011). It is possible that ester-linked glycolipids and phospholipids degrade at similar rates. But alternatively, the similarity in rates calculated from our models instead may reflect a curve-fitting artifact stemming from zonation in IPL production and cycling with depth. Here, glycolipid production is high in the euphotic zone, where phospholipid production is low. Because the most intense remineralization processes likely occur in the fully-oxygenated upper water column, the relative attenuation in the concentration of glycolipids is very high here. Best-fit degradation curves will be heavily influenced by this portion of the data with the greatest change in concentration, and thus will

predict high degradation rates for the glycolipids that may not actually relate to their inherent chemical lability in comparison to the phospholipids. Inclusion of the intense production and remineralization signatures in the photic zone previously has been identified as imparting a similar bias on derived degradation curves for total organic carbon in the water column (Buesseler and Boyd, 2009).

Instead, curves fit to data gathered only from subphotic depths may better represent the degradation patterns that are inherent to biochemical classes within a given whole-water column profile (e.g., Buesseler and Boyd, 2009). We therefore also formulate degradation curves for our modeled lipid pool starting with material present at our first measured depth below the photic zone (170 m; Table 4.1c,d). This might represent better the concentrations typically considered for OM "export" (usually defined as 100 m or the base of the euphotic zone). From this subphotic formulation, values of b for glycolipids (b = 1 to 2) are more similar to those expected for bulk OM (e.g., Martin et al., 1987; Lamborg et al. 2008). This is in contrast to the rates of degradation of phospholipids, which now are predicted to be more labile than glycolipids (b = ~4 to 6). For the rate constants k, values for phospholipids are on the order of those observed for total fatty acid degradation in oxic sediments (k ~0.02 day^{-1}, Canuel and Martens, 1996), if we assume a 1 m d^{-1} sinking rate for these samples. IPLs might be expected to degrade faster than total fatty acids, but here a slow apparent degradation rate for all IPLs could reflect enhanced preservation in the oxygen minimum zone (e.g., Van Mooy et al., 2002); and similar to b values, k values for glycolipids are even slower.

Possible signatures of recycling among fatty acids. The models described here assume that all fatty acid signatures arise from *de novo* biosynthesis within their respective biological sources. However, it may be possible that Bacteria in the marine water column assimilate free fatty acids in the environment as side chain components of IPLs in their cell membranes. Similar uptake of partially-degraded lipid side chains into cellular membranes has been suggested for benthic marine Archaea (Takano et al., 2010). If side-chain recycling were a significant mode of uptake in the water column, this would provide a mechanism by which apparent ^{13}C enrichment

in IPLs could progress during water column degradation. During partial degradation, FA with lighter carbon isotopic content might degrade more quickly, leaving the residual pool ^{13}C-enriched but available for assimilation into membranes. Recycling also could provide a mechanism by which IPL side chains could be altered to contain a greater proportion of saturated compounds. During uptake, Bacteria can transform unsaturated FA into saturated forms, as well as cleave carbon atoms from the side chain. If these altered FA were assimilated into the IPL structure of heterotrophic Bacteria, their lipid signature would include a relatively large amount of saturated components, and, through the effect described above, become relatively enriched in ^{13}C. Both ^{13}C enrichment and predominance of saturated FA (particularly $C_{16:0}$ and $C_{18:0}$) are observed at most subphotic depths in the ETNP. Both of these signatures could arise from intensive recycling of surface-derive material, which is typically rich in unsaturated FA. Production of excess saturated FA from partial degradation of IPLs and their unsaturated side-chains could also explain why the saturated and ^{13}C-enriched signature is common in both polar lipid classes.

Such recycling processes could be incorporated into interpretation of the model synthesis described above. High concentrations of phytoplanktonic biomass would be partially reprocessed in the upper water column, resulting in secondary, saturated membrane lipids. Due to the vanishing oxygen concentrations, these upper-water column, secondary lipids could be well-preserved during sinking, and in fact dominate the lipid signature in the upper OMZ. Then, breakdown of particles would introduce fresh, photic zone-derived OM into the mid-OMZ. Again, intense breakdown of this highly-unsaturated phytoplanktonic biomass would result in a dominant, secondary, saturated signature in lipids in the lower OMZ. This does not necessarily explain the presence and ^{13}C enrichment of PUFAs in the OMZ, however, suggesting there may still be a need for an exogenous source of sinking lipids. Finding more specific and quantitative evidence for such recycling processes thus could help refine models of OM cycling in the water column and could alter existing assumptions regarding the proportionality of dark ocean heterotrophic carbon uptake rates and biomass content.

Conclusions

The models we formulate here calculate the maximum sinking flux "allowable" by measured FA distributions and $\delta^{13}C$ values, within disparate conceptual frameworks. The general agreement between models indicates that intact polar lipids survive as sinking detrital components in all size classes, and that subphotic production also adds significantly to the sinking flux. Calculations of degradation rates from these model formulations indicate that intact polar lipids may survive transit through oxygenated waters with similar fidelity to pigment compounds. Degradation rates for glycolipids appear to slow significantly in low-oxygen waters, by as much as an order of magnitude. Notably, the strong zonation in the production of glycolipids and phospholipids – with the maximum glycolipid production in the upper photic zone and maximum phospholipid production in the lower photic zone – renders it difficult to calculate degradation rates in measured whole-water column concentration profiles of these two pools. However, with the aid of model deconvolution, we are able to separate the two polarity fractions and calculate their degradation rates separately as a function of depth.

All models also suggest the capacity for mid-water column Bacteria to produce glycolipids. Further independent evidence for the plausibility of this outcome would be significant, since production of glycolipids by Bacteria may relate to nutrient availability (e.g., Van Mooy et al., 2009; Popendorf et al., 2011). An additional consideration of heterotrophic recycling of partially-degraded fatty acid side chains also could help explain patterns highlighted in the models. This may be especially important to explain the prevalence of ^{13}C-enriched $C_{16:0}$ and $C_{18:0}$ in most subphotic depths. The capacity for mid-water column Bacteria to assimilate detrital free fatty acids into their membrane lipids is another stimulating question raised by these model results.

A mechanistic model framework appears to be a powerful means to resolve patterns in the sinking versus *in situ* production of lipids. With concurrent measurement of associated geochemical and biological variables, these models could be iteratively tested to determine a best-fit scenario of water column OM cycling. The next steps will be to combine lipid and

isotope data with these other measurements that are indicative of *in situ* metabolic activity. Regardless, all models are consistent with evidence from sedimentary biomarkers that bacterial lipids are incorporated into sinking particulate matter throughout the water column. A major implication is that sediments are not exclusive indicators of photic zone processes.

References

Bacon MP, Anderson RF (1982) Distribution of thorium isotopes between dissolved and particulate forms in the deep sea. *Journal of Geophysical Research,* **87**, 2045-2056.

Bacon M, Huh C, Fleer A (1985) Seasonality in the flux of natural radionuclides and plutonium in the deep Sargasso Sea. *Deep Sea Research Part A.,* **32**.

Buesseler KO, Boyd PW (2009) Shedding light on processes that control particle export and flux attenuation in the twilight zone of the open ocean. *Limnology and Oceanography*, **54**, 1210-1232.

Canuel EA, Martens CS (1996) Reactivity of recently deposited organic matter: degradation of lipid compounds near the sediment-water interface. *Geochimica et Cosmochimica Acta*, **60**, 1793-1806.

Cho B, Azam F (1988) Major role of bacteria in biogeochemical fluxes in the ocean's interior. *Nature,* **332**, 441-443.

Espinosa LF, Pantoja S, Pinto LA, Rullkotter J (2009) Water column distribution of phospholipid-derived fatty acids of marine microorganisms in the Humboldt Current system off northern Chile. *Deep-Sea Research II*, **56**, 1063-1072.

Fowler SW, Knauer GA (1986) Role of large particles in the transport of elements and organic compounds through the oceanic water column. *Progress in Oceanography,* **16**, 147-194.

Harvey HR, Fallon RD, Patton JS (1986) The effect of organic matter and oxygen on the degradation of bacterial membrane lipids in marine sediments. *Geochimica et Cosmochimica Acta*, **50**, 795–804.

Ingalls AE, Shah SR, Hansman RL, Aluwihare LI, Santos GM, Druffel ERM, Pearson A (2006) Quantifying archaeal community autotrophy in the mesopelagic ocean using natural radiocarbon. *Proceedings of the National Academy of Sciences of the United States of America,* **103**, 6442-6447.

Jaeschke A, Ziegler M, Hopmans EC, Reichart G-J, Lourens LJ, Schouten S, Sinninghe Damsté JS (2009) Molecular fossil evidence for anaerobic ammonium oxidation in the Arabian Sea over the last glacial cycle. *Paleoceanography*, **24**, 1-11.

Karl DM, Knauer GA, Martin JH (1988) Downward flux of particulate organic matter in the ocean: a particle decomposition paradox. *Nature,* **332**, 438-441.

Lamborg C, Buesseler K, Valdes J, Bertrand C, Bidigare R, Manganini S, Pike S, Steinberg D, Trull T, Wilson S (2008) The flux of bio- and lithogenic material associated with sinking particles in the mesopelagic "twilight zone" of the northwest and North Central Pacific Ocean. *Deep Sea Research Part II: Topical Studies in Oceanography,* **55**, 1540-1563.

Lichtfouse E, Eglinton T (1995) 13C and 14C evidence of pollution of a soil by fossil fuel and reconstruction of the composition of the pollutant. *Organic Geochemistry,* **23**, 969-973.

Lipp JS, Morono Y, Inagaki F, Hinrichs K-U (2008) Significant contribution of Archaea to extant biomass in marine subsurface sediments. *Nature,* **454**, 991-994.

Martin JH, Knauer GA, Karl DM, Broenkow WW (1987) VERTEX: carbon cycling in the northeast Pacific. *Deep Sea Research Part I,* **34**, 267-285.

Niggemann J, Schubert CJ (2006) Fatty biogeochemistry of sediments from the Chilean coastal upwelling region: sources and diagenetic changes. *Organic Geochemistry*, **37**, 626-647.

Pearson A, Eglinton TI (2000) The origin of *n*-alkanes in Santa Monica Basin surface sediment: a model based on compound-specific $\Delta^{14}C$ and $\delta^{13}C$ data. *Organic Geochemistry*, **31**, 1103-1116.

Podlaska A, Wakeham SG, Fanning KA, Taylor GT. Microbial community structure and productivity in the oxygen minimum zone of the Eastern Tropical North Pacific. *Deep-Sea Research I*, in press.

Popendorf KJ, Lomas MW, Van Mooy BAS (2011) Microbial sources of intact polar diacylglycerolipids in the Western North Atlantic Ocean. *Organic Geochemistry,* **42**, 803-811.

Reemtsma T, Ittekkot V (1992) Determination of factors controlling the fatty acid composition of settling particles in the water column by principal-component analysis and their quantitative assessment by multiple regression. *Organic Geochemistry*, **18**, 121-129.

Repeta DJ (1993) A high resolution historical record of Holocene anoxygenic primary production in the Black Sea. *Geochimica et Cosmochimica Acta*, **57**, 4337-4342.

Russell NJ, Nichols DS (1999) Polyunsaturated fatty acids in marine bacteria- a dogma rewritten. *Microbiology,* **145**, 767-779.

Schouten S, Middelburg JJ, Hopmans EC, Sinninghe Damsté (2010) Fossilization and degradation of intact polar lipids in deep subsurface sediments: a theoretical approach. *Geochimica et Cosmochimica Acta*, **13**, 3806-3814.

Sheridan C, Lee C, Wakeham S (2002) Suspended particle organic composition and cycling in surface and midwaters of the equatorial Pacific Ocean. *Deep Sea Research I,* **49**, 1983-2008.

Sinninghe Damsté JS, Strous M, Rijpstra IC, Hopmans EC, Geenevasen JAJ, van Duin ACT, van Niftrik LA, Jetten MSM (2002) Linearly concatenated cyclobutane lipids form a dense bacterial membrane. *Nature*, **419**, 708-712.

Takano Y, Chikaraishi Y, Ogawa NO, Nomaki H, Morono Y, Inagaki F, Kitazato H, Hinrichs K-U, Ohkouchi N (2010) Sedimentary lipids recycled by deep-sea benthic archaea.

Nature Geoscience, **3**, 858-861.

Van Mooy BAS, Keil RG, Devol AH (2002) Impact of suboxia on sinking particulate organic carbon: Enhanced carbon flux and preferential degradation of amino acids via denitrification. *Geochimica et Cosmochimica Acta,* **66**, 457-465.

Van Mooy BAS, Fredricks HF, Pedler BE, Dyhrman ST, Karl DM, Zoblízek M, Lomas MW, Mincer TJ, Moore LR, Moutin T, Rappé MS, Webb EA (2009) Phytoplankton in the ocean use non-phosphorus lipids in response to phosphorus scarcity. *Nature*, **458**, 69-72.

Van Mooy BAS, Fredricks HF (2010) Bacterial and eukaryotic intact polar lipids in the eastern subtropical South Pacific: Water-column distribution, planktonic sources, and fatty acid composition. *Geochimica et Cosmochimica Acta,* **74**, 6499-6516.

Wakeham SG, Lee C, Hedges JI, Hernes PJ, Peterson ML (1997) Molecular indicators of diagenetic status in marine organic matter. *Geochimica et Cosmochimica Acta*, **24**, 5363-5369.

Wakeham SG, Turich C, Schubotz F, Podlaska A, Li XN, Varela R, Astor Y, Sáenz JP, Rush D, Sinninghe Damsté JS, Summons RE, Scranton MI, Taylor GT, Hinrichs K-U (2012) Biomarkers, chemistry and microbiology show chemoautotrophy in a multilayer chemocline in the Cariaco Basin. *Deep Sea Research I,* **63**, 133-156.

Wuchter C, Schouten S, Wakeham SG, Sinninghe Damsté JS (2006). Archaeal tetraether membrane lipid fluxes in the northeastern Pacific and the Arabian Sea: implications for TEX_{86} paleothermometry. *Paleoceanography,* **21**, 1-9.

Chapter 5

Inverse carbon isotope patterns of lipids and kerogen record heterogeneous primary biomass

This chapter has been published: Close HG, Bovee R, Pearson A (2011) Inverse carbon isotope patterns of lipids and kerogen record heterogeneous primary biomass. *Geobiology*, **9**, 250-265.

Abstract

Throughout the Proterozoic $\delta^{13}C$ values for preserved *n*-alkyl lipids are more positive than for syngenetic kerogen. This pattern is the inverse of biosynthetic expectations. It has been suggested that this isotopic inversion results from selective preservation of lipids from ^{13}C-enriched heterotrophic populations, while the bulk of kerogen derives from primary producers. Here we formulate a degradation model to calculate the ^{13}C content of sedimentary total organic carbon (TOC) and lipid. The model addresses two scenarios. The first scenario explores preferential preservation of heterotrophic lipid, thereby quantifying the existing hypothesis. In the second we suggest that an inverse signature could be the result of prokaryotic phytoplankton contributing the majority of the total ecosystem biomass. Photosynthetic prokaryotes bearing a relative ^{13}C enrichment would contribute much of the resulting preserved lipids, while primary eukaryotic biomass would dominate the TOC. We find that our hypothesis of a mixed primary producer community generates inverse isotopic patterns while placing far fewer requirements on specific degradation conditions. It also provides a possible explanation as to why there are large variations in the ^{13}C content of the isoprenoid lipids pristane and phytane relative to *n*-alkyl lipid, while the difference between *n*-alkyl lipid and kerogen is more constant. Our results suggest that the disappearance of the inverse ^{13}C signature in the late Ediacaran is a natural consequence of the fundamental shift to oceans in which export production has a higher ratio of eukaryotic biomass.

Introduction

Organic matter in Precambrian marine deposits consistently has a carbon isotope relationship between *n*-alkyl lipids and total organic carbon (TOC) that is the reverse of what is observed throughout most of the Phanerozoic (Logan et al., 1995; Brocks et al., 2003b). Nearly all sedimentary rocks from the Phanerozoic have the isotopic ordering expected from direct biosynthetic products of Calvin-Benson-Bassham (Rubisco-utilizing) photoautotrophs (Figure 5.1a), with average kerogen or TOC enriched in ^{13}C relative to bitumen; and within bitumen, isoprenoid lipids are ^{13}C-enriched relative to *n*-alkyl lipids (Hayes et al., 1983; Logan et al., 1997; Hayes, 2001). These compound classes in Proterozoic marine deposits consistently show the opposite ordering (Figure 5.1b). Bitumen or extractable *n*-alkyl lipids (specifically, *n*-alkanes) are the most ^{13}C-enriched fraction; and although isoprenoids such as pristane and phytane can be ^{13}C-enriched or depleted relative to kerogen, consistently they are ^{13}C-depleted relative to *n*-alkyl lipids. The inverse pattern between *n*-alkyl lipids and kerogen disappears in the late Ediacaran (Logan et al., 1995; Logan et al., 1997; Höld et al., 1999; Kelly, 2009), but temporarily returns in the upper Permian where there is geochemical evidence for widespread ocean anoxia and photic zone euxinia (Grice et al., 1996; Schwab and Spangenberg, 2004; Grice et al., 2005; Hays, 2010; Nabbefeld et al., 2010). Inverse ordering of *n*-alkyl lipids versus isoprenoids also occurs in the Phanerozoic (upper Ordovician: Guthrie, 1996; upper Devonian: Joachimski et al., 2001; lower Jurassic: Schwab and Spangenberg, 2007; upper Jurassic: van Kaam-Peters et al., 1997; Dawson et al., 2007; Eocene-Oligocene: Hollander et al., 1993). However, most of these additional instances from the Phanerozoic are not accompanied by data indicating inverse ordering of *n*-alkyl lipids versus TOC.

Although the Precambrian isotope pattern is termed "inverse" because it is the opposite of our biosynthetic understanding, most of Earth history records this pattern. Marine deposits from the middle Proterozoic (~1055 Ma) through the late Neoproterozoic exclusively show

inverse ordering. Additional observations suggest the same signature also was prevalent in the Archean (Brocks et al., 2003a; Brocks et al., 2003b). The Proterozoic data span marine deposits on several modern-day continents and thus potentially can be thought to constitute a global oceanic signature, although Precambrian deposits in general are limited to shelf-slope or epicontinental marine facies.

Before the advent of compound-specific isotope analysis, comparison of Proterozoic bitumens and kerogens exposed the inverse pattern, but it was thought to reflect contamination (Hoering, 1965; Hoering, 1967). Further measurements showed the inverse signature was syngenetic (Hieshima, 1992); and subsequently, compound-specific data revealed the ^{13}C-enriched *n*-alkyl pool within the bitumens (Logan et al., 1995). These early reports of an inverse isotope signature for the Proterozoic focused on the consistency of positive values of $\Delta\delta = \Delta\delta_{n\text{-alkyl}} - \delta_{\text{kerogen/TOC,}}$ which average ~1.5‰ (Figure 5.1b) (Hieshima, 1992; Logan et al., 1995; for discussion of terminological use of kerogen versus TOC, see Chapter 5 Appendix). Isotopic ordering of *n*-C_{17} alkane versus kerogen, pristane versus kerogen, and the average of *n*-C_{17} and *n*-C_{18} alkanes versus pristane all upheld the inverse relationship. Subsequent reports have used these diagnostic compounds, as well as phytane, as the standard methods to monitor inverse isotope signatures (Logan et al., 1997; Kelly, 2009).

Despite the geologic importance of these patterns, a satisfactory explanation remains elusive. Logan et al. (1995) suggested that a specific relationship between organic matter source and degradation existed in the Precambrian. Pristane and kerogen were proposed to derive mostly from photosynthetic species, thereby carrying the isotopic signature of carbon fixation. While kerogen may form from organic matter that survives remineralization due to biochemical resistance to degradation, association with ballast or mineral surfaces, or geopolymerization or reduction reactions (*e.g.*, Hebting et al., 2006; recent review by Zonneveld et al., 2010), the Logan et al. (1995) hypothesis specifically invokes resistant algal biopolymer. After intense

microbial heterotrophy in a water column largely devoid of eukaryotic grazers, *n*-alkyl lipids from primary producers were proposed to be replaced by *n*-alkyl lipids from heterotrophs. Heterotrophs would have been enriched in ^{13}C by the fractionation associated with intense respiration through multiple trophic levels (DeNiro and Epstein, 1978). Consequently, preserved TOC would consist of a mixture of primary kerogen and secondary lipid. With the diversification of multicellular Eukaryotes across the Cambrian boundary, an increase in the flux of faster-sinking particles (fecal pellets or increased biomineralization) concomitantly would increase the preservation potential of total primary material (including primary lipids) while reducing the intensity of water-column heterotrophy. This would decrease the degree of ^{13}C-enrichment in lipids from microbial heterotrophs, as well as the quantity of these lipids, eliminating the inverse isotope pattern.

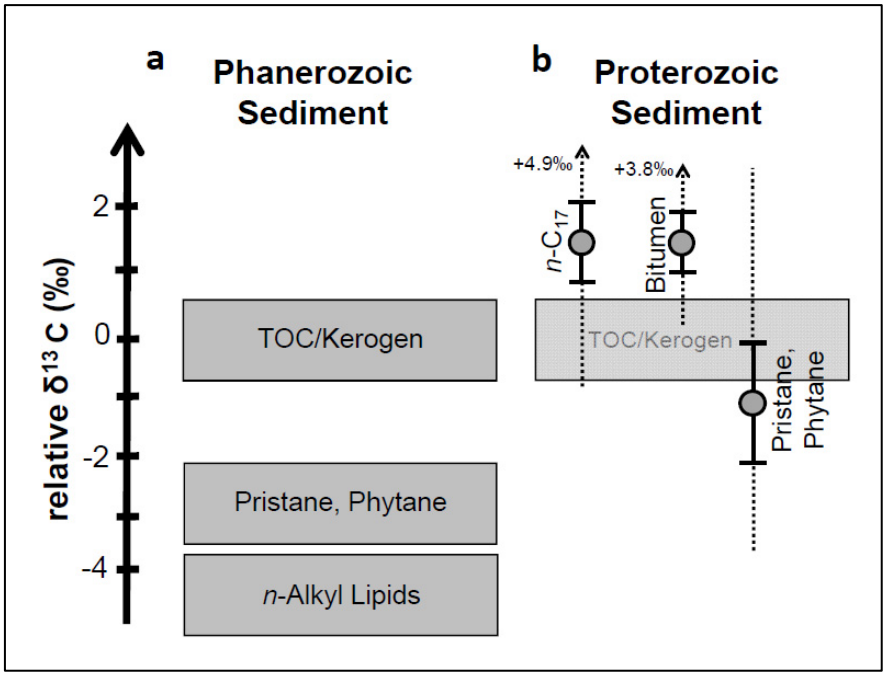

Figure 5.1. (a) Relative values of $\delta^{13}C$ for organic components in typical Phanerozoic sediments, in agreement with expected biochemical patterns of fractionation (Logan et al., 1995; Hayes, 2001). (b) Relative values of $\delta^{13}C$ for lipids relative to TOC or kerogen in Proterozoic sediments, averaged from Hieshima (1992) and Logan et al. (1995, 1997). Values show average and standard deviation (1σ), and the total range of individual values is shown with dotted lines.

The central premise of Logan et al. (1995) is that intense heterotrophy occurred in a water column dominated by small, slowly-sinking cells. However, a persistent question remains as to how lipids from heterotrophs could dominate the total preserved lipids, especially considering that their biomass production rate can only constitute a fraction of total photosynthesis (*e.g.,* del Giorgio and Cole, 1998), and both primary and secondary cells would be subjected to degradation in the same water column. Here we quantitatively model the contributions of primary and heterotrophic organisms to TOC and lipids to answer this question. Our results suggest that the most physically-plausible scenarios that generate inverse ^{13}C signatures are consistent with the origin of the ^{13}C enrichment within primary biomass. The disappearance of the inverse ^{13}C signature in the late Ediacaran would then represent a fundamental shift in the marine primary producer community, while episodic returns to inverse ordering in the Phanerozoic would signal a temporary return to higher prokaryote:eukaryote ratios, similar to Proterozoic oceans.

Heterotrophic enrichment scenario

To yield a carbon isotopic relationship in which preserved *n*-alkyl lipids are ^{13}C-enriched relative to TOC (positive value of $\Delta\delta_{n\text{-alkyl–TOC}}$), the lipid must carry an *integrated* isotopic value that is enriched in ^{13}C sufficiently to overcome what usually is a ~4.5‰ ^{13}C-depletion for lipid biosynthetic products relative to biomass (*e.g.,* Teece et al., 1999; Hayes, 2001). Accordingly, a model that considers the degradation rates (*K*) of all biomolecular classes to be equal cannot yield sufficient ^{13}C partitioning into net preserved lipids to produce a positive value of $\Delta\delta_{n\text{-alkyl-TOC}}$ (Chapter 5 Appendix, Case 1). Therefore, the Logan et al. (1995) explanation implicitly requires different degradation potentials for different classes of biological products. Namely, recalcitrant carbon deriving from primary photosynthetic sources must comprise the majority of kerogen. Lipids also must be resistant to degradation, because they are presumed to

accumulate during late-stage processing. They must outlast the more labile components of biomass during diagenesis.

Following the models of several authors, we assume that both total organic matter and individual compound classes degrade following pseudo-first-order kinetics (Westrich and Berner, 1984; Middelburg, 1989). Since the sedimentary record preserves organic matter after some total extent of degradation, we use "*d*" (degradation) rather than "*t*" (time) to represent the net decay in a particular environment. The parameter *d* is similar conceptually to the idea of total exposure (Hartnett et al., 1998; Hedges et al., 1999), and thus it is not strictly temporal but also can encompass environmental or biological factors relating to degradation intensity (*e.g.* Middelburg et al., 1993; Rothman and Forney, 2007). It is well established that organic molecular classes degrade at different rates, typically $K_{biopolymer} < K_{lipid} < K_{carbohydrate} \sim K_{protein} << K_{nucleic\ acid}$ (Henrichs, 1992; Harvey et al., 1995; Harvey and Macko, 1997; Grossi et al., 2001; Versteegh and Zonneveld, 2002; Nguyen et al., 2003). For the model, we consider the resistant (*R*) fraction to be equivalent in relative reactivity to biopolymer, but not necessarily composed exclusively or specifically of chemically resistant biomolecules such as algaenan, which may be less common than previously thought (Kodner et al., 2009). We aggregate carbohydrate, protein, and nucleic acid as "labile biomass" (*B*); and we treat lipid separately (*L*). The rate constants K_R, K_L, and K_B are modeled accordingly such that $K_R < K_L < K_B$ (Table 1), with a minimum K_L/K_R constrained by the requirement of retaining at least 1 ppm lipid preserved within the sedimentary organic pool (details in Chapter 5 Appendix).

The model also requires assessment of carbon isotopic enrichment within the microbial food web. Critically, microbes do not feed by phagocytosis. They subsist on substrates generally < 1000 Da, and a given organism may consume carbon deriving from lysis of multiple cells of different trophic histories (*e.g.,* Jahnke and Craven, 1995). We introduce the concept here of "molecular trophic level" rather than "species trophic level" to clarify that higher trophic-level

carbon is simply the net material which has been processed (incorporated or exuded) before respiration to CO_2. Thus, the net trophic hierarchy of a mixed microbial community is also a function of "*d*". Consequently, trophic levels are not necessarily separated in time or space, and the net trophic level *N* is a parameter of the community, not of a single cell.

With these considerations, we incorporate differential degradation rates K_R, K_L, and K_B to calculate the total preserved organic carbon (P) as a function of *d*

$$P(d) = \sum P_N(d) \tag{1}$$

and the isotopic composition of this organic carbon (P) and of lipid (L)

$$\delta_P(d) = \sum \frac{P_N(d)\delta_{P_N}(d)}{P(d)} \tag{2}$$

$$\delta_L(d) = \sum \frac{L_N(d)\delta_{\overline{L}}(d)}{L(d)} \tag{3}$$

for two scenarios: uniform exposure *d*, and attenuated exposure *D*(*d*, *N*), in which there is less degradation at higher levels of *N*. Full details of all derivations and equations are given in the Chapter 5 Appendix.

Uniform degradation of all trophic levels. To calculate the amount and isotopic signature of preserved organic matter, it is partitioned into material that remains unaltered from the original primary pool (P_0) and material that builds up from each subsequent addition of heterotrophic biomass (P_N). Photosynthetic biomass is modeled in three components: *R*, *L*, and *B*. Heterotrophic cells are modeled as containing only *L* and *B*, since bacteria are not known to produce chemically resistant biopolymers comparable to those observed in eukaryotic algae (Allard et al., 1997). *E* is the overall heterotrophic efficiency (fraction of carbon incorporated into biomass; 1-*E* = fraction respired as CO_2).

The isotopic signature of organic matter preserved in higher trophic levels ($N > 0$) depends on the isotopic value inherited from the degraded portion of the previous trophic level,

and it subsequently is enriched by a weighted standard effect of heterotrophy, $h(1\text{-}E)$ (h = 1.5‰; DeNiro and Epstein, 1978). Summing weighted isotopic contributions over all trophic levels, according to Equations 2 and 3 above, yields the "sedimentary" isotopic values for TOC and lipids, where lipid in each trophic level (δ_{LN}) is correspondingly offset by the biosynthetic fractionation, ε_L = 4.5‰.

Attenuated degradation. A modified model captures the possibility of shorter exposure times for later molecular trophic levels, N. This simulates potential decreases in the degradation probability due to differences in physical location or environmental conditions; *e.g.*, biosynthesis in sediments rather than in the water column, exposure of higher trophic levels to lower-oxygen environments, variations in rate of lysis, or decreases in reactivity due to geopolymerization and/or reduction via sulfur species (*e.g.*,. Hebting et al., 2006). We model this effective exposure (D) for a given trophic level as an exponentially-decreasing fraction of the maximum exposure: $D(d,N) = de^{-\zeta N}$, where the maximum (d) is experienced only by primary organic matter. Examples of scaling coefficients (ζ) and their influence on effective exposure time are shown in the Chapter 5 Appendix, Figure A5.2.

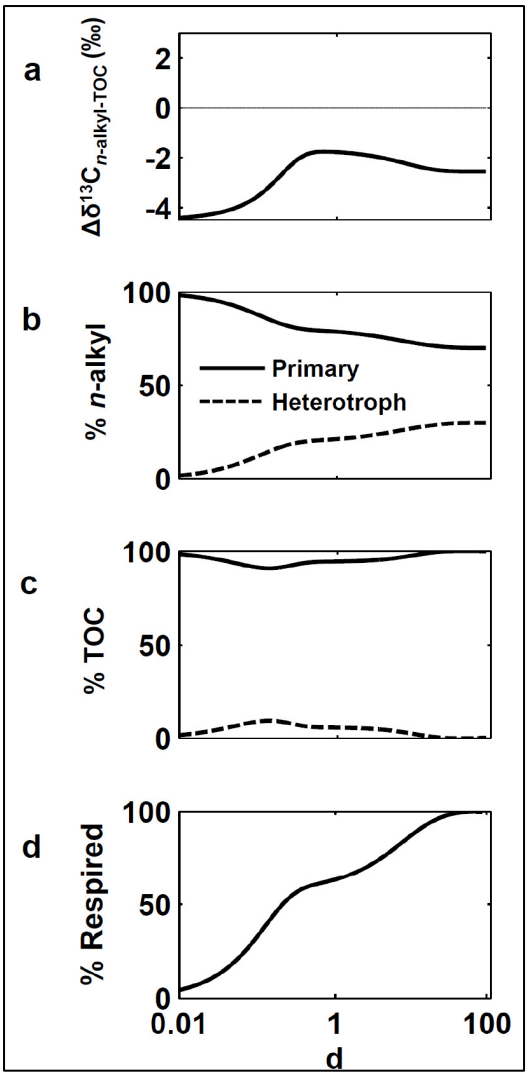

Figure 5.2. Results of Logan-type scenario with d constant for all trophic levels. **(a)** Dependence of $\Delta\delta_{n\text{-alkyl–TOC}}$ on overall degradation, d. **(b, c)** Contributions of primary and heterotrophic populations to final preserved lipid and TOC. **(d)** Net respiration of primary productivity as a function of d.

Parameter values. Both the constant-degradation and attenuated-degradation models were

evaluated with regard to their ability to generate a positive value of $\Delta\delta_{n\text{-alkyl–TOC}}$. The maximum possible $\Delta\delta$ for a given parameterization was calculated using the following three constraints on the terminal level of *d*: (*i*) total preserved organic matter is not less than 0.01% of the original amount of photosynthetic product, comparable to intensive degradation regimes in the modern ocean (Hedges and Keil, 1995; Martin et al., 1987; Wakeham et al., 1997), and (*ii*) total preserved lipid is at least 1 ppm of the total sedimentary organic matter, such that enough would remain for lipid extraction and identification (includes both kerogen-bound and extractable lipid; see Chapter 5 Appendix). We define these conditions as terminal burial. Finally: (*iii*) the total number of trophic levels through which the organic matter is processed increases until the available organic substrate from the preceding trophic level has decreased to 0.00001% of the original photosynthetic product, a value found to consistently approximate food chains that run to infinity. We define this as terminal heterotrophy, and it was found to reach a maximum of 14 trophic levels at E=0.3, with the actual number depending on degree of exposure (*d*) and value of ζ. Model runs were terminated when one of the three boundary limits was reached. The models were initiated with the values shown in Table 1.

Results of heterotrophic enrichment scenarios

Constant *d*. A scenario of intense microbial reworking in the surface ocean would be expected to result in uniform (and high) degradation of organic matter through all trophic levels. Our model shows that such intense processing restricts the ability to create a positive value of $\Delta\delta_{n\text{-alkyl–TOC}}$ (Figure 5.2). The net value of $\Delta\delta$ never exceeds zero, since the compounded decrease in biomass at each subsequent trophic level dictates progressively smaller contributions as N increases. Additionally, because some amount of lipid from P_0 always remains, the theoretical maximum value of $\Delta\delta$ that would arise from purely heterotrophic contribution to lipid cannot be reached at any extent of *d*. Heterotrophic enrichment therefore is maximized at intermediate *d* (Figure 5.2a),

but $\Delta\delta_{n\text{-alkyl–TOC}}$ is still negative. Thus, formation of a positive signature for $\Delta\delta_{n\text{-alkyl–TOC}}$ under this scenario is strictly dependent on the exact fractionations involved in biosynthesis, namely the values of ε_R, ε_L, and h, where $\Delta\delta_{n\text{-alkyl–TOC}} \approx \varepsilon_R - \varepsilon_L + h(1\text{-E})$. In particular, to achieve a positive value of $\Delta\delta$ would require that the biopolymer or other material destined to become kerogen is systematically more isotopically negative, or lipids more isotopically positive, than could be reasonably expected based on known biosynthetic fractionations (Table 5.1).

Table 5.1. Parameters and values, heterotrophic enrichment model

Model Parameters	**Symbol**	**Value used in examples**	**Range for Monte Carlo simulations**
Biosynthetic fractionation, resistant biopolymer	ε_R	1.5‰	-1.5 to 4.5‰
Biosynthetic fractionation, *n*-alkyl lipid	ε_L	4.5‰	3 to 6‰
Degradation rate constant, resistant biopolymer	K_R	0.1	fixed
Degradation rate constant, lipid	K_L	0.27	0.1 to 0.27
Degradation rate constant, labile biomass	K_B	10	fixed
Fraction resistant biopolymer, primary producer cell	F_R	30%	15 to 35% ($1\text{-}F_B\text{-}F_L$)
Fraction lipid, primary producer cell	F_L	10%	5 to 25%
Fraction labile biomass, primary producer cell	F_B	60%	fixed
Fraction lipid, heterotrophic cell	F_{HL}	10%	5 to 25%
Fraction labile biomass, heterotrophic cell	F_{HB}	90%	75 to 95% ($1\text{-}F_{HL}$)
Max. heterotrophic ^{13}C enrichment per trophic level	h	1.5‰	1 to 2‰
Heterotrophic efficiency	E	0.3	0.05 to 0.6

Attenuated *d*. When $D(d,N) = de^{-\zeta N}$, later trophic levels experience less degradation. This leads to preferential preservation of biomass from later-stage heterotrophs, *i.e.* formalization of the scenario presented in Logan et al., (1995). Extreme attenuation (high ζ) favors preservation of heterotrophic material in excess of primary material, while extreme exposure (low ζ) favors preservation of only the most highly resistant primary material. Importantly, such attenuation of exposure time with trophic level does produce a positive value of $\Delta\delta_{n\text{-alkyl–TOC}}$, as postulated by Logan et al. (1995). Figure 5.3a shows that this outcome happens only in systems with moderately attenuated exposure times and over a narrow range of *d*. Under extreme attenuation, the amount of degradation experienced at higher trophic levels (high *N*) relative to level 0 is very small, especially at a high value of *d*. The result is that primary organic matter (P_0) approaches

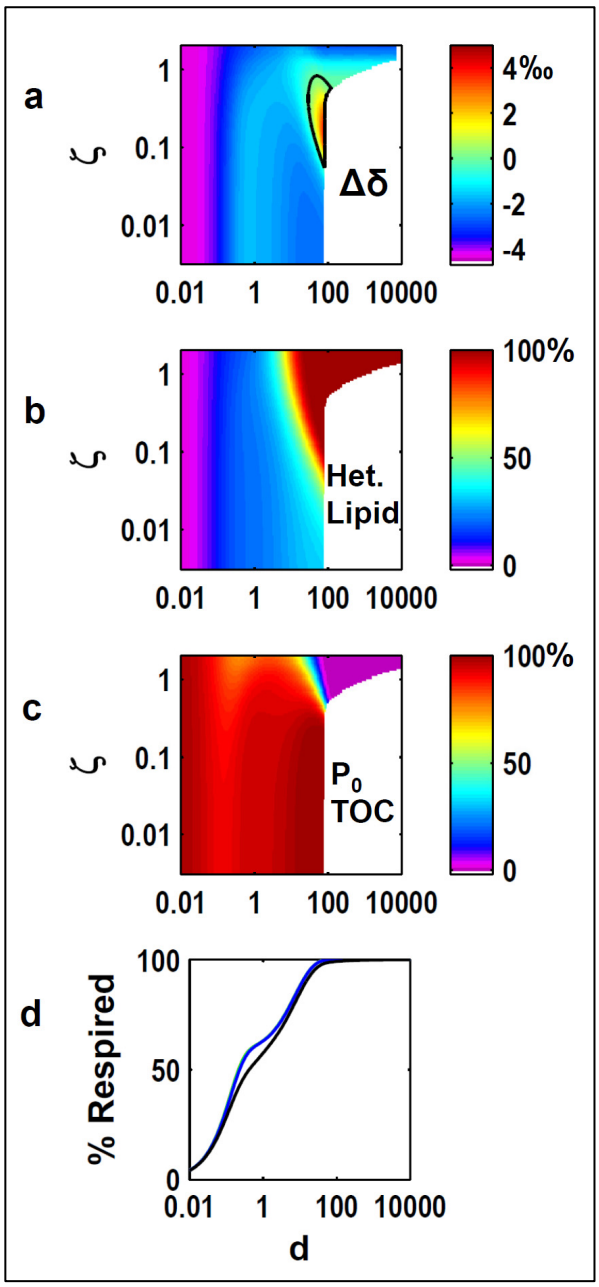

Figure 5.3. Results of Logan-type scenario when exposure time is attenuated in higher trophic levels. **(a)** Dependence of $\Delta\delta_{n\text{-alkyl–TOC}}$ on overall degradation, *d*, and ζ , a scaling coefficient that determines the attenuation of degradation with increasing trophic level. The black contour follows a value of 0 for Δδ. **(b)** Contribution of heterotrophic lipid to total preserved lipid as a function of *d* and ζ. **(c)** Contribution of primary producers to total preserved TOC as a function of *d* and ζ. **(d)** Net respiration of primary productivity as a function of *d* and ζ.

zero concentration, and all preserved lipid *and* total organic matter both derive from heterotrophs (top right corner of Figure 5.3b,c). The final Δδ value approaches zero as the TOC becomes dominated by heterotrophic lipids (top right corner of Figure 5.3a). Conversely, in the limit of a very small attenuation exponent (*i.e.*, extreme exposure; bottom of Figure 5.3a), the Δδ result follows the same pattern as Figure 5.2a, and a positive isotope anomaly is never reached.

Intermediate values of ζ therefore are required to preserve heterotrophic lipids simultaneously with residual primary material. The area of positive $\Delta\delta_{n\text{-alkyl–TOC}}$ values in Figure 5.3a maps well to the intersecting areas of high contribution of heterotrophic lipid to total preserved lipid (Figure 5.3b), while still leaving the majority of total preserved organic matter as resistant biopolymer from P_0 (Figure 5.3c). Values for Δδ become slightly to strongly positive (maximum of ~4.3‰) before the model run terminates. The maximum occurs at ζ ~0.15. The magnitude of the maximum Δδ value is strongly dependent on when the model run is terminated, *i.e.*, on how we choose the imposed

limits of terminal heterotrophy and/or terminal burial. Note that the units of the *d* axes in Figures 5.2 and 5.3 are in units of relative degradation and should not be equated to time. Rather, the distance along this axis represents the fractional approach to one of the criteria *i*-*iii*, above. Accordingly, net respiration of primary productivity as a function of *d* is nearly identical for different values of ζ (Figure 5.3d).

The dual variable space of *d* and ζ potentially can simulate environmental characteristics of the water column. For example, rapid attenuation and low total extent of degradation might occur in shallow water columns (rapid burial). Modest attenuation and degradation might occur in anoxic waters, and no attenuation and high extent of total degradation might reflect well-oxygenated open oceans. The concept of ζ encompasses specifically those environmental factors that would affect the relative reactivity of molecular trophic levels. The exact nature of the ζ function is unknown (here simulated as a first-order decay with increasing trophic level), but degradation probability is known to vary with location and environment (*e.g.,* Hedges and Keil, 1995), and most diagenetic systems are treated using first-order decay approximations such as used here (*e.g.,* Middelburg, 1989). Importantly, regardless of the form that ζ takes, in any given burial regime, only the *local* value of ζ would apply, and it is this value that would be reflected in the preserved value of $\Delta\delta_{n\text{-alkyl–TOC}}$.

In summary, under the heterotrophic enrichment scenario, there are two ways to produce sedimentary organic matter with a positive value of $\Delta\delta_{n\text{-alkyl–TOC}}$: (*i*) a specific relationship between ε_R, ε_L, *h*, and *E* that also meets the unusual condition of $\varepsilon_R > \varepsilon_L$; or (*ii*) an "optimum" diagenetic scenario, which can produce positive $\Delta\delta_{n\text{-alkyl–TOC}}$ over a narrow range of both exposure and attenuation (*d* and ζ).

While these conditions could exist in specific environmental settings, we believe neither is a good candidate to be a controlling mechanism that would be fundamental to the entire Proterozoic, and yet would disappear unequivocally at the end of the eon. Option (*ii*) would be

highly localized and would require specific burial scenarios. It is unreasonable to imagine that all depositional environments would be uniformly poised at attenuation coefficients (ζ) within the required, narrow range. Such environmental constancy appears to be refuted by the appearance of inverse isotopic signatures in samples from diverse water depths and environments, from evaporative carbonate platforms (Hieshima, 1992; Höld et al., 1999) to deeper marine, shale-depositing environments (Logan et al., 1997). In the case of option (*i*), there is no known mechanism for making recalcitrant molecules (algal biopolymers) and/or total kerogen that are systematically isotopically lighter than lipids. However, in some cases, ^{13}C-depleted kerogen has been attributed to the increased preservation of biomass from methanotrophic Archaea or Bacteria (*e.g.*, Hinrichs, 2002; Eigenbrode et al., 2008).

Community hypothesis: ^{13}C difference between primary prokaryotes and eukaryotes

To consider an alternative to the Logan scenario, we examined the extent to which values of $\Delta\delta_{n\text{-alkyl–TOC}}$ could be controlled by the composition of the primary producer community. Presently, both eukaryotes and prokaryotes contribute to primary production in surface marine environments, but eukaryotes dominate primary biomass, C-fixation rate, and even sometimes numerically (*e.g.,* Agawin et al., 2000). Although eukaryotic primary producers were present and active for several hundreds of millions of years prior to the Cambrian transition, they rose to global prominence in the latest Neoproterozoic and earliest Cambrian (*e.g.*, Knoll et al., 2007). This suggests that the total biomass attributable to prokaryotes and eukaryotes changed fundamentally across the end of the Proterozoic. If these biomass sources carried different ^{13}C signatures, this signal could have been transferred to sediments.

Size-population isotope model. In an ocean that contains prokaryotic (S, small) and eukaryotic (G, large) primary producers having different initial average ^{13}C contents, the isotopic signature of primary organic matter depends on the relative biomass ratios of these cell types in

the surface ocean. Importantly, biomass ratios do not scale linearly with cell numbers, due to size:volume relationships. We treat the average size of S and G cells as the fractional radius of the small cells relative to the large cells ($R_z = r_S/r_G$). Similarly, the population of cells is treated as a ratio ($R_p = \text{cells}_S/\text{cells}_G$). We then model the total amount of biomass from a given cell type as $R_p R_z^3$, thereby assuming that the abundance of biomass in a cell is proportional to the cell volume and that the cells are spherical.

Relative ^{13}C enrichment in bacterial photoautotrophs has been observed in multiple taxa (Cyanobacteria, green and purple sulfur and non-sulfur bacteria; Pardue et al., 1976; Sirevåg et al., 1977, Roeske and O'Leary, 1985; Popp et al., 1998; van der Meer et al., 2003) and modern aquatic environments (*e.g.,* open marine: Tolosa et al., 2008; Tchernov and Lipschultz, 2008; and lakes: Vuorio et al., 2006; Gu and Schelske, 1996), and has been implicated in several geologic time periods (*e.g.,* Miocene: Kashiyama et al., 2008b; Cretaceous: Kashiyama et al., 2008a; Sinninghe Damsté et al., 2008; Jurassic: Schwab and Spangenberg, 2007; Permian: Grice et al., 1996; Devonian: Joachimski et al., 2001; Neoproterozoic: Riding, 2006). We model a community in which prokaryotic S primary producer cells are on average isotopically enriched compared to the larger G cells, and define β as the average net isotopic difference between the size classes. The ^{13}C content of large cells is defined as δ_{G0}, and the starting ^{13}C content of small cells is $\delta_{S0} = \delta_{G0} + \beta$. Values of $\delta^{13}C$ of biochemical classes within the bulk S and G pools are offset by the biosynthetic fractionations ε_R and ε_L as described under the Logan scenario.

We formulate primary organic matter as a mixture of prokaryotic *B* and *L*, and eukaryotic *B*, *L*, and *R* (biochemical classes as in the Logan scenario). Although the resistant portion of biomass is prescribed for large cells only, it does not explicitly denote a biosynthetic class of material, but rather implies that resistance to degradation may be imparted due to mechanisms related to cell size, rather than specific chemical composition. Such mechanisms could include physical protection of eukaryotic biomass through cell wall matrix effects (Nguyen et al., 2003)

or reduced exposure time via faster sinking through the water column (*e.g.* Butterfield, 2009; Burd and Jackson, 2009). Similarly, the model does not preclude the incorporation of prokaryotic (or eukaryotic) *L* and *B* into kerogen via geopolymerization. Degradation rates, heterotrophic uptake equations, and all other parameters are also formulated as described previously. Full details of derivations are given in the Chapter 5 Appendix.

Parameter values. To span a wide range of ecological space, we consider ratios of prokaryotic:eukaryotic cells from 10^1 to 10^7. In today's ocean, more productive coastal and estuarine environments can have ratios ~10^1, while oligotrophic, subtropical ocean gyres have ratios ~10^3 (*e.g.* Hall and Vincent, 1990; Li, 1994; Fujieki et al., 2010; Marañon et al., 2010). We consider ranges of degradation extent, *d*, identical to those above, and the simulations are terminated as described previously. Attenuation of *d* with trophic level (ζ) is modeled for two values, $\zeta = 0$ (no attenuation) and $\zeta = 0.15$ (maximum effect on $\Delta\delta_{n\text{-alkyl–TOC}}$), for comparison to the Logan-type scenarios above.

Values for new parameters are shown in Table 2; all other model values were drawn from Table 1. We consider a conservative value of 4‰ for β, based on observations that Cyanobacteria could have values of $\delta^{13}C$ ~3-7‰ more positive relative to eukaryotes grown on the same C source (*e.g.* Popp et al., 1998), while anoxygenic photoautotrophs using Type II Rubisco could have 6-9‰ enrichments (Roeske and O'Leary, 1985; Robinson and Cavanaugh, 1995), and those using the rTCA cycle could be >10‰ enriched (Sirevåg et al., 1977; Preuß et al., 1989; House et al., 2003). Smaller kinetic isotope effects for their C-fixing enzymes and/or the use of carbon concentrating mechanisms (CCMs) could explain these ^{13}C enrichments (Erez et al., 1998; Popp et al., 1998; House et al., 2003). Natural isotopic measurements of modern coexisting cyanobacteria and eukaryotic phytoplankton are sparse, and use varying methods to separate size classes and/or individual taxa. Resulting measurements correspond to a wide range of β values if comparison between individual taxa of cyanobacteria and eukaryotes were

considered (-9 to +19; Gu and Schelske, 1996; Vuorio, 2006; Tolosa et al., 2008). This sort of variability is also reflected in culture studies (Pardue et al., 1976; Falkowski, 1991). However, since we are considering what would constitute a weighted average of values across a diverse marine population, we confine our simulations to a more modest range of β.

Table 5.2. Additional parameters and values, mixed community model

Additional Parameters, Mixed Community model	**Symbol**	**Value used in examples**	**Range for Monte Carlo**
Difference in $\delta^{13}C$ value average biomass, small cells – large	β	4‰	0 to 8‰
Radius size ratio, small/large cells	R_z	1/15	fixed
Fraction labile biomass, primary small cells	F_{SB}	90%	75 to 95% (1-F_{SL})
Fraction lipid, primary small cells	F_{SL}	10%	5 to 25%

To model cell sizes we assume that average marine bacteria are 0.8 μm in diameter and use an R_z of 1/15, resulting in eukaryotic algae smaller than present-day coccolithophorids. This yields a conservative estimate of the contrast in size between cell types. Notably, due to this choice of R_z, primary biomass ratios for S:G are 1:1 when $R_p \sim 10^{3.5}$. In other words, biomass dominance of eukaryotes appears when S:G is $< \sim 10^{3.5}$ or disappears when S:G $> \sim 10^{3.5}$; the latter would be only slightly higher than modern, oligotrophic gyres. Finally, we consider the proportions of *B* and *L* in primary prokaryotes to be the same as in heterotrophic prokaryotes.

Results of size-fractionated scenarios. The size-fractionated biomass model (Figure 5.4) was tested by varying the numerical ratio of small:large cells and the total extent of degradation. A positive value for $\Delta\delta_{n\text{-alkyl–TOC}}$ requires that sedimentary lipid must be dominated by input from S cells and/or heterotrophs, while most sedimentary TOC must originate from G cells. The areas producing positive values of Δδ in Figure 5.4a and 4f correspond to an intermediate contribution of preserved lipid from S cells (Figure 5.4b, g), coincident with an intermediate contribution of preserved TOC from G cells (Figure 5.4d, i).

A positive value of $\Delta\delta_{n\text{-alkyl–TOC}}$ (Figure 5.4a, f) is relatively insensitive to the contribution of heterotrophs to preserved lipid (Figure 5.4c, h). The relative contribution of heterotrophic lipids to a positive $\Delta\delta$ signal is smaller than in the Logan scenarios, because the lipids of heterotrophs and of S cells both are ^{13}C-enriched. The lipids of heterotrophs become significantly abundant only when the upper limit of d is simultaneous with $\zeta > 0$ (Figure 5.4h). This results from extensive degradation of S lipids from trophic level 0, while heterotrophic lipids in trophic level N can accumulate. In the example shown here, the additional heterotrophic contribution causes maximum values for $\Delta\delta$ to become slightly more positive (from ~1.2‰ in Figure 5.4a to ~2.6‰ in Figure 5.4f).

Thus, although the maximum value of $\Delta\delta_{n\text{-alkyl–TOC}}$ is governed by the contribution of preserved heterotrophic lipids, this effect occurs over a small range of d. The majority of positive $\Delta\delta$ space (Figure 5.4a,f) is governed by the differential preservation of components of S and G cells. The absolute value of $\Delta\delta$ depends on our choice of β, specifically in relation to the biosynthetic fractionations prescribed for ε_R and ε_L. In the extreme case of sedimentary lipid contributed *only* by small cells and TOC *only* by large cells, the *maximum* value of $\Delta\delta$ would be equal to $\delta_{SL} - \delta_{GR}$, which reduces to $\varepsilon_R + \beta - \varepsilon_L$, or 1‰ using values from Tables 1 and 2. The larger expressed maximum of ~1.2‰ (Figure 5.4a) is due to a non-zero contribution of heterotrophic lipids slightly overwhelming a small, but continued presence of lipid from ^{13}C-depleted G cells. Accordingly, the $\Delta\delta$ signature more readily stays positive once a large enough ratio of small:large cells is achieved, as δ_{SL} (plus heterotrophic lipids) dominates the total δ_L. Under conditions of very high ratios of S:G, however, there no longer is enough biomass from G to contribute to TOC. Both the total δ_L and δ_{TOC} are dominated by material from S cells and the positive signature for $\Delta\delta$ decreases. When population ratios change in the other direction, the positive signal in $\Delta\delta$ disappears rapidly and completely when S:G falls below ~$10^{3.5}$.

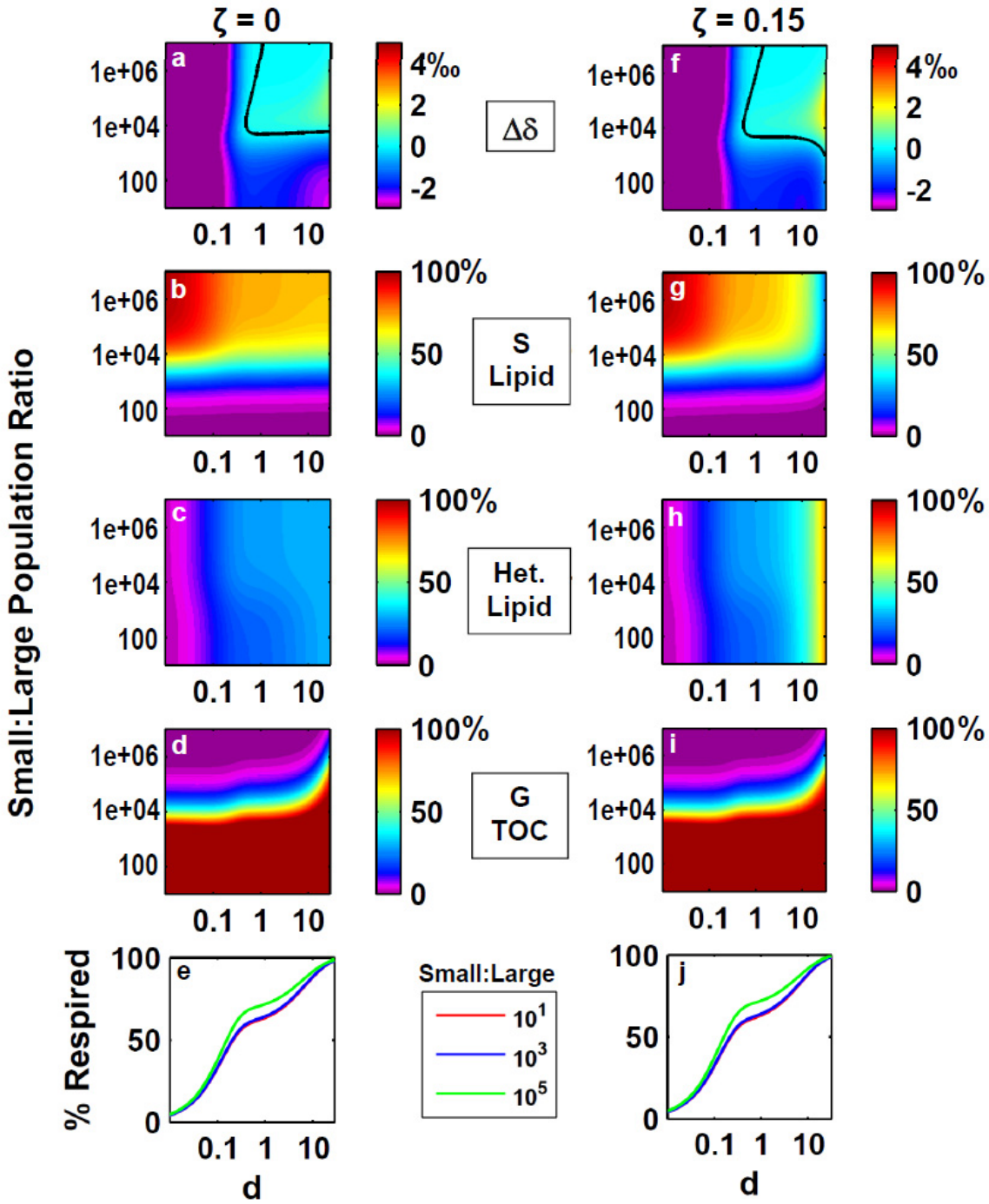

Figure 5.4. Results of mixed-community scenario. The ζ=0 case (a-e) indicates results when *d* remains constant for all trophic levels; the ζ=0.15 case (f-j) is shown for comparison to the Logan scenarios, in which *d* is attenuated at higher trophic levels. **(a, f)** Dependence of $\Delta\delta_{n\text{-alkyl–TOC}}$ on overall degradation, *d*, and population ratio of small(S):large(G) primary producer cells (R_P). The black contour follows a value of 0 for Δδ. **(b, g)** Contribution of lipid from primary S cells to total preserved lipid as a function of *d* and R_P. **(c, h)** Contribution of heterotrophic lipid to total preserved lipid as a function of *d* and R_P. **(d, i)** Contribution of primary G cells to total preserved TOC as a function of *d* and R_P **(e, j)** Net respiration of primary productivity as a function of *d* for several different R_P shows convergence of all models at high *d*, regardless of ζ. Contour values in (b, c, g, h) are % of total lipid; in (d, i) are % of TOC.

Comparison to inverse $\Delta\delta^{13}C_{n\text{-alkyl-isoprenoid}}$

Additional studies have reported the inverse pattern by comparing the isotopic content of selected *n*-alkyl lipids to the isoprenoid lipids pristane and phytane. The latter represent photosynthetic sources as they are thought to derive mostly from chlorophyll *a* (Logan et al., 1995; Logan et al., 1997; Kelly, 2009). The measured $\Delta\delta_{n\text{-alkyl-isoprenoid}}$ offset most commonly varies in magnitude from ~0 to 4‰ (Logan et al., 1995; Logan et al., 1997; Kelly, 2009), although larger offsets have been reported for one Cryogenian horizon (Kelly, 2009).

In samples in which inverse signatures are observed in both $\Delta\delta_{n\text{-alkyl-kerogen}}$ and $\Delta\delta_{n\text{-alkyl-isoprenoid}}$, the isotopic ordering between isoprenoids and kerogen is variable, covering both positive and negative values (Logan et al., 1995; Logan et al., 1997; Figure 5.1). This variability has been attributed to an archaeal contribution to the pool of phytane (Logan et al., 1997; Schouten et al., 1998), and the relative effect has been estimated by assuming that Archaea are responsible for any inconsistency in the pristane to phytane abundance ratio or isotopic values (Logan et al., 1997). However, there are other ways to generate variability in $\Delta\delta_{n\text{-alkyl-isoprenoid}}$ that do not require the presence of Archaea.

To demonstrate this, we incorporated an isoprenoid component into both the Logan scenario and the mixed community scenario. We assume that pristane and phytane are from photosynthetic sources only, that their abundance is proportional to the number of photosynthetic cells (both S and G), and that they are biosynthesized with an average fractionation $\varepsilon_{biomass\text{-isoprenoid}}$ of 3‰ for plastidic lipids (*e.g.*, Schouten et al., 1998; Hayes, 2001).

When *d* is not attenuated by trophic level (ζ =0), values for $\delta_{isoprenoid}$ and for $\delta_{n\text{-alkyl}}$ change in parallel, and the difference between them ($\Delta\delta_{n\text{-alkyl-isoprenoid}}$) must remain equal to the difference expected for biosynthetic control (-1.5‰). It is not possible to make the sign or magnitude of this relationship change unless a non-zero value of ζ is incorporated. Therefore, values of $\Delta\delta_{n\text{-alkyl-TOC}}$ and $\Delta\delta_{n\text{-alkyl-isoprenoid}}$ were modeled for the Logan scenario at three different values of

ζ (Figure 5.5a, d) and for the mixed community scenario at three different population ratios R_p and two different ζ (Figure 5.5b, e, c, f). At low d in all scenarios, the relationship between isoprenoids and *n*-alkyl lipids continues to reflect that of biosynthetic products (Figure 5.5), but at higher d, values of $\Delta\delta_{n\text{-alkyl-isoprenoid}}$ become positive in all models (Figure 5.5 d, e, f).

The mixed community scenario produces a positive $\Delta\delta_{n\text{-alkyl-isoprenoid}}$ signature for values of $\zeta > 0.125$ and moderate to high values of d. Figures 5.5b and 5.5e are shown at $\zeta = 0.15$, the value at which maximum $\Delta\delta_{n\text{-alkyl-TOC}}$ is obtained in the Logan scenario; Figures 5.5c and 5.5f are shown at $\zeta = 0.5$, a value that illustrates a wide range of isotopically positive values for both types of lipids.

At elevated ζ, a changing population ratio R_p can reproduce the variability seen in the isotopic relationship between preserved isoprenoids and kerogen (Figure 5.1b), with both positive and negative offsets occurring in conjunction with positive values of $\Delta\delta_{n\text{-alkyl-TOC}}$ and $\Delta\delta_{n\text{-alkyl-isoprenoid.}}$ In a modestly prokaryotic ocean (blue line, Figure 5.5c, f), between $\sim 10 < d < 40$ (degradational extents from ~85-99%), $\Delta\delta_{n\text{-alkyl-TOC}}$, $\Delta\delta_{n\text{-alkyl-isoprenoid}}$, and $\Delta\delta_{\text{isoprenoid-TOC}}$ all are positive, as seen throughout many Proterozic samples. Approaching maximum d, however, $\Delta\delta_{n\text{-alkyl-isoprenoid}}$ remains positive (Figure 5.5d) while $\Delta\delta_{\text{isoprenoid-TOC}}$ returns to a negative (biosynthetic) value. The former is largely a consequence of the population distribution, while the latter is caused by heterotrophic isotopic enrichment causing an increase in net $\delta^{13}C_{TOC}$.

Importantly, these models can simulate some unusual data from the Cambrian. Continued positive values for $\Delta\delta_{n\text{-alkyl-isoprenoid}}$ occur in the early Cambrian, but they are found alongside negative values for $\Delta\delta_{n\text{-alkyl–kerogen}}$ (Logan et al., 1997). Both the Logan scenario and the mixed community scenario can reproduce this effect. In the Logan scenario, $\delta_{n\text{-alkyl}}$ is more positive than $\delta_{\text{isoprenoid}}$ at high values of d and ζ, although both are negative relative to δ_{TOC} (Figure 5.5a). In the mixed community scenario at $\zeta = 0.15$, $\delta_{n\text{-alkyl}}$ is more positive than $\delta_{\text{isoprenoid}}$ at high values of d and moderate values of R_p, but $\delta_{n\text{-alkyl}}$ can be negative relative to δ_{TOC} if R_p decreases

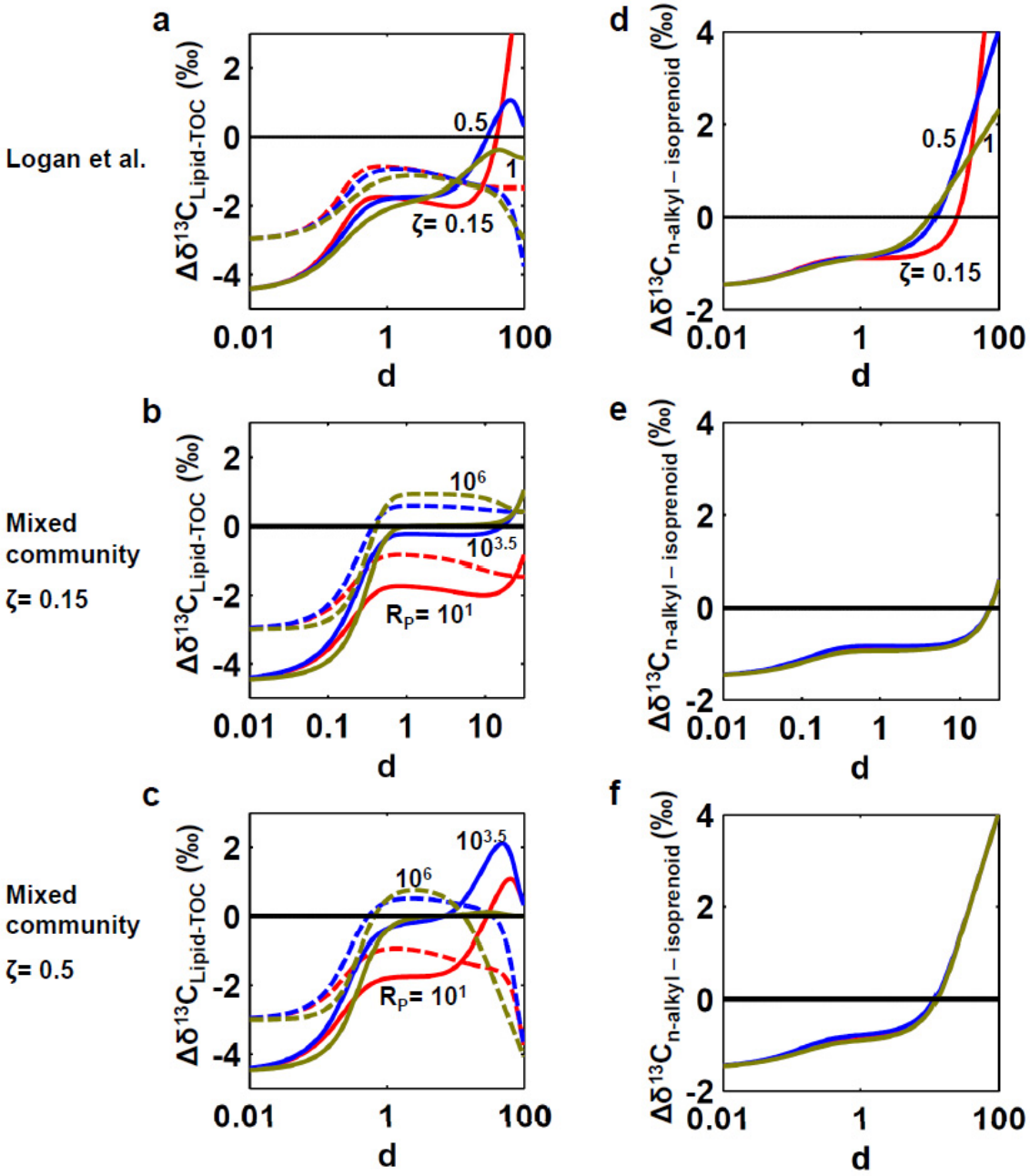

Figure 5.5. Modeled $\Delta\delta_{n\text{-alkyl-isoprenoid}}$ isotope anomalies for the Logan scenario **(a, d)** and mixed-community scenario at ζ=0.15 **(b, e)** and at ζ=0.5 **(c, f)**. Relative isotope anomalies are shown for isoprenoid (dashed) and *n*-alkyl (solid) lipids, each normalized to TOC (black line at 0‰). Colors illustrate results with three different values for the controlling parameter in each scenario: ζ, trophic attenuation factor **(a, d)**; and R_p, population ratio of primary small cells to large cells **(b, e, c, f)**. In the left-hand column, values above zero indicate an inverse signature for $\Delta\delta_{n\text{-alkyl-TOC}}$ and $\Delta\delta_{\text{isoprenoid-TOC}}$; in the right-hand column, values above zero indicate an inverse signature for $\Delta\delta_{n\text{-alkyl-isoprenoid}}$.

(eukaryotes become more abundant; Figure 5.5b). Still another Cambrian formation (Observatory Hills; Logan et al., 1997) shows Phanerozoic (biosynthetic) patterns by having negative values of $\Delta\delta_{n\text{-alkyl-isoprenoid}}$ (isoprenoids heavier than *n*-alkyl lipids) and negative values of $\Delta\delta_{n\text{-alkyl–kerogen}}$ (kerogen heavier than *n*-alkyl lipids), but positive values for isoprenoids in relation to kerogen. This pattern can be reproduced in the community mixing model at moderate values of *d* (Figure 5.5b,c), but not in the Logan model (Figure 5.5a).

Discussion and conclusions

Uncertainty in and sensitivity to parameter values. Most of the parameters in our models have wide ranges of values in the current literature. Properties of water column and sedimentary environments, as well as cell physiologies and phylogenies, remain relatively unknown for the Proterozoic. We have attempted to account for this large range of uncertainty by choosing parameter values conservatively, erring on the side of values that favor success of a Logan-type model, rather than the community model. Our relative results are thus significant, whereas the absolute values are highly dependent on the inputs. Figure 5.6 shows the frequency distribution of results that successfully display a positive value for $\Delta\delta_{n\text{-alkyl–TOC}}$ in a Monte Carlo simulation designed to explore the sensitivities of both models. Parameter values and combinations were chosen at random for each of $> 6\text{x}10^6$ simulations. Ranges of values used for these Monte Carlo simulations are shown in Tables 1 and 2 and are discussed further in the Chapter 5 Appendix.

The frequency distribution of positive $\Delta\delta_{n\text{-alkyl–TOC}}$ in Figure 5.6 is similar to the patterns shown in Figures 5.3 and 5.4. This indicates that the variables shown in Figures 5.3 and 5.4 are indeed the ones to which the models are most sensitive. In all cases, however, the range that results in an inverse signature is expanded in Figure 5.6. It remains true that in the Logan case the bulk of inverse results occur within a small range of high *d* surrounding an intermediate ζ (Figure 5.6a). These variables clearly are interrelated conceptually, as extensive later-stage

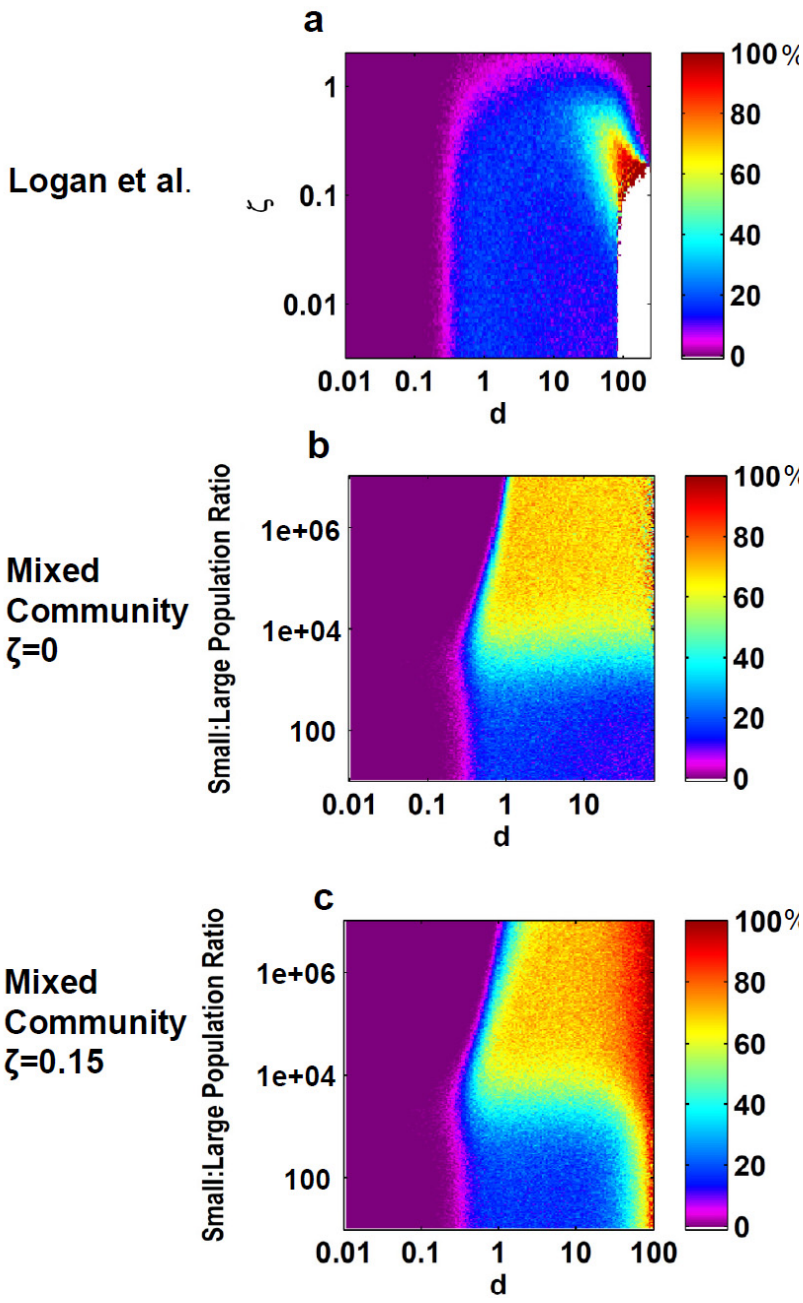

Figure 5.6. . Results of > $6x10^6$ Monte Carlo simulations, drawing from parameter ranges in Tables 1 and 2. Color map indicates percentage of simulations resulting in an inverse (> 0‰) value for $\Delta\delta_{n\text{-alkyl–TOC}}$. Results for the Logan scenario (a) are shown for varying d and ζ and have been limited to d values displaying nonzero outcomes, up to $10^{2.5}$. Results are shown for the mixed community scenario for varying d and R_P, and both for when ζ=0 (b) and ζ=0.15 (c).

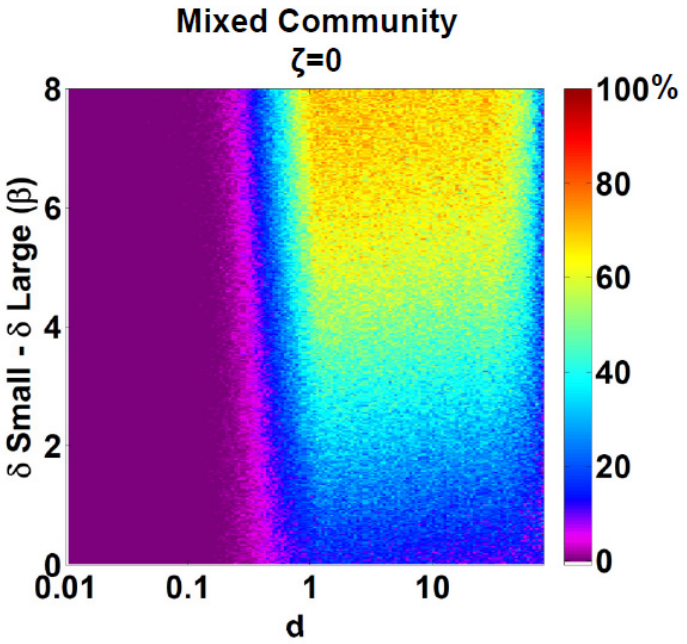

Figure 5.7. . Results of > 6x10^6 Monte Carlo simulations, drawing from parameter ranges in Tables 1 and 2. Color map indicates percentage of simulations resulting in an inverse (> 0‰) value for $\Delta\delta_{n\text{-alkyl–TOC}}$. Explicit dependency on *d* and β is shown; all other parameters were randomized. Results are shown for the mixed community scenario with ζ=0.

heterotrophy necessarily occurs only when the total degradation of primary organic matter is high. The fact that the mixed community scenario also shows a stronger dependency on *d* when a non-zero value of ζ is incorporated (Figure 5.6c) also highlights this connection.

The mixed community scenario is otherwise more dependent on other parameter combinations. It produces a broader range of positive results for $\Delta\delta_{n\text{-alkyl–TOC}}$ across a wider range of ζ, including at ζ = 0 (Figure 5.6b). The major driver of the magnitude of Δδ is of course β, which is the ultimate determinant of isotopic enrichment in a non-eukaryotic source of *n*-alkyl lipids. Although positive values of Δδ also are driven by the small:large population ratio and *d*, specific combinations of these variables alone do not *guarantee* an inverse outcome, especially when ζ = 0 (Figure 5.6b; no cases of 100% success) due to our incorporation of a range of β values. Dependence of inverse results on the value for β is shown in Figure 5.7, which indicates that values of β as low as 3‰ still produce positive values of Δδ in > 40% of trials.

Comparison of models to the Proterozoic environment. The measured inverse signature of $\Delta\delta_{n\text{-alkyl–kerogen}}$ during the Proterozoic manifests as a general trend across a large global extent of shelf and outer shelf-slope facies. While the magnitude of the signature is somewhat variable, the positive sign is almost exclusive to the Precambrian, with a trend toward negative values starting in the latest Ediacaran – early Cambrian (Logan et al, 1995; Logan et al., 1997). The Proterozoic was a time of enormous change in global biogeochemical cycles (*e.g.,* Canfield, 1998; Anbar and Knoll, 2002; Johnston et al., 2009). Marine biogeochemistry likely was controlled by variability in oxygen concentrations and changes in the sulfur cycle (*e.g.* Fike et al., 2006), and the redox environments in different parts of the ocean supported different populations and likely differing rates of diagenesis (*e.g.,* Logan et al., 1999; Canfield et al., 2008; McFadden et al., 2008). Despite this potential for redox heterogeneity, the inverse signature of $\Delta\delta_{n\text{-alkyl–kerogen}}$ remained ubiquitous, suggesting it derived from environmental or ecological conditions that were fundamental to the entire era.

In our formalization of the Logan hypothesis, a ubiquitous inverse signature would derive from consistently very high exposure to degradation (d) for primary organic matter, and intermediate levels of attenuation of this exposure for heterotrophs (ζ), across most preserved environments. Magnitudes of the $\Delta\delta$ signature could then vary widely within the narrow range of allowed d and ζ (Figure 5.3). While water column degradation could be enhanced due to slower sinking rates of photosynthetic cells (*e.g.* Logan et al., 1995; Butterfield, 2009), total respiration may have been limited by low oxidant availability. Therefore, explanations *requiring* very high values of d might not be expected to apply ubiquitously throughout the era. But supposing that environmental conditions did impose a strictly high d, then the switch to a negative value of $\Delta\delta_{n\text{-alkyl–kerogen}}$ mostly likely would derive from a gradual relaxation of the conditions that caused a fixed value of ζ. The questions then are how could a narrow control on ζ be maintained, and how would it be universally relaxed at the Cambrian boundary? It is

difficult to envision how attenuation of degradation would have been uniformly constant during the Proterozoic. The parameter ζ is presumed to integrate many environmental factors such as particle sinking rate and variability in exposure to oxidants. Considering the likely heterogeneity of degradative conditions across the Proterozoic, a consistently narrow range of net ζ appears to be an unreasonably strict requirement. The eventual change in ζ potentially could be related to an increased sinking flux for primary producers, possibly as a result of increased biomineralization. However, inorganic ballast during the Proterozoic has been suggested to be abundant enough to cause high organic burial rates (*e.g.* Hotinski et al., 2004), and modern microbially-dominated ecosystems are capable of sustaining significant export of primary organic matter (*e.g.* Hotinski et al., 2004; Richardson and Jackson, 2007). This suggests that increased sinking particle sizes in the early Cambrian may not have altered the preservation mechanisms sufficiently to produce a monotonic shift in $\Delta\delta_{n\text{-alkyl–kerogen}}$.

Positive values of $\Delta\delta_{n\text{-alkyl–kerogen}}$ across diverse diagenetic histories are accommodated more easily by a mechanism that allows a wider range of total degradation (*d*), and allows but does not require an attenuation factor (ζ). The mixed community model satisfies these requirements. In the mixed community scenario, a ubiquitous positive value of $\Delta\delta_{n\text{-alkyl–kerogen}}$ would result from a relatively high ratio of a ^{13}C-enriched prokaryotic production and variably intermediate to high extent of *d*. Meanwhile, ζ could be ≥ 0 and could be permitted to vary over a wide range. This scenario accommodates redox heterogeneity and would allow the positive isotope signal to be observed in a variety of marine facies. There is no requirement for selective preservation of heterotrophic biomass. Variability in the predicted magnitude of $\Delta\delta_{n\text{-alkyl–kerogen}}$ is somewhat smaller in the mixed community model, but the range of population ratios for which an inverse signature is retained is large. The switch to a negative sign of Δδ in the late Ediacaran would signal a fundamental ecological transition in response to geochemical changes favoring the gradual increase in eukaryotic proportion of primary production over time.

The trend of measured values for $\Delta\delta_{n\text{-alkyl–isoprenoid}}$ in the Proterozoic is similar to that for $\Delta\delta_{n\text{-alkyl–kerogen}}$, but with relatively more outliers, a wider range of magnitudes in some sections, and several measurements of continued inverse signatures in the Cambrian (Logan et al., 1995; Logan et al., 1997; Kelly, 2009). A non-zero value of ζ is required to produce an inverse $\Delta\delta_{n\text{-alkyl-isoprenoid}}$ in both models, and variability in d at a given ζ can reproduce the observed variability in $\Delta\delta_{n\text{-alkyl–isoprenoid}}$. However, only the mixed community scenario is capable of simulating the full range of simultaneous combinations of sign relationships observed for $\Delta\delta_{n\text{-alkyl–TOC}}$, $\Delta\delta_{n\text{-alkyl-isoprenoid}}$, and $\Delta\delta_{\text{isoprenoid–TOC}}$. The overall heterogeneity of the observational data may then be a consequence of heterogeneity in both environmental and ecological parameters. A purely heterotrophy-based model like the Logan scenario is unable to reproduce the same diversity of signatures, and in general is less accommodating of a variable environment in its requirements for creating inverse isotopic signatures.

Our model addresses a conservative formulation of organic matter production and biosynthetic isotope patterns for the Proterozoic, but there are additional mechanisms by which preserved *n*-alkyl lipids could acquire relative ^{13}C enrichment. Most simply, some photoautotrophs during the Proterozoic could have had different pathways of lipid biosynthesis that result in an "inverse" isotopic ordering of their direct biosynthetic products, as seen in rTCA organisms (van der Meer et al., 1998). A second way would be for the isotopically-enriched portion of the community (whether primary or heterotrophic) to have a relatively high cellular lipid content compared to other organisms, thereby contributing disproportionate quantities of ^{13}C-enriched lipids to the sedimentary pool (as suggested for inverse isotope ordering in the Archean; Brocks et al., 2003b). Finally, inverse $\Delta\delta_{n\text{-alkyl–isoprenoid}}$ values specifically could arise from our model without invoking $\zeta > 0$, if the predominant isotopically-enriched photoautrophs had a chlorophyll side-chain based on farnesane, *i.e.* not contributing to pristane and phytane. Although likely present to some extent in the Proterozoic, these alternative mechanisms are

difficult to invoke as controlling factors across all environments spanning the entire eon. Our model is able to show that none of these mechanisms is *necessary* to explain inverse $\Delta\delta$; including some proportion of organisms producing these alternative effects simply would widen the parameter range under which our model produces inverse signatures.

The value chosen for β in our model may err on the side of conservative: Proterozoic ocean conditions may have promoted ^{13}C depletion in eukaryotes while favoring photosynthetic prokaryotes that tend to discriminate less against ^{13}C. While the proportional significance of prokaryotic oxygenic and anoxygenic photoautotrophs remains largely unknown for the Proterozoic (*e.g.,* Eigenbrode and Freeman, 2006; Johnston et al., 2009), both are expected to have discriminated less against ^{13}C than photosynthetic eukaryotes (*e.g.*, Schidlowski, 1987; Badger and Price, 2003; Riding, 2006). Modern prokaryote-dominated areas of the open ocean may provide our closest observable analog to likely conditions that persisted in the Proterozoic. Prokaryotic autotrophy currently dominates some tropical, oligotrophic marine settings (Agawin et al., 2000), where small cell size is likely to impart fundamental physiological advantages (*e.g.* Raven, 1998; Jiang et al., 2005). Contemporary evidence suggests that in these environments, Cyanobacteria are likely to be enriched in ^{13}C relative to coexisting eukaryotic producers (*e.g.,* Popp et al., 1998; Tolosa et al., 2008). Cyanobacteria are suspected to operate CCMs obligately in modern natural settings, and also use them constitutively under high CO_2 conditions (Price et al., 1998). Colonial behavior can also impose local CO_2 limitation, depressing the expressed ^{13}C fractionation in biomass due to the activity of CCMs (Pardue et al., 1976; Tchernov and Lipschultz, 2008).

Although the environmental controls on the expression of ^{13}C discrimination in eukaryotic Rubisco are complex, low growth-rates and/or high CO_2 availability lead to expression of near-maximum fractionation factors in C-fixation in eukaryotic cells (*e.g.* Popp et al., 1998); both of these conditions likely were favored in Proterozoic oceans. Smaller average

cell size of eukaryotic phytoplankton also was likely in the Proterozoic, as is favored in modern oligotrophic environments. The corresponding high surface area would tend to increase CO_2 diffusion into the cell (*e.g.,* Raven, 1998). All of these factors would contribute to ^{13}C-depletion in eukaryotes. Together the prokaryotic and eukaryotic effects could increase the magnitude of β.

Modern observational data support these suggestions. Recent measurements from the Central North Pacific gyre show that ^{13}C-enriched lipids are found among the small size class (0.2 – 0.5 μm organic matter) and might be abundantly exported to mesopelagic depths (Chapter 2). Compound-specific isotopic measurements on oligotrophic water-column filtrates and on sediments recovered from deep-sea cores could help expand our understanding of prokaryote-dominated marine environments and provide valuable analogues to the Proterozoic.

Relative biomarker abundances also may be valuable tools to elucidate populations contributing to inverse isotope signatures. For instance, biomarkers for anoxygenic photosynthesizing bacteria can be helpful in conceptualizing possible sources of organic matter in a mixed phytoplankton community and the isotopic consequences for TOC and/or individual compounds (*e.g.*, Hollander et al., 1993; Schwab and Spangenberg, 2007). Sedimentary hopane:sterane ratios also are frequently interpreted to indicate the possible relative contribution of bacteria (photosynthetic or heterotrophic) to sedimentary organic matter. Given the results of the mixed-community model as shown in Figure 5.4, inverse values of $\Delta\delta_{n\text{-alkyl–TOC}}$ are achieved at a population ratio of primary prokaryotes:eukaryotes $\geq \sim 10^{3.5}$. This corresponds to biomass ratios of $\geq \sim 1{:}1$. Making the very broad assumptions that hopanes and steranes comprise approximately equal fractions of the biomass of their respective sources and that they degrade at rates proportional to *n*-alkyl lipids, hopane:sterane ratios could be ~1:1, even when the $\Delta\delta_{n\text{-alkyl-TOC}}$ signature is still positive. This is consistent with observations from the Proterozoic (Grosjean et al., 2009; Love et al., 2009). Accordingly, the transition of the Δδ signature to negative values need not accompany a major disturbance in the biomarker record. Given the

many uncertainties in translating biomarker ratios to quantitative estimates of the associated biomass, this supports the idea that such ratios benefit from concomitant isotopic measurements.

Conclusions. It has been suggested previously that ^{13}C-enriched lipids in Proterozoic and Archean deposits could derive from a distinct portion of the photosynthetic community (Hieshima, 1992; Logan et al., 1997; Brocks et al., 2003b), but until now this idea has not been explored quantitatively or adopted as an explanation for Proterozoic inverse organic isotopic patterns. Conversely, the suggestion that ^{13}C-enriched lipids derive from preferentially-preserved late-stage heterotrophs (Logan et al., 1995) has been widely adopted, but to date the potential mechanisms for this effect have not been treated quantitatively. Our models support the former idea.

Consistent inverse values for $\Delta\delta_{n\text{-alkyl–kerogen}}$ are most easily and broadly explained by an isotopically heterogeneous community of primary producers, and not solely by preferential preservation of lipids from heterotrophs. However, inverse values observed for $\Delta\delta_{n\text{-alkyl-isoprenoid}}$ are best explained in the model by enhanced preservation of heterotrophs *within* a mixed primary community scenario. The latter signature implicates the importance of non-uniform degradation as a function of trophic level. In turn this suggests that variations in environment-specific factors like stratification, water depth, and oxygen concentrations are more readily expressed within the $\Delta\delta_{n\text{-alkyl-isoprenoid}}$ signal; while the overall fractionations between organic and inorganic carbon are best represented by *n*-alkyl lipids, kerogen, and carbonate. More compound-specific isotopic measurements from all time periods of the Proterozoic and Cambrian – from well-constrained environmental settings – should help to elucidate more detailed controls on these signatures.

Acknowledgments

We would like to thank Dan Rothman, Roger Summons, Alex Bradley, and John Hayes for helpful discussions; and Rita Parai for Matlab advice. This work was supported by an ExxonMobil Geoscience Grant (to H.G.C.), the Harvard University Science and Engineering Committee (HUSEC), and by NSF-OCE-0927290 and the David and Lucille Packard Foundation (to A.P.). We also thank Lee Kump for editorial assistance and four anonymous reviewers for their valuable comments.

References

Agawin NSR, Duarte CM, Agustí S (2000) Nutrient and temperature control of the contribution of picoplankton to phytoplankton biomass and production. *Limnology and Oceanography,* **45**, 591-600.

Allard B, Templier J, Largeau C (1997) Artifactual origin of mycobacterial bacteran. Formation of melanoidin-like artifact macromolecular material during the usual isolation process. *Organic Geochemistry,* **26**, 691-703.

Anbar A, Knoll A (2002) Proterozoic ocean chemistry and evolution: a bioinorganic bridge? *Science,* **297**, 1137-1142.

Badger MR, Price GD (2003) CO_2 concentrating mechanisms in cyanobacteria: molecular components, their diversity and evolution. *Journal of Experimental Botany,* **54**, 609-622.

Brocks JJ, Buick R, Logan Ga, Summons RE (2003a) Composition and syngeneity of molecular fossils from the 2.78 to 2.45 billion-year-old Mount Bruce Supergroup, Pilbara Craton, Western Australia. *Geochimica et Cosmochimica Acta,* **67**, 4289-4319.

Brocks JJ, Buick R, Summons RE, Logan GA (2003b) A reconstruction of Archean biological diversity based on molecular fossils from the 2.78 to 2.45 billion-year-old Mount Bruce Supergroup, Hamersley Basin, Western Australia. *Geochimica et Cosmochimica Acta,* **67**, 4321-4335.

Burd AB, Jackson GA (2009) Particle Aggregation. *Annual Review of Marine Science,* **1**, 65-90.

Butterfield NJ (2009) Oxygen, animals and oceanic ventilation: an alternative view. *Geobiology,* **7**, 1-7.

Canfield D (1998) A new model for Proterozoic ocean chemistry. *Nature,* **396**, 450-453.

Canfield D, Poulton SW, Knoll AH, Narbonne GM, Ross G, Goldberg T, Strauss H (2008) Ferruginous conditions dominated later Neoproterozoic deep-water chemistry. *Science*, **321**, 949-952.

Dawson D, Grice K, Alexander R, Edwards D (2007) The effect of source and maturity on the stable isotopic compositions of individual hydrocarbons in sediments and crude oils from the Vulcan Sub-basin, Timor Sea, Northern Australia. *Organic Geochemistry,* **38**, 1015-1038.

del Giorgio P, Cole J (1998) Bacterial growth efficiency in natural aquatic systems. *Annual Review of Ecology and Systematics,* **29**, 503-541.

DeNiro M, Epstein S (1978) Influence of diet on the distribution of carbon isotopes in animals. *Geochimica et Cosmochimica Acta,* **42**, 495-506.

Eigenbrode J, Freeman K, Summons R (2008) Methylhopane biomarker hydrocarbons in Hamersley Province sediments provide evidence for Neoarchean aerobiosis. *Earth and Planetary Science Letters,* **273**, 323-331.

Eigenbrode JL, Freeman KH (2006) Late Archean rise of aerobic microbial ecosystems. *Proceedings of the National Academy of Sciences,* **103**, 15759-15764.

Erez J, Bouevitch A, Kaplan A (1998) Carbon isotope fractionation by photosynthetic aquatic microorganisms: experiments with Synechococcus PCC7942, and a simple carbon flux model. *Canadian Journal of Botany,* **76**, 1109-1118.

Falkowski PG (1991) Species variability in the fractionation of ^{13}C and ^{12}C by marine phytoplankton. *Journal of Plankton Research,* **13**, 21-28.

Fike DA, Grotzinger JP, Pratt LM, Summons RE (2006) Oxidation of the Ediacaran ocean. *Nature*, **444**, 744-747.

Fujieki L, Santiago-Mandujano F, Lethaby P, Lukas R, Karl D (2010) Hawaii Ocean Time-series Program Data Report 19: 2007. University of Hawaii School of Ocean and Earth Science and Technology, Honolulu, HI, pp. 403. Available Online: http://hahana.soest.hawaii.edu/hot/reports/reports.html.

Grice K, Cao C, Love GD, Böttcher ME, Twitchett RJ, Grosjean E, Summons RE, Turgeon SC, Dunning W, Jin Y (2005) Photic zone euxinia during the Permian-Triassic superanoxic event. *Science,* **307**, 706-709.

Grice K, Schaeffer P, Schwark L, Maxwell JR (1996) Molecular indicators of palaeoenvironmental conditions in an immature Permian shale (Kupferschiefer, Lower Rhine Basin, north-west Germany) from free and S-bound lipids. *Organic Geochemistry,* **25**, 131-147.

Grosjean E, Love GD, Stalvies C, Fike DA, Summons RE (2009) Origin of petroleum in the Neoproterozoic–Cambrian South Oman Salt Basin. *Organic Geochemistry,* **40**, 87-110.

Grossi V, Blokker P, Sinninghe Damsté JS (2001) Anaerobic biodegradation of lipids of the marine microalga Nannochloropsis salina. *Organic Geochemistry,* **32**, 795-808.

Gu B, Schelske CL (1996) Temporal and spatial variations in phytoplankton carbon isotopes in a polymictic subtropical lake. *Journal of Plankton Research,* **18**, 2081-2092.

Guthrie JM (1996) Molecular and carbon isotopic analysis of individual biological markers: evidence for sources of organic matter and paleoenvironmental conditions in the Upper Ordovician Maquoketa Group, Illinois Basin, U.S.A. *Organic Geochemistry,* **25**, 439-460.

Hall J, Vincent W (1990) Vertical and horizontal structure in the picoplankton communities of a coastal upwelling system. *Marine Biology,* **106**, 465-471.

Hartnett H, Keil R, Hedges J, Devol A (1998) Influence of oxygen exposure time on organic carbon preservation in continental margin sediments. *Nature,* **391**, 2-4.

Harvey HR, Macko SA (1997) Catalysts or contributors? Tracking bacterial mediation of early diagenesis in the marine water column. *Organic Geochemistry,* **26**, 531-544.

Harvey HR, Tuttle JH, Bell JT (1995) Kinetics of phytoplankton decay during simulated sedimentation: Changes in biochemical composition and microbial activity under oxic and anoxic conditions. *Geochimica et Cosmochimica Acta,* **59**, 3367-3377.

Hayes JM (1983) Geochemical evidence bearing on the origin of aerobiosis, a speculative hypothesis. In: *Earth's earliest biosphere: Its origin and evolution* (ed Schopf JW). Princeton University Press, Princeton, NJ, pp. 291-301.

Hayes JM (2001) Fractionation of the isotopes of carbon and hydrogen in biosynthetic processes. *Reviews in Mineralogy and Geochemistry,* **43**, 225-278.

Hays LE (2010) *Biogeochemical Proxies for Environmental and Biotic Conditions at the Permian-Triassic Boundary* (Doctoral dissertation). Available from Massachusetts Institute of Technology Libraries. (http://hdl.handle.net/1721.1/59738)

Hebting Y, Schaeffer P, Behrens a, Adam P, Schmitt G, Schneckenburger P, Bernasconi SM, Albrecht P (2006) Biomarker evidence for a major preservation pathway of sedimentary organic carbon. *Science,* **312**, 1627-1631.

Hedges JI, Hu FS, Devol AH, Hartnett HE, Tsamakis E, Keil RG (1999) Sedimentary organic matter preservation: a test for selective degradation under oxic conditions. *American Journal of Science,* **299**, 529-555.

Hedges JI, Keil RG (1995) Sedimentary organic matter preservation: an assessment and speculative synthesis. *Marine Chemistry,* **49**, 81-115.

Henrichs SM (1992) Early diagenesis of organic matter in marine sediments: progress and perplexity. *Marine Chemistry,* **39**, 119-149.

Hieshima, GB (1992). *Organic and isotopic geochemical study of the middle Proterozoic Nonesuch Formation, North American Midcontinent Rift* (Doctoral dissertation). Available from ProQuest Dissertations and Theses Full Text database. (UMI No. AAT 9231552)

Hinrichs K-U (2002) Microbial fixation of methane carbon at 2.7 Ga: Was an anaerobic mechanism possible? *Geochemistry Geophysics Geosystems,* **3**.

Hoering T (1965) The extractable organic matter in Precambrian rocks and the problem of contamination. *Year Book - Carnegie Institution of Washington,* **64**, 215-218.

Hoering T (1967) Criteria for suitable rocks in Precambrian organic geochemistry. *Year Book - Carnegie Institution of Washington,* **65**, 365-372.

Höld IM, Schouten S, Jellema J, Sinninghe Damsté JS (1999) Origin of free and bound mid-chain methyl alkanes in oils, bitumens and kerogens of the marine, Infracambrian Huqf Formation (Oman). *Organic Geochemistry,* **30**, 1411-1428.

Hollander DJ, Sinninghe Damste JS, Hayes JM, de Leeuw JW, Huc AY (1993) Molecular and bulk isotopic analyses of organic matter in marls of the Mulhouse Basin (Tertiary, Alsace, France). *Organic Geochemistry,* **20**, 1253-1263.

Hotinski RM, Kump LR, Arthur MA (2004) The effectiveness of the Paleoproterozoic biological pump: A $\delta^{13}C$ gradient from platform carbonates of the Pethei Group (Great Slave Lake Supergroup, NWT). *Geological Society of America Bulletin,* **116**, 539-554.

House CH, Schopf JW, Stetter KO (2003) Carbon isotopic fractionation by Archaeans and other thermophilic prokaryotes. *Organic Geochemistry,* **34**, 345-356.

Jahnke RA, Craven DB (1995) Quantifying the role of heterotrophic bacteria in the carbon cycle: A need for respiration rate measurements. *Limnology and Oceanography,* **40**, 436-441.

Jiang L, Schofield OME, Falkowski PG (2005) Adaptive evolution of phytoplankton cell size. *The American naturalist,* **166**, 496-505.

Joachimski MM, Ostertag-Henning C, Pancost RD, Strauss H, Freeman KH, Littke R, Sinninghe Damsté JS, Racki G (2001) Water column anoxia, enhanced productivity and concomitant changes in $\delta^{13}C$ and $\delta^{34}S$ across the Frasnian–Famennian boundary (Kowala — Holy Cross Mountains/Poland). *Chemical Geology,* **175**, 109-131.

Johnston DT, Wolfe-Simon F, Pearson A, Knoll AH (2009) Anoxygenic photosynthesis modulated Proterozoic oxygen and sustained Earth's middle age. *Proceedings of the National Academy of Sciences of the United States of America,* **106**, 16925-16929.

Kashiyama Y, Ogawa NO, Kuroda J, Shiro M, Nomoto S, Tada R, Kitazato H, Ohkouchi N (2008a) Diazotrophic cyanobacteria as the major photoautotrophs during mid-Cretaceous oceanic anoxic events: Nitrogen and carbon isotopic evidence from sedimentary porphyrin. *Organic Geochemistry,* **39**, 532-549.

Kashiyama Y, Ogawa NO, Shiro M, Tada R, Kitazato H, Ohkouchi N (2008b) Reconstruction of the biogeochemistry and ecology of photoautotrophs based on the nitrogen and carbon isotopic compositions of vanadyl porphyrins from Miocene siliceous sediments. *Biogeosciences,* **5**, 797-816.

Kelly, A. E. (2009). *Hydrocarbon biomarkers for biotic and environmental evolution through the Neoproterozoic-Cambrian transition* (Doctoral dissertation). Available from ProQuest Dissertations and Theses Full Text database. (UMI No. AAT 0822083)

Knoll AH, Summons RE, Waldbauer JR, Zumberge JE (2007) The geological succession of primary producers in the oceans. In: *Evolution of Primary Producers in the Sea* (eds Falkowski PG, Knoll AH). Elsevier Academic Press, Burlington, MA, pp. 133-163.

Kodner RB, Summons RE, Knoll AH (2009) Phylogenetic investigation of the aliphatic, non-hydrolyzable biopolymer algaenan, with a focus on green algae. *Organic Geochemistry,* **40**, 854-862.

Li WKW (1994) Primary production of prochlorophytes , cyanobacteria, and eucaryotic ultraphytoplankton : measurements from flow cytometric sorting. *Limnology and Oceanography,* **39**, 169-175.

Logan GA, Calver CR, Gorjan P, Summons RE, Hayes JM, Walter MR (1999) Terminal Proterozoic mid-shelf benthic microbial mats in the Centralian Superbasin and their environmental significance. *Geochimica et cosmochimica acta,* **63**, 1345-1358.

Logan GA, Hayes JM, Hieshima GB, Summons RE (1995) Terminal Proterozoic reorganization of biogeochemical cycles. *Nature,* **376**, 53-56.

Logan GA, Summons RE, Hayes JM (1997) An isotopic biogeochemical study of Neoproterozoic and Early Cambrian sediments from the Centralian Superbasin, Australia. *Geochimica et Cosmochimica Acta,* **61**, 5391-5409.

Love GD, Grosjean E, Stalvies C, Fike Da, Grotzinger JP, Bradley AS, Kelly AE, Bhatia M, Meredith W, Snape CE, Bowring Sa, Condon DJ, Summons RE (2009) Fossil steroids record the appearance of Demospongiae during the Cryogenian period. *Nature,* **457**, 718-721.

Marañón E, Fernandez A, Mouriño-Carballido B, Martinez-Garcia S, Teira E, Cermeno P, Choucino P, Huete-Ortega M, Fernandez E, Calvo-Diaz A, Moran X, Bode A, Moreno-Ostos E, Varela MM, Patey MD, Achterberg EP (2010) Degree of oligotrophy controls the response of microbial plankton to Saharan dust. *Limnology and Oceanography,* **55**, 2339-2352.

Martin JH, Knauer GA, Karl DM, Broenkow WW (1987) VERTEX: carbon cycling in the northeast Pacific. *Deep Sea Research Part A. Oceanographic Research Papers,* **34**, 267-285.

McFadden Ka, Huang J, Chu X, Jiang G, Kaufman AJ, Zhou C, Yuan X, Xiao S (2008) Pulsed oxidation and biological evolution in the Ediacaran Doushantuo Formation. *Proceedings of the National Academy of Sciences of the United States of America,* **105**, 3197-3202.

Middelburg J, Vlug T, van der Nat F (1993) Organic matter mineralization in marine systems. *Global and Planetary Change,* **8**, 47-58.

Middelburg JJ (1989) A simple rate model for organic matter decomposition in marine sediments. *Geochimica et Cosmochimica Acta,* **53**, 1577-1581.

Nabbefeld B, Grice K, Twitchett RJ, Summons RE, Hays L, Böttcher ME, Asif M (2010) An integrated biomarker, isotopic and palaeoenvironmental study through the Late Permian event at Lusitaniadalen, Spitsbergen. *Earth and Planetary Science Letters,* **291**, 84-96.

Nguyen R, Harvey HR, Zang X, van Heemst JDH, Hetenyi M, Hatcher PG (2003) Preservation of algaenan and proteinaceous material during the oxic decay of Botryococcus braunii as revealed by pyrolysis-gas chromatography/mass spectrometry and 13C NMR spectroscopy. *Organic Geochemistry,* **34**, 483-497.

Pardue JW, Scalan RS, van Baalen C, Parker PL (1976) Maximum carbon isotope fractionation in photosynthesis by blue-green algae and a green alga. *Geochimica et Cosmochimica Acta,* **40**, 309-312.

Popp BN, Laws EA, Bidigare RR, Dore JE, Hanson KL, Wakeham SG (1998) Effect of phytoplankton cell geometry on carbon isotopic fractionation. *Geochimica et Cosmochimica Acta,* **62**, 69-77.

Preuß A, Schauder R, Fuchs G (1989) Carbon isotope fractionation by autotrophic bacteria with three different CO2 fixation pathways. *Zeitschrift für Naturforschung,* **44c**, 397-402.

Price GD, Sültemeyer D, Klughammer B, Ludwig M, Badger MR (1998) The functioning of the CO_2 concentrating mechanism in several cyanobacterial strains: a review of general physiological characteristics, genes, proteins, and recent advances. *Canadian Journal of Botany,* **76**, 973-1002.

Raven JA (1998) The Twelfth Tansley Lecture, Small is Beautiful: The Picophytoplankton. *Functional Ecology,* **12**, 503-513.

Richardson TL, Jackson Ga (2007) Small phytoplankton and carbon export from the surface ocean. *Science,* **315**, 838-840.

Riding R (2006) Cyanobacterial calcification, carbon dioxide concentrating mechanisms, and Proterozoic-Cambrian changes in atmospheric composition. *Geobiology,* **4**, 299-316.

Robinson JJ, Cavanaugh CM (1995) Expression of form I and form II Rubisco in chemoautotrophic symbioses: implications for the interpretation of stable carbon isotope values. *Limnology and Oceanography,* **40**, 1496-1502.

Roeske CA, O'Leary MH (1985) Carbon isotope effect on carboxylation of ribulose bisphosphate catalyzed by ribulose bisphosphate carboxylase from Rhodospirillum rubrum. *Biochemistry,* **24**, 1603-1607.

Rothman DH, Forney DC (2007) Physical model for the decay and preservation of marine organic carbon. *Science,* **316**, 1325-1328.

Schidlowski M (1987) Application of stable carbon isotopes to early biochemical evolution on Earth. *Annual Review of Earth and Planetary Sciences,* **15**, 47-72.

Schouten S, Klein Breteler W, Blokker P, Schogt N, Rijpstra W, Grice K, Baas M, Sinninghe Damsté JS (1998) Biosynthetic effects on the stable carbon isotopic compositions of algal lipids: Implications for deciphering the carbon isotopic biomarker record. *Geochimica et Cosmochimica Acta,* **62**, 1397-1406.

Schwab V, Spangenberg JE (2004) Organic geochemistry across the Permian–Triassic transition at the Idrijca Valley, Western Slovenia. *Applied Geochemistry,* **19**, 55-72.

Schwab VF, Spangenberg JE (2007) Molecular and isotopic characterization of biomarkers in the Frick Swiss Jura sediments: A palaeoenvironmental reconstruction on the northern Tethys margin. *Organic Geochemistry,* **38**, 419-439.

Sinninghe Damsté JS, Kuypers MMM, Pancost RD, Schouten S (2008) The carbon isotopic response of algae, (cyano)bacteria, archaea and higher plants to the late Cenomanian perturbation of the global carbon cycle: Insights from biomarkers in black shales from the Cape Verde Basin (DSDP Site 367). *Organic Geochemistry,* **39**, 1703-1718.

Sirevåg R, Buchanan B, Berry J, Troughton J (1977) Mechanisms of CO2 fixation in bacterial photosynthesis studied by the carbon isotope fractionation technique. *Archives of Microbiology,* **112**, 35-38.

Tchernov D, Lipschultz F (2008) Carbon isotopic composition of Trichodesmium spp. colonies off Bermuda: effects of colony mass and season. *Journal of Plankton Research,* **30**, 21-31.

Teece M, Fogel M, Dollhopf M, Nealson K (1999) Isotopic fractionation associated with biosynthesis of fatty acids by a marine bacterium under oxic and anoxic conditions. *Organic Geochemistry,* **30**, 1571-1579.

Tolosa I, Miquel J-C, Gasser B, Raimbault P, Goyet C, Claustre H (2008) Distribution of lipid biomarkers and carbon isotope fractionation in contrasting trophic environments of the South East Pacific. *Biogeosciences,* **5**, 949-968.

van Der Meer MTJ, Schouten S, Sinninghe Damsté JS (1998) The effect of the reversed tricarboxylic acid cycle on the 13C contents of bacterial lipids. *Organic Geochemistry,* **28**, 527-533.

van Der Meer MTJ, Schouten S, Sinninghe Damsté JS, de Leeuw JW, Ward DM (2003) Compound-specific isotopic fractionation patterns suggest different carbon metabolisms among Chloroflexus-like bacteria in hot-spring microbial mats. *Applied and Environmental Microbiology,* **69**, 6000-6006.

van Kaam-Peters HME, Schouten S, de Leeuw JW, Sinninghe Damsté JS (1997) A molecular and carbon isotope biogeochemical study of biomarkers and kerogen pyrolysates of the Kimmeridge Clay Facies: palaeoenvironmental implications. *Organic Geochemistry,* **27**, 399-422.

Versteegh GJM, Zonneveld KAF (2002) Use of selective degradation to separate preservation from productivity. *Geology,* **30**, 615.

Vuorio K, Meili M, Sarvala J (2006) Taxon-specific variation in the stable isotopic signatures (delta13C and delta15N) of lake phytoplankton. *Freshwater Biology,* **51**, 807-822.

Wakeham SG, Lee C, Hedges JI, Hernes PJ, Peterson MJ (1997) Molecular indicators of diagenetic status in marine organic matter. *Geochimica et Cosmochimica Acta,* **61**, 5363-5369.

Westrich JT, Berner RA (1984) The role of sedimentary organic matter in bacterial sulfate reduction : The G model tested. *Limnology and Oceanography,* **29**, 236-249.

Zonneveld KAF, Versteegh GJM, Kasten S, Eglinton TI, Emeis K-C, Huguet C, Koch BP, de Lange GJ, de Leeuw JW, Middelburg JJ, Mollenhauer G, Prahl FG, Rethemeyer J, Wakeham SG (2010) Selective preservation of organic matter in marine environments; processes and impact on the sedimentary record. *Biogeosciences,* **7**, 483-511.

Appendix, Chapter 5

Models and parameterization

Case 1: Simple uniform degradation through multiple trophic levels

We begin with the simplest case, where all organic matter degrades to a total extent (or exposure time), d, with a rate constant k. The amount of preserved ("sedimentary") organic matter from a given trophic level N, as a function of P_0, or the starting amount of total primary photosynthetic organic matter, is

$$P_N(d) = e^{-Kd} P_0 E^N \left(1 - e^{-Kd}\right)^N \quad (1)$$

where primary OM is represented as trophic level N = 0, heterotrophy proceeds from trophic levels N = 1 through infinity or some derived terminal level T, E is the heterotrophic efficiency (fraction of OM incorporated into de novo biomass rather than respired as CO_2), e^{-Kd} is the fraction of biomass that is preserved at each trophic level, and $1 - e^{-Kd}$ is the fraction of biomass that is transferred to the next trophic level. The amount of biomass in the cells of a trophic level N, before being degraded further by trophic level N + 1, is thus $P_0E^N(1 - e^{-Kd})^N$.

The total preserved organic matter from all trophic levels then is

$$P(d) = e^{-Kd} P_0 \sum E^N \left(1 - e^{-Kd}\right)^N \quad (2)$$

We can determine the final, net isotopic value for preserved organic matter simply by multiplying the fractional contribution of biomass from each trophic level, $P_N(d)/P(d)$, by its isotopic value, which is determined by compounded heterotophic isotopic enrichment from the primary signature δ_{P0}.

(3) $$\delta_P(d) = \sum \frac{P_N(d)\,(\delta_{P_0} + hN\,(1-E))}{P(d)}$$

where h is the maximum isotopic enrichment at each trophic level and actual enrichment per trophic level depends on the heterotrophic efficiency E as h(1 - E).

In calculating the resulting isotopic content of net preserved organic matter according to these equations, over a range of exposure times d and using the parameter values in Table 1 of the main document, we find that heterotrophic biomass contribution is substrate-limited enough that the $\delta^{13}C$ value of total preserved biomass is only enriched slightly in ^{13}C due to heterotrophic processing, in comparison to starting primary organic matter (Figure A5.1). Because no distinction is made between degradation rates for different biochemical classes, the amount and isotopic content of all compounds types will relate to the trophic level at which they were biosynthesized. Therefore, the $\Delta\delta_{n\text{-alkyl-TOC}}$ value will always reflect that of biosynthetic product.

Case 2a: Heterotrophic enrichment hypothesis- Distinct degradation rates for compound classes

Starting again with total photosynthetic biomass P_0, we now account for differences in degradation rate constants for different compound classes. Photosynthetic biomass is modeled in three components: resistant biopolymer (R), lipid (L), and other, labile biomass (B), which are biosynthesized in photosynthetic cells (N=0) in the corresponding proportions F_R, F_L, and F_B, such that $F_R + F_L + F_B = 1$. Heterotrophic cells are modeled as containing only lipid and labile

biomass (F_R = 0). We will use the notation F_X to refer to generalized heterotrophic (H) components in the following formulations, and simply stipulate that for trophic levels N = 1 and above, $F_R = 0$, $F_B = F_{HB}$ and $F_L = F_{HL}$. Total biomass synthesized in a given trophic level has the isotopic signature δ_{PN}, and isotopic values for resistant biopolymer (δ_R) and lipid (δ_L) are calculated by subtracting biosynthetic fractionations ε_R and ε_L, respectively, from δ_N. The isotopic value of the remaining labile biomass (B) is calculated by difference from the isotopic mass balance

(4) $$\delta_{P_N} = F_{\overline{B}}\delta_B + F_{\overline{L}}\delta_L + F_{\overline{R}}\delta_R$$

If each class of compounds also has a distinctive degradation rate K_X, the amount of preserved organic matter from primary producers alone (N = 0) is

(5) $$P_0(d) = P_0\left(F_R e^{-K_R d} + F_L e^{-K_L d} + F_B e^{-K_B d}\right)$$

and its isotopic content can be calculated as

(6) $$\delta_{P_0}(d) = \frac{F_R e^{-K_R d}\delta_R + F_L e^{-K_L d}\delta_L + F_B e^{-K_B d}\delta_B}{F_R e^{-K_R d} + F_L e^{-K_L d} + F_B e^{-K_B d}}$$

Accounting for fractional contribution and different degradation rates of the compound classes, as well as the presence of resistant biopolymer R only in trophic level N = 0, the analog for Equation 1 above, for trophic levels N = 1 and above only, is

(7)

$$P_N(d) = P_0 E^N \left(F_{\overline{L}} e^{-K_L d} + F_{\overline{B}} e^{-K_B d}\right) \left[1 - F_{\overline{L}} e^{-K_L d} - F_{\overline{B}} e^{-K_B d}\right]^{N-1} \left(1 - F_R e^{-K_R d} - F_L e^{-K_L d} - F_B e^{-K_B d}\right)$$

$$\text{for } N = 1 \text{to } T.$$

The total preserved organic matter, starting from N = 0 (primary producers) is then

(8)

$$P(d) = \sum P_N(d)$$

The isotopic signature of organic matter preserved from each heterotrophic level will depend on the organic matter consumed, the metabolic efficiency and corresponding net isotopic enrichment, isotopic fractionation during biosynthesis of different compound classes, and the differential loss of these classes to degradation by higher trophic levels. Before degradation by the trophic level N + 1, we know that isotopic value is inherited from the degraded portion of the previous trophic level and enriched such that

(9)

$$\delta_{P_N} = \delta_{P_{(N-1)_{Deg}}} + h(1 - E)$$

where $\delta_{P(N-1)\ Deg}$ can be calculated by difference from $\delta_{P(N-1)}$ and $\delta_{P(N-1)}(d)$, and the second term is the isotopic enrichment by a single heterotrophic level N.

Lipid in trophic level N has an isotopic value of

(10)

$$\delta_{\overline{L}} = \delta_{P_{(N-1)_{Deg}}} + h(1 - E) - \varepsilon_L$$

The isotopic value for the more labile components of biomass, by difference, is then

(11)

$$\delta_{\overline{B}} = \left[\delta_{P_{(N-1)_{Deg}}} + h\,(1 - E)\right] \left(1 - F_{\overline{L}}\right) + F_{\overline{L}} \varepsilon_L$$

After degradation by trophic level N + 1, the residual biomass is preserved in new proportions according to the different rates of decay; the amount of preserved organic matter from a given compound class X at trophic level N and after degradation d is

(12)

$$X_N(d) = P_0 E^N F_{\overline{X}} e^{-K_X d} \left[1 - F_{\overline{L}} e^{-K_L d} - F_{\overline{B}} e^{-K_B d}\right]^{N-1} \left(1 - F_R e^{-K_R d} - F_L e^{-K_L d} - F_B e^{-K_B d}\right)$$

The fractional contribution to total preserved organic matter from a compound class X is thus $X_N(d)/P_N(d)$; therefore the net isotopic value for total preserved organic matter from trophic level N after degradation d is

(13)

$$\delta_{P_N}(d) = \frac{B_N(d)}{P_N(d)} \delta_{\overline{B}} + \frac{L_N(d)}{P_N(d)} \delta_{\overline{L}}$$

For the next trophic level, we can calculate the isotopic value of biomass that is degraded from trophic level N by difference, as mentioned:

(14)

$$\delta_{P_{N_{Deg}}} = \frac{F_{\overline{B}}(1 - e^{-K_B d})\delta_{\overline{B}} + F_{\overline{L}}(1 - e^{-K_L d})\delta_{\overline{L}}}{1 - F_{\overline{B}} e^{-K_B d} - F_{\overline{L}} e^{-K_L d}}$$

$$\text{for } N = 1 \text{ to } T.$$

This formula holds for N = 1 and above. The isotopic value of primary organic matter consumed by the first heterotrophic level differs slightly, since it must account for resistant biopolymer from primary producers:

(15)

$$\delta_{P_{0_{Deg}}} = \frac{F_R(1 - e^{-K_R d})\delta_R + F_L(1 - e^{-K_L d})\delta_L + F_B(1 - e^{-K_B d})\delta_B}{1 - F_R e^{-K_R d} - F_L e^{-K_L d} - F_B e^{-K_B d}}$$

Thus we can successively derive both amounts and isotopic values for total organic matter and lipid preserved from each trophic level. After summing the total amount preserved, we then calculate the fractional contribution of each trophic level, and create a weighted average of isotopic values in order to derive the final "sedimentary" isotopic value for TOC and lipid:

(16) $$\delta_P(d) = \sum \frac{P_N(d)\delta_{P_N}(d)}{P(d)}$$

(17) $$\delta_L(d) = \sum \frac{L_N(d)\delta_{\overline{L}}(d)}{L(d)}$$

Case 2b: Logan hypothesis- Attenuation of degradation effects in higher trophic levels

For calculations involving an attenuation of exposure time for increasing trophic levels, amounts of heterotrophic material can no longer be expressed as a simple sum: these must also be calculated successively and summed. Where D(d,N) is some function of exposure time d and trophic level N that determines the attenuation of effective exposure time with trophic level,

(18) $$P_N(d) = EP_{N-1_{Deg}}\left(F_{HB}e^{-K_B D(d,N)} + F_{HL}e^{-K_L D(d,N)}\right)$$

and for the next level, the degraded organic matter from trophic level N, by difference,

(19) $$P_{N_{Deg}} = EP_{N-1_{Deg}} - P_N(d)$$

The isotopic values for each trophic level can be calculated as above, but replacing d in all cases with D(d,N). For the cases presented in which effective exposure time varies with trophic level, we have formulated the function D as

(20) $$D(d,N) = de^{-\zeta N}$$

where d is the "maximum exposure time" experienced by primary photosynthetic organic matter, ζ is some attenuation scaling factor as described (cases discussed include values of 0.16 and 0.5), and N is the trophic level. The influence of ζ on effective exposure time is shown in Figure A5.2.

Case 3: Size-population-dependent signature of primary organic matter

We now model two surface populations with different starting isotopic values and, in one case, with differing amounts of cellular lipid; the composition and isotopic signature of primary organic matter is thus dependent on the relative population of small and large cells in the surface ocean and some proportion or size scaling that determines their lipid content. For two size classes of cells, small (S) and large (G), we treat the average size of each as a ratio of small:large cell radius, or the fractional radius of the small cells R_z relative to the large cells. Similarly, the population of small:large cells is treated as a ratio, and thus this population ratio R_p can be treated as the numerical abundance of small cells for every one large cell. We then model the total amount of biomass from a given cell type as population × radius^3, assuming that the abundance of biomass in a cell is proportional to the cell volume. The amount of total biomass produced by small cells in the surface ocean is thus $P_S = R_p R_z^3$ and by large cells is $P_G = 1 \times 1^3$, and the total amount of photosynthetic biomass is

(21) $$P_0 = R_p R_z^3 + 1$$

The amount of lipid in a cell is modeled as some fraction of its biomass: the respective fractions are the values F_{SL} and F_{GL}. Retaining nomenclature for other compound classes as

before (the fractional contributions of which are calculated by difference from F_L), and assuming resistant biopolymer is only produced by large cells, the amount of biomass from primary producers that remains preserved after some degree of degradation d is

(22) $$P_0(d) = R_p R_z^3 \left(F_{SL} e^{-K_L d} + F_{SB} e^{-K_B d}\right) + F_{GL} e^{-K_L d} + F_{GB} e^{-K_B d} + F_{GR} e^{-K_R d}$$

In calculating the isotopic value of this primary biomass, we introduce an isotopic enrichment in small cells, of magnitude $\beta_{S\text{-}G}$ (per mil). We define the isotopic composition of large cells as δ_{0G}, and the starting isotopic composition of small cells is $\delta_{0S} = \delta_{0G} + \beta_{S\text{-}G}$. Assuming the biosynthetic isotopic fractionations as discussed previously, and calculating isotopic values for biosynthetic components by difference from the cellular total, the isotopic value of total preserved biomass from primary producers after some amount d of degradation is

(23)

$$\delta_{P_0}(d) = \frac{R_p R_z^3 (F_{SL} e^{-K_L d} \delta_{L0_S} + F_{SB} e^{-K_B d} \delta_{B0_S}) + F_{GL} e^{-K_L d} \delta_{L0_G} + F_{GB} e^{-K_B d} \delta_{B0_G} + F_{GR} e^{-K_R d} \delta_{R0_G}}{R_p R_z^3 (F_{SL} e^{-K_L d} + F_{SB} e^{-K_B d}) + F_{GL} e^{-K_L d} + F_{GB} e^{-K_B d} + F_{GR} e^{-K_R d}}$$

Heterotrophic biomass amounts, compound distribution, and isotopic content are calculated as in Case 2a, above.

Kerogen versus TOC terminology

TOC and kerogen for many Proterozoic deposits are observed to have very similar ^{13}C contents, differing by <1o (e.g. Hieshima, 1992 – Nonesuch Formation; Summons, 1992 – Chuar Group). Additionally, it has been estimated that ~90-95% of sedimentary TOC is typically comprised of kerogen (Durand, 1980); therefore, the isotopic signatures of TOC and kerogen

should be very similar, and deviations can sometimes be attributed to fluid migration (Strauss et al., 1992). Most Proterozoic isotopic studies cited report values for kerogen, excluding Hieshima (1992). For modeling purposes, however, we report TOC values, since the fractional partitioning of lipid products into bound kerogen rather than extractable bitumen is unclear, and could result in truncated model runs if extractable lipid concentrations are further limited. Our model-run degradation limit of 1 ppm lipid remaining in TOC would thus reflect all potentially measurable lipid, whether existing as free compounds or released from kerogen during diagenesis or analysis. Our model results are also assumed to be conservative since kerogen is usually slightly isotopically lighter than TOC, if different at all; considering kerogen rather than TOC would therefore increase the positive value of $\Delta\delta$.

Selection of Model Parameters

Degradation rate constants. Relative values for degradation rates of different compound classes are important in determining their effect on the composition and isotopic signature of both preserved primary organic matter and substrate available to heterotrophs. Absolute values are arbitrary since we do not address specific time intervals for degradation. While there are some literature examples of measured degradation rates for specific compound classes (e.g. Nguyen et al., 2003; Henrichs et al., 1992, among many), they address varying levels of chemical specificity, stages of degradation, and purity of source. The resulting rate values vary across many orders of magnitude. We incorporate a labile component of biomass across all organisms; its degradation rate can be addressed as arbitrarily fast, since we are considering mostly scenarios in which "unprotected" labile material is fully consumed or respired. In many published results (e.g. Henrichs et al., 1992) labile biomass is degraded at rates 2-3 orders of

magnitude faster than recalcitrant fractions. In others, it is degraded only a factor of 2 faster (e.g. Nguyen et al., 2003; Versteegh and Zonneveld, 2002).

We formulate degradation rates for lipid and other recalcitrant portions of organic matter so that lipid persists in concentrations of at least 1 ppm (i.e. detectable) in sedimentary scenarios where only a small portion (0.01%) of original primary organic matter is preserved. In order to ensure this, we choose rate constants such that

$$\frac{K_L}{K_R} \leq \left(\frac{\ln\left([L] * \frac{F_{Pres}}{F_L} \right)}{\ln\left(\frac{F_{Pres}}{F_R} \right)} \right) \quad (24)$$

where F_{Pres} is our requirement for minimum fraction of original primary organic matter preserved (0.0001; note this does not imply sedimentary concentration, as that is dependent on corresponding inorganic sedimentation rate) and [L] is the minimum required concentration of lipid in preserved OM in order to be detected (1 ppm). With these constraints, K_L/K_R must not exceed 2.7. We use this value in our examples in order to capture some distinction between free lipid and other resistant, potentially bound/polymerized compounds. In our Monte Carlo simulations, we explore a range down to a 1:1 relationship between K_L and K_R, in order to incorporate the possibility that lipid and the resistant fraction have similar sources and/or modes of protection from degradation.

Chemical and isotopic distribution across cell types. Literature values indicate that cellular lipid content can range from <5 to >25% (dry weight; Fernandez-Reiriz et al., 1989; Fleurence et al., 1992; Brown, 1991) depending on phylogeny and various environmental factors. Phospholipids, the major presumed precursors for preserved n-alkyl lipids, generally comprise some large fraction of total lipid. We therefore use an average value of 10% n-alkyl lipid for all cell types, but we consider a range of 5-25% in the Monte Carlo simulation. We use an average

biosynthetic fractionation of 4.5‰ for n-alkyl lipids as compared to average biomass for a given cell, but we consider a range of 3 to 6‰ in the Monte Carlo simulations, since fully-expressed fractionation factors for the biosynthetic pathway of acetogenic lipids would result in larger expressed fractionation, while high cellular lipid content might result in lower expressed fractionations (Laws, 1991; Hayes, 2001).

The resistant biological component that we account for could encompass a wide range of reported preservational effects in eukaryotes. Most directly, and in keeping with a Logan-type explanation, this could represent a cell-wall biopolymer of eukaryotic algae that is resistant to degradation (e.g. algaenan; Tegelaar et al., 1989, and others). Literature values vary widely as to the commonness, cellular content, and isotopic fractionation of these types of polymers (e.g. Kodner et al., 2009). Reports suggest the cellular content is likely to range from <10% to >30% (de Leeuw and Largeau, 1993), and since these polymers are usually described as strongly aliphatic in origin, some isotopic fractionation is suspected to occur during biosynthesis (e.g. Eglinton, 1994; Höld et al., 1998). Other modes of resistance for a eukaryotic component could stem from preferential physical protection of biomass through cell wall matrix effects (Nguyen et al., 2003), or from reduced exposure time via faster sinking through the water column (e.g. Butterfield, 2009; Burd and Jackson, 2009). In keeping with a biopolymer origin for the resistant fraction, we present cases in which the resistant fraction is isotopically depleted by 1.5‰ (the algaenan model) and comprises 30% of cellular material. However, in our Monte Carlo simulation, we address a 15-35% range of cellular composition and we explore isotopic signatures ranging from 4.5‰ depleted to 1.5‰ enriched in ^{13}C compared to average biomass. The wide range of isotopic values accounts for the possibility that the resistant fraction is instead

an early diagenetic polymerization product that could derive from a wide range of biochemical sources (e.g. Eglinton, 1994).

Heterotrophic efficiency and isotopic enrichment. The efficiency of conversion of organic substrate to *de novo* biosynthetic product by heterotrophic bacteria is commonly referred to as bacterial growth efficiency (BGE; e.g. del Giorgio and Cole, 1998), and is largely responsible for the limitations on trophic isotopic enrichment by the relationship $H = h_{max}(1 - E)$ as described above (where H = actual isotopic enrichment, h_{max} = maximum isotopic enrichment, and E = BGE). A wide range of values from <0.05 to >0.5 for E has been reported from natural environments. Del Giorgio and Cole (1998) related relative values of BGE to environmental/ecologic factors such as oligotrophy and eutrophy. We utilize an intermediate value of 0.3 in our examples, but we consider a wide range (0.05-0.6) in our Monte Carlo simulations, given the uncertainties on the ecological controls likely to be present in various Proterozoic environments.

The maximum isotopic enrichment per trophic level, h_{max}, is modulated by BGE as described. We utilize a maximum value of 1.5‰, a commonly cited value originally deriving from DeNiro and Epstein (1978), but incorporate a small range of uncertainty in this number by using values from 1-2‰ in our Monte Carlo simulations.

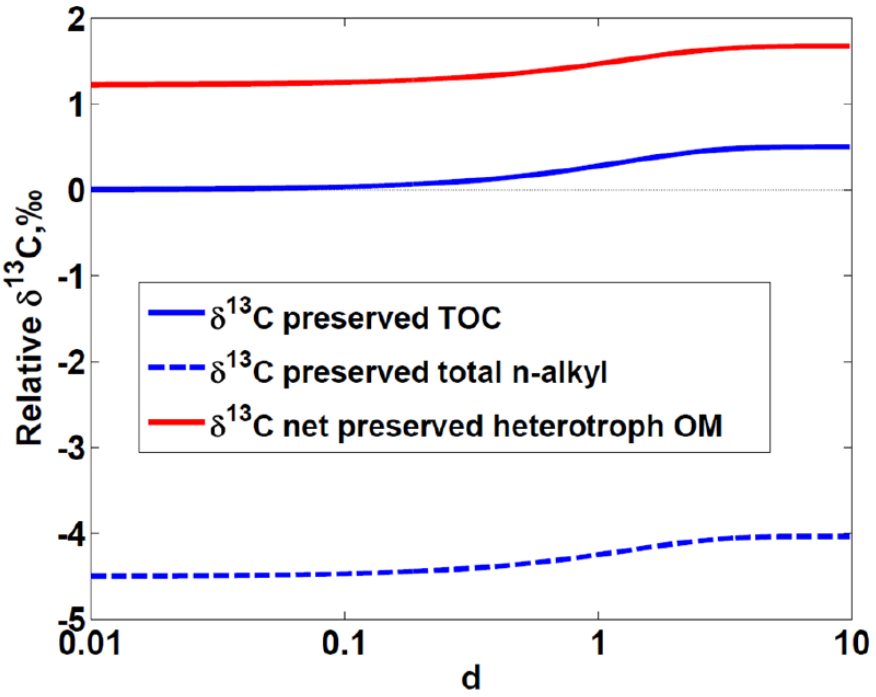

Figure A5.1. Final ^{13}C composition of preserved TOC, total n-alkyl lipid, and net heterotrophic contribution to TOC under Case 1. No distinction is made between compound classes; all are assumed to degrade at a constant rate. As d increases, the ^{13}C content of heterotrophic biomass increases because a larger supply of primary material is available to extend the food chain and increase the relative amount of biomass preserved from later trophic levels. The maximum enrichment is limited, however, by the decreasing amount of substrate available to late trophic levels. Total preserved n-alkyl lipid is preserved with an isotopic offset from TOC that reflects biosynthetic fractionation from the net organic pool. Although heterotrophic organic matter can become significantly positive in its $\delta^{13}C$ value, it cannot become positive enough to drive its associated n-alkyl lipids to values > 0 in relation to preserved TOC.

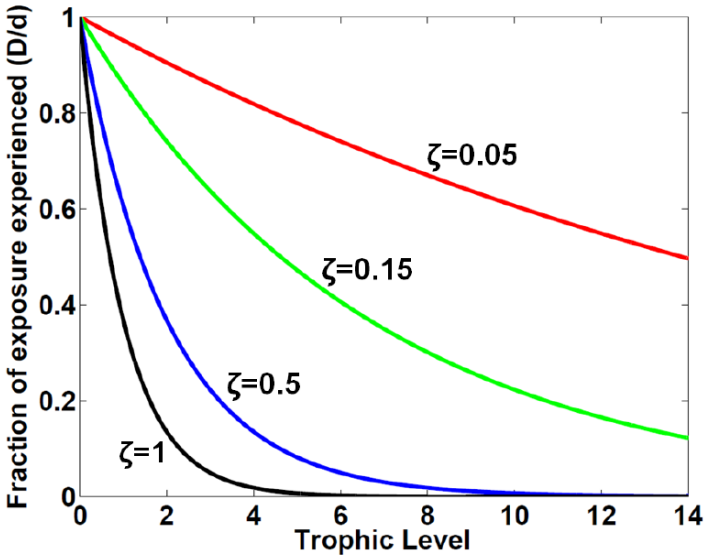

Figure A5.2. Effective attenuation of degradative exposure (D) experienced by trophic level (N), at different values of ζ. Primary producers are denoted by trophic level 0 and always experience the highest degradative exposure (d). Heterotrophic processing begins at trophic level 1; degradative exposure experienced by heterotrophic biomass is less than that experienced by primary producers by a factor of $e^{-\zeta N}$, such that $D = de^{-\zeta N}$.

References

Brown M (1991) The amino-acid and sugar composition of 16 species of microalgae used in mariculture. *Journal of Experimental Marine Biology and Ecology,* **145**, 79-99.

Burd AB, Jackson GA (2009) Particle Aggregation. *Annual Review of Marine Science,* **1**, 65-90.

Butterfield NJ (2009) Oxygen, animals and oceanic ventilation: an alternative view. *Geobiology,* **7**, 1-7.

de Leeuw JW, Largeau C (1993) A review of macromolecular organic compounds that comprise living organisms and their role in kerogen, coal and petroleum formation. In: *Organic Geochemistry: Principles and Applications* (eds Engel MH, Macko SA). Plenum Press, New York, pp. 23-72.

del Giorgio P, Cole J (1998) Bacterial growth efficiency in natural aquatic systems. *Annual Review of Ecology and Systematics,* **29**, 503-541.

DeNiro M, Epstein S (1978) Influence of diet on the distribution of carbon isotopes in animals. *Geochimica et Cosmochimica Acta,* **42**, 495-506.

Durand B (1980) *Kerogen - Insoluble Organic Matter from Sedimentary Rocks,* Éditions Technip, Paris.

Eglinton T (1994) Carbon isotopic evidence for the origin of macromolecular aliphatic structures in kerogen. *Organic Geochemistry,* **21**, 721-735.

Fernandez-Reiriz M, Perez-Camacho A, Ferreiro M, Blanco J, Planas M, Campos M, Labarta U (1989) Biomass production and variation in the biochemical profile (total protein, carbohydrates, RNA, lipids and fatty acids) of seven species of marine microalgae. *Aquaculture,* **83**, 17-37.

Fleurence J, Gutbier G, Mabeau S, Leray C (1994) Fatty acids from 11 marine macroalgae of the French Brittany coast. *Journal of Applied Phycology,* **6**, 527-532.

Hayes JM (2001) Fractionation of the isotopes of carbon and hydrogen in biosynthetic processes. *Reviews in Mineralogy and Geochemistry,* **43**, 225-278.

Henrichs SM (1992) Early diagenesis of organic matter in marine sediments: progress and perplexity. *Marine Chemistry,* **39**, 119-149.

Hieshima, GB (1992). *Organic and isotopic geochemical study of the middle Proterozoic Nonesuch Formation, North American Midcontinent Rift* (Doctoral dissertation). Available from ProQuest Dissertations and Theses Full Text database. (UMI No. AAT 9231552) 12

Höld IM, Schouten S, van Kaam-Peters HME, Sinninghe Damsté JS (1998) Recognition of nalkyl and isoprenoid algaenans in marine sediments by stable carbon isotopic analysis of pyrolysis products of kerogens. *Organic Geochemistry,* **28**, 179-194.

Kodner RB, Summons RE, Knoll AH (2009) Phylogenetic investigation of the aliphatic, nonhydrolyzable biopolymer algaenan, with a focus on green algae. *Organic Geochemistry,* **40**, 854-862.

Laws EA (1991) Photosynthetic quotients, new production and net community production in the open ocean. *Deep-Sea Research,* **38**, 143-167.

Logan GA, Hayes J, Hieshima GB, Summons RE (1995) Terminal Proterozoic reorganization of biogeochemical cycles. *Nature,* **376**, 53-56.

Nguyen R, Harvey HR, Zang X, van Heemst JDH, Hetenyi M, Hatcher PG (2003) Preservation of algaenan and proteinaceous material during the oxic decay of Botryococcus braunii as revealed by pyrolysis-gas chromatography/mass spectrometry and 13C NMR spectroscopy. *Organic Geochemistry,* **34**, 483-497.

Strauss H, Des Marais D, Hayes JM, Summons RE (1992) The Carbon-Isotopic Record. In: *The Proterozoic Biosphere: A Multidisciplinary Study* (eds Schopf Jw, Klein C). Cambridge University Press, Cambridge, pp. 117-128.

Summons RE (1992) Abundance and composition of extractable organic matter. In: *The Proterozoic Biosphere: A Multidisciplinary Study* (eds Schopf JW, Klein C). Cambridge University Press, Cambridge, pp. 101-115.

Tegelaar EW, de Leeuw JW, Derenne S, Largeau C (1989) A reappraisal of kerogen formation. *Geochimica et Cosmochimica Acta,* **53**, 3103-3106.

Versteegh GJM, Zonneveld KAF (2002) Use of selective degradation to separate preservation from productivity. *Geology,* **30**, 615-618.

Chapter 6

Comprehensive extraction of protein, nucleic acids, and lipids from environmental samples for natural isotope analysis, Part I: Extraction procedure and lipid recovery

Introduction

The following chapter describes the development and optimization of a detergent-based method for the extraction of organic matter from environmental samples. Development of this method has allowed for the extraction of environmental lipids from polyethersulfone filters as described in Chapter 3. This method has helped overcome a significant barrier in analysis of organic matter at the bacterial size scale due to the use of detergent rather than organic solvents, which dissolve the polymer components of many membrane filters. The extraction method is suitable for simultaneous recovery of total lipid, proteins, and nucleic acids, thus expanding the analytical yield and potential applications for a given (often biomass-poor) sample. This chapter describes "Part I" of quantitative extraction yields for this "total extraction protocol" (TEP): optimization of method and quantification of yield for intact polar lipids (IPL). Yields are quantified from the extraction of cultured bacterial biomass in both pellet and filter-retained form, and from environmental (filter) samples. Recovery of IPLs from environmental samples has recently become a priority in many organic geochemical applications.

Methods

Preparation of samples and standards.

Preparation of biomass from Synechocystis sp. PCC6803. Axenic cultures of freshwater cyanobacterium *Synechocystis* sp. PCC6803 were grown to concentrations of 10^9 cells/mL. Three measured volumes (Filter A = 1 mL, Filter B = 10 mL, Filter C = 100 mL; Table 6.1) of living culture were filtered via peristaltic pump onto separate 0.2 μm cartridge filters (Pall AcroPak™ 500, Supor® polyethersulfone) that had been pre-rinsed with a 10% HCl solution and autoclaved water. Filters were flushed with small volumes of autoclaved growth medium to

distribute cells, and were immediately frozen and stored at -80°C. Filters remained frozen during removal of Supor components from the filter housing. Filters were cut into pieces with solvent-clean blades and placed in a methanol-rinsed polycarbonate bead-beating chamber with pre-combusted 0.1 mm silica-zirconia beads (BioSpec). Several cell pellets were prepared from the same continuous culture by centrifugation of 50-mL aliquots (Table 6.1). Pellets were stored in polypropylene centrifuge tubes and immediately frozen at -80°C.

Table 6.1. Summary of culture samples and content

Sample ID	Extraction Method	IPL standards added	Other lipid standards added	Protein and DNA standards added	Synechocystis sp. PCC 6803 culture	Days of growth	Approximate cells/mL	Volume of culture extracted (mL)
Standards baseline test	none	X	X					
Standards-only TEP	TEP	X	X	X				
Pellet Q TEP	TEP	X			X	equivalent to Pellet N		12.5
Pellet R-a TEP	TEP	X	X		X	16	~6x10^8	10
Filter A TEP	TEP	X	X		X	9	~3x10^8	1
Filter B TEP	TEP	X	X		X	9	~3x10^8	10
Filter C TEP	TEP	X	X		X	9	~3x10^8	100
Pellet N Bligh & Dyer	Bligh & Dyer	X			X	equivalent to Pellet Q		12.5
Pellet R-b Bligh & Dyer	Bligh & Dyer	X	X		X	16	~6x10^8	10

Preparation of environmental (marine) samples. Samples were collected from several depths in the water column of the Eastern Tropical North Pacific during a large-scale sampling effort described in Chapter 3. Samples described here were obtained from 91 m depth, where a secondary chlorophyll maximum coincides with the top of a pronounced oxygen minimum zone. Approximately 1500 L of seawater was filtered *in situ* (McLane Water Transfer System) sequentially through a 53 µm Nitex screen and 0.7 µm-pore size glass fibers filters (GF/F, two, stacked). Filters were frozen immediately at -70°C and remained at -70°C or -80°C until laboratory processing. The GF/F filters were split into pieces and weighed so extraction yields could be determined quantitatively. An aliquot representing 580 L of water was extracted via the Bligh and Dyer (1959) method; the aliquot extracted via the TEP method represented 670 L of seawater. All reported yields are normalized to the original volume of seawater. The Bligh and Dyer extraction method varied slightly from the published version by replacing the same volume of phosphate buffer with trichloroacetic acid. The filter aliquot for this extraction was torn with

clean instruments, and several mL of combusted silica-zirconia beads were added to aid in cell lysis during physical disruption stages of the extraction.

Preparation and addition of standards. Stock solutions of lipid standards representing major compound classes of interest in environmental samples were prepared in dichloromethane from compounds weighed in powder form (ketone, sterol, free fatty acid). Stock solutions of intact polar lipids representing three different classes of headgroups were prepared by diluting a concentrated solution obtained from the manufacturer.

Lipid standards were added to *Synechocystis* lysate as full-process recovery standards for the extraction methods tested here (Tables 6.1, 6.2). Additionally, a mixture of these standards was dried, extracted, and purified according to the full TEP method presented here to determine recovery yields for the process without the effects of biological matrix. Two protein standards and DNA purified from lab culture of *Escherichia coli* were also added to determine TEP recovery yield for these compounds. Protein standards were weighed in powder form and prepared in Nanopure H_2O; DNA from *E. coli* was roughly quantified via Nanodrop, and added to the standards mixture according to the derived concentration. Results from protein and nucleic acid extracts will be presented elsewhere.

Fatty acid methyl ester (FAME) and sterol standards added for quantitation during GC-MS analysis were prepared similarly to other lipid standards. A nonadecanoate ($C_{19:0}$ FAME) standard solution was prepared from powdered nonadecanoic acid ($C_{19:0}$ fatty acid). The

Table 6.2. Yields of lipid recovery standards relative to baseline response (as a fraction).

Compound	Standards-only TEP	Pellet R-b Bligh&Dyer extraction	Pellet R-a TEP	Pellet Q TEP	Filter A TEP (10^8 cells)	Filter B TEP (10^9 cells)	Filter C TEP (10^10 cells)
12-Tricosanone	1.8	2.6	2.0	n/a	1.3	0.7	1.7
Tetracosanoic acid	0.2	1.1	0.9	n/a	0.6	0.5	0.5
Stigmasterol	0.9	1.2	1.0	n/a	0.5	*unable to resolve*	*unable to resolve*
di-C17 PE (1,2-diheptadecanoyl-*sn*-glycero-3-phosphoethanolamine)	0.5	0.5	0.7	0.5	0.9	n/a	n/a
di-C23 PC (1,2-ditricosanoyl-*sn*-glycero-3-phosphocholine)	0.2	0.1	0.1	0.1	n/a	0.4	0.2

powdered standard was weighed and dissolved into a precise volume of dichloromethane to yield a known concentration, and a precise aliquot was transesterified to FAME. A standard solution of cholesterol was prepared similarly by weighing as powder and mixing volumetrically into dichloromethane.

Extraction and purification of lipids

Cell lysis and extraction of organics. Cell lysis and organic extraction were maximized by a combination of physical disruption, multiple freeze-thaw cycles, and detergent treatment. Frozen samples were thawed into a solution of 1:1 Y-PER/B-PER detergents (Yeast- and Bacterial- Protein Extraction Reagents, Pierce Protein Research Products) and bead-beaten (BioSpec BeadBeater) for five minutes in pulses, surrounded by ice. The samples were frozen for a second time at -20°C for a minimum of two hours to enhance lysis. After thawing, samples were bead-beaten again, and organic lysate was removed into solvent-rinsed Teflon tubes. Remaining filter and bead components were rinsed with small aliquots of 1:1 YPER/BPER to maximize organic yield. Gentle centrifugation at 4°C was sometimes needed to further separate solid components.

The initial extraction protocol was modified slightly for environmental filter samples. Small bead-beating chambers (25 mL volume, polypropylene; BioSpec) were used to minimize detergent needed. Chambers were thoroughly cleaned with detergent, deionized water, dilute HCl, and methanol before use. After initial addition of detergent and bead-beating, samples were frozen overnight. After a second thaw and bead-beating, GF/F filters were effectively torn into uniform pulp. Filter pulp was centrifuged gently and rinsed with small aliquots of detergent repeatedly in order to effectively separate the organic extract from the filter remnants. Rinse volumes were restricted such that the final detergent extract volumes totaled 14-17 mL.

Separation of nucleic acid, protein, and lipid phases. Separation of an aqueous phase containing RNA was achieved by standard protocol (Chomczynski and Sacchi, 1987) using Trizol LS (RNA extraction reagent, Invitrogen). Reagent was added 1:1 v/v to the detergent-

extracted lysate, mixed, and held on ice. 20% v/v $CHCl_3$ was added to improve phase separation. Lipid standards dissolved in $CHCl_3$ were added at this stage for recovery quantitation. After centrifugation at 10,000 g and 4°C for 15 minutes, the top aqueous phase was removed to a separate container. An interphase containing DNA was removed and stored separately; this component has not been analyzed further here. The remaining phenol/$CHCl_3$ phase contains lipids and protein; chilled isopropyl alcohol (IPA) was added approximately 1:1 to 2:1 v/v to the organic phase in order to precipitate proteins, but should be added in excess for more efficient recovery. IPA was also added to the aqueous phase at approximately 1:1 v/v for preservation of nucleic acids. All were immediately stored at -20°C. After allowing at least one hour at -20°C for protein precipitation, the organic phase was centrifuged at 10,000 g and 4°C for 15 minutes to form a pellet of protein. The supernatant was removed to a separatory funnel for lipid extraction and the protein was returned to -20°C or -80°C.

Lipid extraction. Lipid was extracted from the phenol/$CHCl_3$ solution in 150 mL chilled $CHCl_3$. Phenol was partitioned into an aqueous phase via washes with 5 × 20-mL aliquots of pre-chilled 5 mM NaOH in nanopure water. Occasionally separation of the phases was poor and the volume at the phase interface required brief centrifugation. To ensure reprotonation of polar lipids after removal of phenol, the $CHCl_3$ (lipid) phase was washed against two 20-mL aliquots of chilled nanopure water before concentrating under high-purity N_2 (g). Care was taken to preserve polar lipids by heating to < 40ºC and removing from heated evaporation chambers after an acceptable concentration had been reached. The total lipid extract would not dry completely, and usually was concentrated to a minimum of ~2 mL.

Silica gel column chromatography and derivatization. Lipid classes were separated by polarity via column chromatography on 100 mL, 100-200 mesh, 60 Å, fully activated pre-combusted SiO_2 gel (~4 cm × 8 cm). The column was prepared in dichloromethane and equilibrated in hexane with 1% each toluene and ethyl acetate (solvent mix "A") to elute residual phenol. Concentrated TLE was homogenized into 100 mL of solvent A and introduced to the column as the first solvent aliquot in order to minimize the polarity effects of any remaining

phenol. Nonpolar recovery standards were eluted in 90:10 hexane/ethyl acetate (v/v; "fraction 5", ketone) and 75:25 hexane/ethyl acetate (v/v; "fraction 8", sterol and free fatty acid). Intact glycolipids were eluted either in 100% ethyl acetate (v/v; "fraction 9") or 75:25 ethyl acetate/methanol (v/v; Fraction 9'). Intact phospholipids were eluted in 100% methanol ("fraction 10").

All collected fractions were dried gently under high purity N_2(g). Acid hydrolysis with 5% HCl in MeOH for 4 h at 70°C effectively cleaved polar head groups and formed FAMEs from free fatty acids and cleaved fatty acid side chains. Products were extracted in 9:1 hexane/chloroform and further derivatized as trimethylsilyl (TMS) ethers in 1:1 pyridine/*N,O*-Bis(trimethylsilyl)trifluoroacetamide (BSTFA). Nonadecanoate ($C_{19:0}$ FAME) and/or cholesterol were added in known concentrations before TMS derivatization as standards for GC-MS quantitation.

Polar lipid fractions from environmental samples were instead saponified in 0.5 N KOH in methanol to cleave head groups. Neutral lipids were extracted, and the remaining reaction mixture was acidified to pH ~2 with hydrochloric acid. Fatty acids were extracted with multiple aliquots of 9:1 hexane/dichloromethane and washed against 5% NaCl in nanopure water and plain nanopure water. Fatty acids were converted to fatty acid methyl esters (FAME) by heating in boron trifluoride/methanol (10% BF_3 in MeOH; Fluka Analytical, Lot BCBC0847) at 70^{o}C for 20-30 minutes. Water was added to stop the reaction and FAMEs were extracted with hexane. Fatty acid standards of known ^{13}C content were routinely methylated with sample batches in order to determine the ^{13}C content of the carbon added from the BF_3/MeOH solution.

Several mixtures of lipid recovery standards were analyzed to establish an in-lab baseline and for maximum yield for these standards after derivatization to FAME or TMS ethers. Recovery standards from stock solutions were mixed in a vial at known concentrations, dried to near completion under high-purity N_2 gas. Without further treatment the mixtures were acid hydrolyzed and derivatized to FAME and TMS ethers as described. The derivatized mixture was analyzed via GC-MS and quantified by comparison of peak area with lipid standards added at

known concentrations. Recovery yields for extracted samples are presented as yields relative to this baseline (Table 6.2). Baseline-relative yields for standards undergoing full extraction and purification stages thus represent integrated potential losses during separation of lipid/protein and nucleic acid phases, lipid extraction (NaOH washes), and SiO_2 column chromatography. Nonadecanoate and cholesterol standards were measured externally for GC-MS quantitation on the same column and temperature-ramping program as full-process standards.

Analysis of lipids via GC-MS. Lipid standards and purified lipid samples were analyzed by gas chromatography-mass spectrometry (GC-MS; Agilent 6890N GC – 5973 mass selective detector) equipped with a 30 m HP5-MS column. Samples were injected in hexane via a programmable temperature vaporization (PTV) inlet with a temperature ramp from 65ºC to 450ºC. The GC oven was held at 65ºC for 1.5 minutes, heated at 60ºC/minute to 115ºC, 20ºC/minute to 130ºC, 6ºC/minute to 280ºC, and 3ºC/minute to 320ºC, where is was held for 25 minutes. Eluent peaks were integrated using the AMDIS (Automated Mass Spectral Deconvolution and Identification System) software, Version 2.65, from the National Institute of Standards and Technology. Only peaks determined to have >90% compound purity are considered here. Relative peak sizes were compared only within a given sample run.

To quantify yields, the relative ratio between the peak area for each analyte and a chemically-similar added standard was determined:

Compound relative abundance = Compound peak area / Standard peak area

Efficiency of extraction and purification procedures was determined by comparison to the known quantity of recovery standards added. If all procedures were 100% efficient, we would have:

100% yield = Proportion of sample injected * Mass of recovery standard added to whole sample / Mass of GC-MS standard added .

For polar lipid standards, the analyte measured (derivatized fatty acid side chain) represents only 69-76% of the original mass of the intact polar lipid added, calculated as the molecular weight of full IPL compound versus diacyl side chains. 100% yield for fatty acids from IPLs was thus adjusted by an average factor of 0.75. The actual yield for full-process recovery standards is thus:

Actual yield = Compound relative abundance / (100% yield) .

Actual yields for recovery standards are further corrected by comparison to baseline yields for the same standards (Table 6.2). Otherwise, the yield described above could be biased by variations in GC-MS responses relating to chain length and other chemical properties, particularly for the C_{23} ketone, which is quantified in relation to the $C_{19:0}$ FAME standard.

The natural ^{13}C content of individual fatty acids extracted from environmental samples was measured via gas chromatography-isotope ratio monitoring mass spectrometry. Methods for this analysis are described in Chapter 3.

Results and Discussion

Recovery of Intact Polar Lipids (IPL). Polar lipids with acyl side chains were determined to be recovered intact based on two observations. (1) An added free fatty acid standard was recovered in less polar fractions (75:25 hexane/EtOAc or less polar). (2) Fatty acids are recovered after hydrolysis of the two polar fractions, but not when these fractions are derivatized directly as TMS ethers.

Recovery of polar lipid standards was achieved in all extraction tests. Generally, the di-C_{23}-glycero-phosphocholine standard was recovered in much lower abundance (10-40% of original, as calculated relative to baseline) than the di-C_{17}-glycero-phosphoethanolamine (50-90% of original). IPL standards were recovered in similar abundance for TEP-extracted samples and the Bligh and Dyer-extracted sample (Table 6.2).

Sturt et al. (2004) report recovery of glycolipids in an acetone fraction and phospholipids in a methanol fraction during SiO_2-gel column chromatography of Bligh and Dyer (1959)-extracted TLE. Van Mooy et al. (2006) found that 70% of IPL biosynthesized by *Synechocystis sp. PCC 6803* were glycolipids. Our 100% ethyl acetate ("glycolipid") fraction thus should contain the bulk of *Synechocystis* biolipids. However, we recovered only ~30-50% of IPL from *Synechocystis* in the ethyl acetate fraction, and the rest in the methanol fraction. Our "glycolipid" fraction is slightly less polar than Sturt et al. (2004), so it is likely that some portion of our glycolipids was eluted in the methanol fraction. In tests of IPL standards, the di-$C_{16:0}$ MGDG was recovered mostly (~75%) from the EtOAc fraction, with some (~25%) eluting in MeOH. However, 100% ethyl acetate also was used to elute glycolipids by Pitcher et al. (2009).

We modified the solvent used to elute the glycolipid fraction to 75:25 EtOAc/MeOH for one extraction test (P-R-b, Bligh and Dyer test). Using this solvent (dubbed fraction 9'), > 90% of *Synechocystis* fatty acids were recovered from this fraction. Phosphoethanolamine- and phosphocholine-headgroup IPL standards were still recovered only in the 100% MeOH fraction. The 75:25 EtOAc/MeOH mixture is therefore a suitable analogue for elution of glycolipids.

Recovery of Nonpolar Lipids. Lipid standards were recovered with relatively consistent yields among the extraction tests (Table 6.2). Baseline-relative yields range from ~50-100% (Table 6.3), although GC-MS responses varied highly between the different compounds and resulted in calculated yields above 100% in many cases. Baseline-relative yields were comparable between the Bligh and Dyer extraction and the TEP standards-only or pellet extractions. The yields of nonpolar standards added to filtered *Synechocystis* culture before TEP extraction were generally slightly lower.

Separation of lipid classes by column chromatography was sometimes compromised by residual phenol compounds from the TEP extraction. Dilution of TLE into a large volume of low-polarity solvent as the first aliquot of mobile phase in SiO_2 column chromatography was found to minimize the polarity effects of any persistent phenol. Nonpolar lipid standards separated using this technique were recovered in the same solvent fraction as those separated

from a Bligh and Dyer extract, with the exception of the $C_{24:0}$ fatty acid. This compound was recovered almost completely in fraction 8 in the TEP sample and in approximately equal proportions in fractions 8 and 9 in the Bligh and Dyer sample.

Samples for which this optimized elution scheme was not performed contained lipids in fractions more nonpolar than expected. Results presented in Table 6.2 represent the sum of compounds recovered across all fractions.

Recovery of Synechocystis biolipids. Polar lipids extracted from *Synechocystis* yielded large peaks of $C_{16:0}$, $C_{18:3\Delta6,9,12}$, and $C_{18:2\Delta9,12}$ FAMEs (isomers identified by comparison to mass spectra at http://lipidlibrary.aocs.org/ms/ms03d/index.htm). This distribution matches well with published fatty acid abundances for *Synechocystis sp. PCC 6803* (Murata et al., 1992; Gombos et al., 1996). Fatty acids were quantified by comparison of peak area with an added standard, and the yield from the total sample was calculated.

Total biolipid yield = (Measured ratio * mass of quantitation standard)/(fraction of total extracted lipid injection)

Results are presented as a per-cell yield of fatty acids in order to compare separate extractions.

Per cell yield = Total biolipid yield / Number of cells extracted

The highest yields calculated were on the order of 10^{-3} pg/cell, for the $C_{16:0}$ and $C_{18:3}$ FAMEs from intact lipids (Table 6.3). All extracts from pelleted cells, whether extracted via the TEP method or the Bligh and Dyer method, yielded 0.002-0.004 pg (2-3 fg) per cell of these two fatty acids. Filtered cultures resulted in lower yields: Filter C extracts yielded ~50% less fatty acids than extracts from pellets, and Filter B yielded ~80% less of the $C_{18:3}$ FAME. For most extracts, the proportion 18:3 to 16:0 was ~1 (+/- 0.2). Environmental variables were held constant in the

continuous culture we sample, so we expect this ratio to remain similar for all extracts. Our observed ratio is slightly different from other published results (~0.6; Murata et al., 1992).

Yields for biolipids from Filter A were difficult to obtain due to potential $C_{16:0}$ contamination, as well as poor resolution of the unsaturated C_{18} FAMEs. A lower limit of filtered biomass for which detectable intact polar lipids can be retrieved thus might be placed around 10^9 cells. However, the spiral-wound filters used in this study required a large volume of detergent to cover the filter surface area. The background of residual detergent-derived analytes is thus relatively high. Disc-type, or flat filters were instead used to collect environmental samples. The surface area of these filters is much lower than that of the spiral-wound cartridge type. The volume of detergent needed and thus the detergent background were each minimized. For applications in which retention of intact lipids is not required, lipids can be cleaved initially and separated from detergent compounds during column chromatography, thus eliminating some of the crossover between sample and reagent.

Purity of TEP extracts. Several compounds appear on GC-MS chromatograms that are not attributable to our cultures or standards. The volume of detergent used in initial TEP extraction correlates with the magnitude of these compounds. The active detergent components are amphiphilic compounds, so any detergent remaining in a sample during column chromatography is likely to elute in the IPL fractions. Compounds in Y-PER and B-PER have been identified by Yang-Boja et al. (2004) as N-tetradecyl-N,N-dimethyl-3-ammonio-1-propanesulfonate and *n*-octyl-beta-D-thioglucopyranoside, respectively. We tentatively attribute one consistently-detected compound to breakdown and disulfide bond formation of B-PER

Table 6.3. Per-cell yields of major *Synechocystis* biolipids (FAMEs recovered from hydrolyzed polar fractions). Units are picograms per cell (pg/cell).

Compound	Pellet N Bligh&Dyer extraction	Pellet Q TEP	Pellet R-b Bligh&Dyer extraction	Pellet R-a TEP	Filter A TEP (10^8 cells)	Filter B TEP (10^9 cells)	Filter C TEP (10^10 cells)
C16:0 FAME from IPL	2.0E-03	2.0E-03	3.6E-03	2.1E-03	6.6E-03	3.7E-03	1.5E-03
C18:3 FAME from IPL	2.4E-03	1.7E-03	3.4E-03	2.5E-03	0**	6.4E-04	1.4E-03
C18:2 FAME from IPL	6.4E-04	5.2E-04	1.0E-03	5.0E-04	0**	0**	1.2E-04
18:3/16:0 ratio	1.18	0.83	0.94	1.16	--	0.17	0.92
18:2/16:0 ratio	0.32	0.25	0.29	0.23	--	--	0.08

during the transesterification procedure. The compound manifests as M^+ 290 in its mass spectrum, eluting problematically close to and/or coeluting with $C_{18:0}$ FAME. The mass spectrum matches a compound identified in the NIST database as dioctyldisulphide.

Transesterification otherwise reduces the number of non-biolipid compounds detectable by GC-MS. Furthermore, purity of polar fractions analyzed by GC-MS was significantly improved by subjecting transesterified products to further polarity separation on a second SiO_2 column, on which methylated fatty acids can be eluted in a low-polarity solvent (here, 90:10 hexane/EtOAc).

Environmental samples cleaved by saponification contained far fewer extraneous compounds. This method was found to be preferable for preparing samples for isotopic analysis, as $C_{18:0}$ is a major environmental compound and isotope analysis requires well-resolved peaks.

Environmental yields and natural ^{13}C analysis. Absolute yields for mass-weighted total fatty acids from each polar lipid fraction were calculated by summing the absolute yields for all resolvable compounds. This absolute yield showed more variability between extract types than any other compared measurement. The Bligh and Dyer method yielded more than twice the total glycolipids that the detergent method recovered, but the detergent method recovered ~67% more phospholipids than the Bligh and Dyer method (Table 6.4). The mass-weighted $\delta^{13}C$ value for total fatty acids, however, was nearly identical for the two extraction methods (within error). On a compound-by-compound basis, almost all $\delta^{13}C$ values were within error range between the two extraction methods. All compounds for which the error ranges for $\delta^{13}C$ values of the two extraction samples did not overlap were minor constituents of the total (Table 6.4, bold type). We suspect that in these cases small and/or irregularly-shaped peaks might have led to slightly poorer auto-integration parameters in the IRMS software. There is slightly more variability in the quantitative distribution of compounds between the TEP and BD samples (i.e., their fatty acid "profiles"). Six to 7 individual compounds per sample displayed relative content (mole fraction, or percent of the total fatty acid) that was > 15% different between the two extracts. However, for all but one compound in the phospholipids, these compounds were minor components,

Table 6.4. Relative yield and $\delta^{13}C$ values of individual compounds from water column filter samples, comparing the Bligh and Dyer (BD; 1959) method with the detergent (TEP) method. a—fatty acids cleaved from the glycolipid fraction; b—fatty acids cleaved from the phospholipid fraction. Bold typeface indicates compounds for which difference in $\delta^{13}C$ values between the two extraction methods is greater than the replicate error range on the measurements. Grey indicates compounds for which the relative proportion (mole fraction) of the compound is > 15% different between the two extraction methods.

a)

Fraction 9: "Glycolipids"

Mass-weighted FA yield		Mass-weighted $\delta^{13}C$	
TEP	52 ng/L	TEP	-28.5‰
BD	140 ng/L	BD	-29.0‰

	$\delta^{13}C$ (‰) Detergent (TEP)	err	$\delta^{13}C$ (‰) Bligh & Dyer (BD)	err	ΔBD-TEP	ΔBD-TEP outside of err range?	Mole Fraction TEP	Mole Fraction BD	% Diff
14:0	-28.5	0.7	-28.3	1.0	0.2	--	0.26	0.25	-2
14:1	-29.5	0.7	-30.2	1.1	-0.7	--	0.08	0.06	-16
15:0	**-28.5**	**0.8**	**-29.8**	**1.1**	**-1.3**	**yes**	**0.01**	**0.01**	**-6**
i-15:0	-25.0	0.7	-25.5	1.1	-0.5	--	0.01	0.01	12
a-15:0	-24.7	0.7	-25.2	1.0	-0.5	--	0.01	0.01	10
16:0	-27.9	0.7	-28.8	1.0	-0.9	--	0.16	0.15	-4
16:1	-29.5	1.0	-29.9	1.1	-0.4	--	0.30	0.30	2
16:1-c	-23.8	1.0	-24.0	5.9	-0.1	--	0.02	0.02	27
17:0	-26.3	1.0	-25.4	0.7	0.9	--	0.01	0.01	-72
18:0	**-25.9**	**0.8**	**-29.4**	**1.0**	**-3.5**	**yes**	**0.03**	**0.02**	**-19**
18:1	-26.9	0.8	-27.1	1.1	-0.2	--	0.02	0.03	15
18:1-b	-29.5	0.8	-30.4	1.2	-1.0	--	0.02	0.02	5
18:4	-33.5	0.7	-32.8	1.2	0.7	--	0.01	0.02	18
20:5	-31.5	4.9	-28.5	0.8	3.0	--	0.02	0.02	7
22:6	-28.8	2.3	-27.2	0.9	1.6	--	0.04	0.05	18

b)

Fraction 10: "Phospholipids"

Mass-weighted FA yield		Mass-weighted $\delta^{13}C$	
TEP	50 ng/L	TEP	-26.7‰
BD	30 ng/L	BD	-26.5‰

	$\delta^{13}C$ (‰) Detergent (TEP)	err	$\delta^{13}C$ (‰) Bligh & Dyer (BD)	err	ΔBD-TEP	ΔBD-TEP outside of err range?	Mole Fraction TEP	Mole Fraction BD	% Diff
14:0	-26.6	0.7	-26.7	0.6	-0.1	--	0.12	0.12	4
br-14:0	-26.0	1.0	-26.2	1.0	-0.3	--	0.01	0.01	-44
14:1	**-22.0**	**0.9**	**-20.8**	**1.0**	**1.2**	**yes**	**0.01**	**0.01**	**0**
15:0	-28.6	0.9	-28.6	1.0	0.0	--	0.02	0.02	8
i-15:0	-24.6	0.8	-24.4	1.0	0.3	--	0.02	0.02	-3
a-15:0	-25.2	0.7	-25.1	1.0	0.1	--	0.02	0.01	-58
16:0	-27.5	0.6	-27.6	0.5	0.0	--	0.21	0.29	28
16:1	-26.2	0.9	-26.1	0.6	0.1	--	0.26	0.23	-14
16:1-b	-25.2	1.0	-24.7	1.0	0.5	--	0.05	0.04	-23
16:1-c	-25.2	0.5	-24.8	1.0	0.4	--	0.03	0.03	-12
17:0	**-25.8**	**1.0**	**-26.9**	**1.0**	**-1.1**	**yes**	**0.01**	**0.01**	**28**
18:0	-27.9	0.7	-27.9	1.2	0.0	--	0.02	0.03	20
18:1	-25.5	0.5	-25.4	1.0	0.2	--	0.08	0.07	-14
br-19:1	**-23.8**	**0.4**	**-26.8**	**1.0**	**-3.0**	**yes**	**0.01**	**0.01**	**-8**
20:5	**-28.5**	**0.6**	**-27.6**	**0.4**	**0.8**	**yes**	**0.04**	**0.02**	**-88**
22:6	-27.3	1.1	-27.1	1.0	0.2	--	0.10	0.08	-14

representing only 1-6% of the total. In addition, the concentrations of fatty acids in the BD phospholipid sample were low enough that several compounds were only measured once for concentration and $\delta^{13}C$. Other compounds were measured 2 to 6 times, and the average values are used. Discrepancies between extracts in the phospholipids are explained largely by this sampling effect.

Conclusions

The detergent method is effective for extracting intact polar lipids in concentrations comparable to that of the Bligh and Dyer technique. There is some evidence that the detergent extraction technique is relatively more efficient at extracting phospholipids and relatively less efficient at extracting glycolipids than the Bligh and Dyer technique. However, based on comparison of extracts from a complex environmental setting, these differences in yield do not appear to affect the measured $\delta^{13}C$ value of lipids derived from either extract; fatty acid profiles derived from the two extracts also are nearly identical.

The detergent extraction technique requires an extended extraction and purification process, but this must be weighed against the increased analytical capabilities offered by simultaneous extraction of other organic constituents (i.e., proteins and nucleic acids). Recovery of nonpolar and/or neutral lipids from the detergent extract is slightly complicated by carryover of extraction reagents. However, clean-up steps were effective in purifying both free fatty acids and sterols. This method was successfully employed on a large sample set from the modern marine water column (Chapter 3). Enough biomass was recovered even from mesopelagic depths for natural ^{13}C analysis, providing unprecedented opportunities to analysis organic matter on the bacterial size scale from the ocean interior.

Acknowledgments

Thanks to Ann Pearson and Roderick Bovee for initiating the efforts and establishing the base protocol for this extraction method, and for continued support with complementary protein and nucleic acid analysis. Thanks also to Yelun Qin for growing the *Synechocystis* biomass that was used for testing this method.

References

Bligh EG, Dyer WJ (1959) A rapid method of total lipid extraction and purification. *Canadian Journal of Biochemistry and Physiology*, **37**, 911-917.

Chomczynski P, Sacchi N (1987) Single-step method of RNA isolation by acid guanidinium thiocyanate-phenol-chloroform extraction. *Analytical Biochemistry*, **162**, 156–159.

Gombos Z, Wada H. Varkonyi Z, Los Da MN (1996) Characterization of the Fad12 mutant of Synechocystis that is defective in delta 12 acyl-lipid desaturase activity. *Biochimica Biophysica Acta,* **1299**, 117–123.

Murata N, Wada H, Gombos Z (1992) Modes of fatty-acid desaturation in Cyanobacteria. *Plant Cell Physiology*, **33**, 933-941.

Pitcher A, Hopmans E, Schouten S (2009) Separation of core and intact polar archaeal tetraether lipids using silica columns: insights into living and fossil biomass contributions. *Organic Geochemistry,* **40**, 12-19.

Sturt HF, Summons RE, Smith K, Elvert M, Hinrichs K-U (2004) Intact polar membrane lipids in prokaryotes and sediments deciphered by high-performance liquid chromatography/electrospray ionization multistage mass spectrometry--new biomarkers for biogeochemistry and microbial ecology. *Rapid communications in mass spectrometry,* **18**, 617-628.

Van Mooy BAS, Rocap G, Fredricks HF, Evans CT, Devol AH (2006) Sulfolipids dramatically decrease phosphorus demand by picocyanobacteria in oligotrophic marine environments. *Proceedings of the National Academy of Sciences of the United States of America*, **103**, 8607–8612.

Yang-Boja E, DeFilippes F, Fales HM (2000) Electrospray mass spectra of three proprietary detergents. *Analytical Biochemistry*, **285**, 105-2010.

Appendix

Fatty acid data from the Eastern Tropical North Pacific

Table A.1. Full fatty acid data from ETNP Station 1 (13ºN 105ºW) polar lipids. Left: fatty acids cleaved from glycolipids; right: fatty acids cleaved from phospholipids. $\delta^{13}C$ values (δ), error, and relative concentration (% of total measured fatty acid mass in sample) of individual compounds, for two size classes (G: 0.7-53 µm; S: 0.2-0.7 µm). Compound names appended by -b, -c, or –d are isomers for which the position of double bonds could not be determined conclusively, but which are consistently identified by retention time across samples. (*) indicates an absolute abundance that has been corrected for estimated loss during processing.

Station 1, Fraction 9' ("glycolipids")
G = 0.7-53 µm / S = 0.2-0.7 µm

Depth & ng/L	FA cmpd	δ_G (‰)	G err	G %	δ_S (‰)	S err	S %
3 m	12:0	-27.9	0.8	1.1	*not collected*		
G 36.3	14:0	-29.0	0.7	30.8			
	14:1	-29.0	0.7	2.6			
	15:0	--	--	0.6			
	i-15:0	--	--	0.3			
	a-15:0	--	--	0.3			
	16:0	-27.4	0.7	28.6			
	16:1-b	-29.2	0.7	15.0			
	16:2	--	--	1.2			
	18:0	-28.3	0.9	9.0			
	18:1ω7	-23.1	0.8	1.5			
	18:1ω9	-27.1	0.7	3.0			
	18:2	-28.1	0.8	1.0			
	18:4	-27.5	0.9	1.4			
	18:4-b	--	--	0.7			
	20:5	--	--	0.7			
	22:6	-25.1	0.5	2.1			
	MW ave	*-28.2*					
52 m	12:0	-28.4	0.8	0.9	*not collected*		
G 183.3	14:0	-30.8	0.7	17.5			
	14:1	-32.8	0.7	1.8			
	15:0	-29.6	0.6	0.6			
	i-15:0	-25.8	0.6	0.4			
	a-15:0	--	--	0.3			
	16:0	-29.1	0.9	13.8			
	16:1	-29.0	0.6	1.0			
	16:1+16:2	-32.1	0.8	12.9			
	16:3	-32.7	0.6	0.8			
	16:4	-33.8	0.8	2.5			
	17:0	--	--	0.9			
	18:0	-28.9	1.5	3.9			
	br-18:0	--	--	0.3			
	18:1ω7	-26.8	0.8	1.5			
	18:1+18:3	-31.4	0.7	3.9			
	18:2	-33.9	0.8	1.9			
	18:3	-32.0	0.7	3.2			
	18:3+18:4	-34.3	0.5	12.9			
	18:4	-34.7	0.5	10.4			
	br-19:0	-30.4	1.0	1.1			
	20:5	-27.6	0.5	2.2			
	20:5-b	--	--	0.4			
	22:6	-27.9	0.5	3.8			
	22:6-b	--	--	0.3			
	22:6-c	--	--	0.4			
	22:6-d	--	--	0.3			
	MW ave	*-31.5*					

Station 1, Fraction 10 ("phospholipids")
G = 0.7-53 µm / S = 0.2-0.7 µm

Depth & ng/L	FA cmpd	δ_G (‰)	G err	G %	δ_S (‰)	S err	S %
3 m	12:0	--	--	1.7	*not collected*		
G 10.3	13:0	--	--	1.1			
	14:0	-27.5	0.6	14.4			
	14:1	--	--	0.8			
	15:0	--	--	1.4			
	i-15:0	--	--	0.9			
	a-15:0	--	--	0.8			
	16:0	-26.7	0.6	31.1			
	16:1	-25.9	0.5	9.4			
	18:0	-28.9	1.4	17.2			
	18:1ω7	-24.1	0.4	6.9			
	18:1ω9	--	--	4.3			
	18:2	--	--	1.4			
	18:3	--	--	0.9			
	20:05	--	--	2.7			
	22:6	-26.2	0.4	4.9			
	MW ave	*-26.9*					
52 m	12:0	--	--	1.0	*not collected*		
G 20.2	14:0	-29.4	0.7	10.2			
	14:1	--	--	0.3			
	15:0	--	--	1.2			
	i-15:0	-23.7	0.6	1.5			
	a-15:0	--	--	1.0			
	16:0	-29.0	0.6	20.3			
	16:1	-28.9	0.6	8.3			
	16:1-c	--	--	1.1			
	16:1+16:2	--	--	**1.7**			
	16:2	**-37.2**	**0.6**	**2.1**			
	16:4	**-35.2**	**1.0**	**1.8**			
	17:0	--	--	0.7			
	18:0	-28.1	0.5	8.6			
	18:1ω7	-27.0	0.5	5.4			
	18:1ω9	-32.1	0.5	5.0			
	18:1-c	--	--	**1.2**			
	18:2	**-36.9**	**0.5**	**3.0**			
	18:3	--	--	**1.3**			
	18:4	**-36.4**	**0.5**	**3.3**			
	18:4-c	--	--	**0.8**			
	br-19:1?	--	--	**0.7**			
	20:0	--	--	0.5			
	20:5	-29.7	0.6	4.3			
	20:5-b	--	--	0.7			
	20:5-c	--	--	0.4			
	22:6	-28.9	1.1	11.9			
	22:6-b	--	--	1.0			
	22:6-c	--	--	0.7			
	MW ave	*-29.8*					

Table A.1 (Continued).

glycolipids, cont.

Depth & ng/L	FA cmpd	δ_G (‰)	G err	G %	δ_S (‰)	S err	S %
91 m	12:0	-27.7	0.8	1.0	*not collected*		
G 51.8	14:0	-28.5	0.7	23.3			
	14:1	-29.5	0.7	7.0			
	15:0	-28.5	0.8	1.4			
	i-15:0	-25.0	0.7	1.0			
	a-15:0	-24.7	0.7	0.9			
	16:0	-27.9	0.7	14.9			
	16:1	-29.5	1.0	28.2			
	16:1-b	-28.1	1.0	1.4			
	16:1-c	-23.8	1.0	1.5			
	16:2	-29.3	1.0	1.2			
	17:0	-26.3	1.0	1.4			
	18:0	-25.9	0.8	2.5			
	18:1ω7	-26.9	0.8	2.1			
	18:1ω9	-29.5	0.8	2.0			
	18:2	--	--	0.7			
	18:3	--	--	0.5			
	18:3+18:1?	--	--	0.5			
	18:4	-33.5	0.7	1.2			
	20:5	-31.5	4.9	1.8			
	22:1	--	--	0.3			
	22:6	-28.8	2.3	3.8			
	22:6-b	--	--	0.9			
	22:6-c	--	--	0.6			
	MW ave	*-28.6*					
128 m	12:0	-27.9	0.9	3.3	-27.7	0.8	2.0
G 14.4	14:0	-30.9	0.8	21.0	-29.7	0.7	20.2
S 15.0	14:1	-33.1	1.0	2.7	-29.0	1.0	1.8
	15:0	-29.4	1.0	1.6	--	--	1.4
	i-15:0	-24.6	1.0	1.1	-22.1	0.7	2.1
	a-15:0	-24.5	1.0	0.7	-25.7	0.7	1.3
	16:0	-27.5	1.1	26.4	-27.2	0.6	22.0
	16:1	-32.3	0.6	13.0	--	--	18.1
	16:1-b	--	--	--	--	--	1.3
	16:1-c	-29.9	1.0	1.8	--	--	2.1
	17:0	--	--	--	--	--	3.4
	18:0	-26.9	0.8	14.4	-26.9	0.7	8.8
	18:1ω7	-29.4	1.0	2.7	-23.2	1.2	6.8
	18:1ω9	--	--	--	--	--	2.3
	18:1-c	-27.8	1.0	2.8	--	--	--
	18:2	--	--	0.7	--	--	0.6
	20:5	-32.1	1.0	1.8	--	--	1.5
	20:5-b	--	--	0.2	--	--	--
	22:1	-35.1	1.0	1.3	-30.2	1.0	2.0
	22:6	-26.7	0.9	4.3	--	--	1.8
	22:6-c	--	--	--	--	--	0.4
	MW ave	*-29.2*			*-27.0*		

phospholipids, cont.

Depth & ng/L	FA cmpd	δ_G (‰)	G err	G %	δ_S (‰)	S err	S %
91 m	12:0	-26.9	1.0	0.5	*not collected*		
G 49.7	i-13:0	--	--	0.3			
	14:0	-26.6	0.7	10.3			
	br-14:0	-26.0	1.0	0.8			
	14:1	-22.0	0.9	1.2			
	14:1-b	--	--	0.5			
	15:0	-28.6	0.9	1.6			
	i-15:0	-24.6	0.8	1.7			
	a-15:0	-25.2	0.7	1.8			
	16:0	-27.5	0.6	18.5			
	br-16:0	--	--	0.4			
	16:1	-26.2	0.9	23.2			
	16:1-b	-25.2	1.0	4.3			
	16:1-c	-25.2	0.5	2.3			
	17:0	-25.8	1.0	0.5			
	17:1	--	--	0.8			
	18:0	-27.9	0.7	1.7			
	br-18:0	--	--	0.5			
	18:1ω7	-25.5	0.5	7.0			
	18:1ω9	-28.6	0.6	3.6			
	18:1-c	--	--	1.1			
	18:1?	--	--	0.9			
	18:2	**-33.2**	**1.0**	**1.0**			
	18:3	--	--	**0.2**			
	18:4	--	--	**0.5**			
	br-19:1	**-23.8**	**1.0**	**0.6**			
	20:5	-28.5	0.6	3.8			
	20:5-b	--	--	0.5			
	22:6	-27.3	1.1	8.5			
	22:6-c	-27.6	1.5	1.6			
	MW ave	*-26.7*					
128 m	12:0	--	--	1.3	--	--	0.4
G 3.6	13:0	--	--	1.2	--	--	0.3
S 11.6	i-13:0	--	--	1.8	--	--	0.3
	a-13:0	--	--	--	--	--	0.2
	14:0	-26.5	1.0	7.6	-24.5	0.6	5.4
	br-14:0	--	--	--	--	--	0.3
	14:1	--	--	1.8	*-10.2*	*1.0*	*1.1*
	15:0	--	--	1.6	-24.7	1.0	1.4
	i-15:0	-21.9	1.0	2.7	-22.0	1.1	3.0
	a-15:0	-22.7	1.0	2.5	-22.3	1.3	1.7
	br-15:0	--	--	--	*-43.8*	*1.0*	*1.3*
	br-15:0	--	--	--	--	--	0.4
	16:0	-27.0	1.0	25.0	-25.2	0.7	24.2
	br-16:0	--	--	--	--	--	0.4
	16:1	-23.4	1.0	12.4	-22.9	0.7	25.0
	16:1-b	--	--	1.2			1.9
	16:1-c	--	--	2.2	-22.2	0.5	3.2
	17:0	--	--	--	--	--	0.5
	br-17:0	--	--	0.9	-31.7	1.0	1.5
	17:1	-25.0	1.0	8.6	--	--	1.3
	18:0	-28.9	0.6	17.5	-27.9	0.5	6.6
	18:1ω7	-24.5	1.0	5.2	-22.2	0.6	12.4
	br-19:0	--	--	--	--	--	1.8
	19:1	--	--	1.0	--	--	--
	20:5	--	--	1.7	-24.0	0.7	2.7
	20:5-b	--	--	0.9	--	--	0.7
	22:6	-27.4	1.0	2.9	-26.9	0.4	1.9
	22:6-c	--	--	--	--	--	0.1
	MW ave	*-26.1*			*-24.2*		

Table A.1 (Continued).

glycolipids, cont.

Depth & ng/L	FA cmpd	δ_G (‰)	G err	G %	δ_S (‰)	S err	S %
G 8.2	14:0	-30.2	0.7	13.6	-30.0	0.6	18.1
S 10.5	15:0	--	--	1.2	--	--	0.7
	i-15:0	--	--	1.1	--	--	1.3
	a-15:0	--	--	0.8	--	--	0.8
	16:0	-27.1	0.5	29.4	-24.9	0.6	28.7
	16:1	-27.0	1.0	2.9	-22.6	0.5	5.4
	16:1-c	--	--	1.2	--	--	1.4
	18:0	-26.9	0.5	23.6	-24.3	0.6	30.1
	18:1ω7	--	--	4.0	-24.7	1.0	4.0
	18:1ω9	-26.2	0.5	4.4	--	--	--
	18:2	--	--	0.9	--	--	--
	20:1	--	--	2.0	--	--	--
	20:5	--	--	1.1	--	--	1.5
	22:1	-32.8	0.8	3.2	-34.2	1.0	2.5
	22:6	-25.8	0.5	3.6	--	--	1.0
	22:6-c	--	--	2.3	--	--	--
	MW ave	*-27.7*			*-25.9*		
502 m	12:0	-27.8	0.7	2.5	*not collected*		
G 7.9	14:0	-29.4	0.8	10.1			
	15:0	--	--	1.1			
	i-15:0	--	--	1.0			
	a-15:0	--	--	0.8			
	16:0	-27.6	0.6	30.2			
	16:1	-27.4	0.5	4.6			
	16:1-c			1.2			
	17:0	-26.9	1.0	3.4			
	18:0	-27.3	0.7	20.2			
	18:1ω7	-28.5	0.7	4.7			
	18:1ω9	-27.0	0.5	3.7			
	18:2	--	--	0.6			
	20:5	--	--	1.2			
	22:1	-32.5	1.5	10.1			
	22:6	-25.2	0.7	3.6			
	22:6-c	--	--	1.1			
	MW ave	*-28.2*					
778 m	12:0	--	--	2.2	*not collected*		
G 20.0	14:0	--	--	9.8			
	16:0	-28.8	0.6	32.9			
	18:0	-28.3	0.5	46.5			
	22:1	--	--	8.6			
	MW ave	*-28.5*					

phospholipids, cont.

Depth & ng/L	FA cmpd	δ_G (‰)	G err	G %	δ_S (‰)	S err	S %
326 m	12:0	--	--	0.9	--	--	0.3
G 3.1	13:0	--	--	1.4	--	--	0.4
S 7.4	i-13:0	--	--	--	--	--	0.2
	a-13:0	--	--	--	--	--	0.1
	14:0	-24.8	1.0	4.9	-25.2	0.6	3.2
	br-14:0	--	--	--	--	--	0.2
	14:1	--	--	--	--	--	0.3
	15:0	--	--	1.4	-22.9	1.0	0.7
	i-15:0	--	--	2.7	-21.3	1.7	2.0
	a-15:0	-20.8	1.0	3.2	-20.3	1.5	1.4
	br-15:0	--	--	--	**-41.9**	**1.0**	**1.4**
	br-15:0-c	--	--	--	**-38.9**	**1.0**	**0.6**
	16:0	-26.0	0.6	22.7	-24.9	1.7	24.4
	16:1	-27.0	0.6	18.8	-22.4	0.8	21.1
	16:1-b	--	--	1.5	--	--	1.6
	16:1-c	--	--	3.7	-22.4	1.0	2.6
	17:0	--	--	1.0	--	--	0.7
	br-17:0	--	--	1.9	-26.4	0.5	4.0
	17:1	-23.1	1.0	5.1	-26.3	5.3	3.5
	18:0	-26.7	0.6	10.5	-27.3	0.7	4.5
	18:1ω7	-28.8	0.5	13.0	-22.7	0.6	13.3
	18:1ω9	--	--	--	-26.3	0.8	8.2
	18:1-c	--	--	--	--	--	0.9
	20:5	--	--	2.9	-23.5	1.3	1.9
	20:5-b	--	--	--	--	--	0.5
	22:6	-25.3	1.0	4.5	-27.4	1.0	1.4
	22:6-b	--	--	--	--	--	0.4
	22:6-c	--	--	--	--	--	0.1
	MW ave	*-26.3*			*-24.5*		
502 m	12:0	--	--	1.0	*not collected*		
G 3.1	13:0	--	--	0.8			
	14:0	-25.1	1.0	4.5			
	15:0	--	--	1.1			
	i-15:0	--	--	2.0			
	a-15:0	-21.8	1.0	2.2			
	16:0	-26.6	0.9	26.1			
	16:1	-25.7	0.7	17.6			
	16:1-c	--	--	3.4			
	br-17:0	--	--	1.8			
	18:0	-27.7	0.5	20.8			
	18:1ω7	-29.5	0.5	9.9			
	18:1ω9	--	--	4.1			
	20:5	--	--	1.7			
	20:5-b	--	--	0.7			
	22:6	--	--	2.3			
	MW ave	*-26.8*					

Table A.2. Full fatty acid data from ETNP Station 8 (9ºN 90ºW) polar lipids. Left: fatty acids cleaved from glycolipids; right: fatty acids cleaved from phospholipids. $\delta^{13}C$ values (δ), error, and relative concentration (% of total measured fatty acid mass in sample) of individual compounds, for two size classes (G: 0.7-53 µm; S: 0.2-0.7 µm). Compound names appended by -b, -c, or –d are isomers for which the position of double bonds could not be determined conclusively, but which are consistently identified by retention time across samples. (*) indicates an absolute abundance that has been corrected for estimated loss during processing.

Station 8, Fraction 9' ("glycolipids")
G = 0.7-53 µm / S = 0.2-0.7 µm

Depth & ng/L	FA cmpd	δ_G (‰)	G err	G %	δ_S (‰)	S err	S %
30 m	12:0	-28.1	0.7	0.5	-27.7	0.9	1.2
G 75.7	14:0	-29.5	0.8	13.7	-29.9	0.6	21.9
S 56.3	14:1	-30.9	0.6	0.9	-30.9	0.6	1.6
	15:0	-29.1	0.7	0.5	--	--	0.4
	i-15:0	-27.4	1.0	0.4	-25.6	1.0	0.9
	a-15:0	--	--	0.2	--	--	0.3
	16:0	-28.8	0.6	39.9	-29.0	0.7	26.2
	16:1	--	--	0.6	-30.1	1.0	0.9
	16:1-c	--	--		--	--	0.8
	16:1+16:2	-31.0	0.8	9.2	-30.9	0.9	17.2
	16:4	-33.2	0.5	1.1	--	--	--
	17:0	-27.4	1.0	0.3	--	--	0.2
	17:1	--	--	0.1	-23.8	1.0	1.3
	18:0	-29.0	0.6	16.6	-28.9	0.6	13.1
	18:1ω7	-27.7	0.5	1.4	-25.9	0.5	3.7
	18:1ω9	-31.0	0.5	2.6	-30.3	0.5	2.5
	18:1+18:2	--	--	1.7	--	--	--
	18:2	-32.2	0.5	1.0	-32.3	1.0	1.0
	18:4	-34.9	0.9	3.2	-34.5	1.0	1.4
	18:4-b	-30.6	1.3	1.7	-29.2	1.0	0.8
	20:5	-27.0	0.4	1.1	-28.4	1.0	1.0
	22:6	-29.8	3.6	2.9	-30.5	4.5	2.1
	22:6-c	--	--	0.4	--	--	0.2
	22:6-d	--	--	--	--	--	0.3
	MW ave	*-29.6*			*-29.5*		
170 m	12:0	-27.4	0.8	3.7	-27.3	0.7	4.1
G 4.0	14:0	-29.5	0.6	11.0	-29.5	0.7	20.5
S 2.3	15:0	--	--	1.0	--	--	0.7
	16:0	-28.7	0.6	39.7	-26.5	0.6	26.4
	16:1	--	--	1.2	-25.3	6.4	3.3
	17:0	--	--	--	--	--	0.9
	17:1	--	--	--	--	--	0.6
	18:0	-28.9	0.8	36.7	-27.2	0.5	37.9
	18:1ω7	--	--	0.9	--	--	1.9
	18:1ω9	-26.5	1.0	2.3	--	--	1.3
	20:5			1.2	--	--	--
	22:1	--	--	--	--	--	1.5
	22:6	-30.6	1.0	2.5	--	--	0.9
	MW ave	*-28.8*			*-27.5*		

Station 8, Fraction 10 ("phospholipids")
G = 0.7-53 µm / S = 0.2-0.7 µm

Depth & ng/L	FA cmpd	δ_G (‰)	G err	G %	δ_S (‰)	S err	S %
30 m	12:0	--	--	0.9	--	--	0.4
G 29.3	14:0	-29.4	0.9	11.6	-28.8	0.6	6.3
S 41.8	14:1	--	--	0.7	--	--	--
	15:0	--	--	2.1	--	--	0.7
	i-15:0	--	--	1.8	--	--	0.7
	a-15:0	--	--	2.8	--	--	--
	16:0	-28.7	0.8	29.7	-27.6	0.6	30.8
	16:1	--	--	--	--	--	5.5
	16:1-c	-29.0	1.0	4.3	--	--	--
	16:1+16:2	-30.9	1.9	8.8	-24.7	0.5	5.1
	17:1	--	--	1.8	--	--	1.0
	18:0	-29.2	0.5	11.4	-26.7	0.5	35.0
	18:1ω7	-28.3	0.5	3.0	-27.2	1.0	4.6
	18:1ω9	-34.0	1.0	3.5	--	--	2.1
	18:2	-34.9	1.0	2.0	--	--	1.5
	18:4	-34.4	0.5	3.1	--	--	1.5
	18:4-b	--	--	1.5	--	--	--
	20:5	-29.2	0.7	3.1	--	--	1.2
	22:6	-31.4	2.7	7.9	-31.5	1.0	3.5
	MW-ave	*-30.0*			*-27.3*		
170 m	12:0	--	--	1.1	--	--	4.5
G 1.1	14:0	--	--	5.9	-29.7	0.6	14.7
S 7.2	15:0	--	--	8.9	--	--	--
	16:0	-28.0	0.9	29.0	-26.7	0.7	31.0
	16:1	--	--	2.0	-24.5	1.0	4.0
	16:1+16:2	-26.7	1.0	11.2	--	--	--
	17:1	--	--	2.6	--	--	0.7
	18:0	-29.4	0.5	33.5	-27.5	0.6	43.1
	18:1ω7	--	--	--	--	--	2.0
	20:5	--	--	2.0	--	--	--
	22:6	--	--	3.8	--	--	--
	MW-ave	*-28.3*			*-27.6*		

Table A.2 (Continued).

glycolipids, cont.

Depth & ng/L	FA cmpd	δ_G (‰)	G err	G %	δ_S (‰)	S err	S %
274 m	12:0	-27.5	0.8	5.7	-27.6	0.7	4.6
G 3.9	14:0	-29.1	0.7	11.7	-29.3	0.9	28.0
S 2.7	15:0	--	--	0.9	--	--	--
	16:0	-27.7	0.5	30.0	-26.9	0.6	23.0
	16:1	--	--	2.0	-21.1	0.8	4.7
	18:0	-28.1	0.5	29.7	-28.4	0.5	28.7
	18:1ω7	--	--	2.5	--	--	2.9
	18:1ω9	-27.3	0.6	7.7	--	--	1.5
	18:2	--	--	1.4	--	--	1.7
	20:5	--	--	1.2	--	--	--
	22:1	-32.0	1.4	5.1	--	--	3.8
	22:6	-24.9	1.0	2.1	--	--	1.2
	MW ave	*-28.1*			*-27.9*		
398 m	12:0	-27.9	1.0	3.4	-27.5	0.7	6.6
G 5.3	14:0	-28.5	0.9	12.0	-28.9	0.8	17.9
S 9.5	15:0	--	--	1.9	--	--	--
	i-15:0	--	--	1.4	--	--	--
	a-15:0	--	--	1.0	--	--	--
	16:0	-25.7	0.6	29.5	-27.6	0.6	28.8
	16:1	-26.3	1.0	3.4	--	--	2.2
	16:1-c	--	--	1.3	--	--	--
	17:1	--	--	1.2	--	--	--
	18:0	-28.3	0.5	23.3	-27.7	0.5	23.5
	18:1ω7	-28.0	1.0	4.2	-27.4	1.0	4.4
	18:1ω9	--	--	2.2	-26.9	0.5	9.4
	18:1+18:2	--	--	1.7	--	--	--
	18:2	--	--		--	--	1.5
	20:5	--	--	1.3	--	--	
	22:1	--	--		--	--	1.2
	22:6	-27.8	5.2	8.0	--	--	0.8
	22:6-c	--	--	4.1	--	--	--
	OH-20:0?	--	--	--	--	--	1.7
	OH-21:1?	--	--	--	--	--	2.1
	MW ave	*-27.3*			*-27.8*		
580 m	12:0	-27.6	0.9	7.9	-27.7	0.8	9.3
G 2.6	14:0	-29.8	1.0	17.1	-29.7	0.7	25.4
S 3.7	16:0	-27.6	0.6	26.0	-28.3	1.1	22.5
	16:1	--	--	--	--	--	3.6
	18:0	-28.4	0.6	43.0	-28.7	0.8	24.8
	18:1ω7	--	--	--	--	--	2.0
	18:1ω9	--	--	--	-27.6	0.7	7.9
	22:1	--	--	3.3	--	--	4.6
	22:6	--	--	2.8	--	--	--
	MW ave	*-28.4*			*-28.7*		
730 m	12:0	-28.5	1.0	6.0	-27.7	0.9	5.0
G 1.8*	14:0	-30.0	0.7	19.6	-29.8	1.1	21.6
S 3.4	16:0	-27.6	0.6	29.9	-29.1	0.7	26.5
	16:1	--	--	2.5	--	--	1.3
	18:0	-28.7	0.7	32.0	-29.0	0.5	23.6
	br-18:1?	--	--	2.3	--	--	1.3
	18:1ω9	--	--	1.7	-26.5	1.0	2.9
	22:1	--	--	3.1	-31.3	0.8	4.5
	22:6	--	--	3.0	--	--	--
	OH-20:0?	--	--	--	-30.0	0.6	10.7
	OH-21:1?	--	--	--	--	--	2.7
	MW ave	*-28.6*			*-29.3*		

phospholipids, cont.

Depth & ng/L	FA cmpd	δ_G (‰)	G err	G %	δ_S (‰)	S err	S %
274 m	12:0	--	--	--	--	--	0.5
G 1.9*	14:0	--	--	4.3			2.3
S 3.2	16:0	-27.3	0.6	39.7	-27.1	0.9	32.8
	16:1	--	--	4.6	-27.0	0.6	8.2
	17:1	--	--	--	--	--	1.3
	18:0	-29.0	0.8	43.9	-27.2	0.6	51.1
	18:1ω7	--	--	--	--	--	2.8
	br-18:1	--	--	7.4	--	--	1.1
	MW-ave	*-28.2*			*-27.2*		
398 m	12:0	--	--	0.7	--	--	--
G 4.0*	14:0	-25.1	1.0	4.1	--	--	2.4
S 4.2*	15:0	--	--	2.2	--	--	--
	i-15:0	--	--	2.0	--	--	--
	a-15:0	--	--	2.5	--	--	--
	16:0	-26.1	0.6	25.9	-27.0	0.7	35.4
	16:1	-28.8	3.9	10.6	-27.3	4.1	8.7
	16:1-b			2.9	--	--	--
	17:1	-23.9	0.7	7.8	--	--	4.0
	18:0	-28.5	0.5	21.2	-27.4	0.7	45.5
	18:1ω7	-29.3	0.5	8.2	--	--	3.9
	18:1ω9	--	--	1.6	--	--	--
	20:5	--	--	2.2	--	--	--
	22:6	-22.9	0.4	8.1	--	--	--
	MW-ave	*-26.8*			*-27.2*		
580 m	14:0	--	--	5.4	--	--	4.3
G 0.8	16:0	-27.3	0.8	33.1	-26.9	0.7	36.5
S 0.4*	16:1	--	--	7.4	-26.6	0.9	13.8
	18:0	-28.4	0.5	48.3	-28.4	0.5	35.2
	18:1ω7	--	--	--	--	--	3.3
	br-18:1	--	--	--	--	--	6.8
	22:6	--	--	5.8	--	--	--
	MW-ave	*-27.9*			*-27.5*		
730 m	12:0	--	--	1.4	--	--	--
G 0.5	14:0	-25.2	1.0	5.8	--	--	3.3
S 0.6	16:0	-27.1	0.6	27.9	-27.3	0.7	37.0
	16:1	-29.1	1.0	13.3	-24.2	1.8	12.7
	17:1	--	--	4.0	--	--	--
	18:0	-28.8	0.5	39.9	-28.2	0.5	44.2
	18:1ω7	--	--	2.1	--	--	2.7
	20:5	--	--	2.1	--	--	--
	22:6	--	--	3.6	--	--	--
	MW-ave	*-28.0*			*-27.3*		

Table A.3. Full fatty acid data from ETNP Station 8 (9ºN 90ºW), free fatty acids. $\delta^{13}C$ values (δ), error, and relative concentration (% of total measured fatty acid mass in sample) of individual compounds, for two size classes (G: 0.7-53 µm; S: 0.2-0.7 µm). Compound names appended by -b, -c, or –d are isomers for which the position of double bonds could not be determined conclusively, but which are consistently identified by retention time across samples. (*) indicates an absolute abundance that has been corrected for estimated loss during processing.

.

Station 8, Fraction 6 (free fatty acids)
G = 0.7-53 µm / S = 0.2-0.7 µm

Depth & ng/L	FA cmpd	δ_G (‰)	G err	G %	δ_S (‰)	S err	S %
30 m	16:0	-29.3	0.8	29.8	-29.6	0.5	43.0
G 79.1	16:1	-31.9	2.6	5.4	-28.7	1.0	5.5
S 15.4*	18:0	-29.9	0.8	8.9	-30.2	0.7	32.4
	18:1ω7	-25.9	1.0	2.8	--	--	3.7
	18:1ω9	-29.9	1.0	8.1	-28.4	1.0	5.3
	18:1+18:2	-30.6	1.0	12.8	--	--	--
	18:2	-31.7	0.7	4.2	--	--	3.6
	18:4	-33.9	0.9	7.9	--	--	1.4
	18:4-b	-30.5	1.0	3.2	--	--	1.0
	20:0	--	--	0.5	--	--	1.5
	20:5	-30.6	1.2	3.3	--	--	--
	22:6	-30.4	1.1	13.0	--	--	2.7
	MW ave	*-30.3*			*-29.7*		
170 m	16:0	--	--	--	-27.4	0.7	29.5
(G lost)	18:0	--	--	--	-29.6	0.6	70.5
S 1.1	*MW ave*	*--*			*-29.0*		
274 m	16:0	-27.3	0.9	26.7	-27.7	0.9	31.0
G 2.9	16:1	-27.5	1.0	11.0	--	--	5.6
S 0.6	18:0	-29.9	0.9	34.4	-30.8	1.1	42.5
	18:1ω7	-24.8	1.0	3.1	--	--	2.9
	18:1+18:2	-27.9	1.0	15.2	-28.3	0.8	13.0
	20:5	-28.2	1.0	4.0	--	--	1.4
	22:6	-29.7	2.9	5.7	--	--	3.6
	MW ave	*-28.4*			*-29.3*		
398 m	16:0	-26.0	1.0	30.7	-28.2	0.7	25.2
G 7.1*	16:1+16:2	-26.5	1.0	6.6	--	--	1.6
S 3.3	18:0	-30.2	0.9	26.9	-29.4	0.7	46.1
	18:1ω7	-28.7	1.0	4.9	--	--	4.2
	18:1ω9	-26.6	1.0	6.9	-29.2	1.0	7.6
	18:2	-30.7	1.0	4.6	-31.4	1.0	7.7
	18:4	--	--	--	--	--	7.7
	20:5	-25.1	1.0	3.7	--	--	--
	22:6	-29.5	5.5	15.7	--	--	--
	MW ave	*-28.0*			*-29.3*		
580 m	16:0	-26.4	0.6	23.7	-31.9	1.0	28.4
G 0.8	16:1+16:2	--	--	2.8			3.9
S 1.2	18:0	-29.6	0.5	39.2	-29.4	1.0	50.6
	18:1ω7	--	--	2.5	--	--	12.8
	18:1ω9	--	--	4.8	--	--	4.2
	18:1+18:2	-27.1	1.0	6.1	--	--	--
	20:5	--	--	3.6	--	--	--
	22:6	-25.1	1.0	17.3	--	--	--
	MW ave	*-27.6*			*-30.3*		
730 m	16:0	-27.2	0.8	23.2	-28.3	0.6	26.1
G 1.6	16:1	--	--	2.3	--	--	--
S 0.6	18:0	-30.2	0.8	54.3	-29.4	0.5	59.7
	18:1ω7	--	--	3.2	--	--	6.0
	18:1+18:2	--	--	7.5	--	--	8.2
	20:5	--	--	2.7	--	--	--
	22:6	-31.7	1.0	6.8	--	--	--
	MW ave	*-29.5*			*-29.1*		